Assessing and Improving Clinical Outcomes of the Cementless Oxford Unicompartmental Knee Replacement Tibial Component



A DISSERTATION SUBMITTED TO THE UNIVERSITY OF OXFORD
IN PARTIAL FULFILMENT OF THE REQUIREMENTS FOR THE DEGREE OF

Doctor of Philosophy

Azmi Sultan Sikander Rahman

Oriel College

Trinity Term 2022

ABSTRACT

Assessing and Improving Clinical Outcomes of the Cementless Oxford Unicompartmental Knee Replacement Tibial Component

Azmi Rahman, Oriel College **DPhil, Trinity Term 2022**

Cementless Oxford Unicompartmental Knee Replacements (OUKR) are known to have a lower revision rate than cemented, but have a higher incidence of early tibial fracture, and is not known how their symptoms compare. The aims of this thesis were firstly to compare the symptoms following cemented and cementless OUKR and explore factors that may influence them, and secondly to assess design changes which may reduce their risk of fracture.

A study comparing Cemented and Cementless OUKR demonstrated that most pain reported by patients is intermittent, and that 42% more patients with Cementless OUKR report having no pain compared to Cemented OUKR.

Radiolucencies at the tibial wall, and bone density around the tibial keel, are characterised for the first time in literature. Radiolucencies around the tibial component were found only where there was no porous coat, and these radiolucencies were associated with an increased likelihood of patients reporting pain. This suggests that the porous coating should be applied to all bone-implant interfaces. Bone density around the keel changes in the years following surgery, but this change is unrelated to pain.

Despite the benefits of Cementless OUKR, cemented tibial components are still used, in part due to concerns about periprosthetic tibial fractures in Cementless OUKR. These occur most commonly around very small components. The keel has the same depth for all sizes, suggesting that the relatively larger keels are an important risk factor for the smaller tibias. To address this, changes to keel design were studied using a plastic bone test in which the push-in force was considered to be related to the fracture risk and the pull-out force was considered to be related to primary fixation. From these tests, two new keel designs were proposed: a small porous keel without a window, and a small porous-walled smooth-edged keel. A more radical redesign replacing keels with two anterior angled pegs was also proposed to address fundamental limitations of a keel.

More physiologically relevant tests were developed using plastic bone blocks machined to the shape of a very small tibia that experienced a fracture. These tests used load-to-fracture to assess fracture risk and anterior lift-off with posterior loading to assess primary fixation. Important assumptions about the effect of keel size and interference are assessed with these tests. The small porous keel, compared to the standard keel, reduced fracture load, and had similar fixation. The smooth-edged keel similarly reduced the fracture load but had better fixation. The two-peg component greatly reduces fracture risk and virtually eliminates pathological implant micromotion.

The thesis concludes with proposed next steps leading to clinical use of these new designs. The small porous and porous-walled smooth-edged keels require minor modifications to manufacturing, while the two-peg device requires modifications to manufacturing, surgical technique, and instrumentation. The new small keels could be introduced relatively rapidly after short clinical studies, whereas the two-peg device would require more in-depth safety assessments. Whichever design is introduced, all surfaces interfacing with bone in the tibial component should have a porous coating.

"The two absolute requirements of an arthroplasty of the knee are relief of pain and stability."

H Phillips and J G Taylor
Journal of Bone and Joint Surgery (Britain), 1975.

ACKNOWLEDGEMENTS

I am incredibly grateful to my supervisors David Murray and Stephen Mellon for their willingness to walk with me on a journey usually taken by more senior orthopaedic colleagues, yet enabling me to develop my ideas freely and productively all the same. I now think differently, and probably for the better.

I am grateful to Barbara Marks and Jo Brown, the stalwarts of the Oxford Orthopaedic Engineering Centre, for facilitating my ideas and making them a reality. I am grateful to Jack Tu, Hasan Mohammad, Michael Beverly, Louise Strickland, Tom Hamilton, Irene Yang, Alexander MacAulay, David Heath, Lachlan Arthur, and Xiaoyi Min for their companionship and collaborations. Our times at OOEC might come and go, but these ties will last.

I am indebted to my many collaborators who were committed to our work despite the challenges of a difficult pandemic – Cathy Jenkins, Benjamin Martin, Jack Aspinall, Gabrielle Omoregie, Katerina Dangas, Simon Hook, Sanpreet Johal, Amber Butler, Aditya Desai, Henry Searle, and Ali Amin. I am also grateful to the wider orthopaedic community – the surgeons, physiotherapists, and radiographers at the Nuffield Orthopaedic Centre and Manor Hospital, the Oxford Knee team, and fellow academics in the field, for enabling the work in this thesis in many ways.

I am grateful to A*STAR for supporting my research, and indebted to Rinawati Rahmat and Lisa Ng for supporting me through highs and lows.

I am thankful for the Oriel College Decanal Team, for welcoming me into their team, becoming close friends, and entertaining my peculiar interest in ‘the bottom bit of the inside half of the knee’. My academic and collegiate lives have been intimately intertwined, and Oriel will forever hold a special place in my heart; floreat Oriel.

Gliding became an important pastime over the course of this research, and I am thankful for my fellow university pilots and the Oxford Gliding Club for flying with me. My time in the air is always a respite from the stresses on the ground.

I cannot capture how grateful I am to my parents Mallick and Sirajunisa, and my sisters Sultana, Yasmin, and Nurlina, for their unwavering support, and for reaching past the distance and time differences to be there for me, and for driving me to reach higher. I am beholden to my nephew Amir and niece Alisha, for patiently putting up with my absence in their lives – you have grown so quickly, and you always make me proud.

I am incredibly grateful to the innumerable patients who will go unnamed in this thesis – everything within these pages stems from you, is based on you, and is meant for you. Without you, this thesis is meaningless.

And finally, I thank you, the reader, for sharing a fondness in improving the daily lives of our patients. I hope that when you are reading this, more problems have been solved, more patients are doing better, and the world is a better place.

COVID-19 STATEMENT

The work presented in this thesis was performed between Michaelmas (October) 2019 and Trinity (June) 2022, totalling nine terms over three academic years.

Five of these nine terms were during periods of lockdown due to the Covid-19 pandemic, where laboratory access and in-person meetings were severely limited.

FUNDING STATEMENT

This DPhil studentship was funded by the Agency for Science, Technology, and Research (A*STAR). Further support was offered by Oriel College and the Nuffield Department of Orthopaedics, Rheumatology, and Musculoskeletal Sciences in the University of Oxford.

ABBREVIATIONS

ACL – Anterior Cruciate Ligament

AKSS-O/F/P – American Knee Society Score (Objective/Functional/Pain)

AP – Antero-Posterior

ANOVA – One Way Analysis of Variance

BMD – Bone Mineral Density

BMI – Body Mass Index

CAD – Computer Aided/Assisted Design

CI – Confidence Interval

DEXA – Dual-Energy X-ray Absorptiometry

DICOM – Digital Imaging and Communications in Medicine (used as a digital image encoding format)

DIMM – Dynamically Induced Micromotion

EQ-5D-5L – Euro-Qol Five Dimension Scale – 5 Levels

HA – Hydroxyapatite

ICOAP 'A'/'B' – Intermittent and Constant Osteoarthritis Pain score, of which 'A' is a score of constant pain and 'B' is a score of intermittent pain

ISO – International Standardization Organization

IEC – International Electrotechnical Commission

JPEG – Joint Photographic Experts Group (used as a digital image encoding format)

mm – Millimetres

μm – Micrometres

$MaxF_{in}$ – Maximum Push-In Force

$MaxF_{out}$ – Maximum Pull-Out Force

MCID – Minimum Clinically Important Difference

MCL – Medial Collateral Ligament

MUA – Manipulation Under Anaesthesia

N – Newton

NHS – National Health Service

NJR – National Joint Registry of England, Wales, Northern Ireland, and Isle of Man

NZJR – New Zealand Joint Registry

OKS – Oxford Knee Score

PIPO – Push-In Pull-Out (a form of testing used in **Chapters 5 and 6**)

PROM – Patient Reported Outcome Measure

RCT – Randomised Control Trial

RSA – Radiostereometric Analysis

SEM – Scanning Electron Microscope/Microscopy

SD – Standard Deviation

SONK – Spontaneous Osteonecrosis of the Knee

SOV – Standardised Opacity Value (ΔSOV: Change in SOV)

TAS – Tegner Activity Scale

TKA/R – Total Knee Arthroplasty/Replacement

TWF/TFF/TKF – Tibial Wall/Floor/Keel Fixation

UK – United Kingdom

UKA/R – Unicompartmental Knee Arthroplasty/Replacement

USA – United States of America

VAS – Visual Analogue Scale

YLD – Years Lived with Disability

TABLE OF CONTENTS

ABSTRACT ..... **II**

ACKNOWLEDGEMENTS ..... **IV**

COVID-19 STATEMENT ..... **V**

FUNDING STATEMENT ..... **V**

ABBREVIATIONS ..... **VI**

TABLE OF CONTENTS ..... **VIII**

FIGURE INDEX ..... **XV**

TABLE INDEX ..... **XXIV**

1 INTRODUCTION **1**

1.1 The Knee 1

1.2 History of Knee Replacement: Total and Unicompartmental 4

1.3 Osteoarthritis and Knee Replacement 6

1.3.1 Pathophysiology of Osteoarthritis 6

1.3.2 Presentation of Osteoarthritis 6

1.3.3 Clinical Management of Osteoarthritis and the Role of Knee Replacement 8

1.4 Other indications for Knee Replacement 10

1.4.1 Inflammatory Arthropathies 10

1.4.2 Osteonecrosis with Cartilage Destruction 10

1.4.3 Post-Traumatic Arthritis 11

1.5 Arthritis, Isolated Medial Osteoarthritis, and Knee Replacement 12

1.5.1 Incidence 12

1.5.2 TKR vs UKR for Isolated Medial Osteoarthritis 13

1.6 Implants Commonly used in Medial Unicompartmental Knee Replacement 14

1.7 The Oxford Unicompartmental Knee Replacement (UKR) 16

1.7.1 History of the Implant 16
1.7.2 The Cementless Oxford UKR Design 18
1.7.3 Specific indications for Oxford Medial UKR 21
1.7.4 Outcomes following Cementless Oxford UKR 21
1.8 Thesis Objectives 23
1.9 Structure of Thesis 24
2 MID-TERM PATIENT REPORTED OUTCOMES OF CEMENTLESS AND CEMENTED OXFORD UKR 26
2.1 Motivation for Chapter 26
2.2 Introduction and Study Aims 27
2.3 Design of Study 30
2.4 Pre-Operative Results 35
2.5 Post-Operative Clinical Outcomes 36
2.6 Post-Operative Patient-Reported Outcomes (PROMs) 38
2.6.1 General PROMs 38
2.6.2 Pain-Specific PROMs 42
2.6.3 Neuropathy and Pain 45
2.6.4 Co-Morbidity and Pain 46
2.7 Impact of Non-Contemporaneity 49
2.8 Discussion of Findings 53
2.9 Chapter Summary 59
3 TIBIAL COMPONENT FIXATION AND PAIN 60
3.1 Motivation for Chapter 60
3.2 Bone-Implant Interfaces of the Tibial Component 61
3.3 Current Knowledge and Chapter Aims 62
3.4 Surface Microstructure of Bone-Facing Surfaces of the Oxford UKR Tibial Component 63

3.5 Assessing Tibial Wall Fixation 66
3.5.1 Collecting Radiographs 66
3.5.2 Quantifying Horizontal Alignment in Radiographs 67
3.5.3 Quantifying Wall Fixation in Radiographs 68
3.6 Tibial Wall Fixation in variants of Oxford UKR 69
3.6.1 Study Aims and Method 69
3.6.2 Study Cohort 69
3.6.3 Software and Statistics 70
3.6.4 Results 71
3.6.5 Discussion of Findings 78
3.6.6 Conclusion 82
3.7 The Effect of Tibial Component Fixation on Pain 83
3.7.1 Limitations in Current Knowledge 83
3.7.2 A Protocol to Assess Radiolucencies around the Tibial Component 84
3.7.3 Software and Statistics 86
3.7.4 Tibial Wall Fixation in 5-year cohort 87
3.7.5 Tibial Radiolucencies and the Incidence of Pain in 5-year cohort 89
3.7.6 Discussion of Findings 94
3.7.7 Conclusion 97
3.8 Chapter Summary 98
4 PERI-KEEL BONE DENSITY AND PAIN 99
4.1 Motivation for Chapter 99
4.2 Peri-Prosthetic Effects of Inserting a Cementless Keel 100
4.3 Concerns about varying Bone Radio-Opacity around the Tibial Keel. 102
4.4 Chapter Aims 103

4.5 A Protocol to Assess Bone Density in Plain-Film Radiographs 104

4.6 Study Cohort and Method 108

4.7 Bone Density Changes around the Cementless Keel 110

4.8 Discussion of Findings 116

4.9 Chapter Summary 120

5 REDUCING KEEL SIZE IN THE CEMENTLESS OXFORD UKR TIBIAL COMPONENT 121

5.1 Motivation for Chapter 121

5.2 The Nature and Risk of Fracture in the Cementless Oxford UKR 122

5.2.1 Fractures in Smaller Tibial Components 122

5.2.2 Fractures in Extended Keel Cuts 124

5.3 Depth and Length of Tibial Component Keel across Implant Sizes 126

5.4 Designing a New Keel 128

5.4.1 Design Aims 128

5.4.2 Implementing Design Aims 129

5.4.3 Testing Design Aims 129

5.5 Testing Design Changes 131

5.5.1 Study Design 131

5.5.2 Data Processing 132

5.5.3 Design Elements Tested 134

5.5.4 Results 138

5.5.4.1 Maximum Push-In and Pull-Out Forces 138

5.5.4.2 Total Push-In and Pull-Out Energies 139

5.5.4.3 Forces and Energies on Reinsertion 140

5.5.5 Discussion of Findings 142

5.5.6 Conclusion 147

5.6 Chapter Summary 148

6 PEGS AS AN ALTERNATIVE TO THE KEEL IN THE CEMENTLESS OXFORD UKR TIBIAL COMPONENT 149

6.1 Motivation for Chapter 149

6.2 Limitations of a Keel 150

6.3 Pegs as an Alternative Fixation Element 151

6.4 Design Aims 153

6.5 Optimising Peg Profile 154

6.5.1 Study Design 154

6.5.2 Design Elements Tested 156

6.5.3 Results 162

6.5.3.1 Effect of Diameter 162

6.5.3.2 Effect of Taper 164

6.5.3.3 Effect of Surface Roughness 165

6.5.3.4 Effect of Tip Profile 166

6.5.3.5 Effect of Base Gap 167

6.5.3.6 Effect of Insertion Depth 168

6.5.3.7 Effect of Angle 169

6.5.3.8 Effect of Tip Surface Roughness 170

6.5.4 Discussion of Findings 171

6.6 A New Tibial Component with Peg Fixation 175

6.6.1 Proposed Peg Profile 175

6.6.2 Proposed Peg Number and Distribution 177

6.7 Chapter Summary 179

7 FRACTURE RISK IN A VERY SMALL TIBIA: THE EFFECT OF DIFFERENT FIXATION ELEMENTS ON LOAD-TO-FRACTURE 180

7.1 Chapter Motivation and Aims 180

7.2 Why a keel may cause a fracture 181

7.3 Testing Load-to-Fracture 182

7.3.1 Study Aims and Methods 182

7.3.2 Results 187

7.3.2.1 Effect of Slot and Keel Depth 187

7.3.2.2 Effect of Loading Position 188

7.3.2.3 Load-to-Fracture in New Fixation Elements 189

7.3.2.4 Fracture Path Angle 190

7.3.3 Discussion of Findings 192

7.4 Chapter Summary 198

8 PRIMARY FIXATION IN A VERY SMALL TIBIA: THE EFFECT OF DIFFERENT FIXATION ELEMENTS ON SAGITTAL MICROMOTION 199

8.1 Chapter Motivation and Aims 199

8.2 Primary Fixation, Micromotion, and Subsidence of the Tibial Component 201

8.2.1 Implications of Inadequate Primary Fixation 201

8.2.2 Implant Factors Affecting Sagittal Micromotion 204

8.3 Measuring Micromotion 206

8.3.1 Available Methods for Implant Motion Tracking 206

8.3.2 A Low-Cost, High-Resolution, Micromotion Measurement Protocol 207

8.4 Measuring Sagittal Micromotion using Anterior Lift-Off 210

8.4.1 Study Aims and Methods 210

8.4.2 Results 215

8.4.2.1 Effect of Interference and Keel Size on Anterior Lift-Off 215

8.4.2.2 Anterior Lift-Off in New Fixation Designs 220

8.4.3 Discussion of Findings 224

8.5 Chapter Summary 229

9 CONCLUSION 230

9.1 Summary of Findings 230

9.2 Further Work on Outcome Assessment 233

9.3 Further Work on Design Changes 235

9.3.1 Expanding the Porous Surface of the Tibial Component 235

9.3.2 Testing Fracture and Fixation in Larger Tibial Sizes and with Cortex 236

9.3.3 Replicating Findings with True Porous Surfaces 236

9.3.4 Producing New Component Designs with Clinical Manufacturing Techniques 237

9.3.5 Safety and Regulatory Approval 239

9.3.6 Clinical Assessment 240

9.3.6.1 Assessing Safety and Primary Fixation 240

9.3.6.2 Assessing Secondary Fixation 241

9.3.6.3 Assessing Patient-Reported Outcomes 242

BIBLIOGRAPHY 243

APPENDICES 263

APPENDIX A PROMS USED IN 5-YEAR CLINICAL STUDY 264
APPENDIX B ADDITIONAL RESULTS FOR TIBIAL COMPONENT FIXATION 273
APPENDIX C ADDITIONAL RESULTS FOR PERI-KEEL REMODELLING 277
APPENDIX D CODE FOR DATA EXTRACTION IN PIPO TESTING 278
APPENDIX E ADDITIONAL RESULTS FROM PEG PIPO TESTING 280
APPENDIX F ADDITIONAL RESULTS FROM FRACTURE TESTING 282

FIGURE INDEX

Figure 1.1: Key Ligaments of the Knee Joint. Key structures not shown: Ilio-tibial band, patellar tendon, articular cartilage of tibia. Image adapted from [3]. 2

Figure 1.2: Articular surfaces and joints in the knee. Taken from [4]. 3

Figure 1.3: The Walldius Hinge Prosthesis. Taken from [8]. 4

Figure 1.4: Commonly used views in Plain Film Knee Radiography. **(a)** AP, **(b)** Lateral, **(c)** Skyline, **(d)** AP with varus stress, **(e)** AP with valgus stress. 7

Figure 1.5: Most commonly used Unicondylar Knee Implants between 2012 and 2020 as reported in the UK National Joint Registry. Figure from [52].....14

Figure 1.6: All iterations of the Oxford UKR to date. **(a)** Phase 1, **(b)** Phase 2, **(c)** Phase 3, **(d)** Twin-Peg, **(e)** Cementless, **(f)** Lateral Domed, **(g)** Lateral Fixed. Images adapted from [75] and [76].....16

Figure 1.7: Components of the Cementless Oxford UKR. **(a)** Femoral Component, **(b)** Bearing, **(c)** Tibial Component. Images adapted from [76, 86]. 19

Figure 2.1: Implants assessed in this study. **(a)** Cemented Phase 3 Oxford UKR. **(b)** Cementless Oxford UKR. Photos from Zimmer Biomet. 27

Figure 2.2: 5-year Oxford Knee Score, American Knee Society Score and EQ-5D Index, scaled to 100, for cemented and cementless cohorts.....39

Figure 2.3: 5-year OKS for cemented and cementless cohorts, categorised into Kalairajah categories 40

Figure 2.4: 5-year EQ-5D-5L domain scores for cemented and cementless cohorts.....41

Figure 2.5: Histogram of Tegner Activity Score in cemented and cementless cohorts.41

Figure 2.6: Mean ± 95% CI scores for ICOAP and PainDETECT for cemented and cementless cohorts. All scores scaled from 0-100 and inverted where necessary such that higher is better (ICOAP A and B inverted, painDETECT multiplied by a factor of 10 from 0-10 to 0-100 and inverted). 42

Figure 2.7: Histogram of 5-year ICOAP (Total) score, for cemented and cementless cohorts. 2-sided Chi-Square Test across all categories had a significant difference to p=0.0006. 2-sided Chi-Square Test between ‘x=0’ and other categories had a significant difference to p<0.0001.....43

Figure 2.8: Percentage of 5-year ICOAP ‘A’, ’B’, and Total scores with score 0 of 100, in cemented, cementless, and combined cohorts.....44

Figure 2.9: Histograms of 5-year painDETECT Scales scores. p-values given for Mann-Whitley U-Tests performed between scores for cemented and cementless cohorts. 45

Figure 2.10: ICOAP 'Total' scores in cemented and cementless cohorts, split by Charnley grades A+B (knee arthritis only) and Charnley C (non-knee arthritis or external morbidity). V Mild: Very Mild, Mod: Moderate, Sev: Severe, Ext: Extreme. ** - $p<0.001$. 47

Figure 2.11: Mean (± 95% CI) responses to ICOAP, painDETECT VAS, OKS (Pain), and AKSS (Pain) categorised into Charnley scores. All distributions are non-parametric (Shapiro-Wilk $p<0.05$), and differences tested with Mann-Whitley U test. 48

Figure 2.12: Histogram of Years of Study and corresponding number of cemented and cementless procedures performed in each year for recruited participants. 49

Figure 2.13: Mean ± 95% CI values for OKS, AKSS (UKR Variant), and EQ-5D (Pain/Discomfort domain and Index score), for cemented and cementless cohorts, further classified into early and late subgroups. 50

Figure 2.14: Mean ± 95% CI scores for ICOAP and painDETECT scales, for cemented and cementless cohorts, further classified into early and late subgroups. All scores scaled from 0-100 (ICOAP already 0-100, painDETECT scales multiplied by a factor of 10 from 0-10 to 0-100). 51

Figure 3.1: (a) The Tibial Component of the Cementless Oxford UKR showing porous transverse surface and smooth wall surface. Image adapted from Campi et al [142]. **(b)** An AP radiograph of a Cementless Oxford UKR, demonstrating the transverse/horizontal cut, sagittal/vertical wall cut, and slot cut. 61

Figure 3.2: Scanning Electron Micrographs of Bone Contact Surfaces in Oxford UKR tibial components. (**a**) Tibial Wall/Floor/Keel in Cemented UKR, without hydroxyapatite. (**b**) Tibial Wall in Early Cementless UKR, with hydroxyapatite. (**c**) Tibial Wall in Later Cementless UKR, with microporous titanium and hydroxyapatite. (**d**) Tibial Floor/Keel in cementless UKR, with porous titanium and hydroxyapatite. (**e**) Close-up view of Cemented UKR surface showing absence of hydroxyapatite. (f) Close-up view of Cementless UKR surface showing hydroxyapatite coating. 64

Figure 3.3: Three progressively rotated AP knee radiographs from a patient, demonstrating how rotation can cause masking of a radiolucency adjacent to the tibial wall. Horizontal Rotation Ratios for each radiograph were **(a)** 32%, **(b)** 82%, **(c)** 223%. 67

Figure 3.4: Comparison of Wall Fixation Ratio (WFR) measured by both observers, separated by coating type. 72

Figure 3.5: Mean Wall Fixation Ratio at the tibial wall in all aligned radiographs, separated by coating at tibial wall. 73

Figure 3.6: Histogram of Wall Fixation Ratio at the tibial wall in all aligned radiographs, separated by coating at tibial wall. FR is split into 20% groups from poor fixation (FR = 0-20%) to excellent fixation (FR = 81-100%). 74

Figure 3.7: Bone growth found in some radiographs where fixation to the tibial wall is poor (FR<20%). Feature is radiographically characterised as a generally hemi-lenticular opacity between implant and sclerosed vertical bone surface. (**a**) Radiograph of a

cementless implant, (**b**) Graphical representation with hemi-lenticular opacity highlighted in yellow. 76

Figure 3.8: Regions assessed and region grouping used to assess presence of radiolucencies in 5-year study cohort. 86

Figure 3.9: Fixation Ratio at Tibial Wall in 5-year Cemented and Cementless Oxford UKR cohorts. 88

Figure 3.10: Radiolucencies around the tibial component in 5-year Cemented and Cementless (HA) Oxford UKR cohorts. *: $p<0.05$. **: $p<0.01$. ***: $p<0.001$. 90

Figure 3.11: Radiolucencies at the Tibial Wall/Floor/Keel and Incidence of Pain in 5-year Cemented and Cementless (HA) Oxford UKR cohorts. ns: $p\geq0.05$. *: $p<0.05$. 92

Figure 3.12: ICOAP (Total) scores against Radiolucency at the Tibial Wall/Floor/Keel in Cemented and Cementless cohorts. 93

Figure 3.13: Overlay of an AP radiograph of a Cementless Oxford UKR assessed in this study, against a model of a tibial component and it is bone-facing surfaces. Overlay demonstrates the alignment of the radiolucency locations at the tibial floor with the regions where porous coat is absent. White arrows indicate transition points where radiolucencies begin/end. 95

Figure 4.1: Three 5-year AP radiographs demonstrating consistent patterns of varying radio-opacity in bone. 102

Figure 4.2: Regions assessed in study. Size of keel, which is constant for all implant sizes, was used as a reference for region size. Regions were termed U1-U5 at the level of the keel and L1-L5 at the level immediately below the keel, where '1' referred to the most medial region. U3 was the keel itself and was left out of analyses. 105

Figure 4.3: Comparison of raw grey values measured by both observers. 110

Figure 4.4: Post-operative (black) and 5-year (green) Standardised Opacity Values in regions assessed. 111

Figure 4.5: Change in Standardised Opacity Values for each region between postoperative and 5-year radiographs, indicating relative changes in bone density for each region. **(a)** Change in Standardised Opacity Values for each region, with significant differences shown ****: $p<0.0001$. **(b)** Mean changes in Standardised Opacity Values overlayed on a radiograph to demonstrate average change in each region. 112

Figure 4.6: Peri-keel Composite Remodelling Score by Tibial Component Size. Effect of size significantly related to remodelling. **: $p<0.01$. 113

Figure 4.7: Post-operative and 5-year radiographs for Size A and one Size F patient included in study. Post-operative radiographs in both knees indicate similar bone density around keel. 5-year radiographs indicate greater remodelling around keel in Size A than Size F, consistent with study findings. 113

Figure 4.8: (a, left) Peri-keel Composite Remodelling Score for each tibial component size from Size A to Size F (no patients in study had a size AA implant), split by female (pink) and male (blue). **(b, right)** A size-matched comparison of Peri-keel composite remodelling score by sex. *:p<0.05.....114

Figure 4.9: The relationship between patient-reported pain and function outcomes and the remodelling observed in their keel. Peri-keel composite remodelling score represents magnitude of remodelling. Patient-reported outcomes all scaled from 0-100, and higher is better. Individual values shown as dots, linear regressions shown as solid black lines, 95% confidence intervals for linear regressions shown as in grey. **(a)** Oxford Knee Score (Pain sub-score). **(b)** Oxford Knee Score (Function sub-score). **(c)** Oxford Knee Score (Total score). **(d)** Intermittent and Constant Osteoarthritis Pain Score ('A' Constant Pain score). **(e)** Intermittent and Constant Osteoarthritis Pain Score ('B' Intermittent Pain score). **(f)** Intermittent and Constant Osteoarthritis Pain Score (Combined Pain score). **(g)** Tegner Activity Score against peri-keel remodelling. **(h)** Remodelling in patients split into those who experienced pain vs no pain based on ICOAP Total scores.....115

Figure 5.1: Preparing the keel slot using a reciprocating keel-cut guided by a template held with a pin, placed on a prepared tibial floor. Image adapted from [86]. 125

Figure 5.2: The size of the Cementless Oxford UKR Tibial Component. (**a, b**) AP and lateral views of relative size of the smallest (AA), middle (C), and largest (F) components. Lines at the posterior aspect of keels in (b) indicate the posterior edge of Size F (green), C (blue), and AA (orange) keels. **(c, d)** AP and lateral views of the tibial components, scaled to implants.....127

Figure 5.3: (a) A typical keel PIPO test setup. Polyurethane foam is constrained from vertical motion, **(b)** Diagram representing interference. **(c)** Depiction of key components of keel PIPO test setup components.....132

Figure 5.4: A sample force-displacement graph from a PIPO test, indicating the Push-In, Unload, and Pull-Out phases, as well as the maximum Push-In and Pull-Out forces. Graph generated on MATLAB. The areas shaded in orange and green highlight the Push-In and Pull-Out energies respectively. 133

Figure 5.5: Keel designs explored in this study. **(a)** Standard clinical keel design, and **(b)** a new smaller keel. **(c)** Overlay of standard and new keel designs, demonstrating the difference in depth and distance from posterior cortex. All keels are based on the Size 'AA' tibia of the Cementless Oxford UKR.....135

Figure 5.6: Scanning Electron Micrographs of keel surfaces used in this study and the surfaces they are meant to represent. **(a)** Printed porous surface, **(b)** Printed smooth surface, **(b)** Clinical porous surface made with porous spray coated with hydroxyapatite, **(d)** Clinical smooth surface which is cast and coated with hydroxyapatite. Keels used in this study: Porous, Porous Walled with Smooth Edged (PWSE), and Smooth, are shown above.....136

Figure 5.7: (a) The template for a standard 'Size AA' tibial component keel cut. **(b)** A 3D-printed clip-on template riser, used to make smaller slots for smaller keels with same clearance as standard template. Riser used the posterior limiting peg and another

accessory peg to secure riser to template, leaving one hole for pin insertion to secure template during keel cut (see **Section 5.2.2**). 137

Figure 5.8: Maximum push-in and pull-out forces for keel and slot designs. Horizontal lines are drawn at the level of the maximum push-in and pull-out forces of the standard keel in standard slot, for comparison. 139

Figure 5.9: Total Push-In and Pull-Out Energy for keel and slot designs. A horizontal line is drawn at the level of the maximum Push-In and Pull-Out forces of the standard keel in standard slot for comparison. 140

Figure 5.10: Maximum push-in and pull-out forces for keel and slot designs on re-insertion into slots. Horizontal lines are drawn at the level of the maximum push-in and pull-out forces of the standard keel in standard slot, for comparison. 141

Figure 5.11: Total push-in and pull-out energies for keel and slot designs on re-insertion into slots. Horizontal lines are drawn at the level of the total push-in and pull-out energies of the standard keel in standard slot, for comparison. 141

Figure 5.12: Representative force-displacement curve profiles for the pull-out phase of testing for each sample variant, scaled to average $MaxF_{out}$ of all repeats for each variant. Area under curve represents total energy of pull-out phase. Note the sharp drop-off with smooth keel, and further smooth tapered keel. **Blue:** Small porous-walled, smooth-edged non-tapered 6mm keel - mean $FMax_{out}$=234 N and E_{out}=611 N.mm. **Grey:** Small smooth non-tapered 6 mm keel - mean $FMax_{out}$=208 N and E_{out}=434 N.mm. **Red:** Small smooth tapered 6 mm keel - mean $FMax_{out}$=204 N and E_{out}=328 N.mm. **Green:** Standard (porous, non-tapered) 9 mm keel - mean $FMax_{out}$=178 N, mean E_{out}=642 N.mm. **Yellow:** Small porous, non-tapered 6 mm keel - mean $FMax_{out}$=113 N, mean E_{out}=243 N.mm. 144

Figure 6.1: (a) A typical peg PIPO test setup. PU foam is constrained from vertical motion, **(b)** Diagram representing interference. **(c)** Depiction of key components of PIPO test setup components. 155

Figure 6.2: (a) A load being applied at the location of the red arrow in the sagittal plane. **(b)** The predicted tilting implant motion that would result indicated with black arrows, demonstrating constrained vertical lift-off of the anterior aspect of the tibial component. 158

Figure 6.3: Test setup for pull-out of an angled peg with vertical constraint, highlighting spindle position for push-in. 159

Figure 6.4: (a) A depiction of the stress concentration resulting at the base of an angled peg of a constant diameter, indicated in red. **(b)** A depiction of a 'base gap' and how it mitigates stress concentrations. 160

Figure 6.5: Difference in surface area of interaction between peg and superior surface of the hole with **(a)** round-bottomed and **(b)** flat-bottomed pegs inserted the same vertical distance, demonstrated by the red line. 161

Figure 6.6: Maximum Push-In, Pull-Out Forces, and ratio of values, with varying peg diameter and interference in a porous peg. Quadratic regression was performed for each variant across interferences. 163

Figure 6.7: Maximum Push-In, Pull-Out Forces, and ratio of values, with varying peg taper angle and interference in a porous peg. Quadratic regression was performed for each variant across interferences. 164

Figure 6.8: Maximum Push-In, Pull-Out Forces, and ratio of values, with varying interference in a 4.7mm smooth and porous pegs. Quadratic regression was performed for each variant across interferences. 165

Figure 6.9: Maximum Push-In, Pull-Out Forces, and ratio of values, with varying interference in a rounded tip vs a flat-angled tip. Quadratic regression was performed for each variant across interferences. 166

Figure 6.10: Maximum Push-In, Pull-Out Forces, and ratio of values, with varying interference in without a gap at the base, and a 2mm base gap. Quadratic regression was performed for each variant across interferences. 167

Figure 6.11: Maximum Push-In, Pull-Out Forces, and ratio of values, with varying peg insertion depth in smooth and porous pegs. Quadratic regression was performed for each variant across insertion depths. 168

Figure 6.12: Maximum Pull-Out Forces with a straight peg and with pegs angled 20°, 30°, and 40° against vertical, with smooth and porous pegs. Linear regression was performed between the angled pegs. 169

Figure 6.13: Maximum Push-In and Pull-Out Forces with a porous vs smooth tip. 170

Figure 6.14: Proposed peg profile incorporating all suggested design elements (not to scale). 176

Figure 6.15: (a) Position of the two pegs in new design in a lateral view of the tibial component (in green), overlayed on the positions of the small keel (in blue), and standard keel (in orange). **(b)** A custom designed template for the positioning and congruent alignment of holes to be drilled for a Two-Peg tibial component. 178

Figure 7.1: (a) Image of setup for load-to-fracture testing. **(b)** Diagram of components in test setup. 183

Figure 7.2: Keel Designs explored in this study. **(a)** Standard keel found in currently used clinical components, **(b)** Small porous keel, **(c)** Small porous-walled smooth-edged keel, **(d)** Two-Peg, and **(e)** no keel. **(f)** Different fixation elements overlayed – standard in orange, small in blue, Two-Peg in green. Small keel designs are as described in **Chapter 5**. Two-Peg design is as described in **Chapter 6**. 184

Figure 7.3: Effect of Slot and Keel on load needed for fracture in standard, small, and no keel designs. 187

Figure 7.4: Effect of loading position and keel design on load needed for failure, in standard keel design and a smaller keel design. 188

Figure 7.5: Fracture loads in the standard, small, small porous-walled smooth-bottomed (PWSE), Two-Peg, an no fixation elements, at central loading. 189

Figure 7.6: Coronal Fracture Path Angle (CFPA) with and without slot, and with standard, small, Two-Peg, and no keels/pegs. 191

Figure 7.7: Visualisation of fracture paths in standard, small, Two-Peg, and no keel variants. 191

Figure 7.8: Anterior-Posterior radiograph of peri-prosthetic tibial fracture occurring in knee used as model for this study. The implant used would have the standard keel. .. 195

Figure 7.9: Consecutive frames of a fracture test in this study with a standard keel, recorded at 240 frames per second. Changes from **7a-c** demonstrate fracture propagating inferiorly keel to bone below, with fracture path similar to clinical findings (see **Figure 7.8**). 196

Figure 8.1: First presented in Figure 6.2 and are re-presented here**. (a)** A load being applied at the location of the red arrow in the sagittal plane. **(b)** The predicted tilting implant motion that would result indicated with black arrows, demonstrating constrained vertical lift-off of the anterior aspect of the tibial component**. (c,d,e,f)** Lateral views of a knee experiencing pain and stiffness, post-operatively, and 1,8, and 10 years after surgery. **(d)** presents increased posterior slope, and radiolucencies in the anterior keel slot and anterior tibial floor, demonstrating anterior lift-off at 1-year. **(e)** presents minimal further change in posterior slope and in-fill of apparent space in anterior keel slot, demonstrating arrest of subsidence by 8 years, **(f)** presents no further change at 10 years. 203

Figure 8.2: (a) Image Acquisition Setup for DIC. **(b)** Example overall image acquired, demonstrating distortion at the lateral ends of image. **(c)** Zoomed-in image presenting high speckle fidelity and low image blur required for DIC. Note that two black dots in (b) are reference points for two identical lines 10.00mm apart, used were used as reference for image scaling in post-processing. Line at the front of component seen in (b) and (c) was used as measurement marker for anterior lift-off. 208

Figure 8.3: Comparison of displacement calculated from Digital Image Correlation to real displacement, for setup validation. Standard deviations for 1.00mm was 1.1%, 0.50mm was 1.5%, 0.20mm was 2.8%, 0.10mm was 4.9%, 0.05mm was 6.2%, 0.02mm was 31.9% and 0.01mm was 51.0%. 209

Figure 8.4: Keel Designs explored in this study. **(a)** Standard keel found in currently used clinical components, **(b)** Standard keel with no interference, **(c)** no fixation element, **(d)** Small porous keel, **(e)** Small porous-walled smooth-edged keel, and **(f)** Two-Peg. **(g)** Fixation elements overlayed – standard in orange, small in blue, and Two-Peg in green. Small keel designs are as described in **Chapter 5**. Two-Peg design is as described in **Chapter 6**. 211

Figure 8.5: (a) Image of setup for sagittal micromotion testing. **(b)** Diagram of components in test setup. 213

Figure 8.6: A sample of how anterior lift-off was measured mid-sequence. **(a)** Mid-sequence image frame under study. **(b)** Surface components applied with a colour map of displacement (blue indicates less motion and red indicates more motion), and two-point distance was measured a at fixed distance from posterior edge of tibial component across all tests. Duplicate measurements were taken at different heights and were found to be within 20 μm in all cases. 214

Figure 8.7: Anterior Lift-Off during posterior loading of tibial components with a standard keel, standard keel with no interference (NI), and no fixation element, loaded at posterior-most position experienced in step-up loading position, located 8 mm posterior to midpoint of implant on the sagittal plane. Anterior lift-off measured using DIC at 50 N increments, with mean values in dots and linear regressions of data represented with solid lines. 216

Figure 8.8: Anterior Lift-Off during posterior loading of tibial components with a standard keel, standard keel with no interference (NI), and no fixation element, located 15 mm posterior to midpoint of implant on the sagittal plane. Anterior lift-off measured using DIC at 50 N increments, with mean values in dots and linear regressions of data represented with solid lines. 218

Figure 8.9: Maximum anterior lift-off measurements, occurring during maximal loading of 200 N in a tibial component with a standard keel, standard keel with no interference (NI), and no fixation element. Tests statistically compared. ns: not significant, *:$p<0.05$. 219

Figure 8.10: Anterior Lift-Off during posterior loading of tibial components with a standard keel, small (porous) keel, small porous keel, small PWSE keel, and Two-Peg, located 15 mm posterior to midpoint of implant on the sagittal plane. Anterior lift-off measured using DIC at 50 N increments, with mean values in dots and linear regressions of data represented with solid lines. 221

Figure 8.11: Anterior Lift-Off during posterior loading of tibial components with a standard keel, small (porous) keel, small porous keel, small PWSE keel, and Two-Peg, located 15 mm posterior to midpoint of implant on the sagittal plane. Anterior lift-off measured using DIC at 50 N increments, with mean values in dots and linear regressions of data represented with solid lines. 222

Figure 8.12: Maximum anterior lift-off measurements, occurring during maximal loading of 200 N in a tibial component with a standard keel, small porous keel, small PWSE keel, and Two-Peg. Tests statistically compared. ns: not significant, *: $p<0.05$, ***: $p<0.001$. 223

Figure 9.1: Current Surfaces on (**a)** lateral and **(b**) inferior views of the current Cementless Oxford UKR presenting implant surfaces that interface with bone. 235

Figure 9.2: Differences in small PWSE keels when **(a)** 3D printed, and **(b)** manufactured using clinical techniques. **(c)** Rasping effect of upper lip of clinically manufactured keel. **(d)** Removal of lip from clinically manufactured keel by planing and filing. 238

Figure 9.3: Maximum Push-In and Pull-Out Forces in clinically manufactured standard and small PWSE keels, and a small PWSE keel where the lip is planed and filed. Tests performed at n=3. 239

TABLE INDEX

Table 2.1: Pre-operative characteristics of cemented and cementless cohorts. 35

Table 2.2: Post-operative revision, re-operation, and complication rates. 36

Table 2.3: 5-year response rates and responses for Oxford Knee Score and American Knee Society Score 39

Table 2.4: Likelihood of having a neuropathic component to pain (based on PainDETECT PD-Q score) at different pain levels, scored on the PainDETECT VAS Strongest (Str) scale. Results (n and %) from cemented and cementless cohorts. 46

Table 2.5: Comparison early and late cemented and cementless cohorts. 52

Table 3.1: Representative images of Oxford UKR tibial components and bone-implant interfaces at the tibial wall, separated by coating type. Note that the mean WFR progressively increases from the Cemented, to the HA, to the HA+MPC variants. 75

Table 3.2: HA and HA+MPC cohort radiographs with features of delaminated bone growth 77

Table 3.3: Fixation Ratio in studies performed. 88

Table 3.4: Comparison of Radiolucency Score in Specific Regions and Combined Scores in 5-year Cemented and Cementless (HA) Oxford UKR cohorts. Difference between cohorts across regions is visualised using a colour scale, where red indicates a relatively greater difference. 90

Table 4.1: Cohort characteristics. 108

Table 6.1: Design elements and variants tested, with reasons for exploring the rationale and ideal outcome for each measurement. 156

Table 7.1: Load to Fracture and Maximum Push-In Force of keel designs tested. 194

Table 8.1: Maximum Anterior Lift-Off and Maximum Push-In Force of keel designs tested. 227

1 Introduction

1.1 The Knee

The knee is a key joint in the human body connecting the femur to the tibia. It is a load-bearing joint fundamentally involved in bipedal motion. It is therefore involved in many activities of daily living, and healthy joint function is vital to daily life.

The knee is capable of flexion and extension over a large range of motion – this is the primary motion of the joint. It is also capable of smaller ranges of abduction/adduction, internal/external rotation, and compression/distraction motions. These secondary motions enable greater joint flexibility [1].

The distal femur, proximal tibia, and patella are encapsulated by the joint capsule. This capsule is filled with synovial fluid produced by the inner lining of the capsule known as the synovium. The femoral, tibial, and patellar articular surfaces are lined with cartilage, and these cartilaginous surfaces contact one another directly. The tibio-femoral interfaces are further supported by menisci, which are C-shaped cartilaginous tissue that help cushion the joint interface [1].

The joint is stabilised by surrounding muscles and ligaments (**Figure 1.1**). The two key muscle groups, the anterior group (quadriceps) and posterior group (hamstrings), induce knee extension and flexion respectively. When activated together, they induce stabilising compressive forces in the joint [2]. The knee is further stabilised by ligaments – the medial and lateral collateral ligaments (MCL, LCL) provide medial and lateral joint stability, and the anterior and posterior cruciate ligaments (ACL, PCL) limit excess

anterior or posterior tibial draw [1]. The iliotibial band is a thick band of fascia on the lateral aspect of the thigh that further supports lateral joint stability [1].

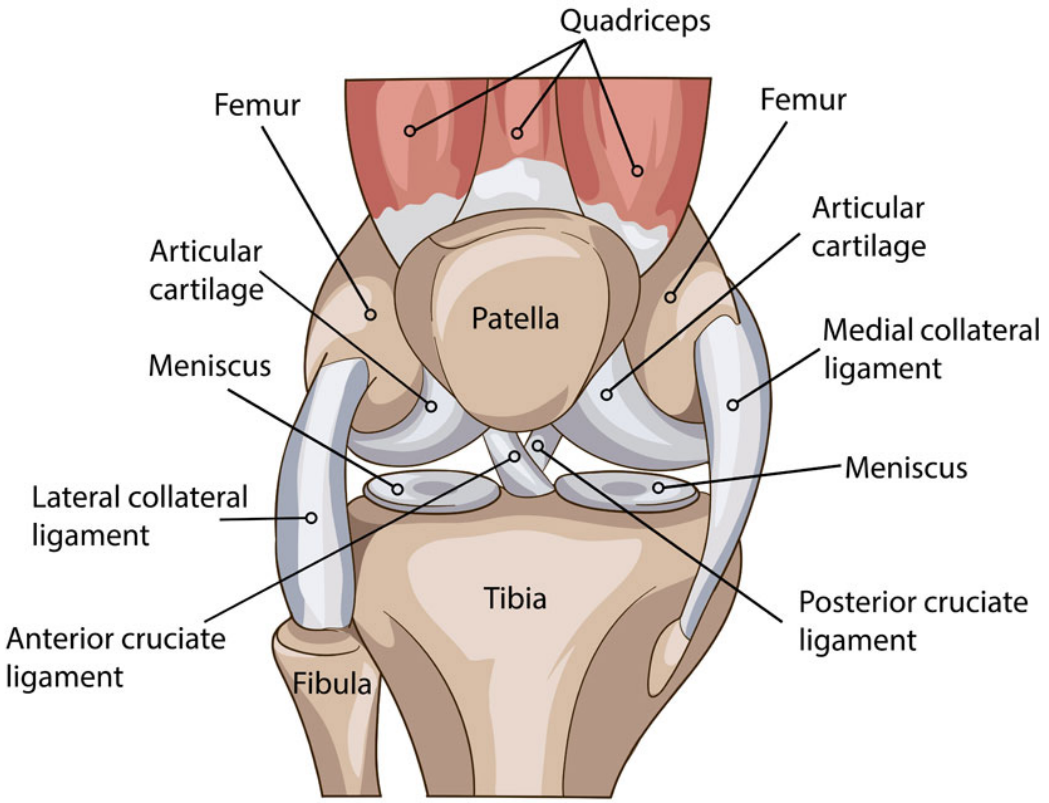


Figure 1.1: *Key Ligaments of the Knee Joint. Key structures not shown: Ilio-tibial band, patellar tendon, articular cartilage of tibia. Image adapted from [3].*

The knee joint can be subdivided into three articular regions – the medial tibio-femoral joint, the lateral tibio-femoral joint, and the patello-femoral joint (**Figure 1.2**). These joints can be surgically replaced using knee arthroplasty, also known as knee replacement.

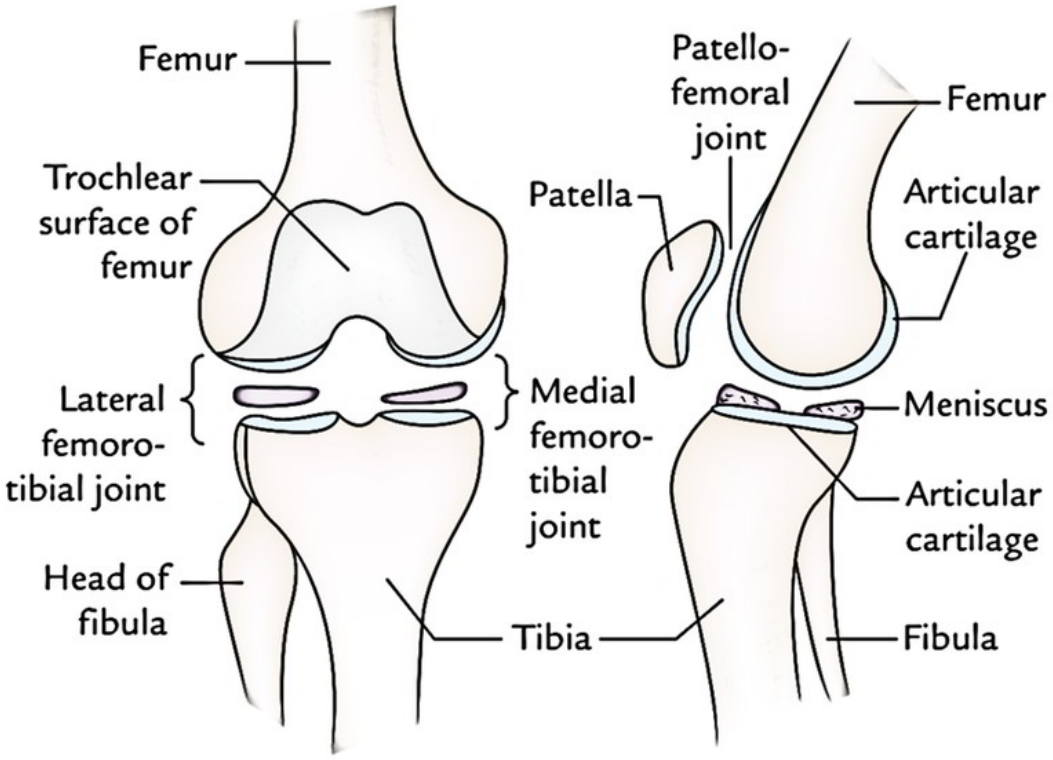


Figure 1.2: *Articular surfaces and joints in the knee. Taken from [4].*

1.2 History of Knee Replacement: Total and Unicompartmental

Knee replacement surgery involves the insertion of implants into and around the articular regions of the knee joint to replace the human tissue. The first recorded knee replacement was the implantation of an ivory hinge joint in 1860, performed on a 17 year old female [5]. The Walldius hinge implant was the first routinely used knee replacement in 1951, and was used in elderly and less mobile patients to reduce pain and enable joint function [5, 6]. Variants with similar design and materials followed. These implants were designed to be highly constrained for joint stability, offering only flexion/extension motion, and less range of motion than an intact knee. Studies found that this implant had a high risk of loosening-related failure, suggested to be due to this constrained of range of motion, resulting in large forces acting on the implant and inducing loosening [7].

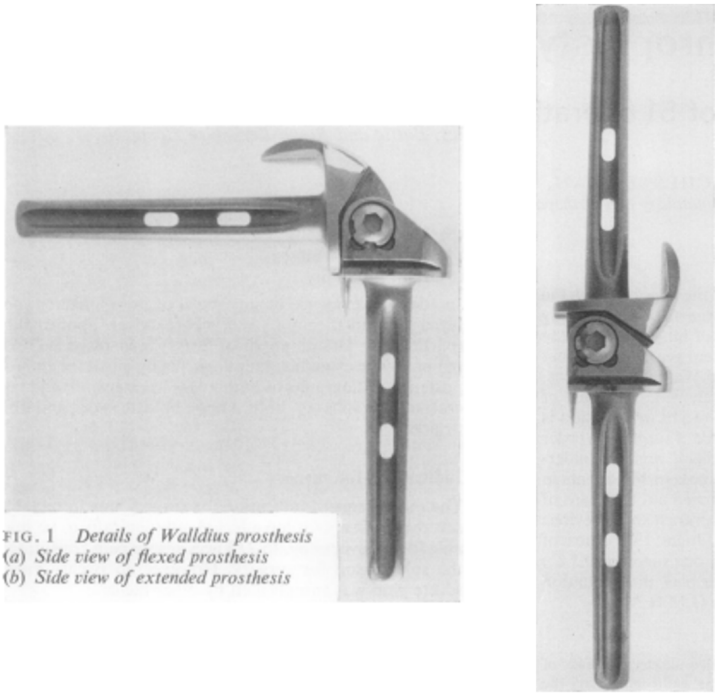


Figure 1.3: *The Walldius Hinge Prosthesis. Taken from [8].*

Following this, two key paradigm shifts occurred in knee replacement design. First, most designs mechanically de-linked the femoral and tibial components to reduce constraint. Second, several designs drew from the successful Charnley metal-on-polyethylene total hip arthroplasty, and introduced metal-on-polyethylene knee replacement implants.

Other design elements included:

- the option of polymethylmethacrylate (PMMA) cement as a fixation aid [9]
- the option of cruciate ligament preservation or sacrifice [5]
- the option of a Total Knee Replacement vs Unicompartmental Knee Replacement [5]

Total Knee Replacement (TKR) generally involves the use of a single implant to replace all articular surfaces, whilst Unicompartmental Knee Replacement (UKR) generally involves using an implant that replaces the medial tibio-femoral joint, lateral tibio-femoral joint, or patello-femoral joint.

Most clinically used knee replacement are categorised into TKR and UKR [10]. Modern commonly-used TKR and UKR have three components – the femoral component, the tibial component, and an interfacing bearing. Most femoral and tibial components are made of hard, low-wear metal alloys, while most bearings are made of a moulded polyethylene bearing. The bearing can be fixed in place on the tibial component surface, or mobile – moving between the femur and tibia. UKR and TKR enable restoration of joint motion that was restricted by pain or structural impediment [10]. TKR designs with a hinge structure continue to be used occasionally when high constraint is required (e.g., in salvage procedures following failed TKR) [11].

1.3 Osteoarthritis and Knee Replacement

1.3.1 Pathophysiology of Osteoarthritis

Over 97% of knee replacement surgery is performed for end-stage osteoarthritis [12]. The precise aetiology of primary osteoarthritis is unknown, but is understood to be a bio-mechanical process involving the joint cartilage, subchondral bone, and the synovium [13, 14]. In osteoarthritis, there is fibrillation and erosion of the cartilage starting in superficial layers which progress into deeper layers of the cartilage [15]. The highly innervated subchondral bone experiences sclerosis and cyst formation, which is likely to contribute to pain [16]. Synoviocytes downregulate production of lubricants and upregulate processes which degenerate synovial and extracellular matrix proteins, further reducing function [14].

Osteoarthritis can also occur secondary to joint trauma which results in abnormal loading of the cartilage, and which accelerates destruction of cartilage. ACL injury predisposes a four times increased odds of developing knee osteoarthritis, and injury also involving the meniscus further increases this to six times increased odds [17].

1.3.2 Presentation of Osteoarthritis

Patients with osteoarthritis tend to experience pain that is relieved by rest and worsening over the day, along with knee instability, and morning stiffness. The pain generally is limited to the knee and worsens as disease progresses, beginning with intermittent pain on activity and progressing to constant pain [18].

Radiographic signs of osteoarthritis include reduced joint space and the presence of osteophytes, subchondral cysts and/or sclerosis [19]. The tibiofemoral joints are assessed using antero-posterior (AP) and lateral views with plain-film radiography of weightbearing knees. The patellofemoral joint is assessed using a skyline view. Where more precise assessment of joint space width in specific condyles is desired, valgus and varus stress radiographs can also be used (**Figure 1.4**) [20].

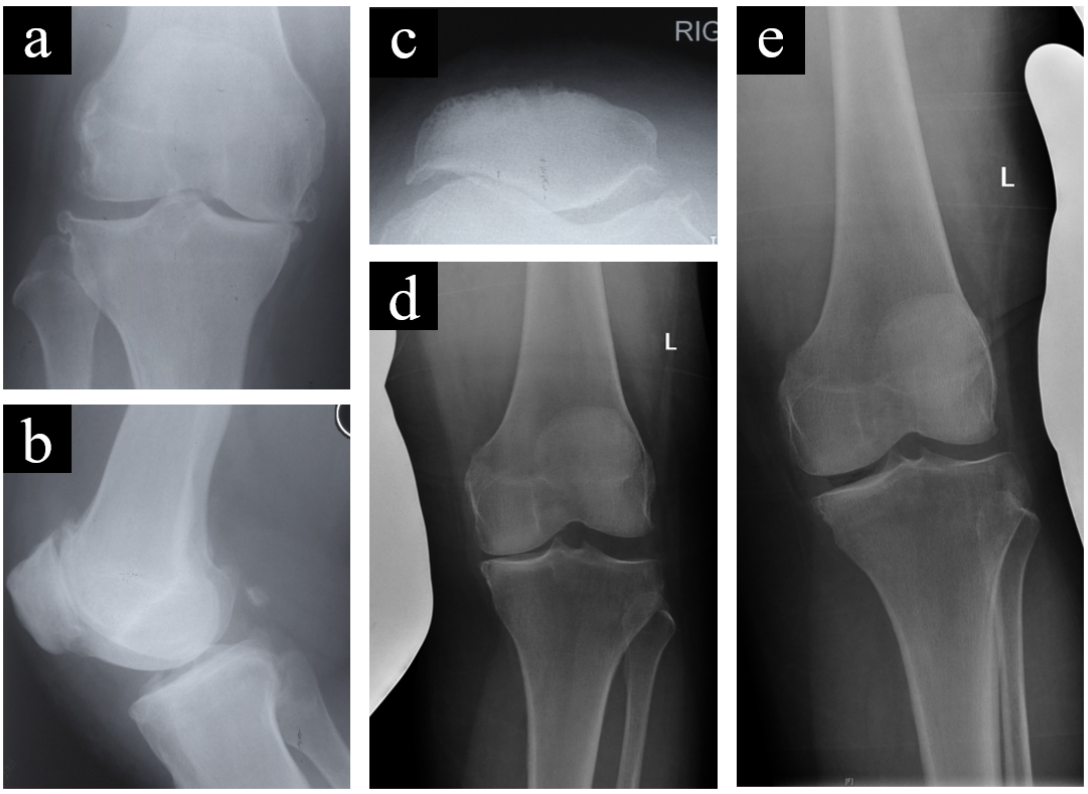


Figure 1.4*: Commonly used views in Plain Film Knee Radiography.* ***(a)*** *AP,* ***(b)*** *Lateral,* ***(c)*** *Skyline,* ***(d)*** *AP with varus stress,* ***(e)*** *AP with valgus stress.*

1.3.3 Clinical Management of Osteoarthritis and the Role of Knee Replacement

Obesity is associated with a doubling in knee osteoarthritis risk [21], and weight loss in obese patients aids osteoarthritis-related pain and disability [22]. Therefore, lifestyle modifications such as increased physical activity [23] and calorie deficits are recommended for conservative management of knee osteoarthritis. Muscle strength supports joint function, and therefore low-impact exercise is recommended [24]. Biomechanical aids such as braces, sleeves, and walking sticks are regularly used, and professional bodies endorse their use if recommended by a specialist. However, scientific evidence for their use is unclear [25], with the use of aids such as walking sticks having been shown to diminish pain and improve function [26], but also induce abnormal changes in gait which can worsen outcomes [27].

Pharmacologically, paracetamol and non-steroidal anti-inflammatory drugs are routinely prescribed for pain management, though side effects need to be carefully managed as the medications will likely be routinely taken. Intra-articular corticosteroid injections offer short-term pain relief and are routinely used, but consecutive injections have diminished pain relief and worsening side effects [28, 29].

Wedge osteotomy of the distal femur or proximal tibia, which involves resection of a wedge of bone to relieve pressure on one compartment of the knee, can be performed if osteoarthritis is secondary to bony malalignment, and can help reduce progression of knee osteoarthritis [30-33].

Arthroscopic lavage and debridement were commonly used to remove cartilage fragments and calcium crystals within the synovium and smoothen articular surfaces, with the aim to reduce synovitis. However, this procedure has become obsolete for this purpose, due to findings that it offers no added benefit over placebo surgery [34, 35].

Knee replacement is indicated for end-stage knee osteoarthritis which is broadly defined as full-thickness cartilage loss (resulting in bone-on-bone contact) between the femur and tibia. Clinical diagnosis of end-stage knee osteoarthritis is done using plain film radiography, often with a series of weight-bearing and stress radiographs (see **Figure 1.4**) to assess joint space narrowing and radiographic bone-on-bone contact.

1.4 Other indications for Knee Replacement

If not performed for osteoarthritis, knee replacement surgery is performed for inflammatory arthropathies, osteonecrosis, or trauma, where alternative medical and surgical management options are unviable or not beneficial.

1.4.1 Inflammatory Arthropathies

Inflammatory arthropathies are distinguished from osteoarthritis due to the involvement of inflammation and autoimmunity [36]. They include inflammatory connective tissue disorders such as rheumatoid arthritis and systemic lupus erythematosus, crystal arthritis such as gout and pseudogout, seronegative spondyloarthropathies such as ankylosing spondylitis, psoriatic arthritis, infectious arthritis, and reactive arthritis [37].

The majority of early knee replacement was performed for rheumatoid arthritis [38, 39]. The success of disease-modifying anti-rheumatic drugs in the 1980s reduced the progression of arthritis in most patients, greatly reducing the need for knee replacement.

However, in advanced disease, total knee replacement remains the most successful intervention that reduces knee pain and improves physical function in rheumatoid arthritis [40].

1.4.2 Osteonecrosis with Cartilage Destruction

Osteonecrosis of the knee, also known as avascular necrosis, refers to the ischemia-induced death of bone around the knee joint [41]. Its pathophysiology is not well

understood. It can be primary/spontaneous, secondary to a variety of pathologies, or rarely, post-arthroscopic. Primary osteonecrosis is classically described as a focal, superficial subchondral lesion, mainly affecting the medial femoral condyle [42]. Secondary and post-arthroscopic osteonecrosis often involves both medial and lateral condyles.

Osteonecrosis is initially managed pharmacologically, or with joint-preserving procedures such as arthroscopy, chondroplasty, or core decompression [43]. However, if osteonecrosis progresses to joint surface collapse, knee replacement is indicated [44].

1.4.3 Post-Traumatic Arthritis

Trauma involving knee anatomy can cause damage to cartilage [45], intra and extra articular deformities, as well as limb malalignment and soft tissue compromise [46]. Resultant necrosis of chondrocytes and/or abnormal loading patterns can result in knee arthritis [46]. Knee replacement is routinely used to preserve knee anatomy and function in knee trauma, and long-term outcomes are similar to knee replacement performed for other indications [47].

1.5 Arthritis, Isolated Medial Osteoarthritis, and Knee Replacement

1.5.1 Incidence

The pain and loss of function due to knee osteoarthritis limits lower extremity function, which is vital for ambulation and several other activities of daily living [48].

Latest analyses of Global Burden of Disease estimate that 22% of the world population have musculoskeletal conditions, of which high-income countries are most affected [49]. Furthermore, they are the biggest contributor to years lived with disability (YLD) worldwide, with 17% of YLDs linked to these conditions [49]. Symptomatic, radiographically confirmed osteoarthritis comprises 20% of the global prevalence of musculoskeletal disorders, and is the fastest growing musculoskeletal disorder, having increased by 114% from 1990 to 2019 [49].

The lifetime risk of knee osteoarthritis in high-income countries is 50%, with obese patients having double the risk of normal/underweight patients – lifetime risk 61% vs 30% [21]. These figures are estimated to grow rapidly in coming years with increasingly ageing [50] and obese [51] population.

Registry data from the United Kingdom shows that over 100 000 knee replacements have been performed annually since 2015 (until the Covid-19 pandemic) [52]. Due to the growing risk factors mentioned above, this is estimated to rise, with some projections estimating over 1 000 000 procedures by 2035 [53, 54].

As of 2019, approximately 1 in 10 knee replacements in the United Kingdom are unicondylar i.e. replacing the medial or lateral tibio-femoral joint [52]. However, candidacy for unicondylar knee replacement is estimated to be around 50% of all knee

replacement procedures [55], a figure supported by the improving outcomes with increased UKR usage up to 50% [56].

1.5.2 TKR vs UKR for Isolated Medial Osteoarthritis

UKR is indicated in severe, isolated medial unicondylar osteoarthritis [57]. However, TKR can also be performed for the same indication. The choice between the two procedures is the centre of much discussion.

UKR provides faster recovery, better function, lower cost, and fewer and less severe complications compared to TKR [58-60]. There is considerable heterogeneity in revision rates reported in literature across cohort and registry data. The annual revision rate for UKR is shown to be approximately 1%, which is double that of TKR [61-63]. However, single-centre studies from the 'designer' Oxford group [64] and other 'non-designer' groups in the Netherlands [65] and South Korea [66] have demonstrated that similar revision rates can be achieved for UKR and TKR.

This heterogeneity in results across registry and cohort study data is suggested in literature to arise from inconsistent selection criteria and varying use of implant designs across practices [67, 68], lower thresholds for revision of UKR compared to TKR [69], and varying UKR usage - analysis of data from Swedish, Nordic, and UK registries shows reduced revision rates if surgeons have a higher case load of UKR [56, 70, 71], stemming from higher usage (defined as the proportion of a surgeon's knee arthroplasty practice comprised by UKR) [56].

1.6 Implants Commonly used in Medial Unicompartmental Knee Replacement

The five most commonly used Unicondylar Knee Replacements in the United Kingdom are (in order of use): Oxford Cementless UKR (Zimmer Biomet UK Limited, Bridgend, UK), Physica ZUK UKR (LimaCorporate, Udine, Italy), Sigma HP UKR (DePuy Synthes, Warsaw, Indiana, USA), Persona UKR (Zimmer Biomet, Warsaw, Indiana, USA), and Oxford Twin Peg Cemented UKR (Zimmer Biomet UK Limited, Bridgend, UK). These constitute over 90% of all UKR implanted in the United Kingdom (**Figure 1.5**).

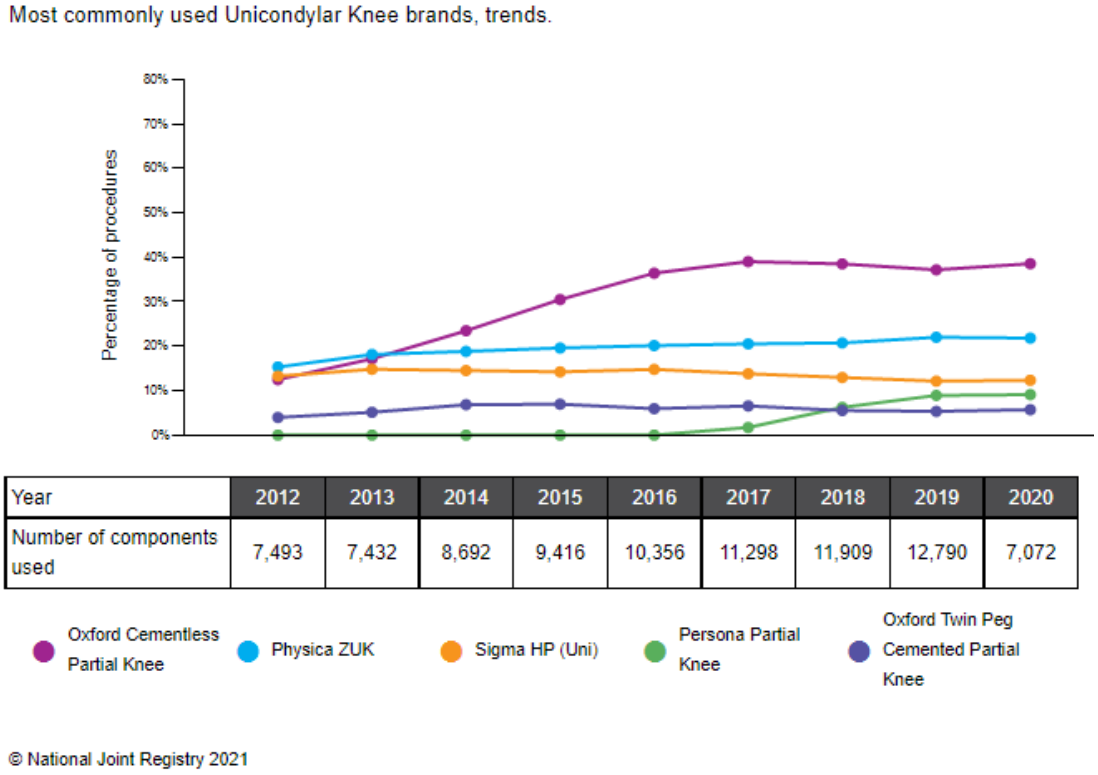


Figure 1.5: *Most commonly used Unicondylar Knee Implants between 2012 and 2020 as reported in the UK National Joint Registry. Figure from [52].*

All five implants consist of femoral and tibial components interfaced with a polyethylene bearing. The Cementless and Cemented Oxford UKR are mobile-bearing implants, while the rest have a bearing fixed to the tibial component tray.

Of the five, the Cementless Oxford UKR is the only cementless implant, and was developed in an attempt to reduce revisions due to aseptic loosening. Direct comparisons of revision rates between this implant and TKR have shown consistently similar or lower revision rates in cementless UKR in high-usage surgeons [72, 73].

1.7 The Oxford Unicompartmental Knee Replacement (UKR)

1.7.1 History of the Implant

The Oxford UKR was developed by Mr John Goodfellow and Professor John O'Connor in 1976. It was designed to explore a unicondylar implant design with a spherically convex femoral component, flat tibial component, and freely mobile bearing which is spherically concave above and flat below, interfacing congruously with both metal components [74].

There have been seven major design iterations of the Oxford Knee UKR, summarised in **Figure 1.6**.

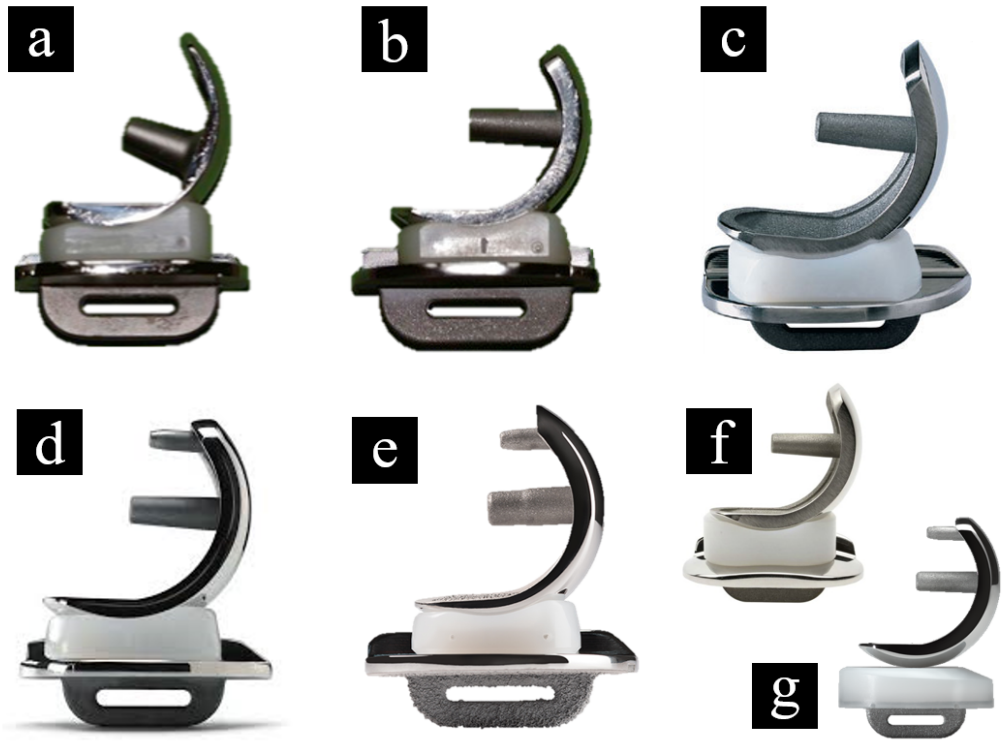


Figure 1.6: *All iterations of the Oxford UKR to date.* ***(a)*** *Phase 1,* ***(b)*** *Phase 2,* ***(c)*** *Phase 3,* ***(d)*** *Twin-Peg,* ***(e)*** *Cementless,* ***(f)*** *Lateral Domed,* ***(g)*** *Lateral Fixed. Images adapted from [75] and [76].*

The Phase 1 implant **(Figure 1.6a)** was developed to be a bi-compartmental implant [74]. There were difficulties with femoral component positioning and matching the flexion-extension gap, resulting in inconsistent ligament tension through knee flexion [75]. It was also determined that the majority of end-stage knee osteoarthritis where the ACL was intact was anteromedial [77, 78].

The Phase 2 implant **(Figure 1.6b)** introduced changes to enable better positioning of the femoral component, and better matching of the flexion-extension gap. It introduced a flat posterior and concave inferior facet to the non-articulating surfaces of the femoral component, along with the use of a new femoral milling instrument to remove bone more precisely, allowing for better matching of flexion-extension gaps [75]. The implant was designed for unicompartmental use. Cohort studies by the designer group [79] and independent groups [80] showed that long term implant survival could be similar to TKR.

The Phase 3 implant **(Figure 1.6c)** introduced the use of new instrumentation and technique, which allowed for a minimally invasive medial parapatellar approach without patellar eversion or dislocation [81]. The Phase 3 had superior functional and recovery times compared to the Phase 2 [82].

The Twin-Peg **(Figure 1.6d)** and Cementless **(Figure 1.6e)** implants introduced a two-peg femoral component for better fixation. The cementless implant additionally had porous sprayed titanium and hydroxyapatite coating on some aspects of its non-articular surfaces. Later versions of the cementless Oxford also had a microporous coat added to non-porous surfaces including the tibial wall. The Cementless Oxford UKR was introduced to improve fixation, but was under careful review as cementless TKR were underperforming compared to cemented TKR in literature [83]. The two-peg cemented

component had improved survival over the Phase 3 ‘single-peg’ [84, 85]. The outcomes of the Cementless Oxford UKR will be discussed in **Section 1.7.2**.

The Lateral Domed **(Figure 1.6f)** and Fixed Bearing **(Figure 1.6g)** implants were designed to address specific needs of lateral compartment arthroplasty, and have been included here for completeness. However, this thesis will focus on medial arthroplasty and therefore will not explore these implants in more detail.

1.7.2 The Cementless Oxford UKR Design

The Cementless Oxford UKR consists of three components: the femoral component (**Figure 1.7a**), the bearing (**Figure 1.7b**), and the tibial component (**Figure 1.7c**). The femur-bearing interface is perfectly spherical and allows for rotation, while the tibia-bearing interface is planar and allows for translation. The femoral and tibial components are produced in various sizes (Femur: X-Small, Small, Medium, Large, X-Large, Tibia: AA (smallest), A, B, C, D, E, F (largest) [86], to allow surgeons to personalise the implant to joint size. The bearing is produced in different thicknesses (3-9 mm) to allow for varying gap width between the femur and tibia whilst maintaining ligament balance [75, 86].



Figure 1.7: *Components of the Cementless Oxford UKR.* ***(a)*** *Femoral Component,* ***(b)*** *Bearing,* ***(c)*** *Tibial Component. Images adapted from [76, 86].*

The femoral and tibial components are machined from a cobalt-chromium-molybdenum alloy which is cast and finished with machining and polishing [75]. Interfaces with the bearing are polished to reduce friction and wear. Interfaces with bone have a porous titanium surface applied using plasma spray technique with an added layer of hydroxyapatite, to enable bone ingrowth into porous surfaces during remodelling and improve fixation [75, 87]. The cementless components are impacted until seated [86]. Therefore, this porous coat is applied to an inset region of the components to ensure that the added thickness does not interfere with implant seating.

Prior to bone remodelling and ingrowth, fixation of the femoral component is achieved using two pegs: a central main peg which extends to the centre of the sphere, and an accessory anterior peg to improve primary stability. The pegs are inserted with an interference fit, with the hole sizes being marginally smaller than the peg size, ensuring a compressive fit [75].

In cementless implants, fixation prior to remodelling and fixation post-remodelling have different characteristics, and therefore should be described separately. In this thesis, the term primary fixation refers to the fixation of the component prior to bone remodelling,

while secondary fixation refers to the fixation of the component post-remodelling, where bone has grown into porous surfaces.

Primary (pre-remodelling) fixation of the tibial component is achieved using its keel, a vertical protrusion at the bottom of the tibial floor. It is inserted into a slot made in the tibia with an interference fit [86]. The keel is of constant width, and has a window in the middle, which is a remnant from the cemented keel for cement in-fill. The tibial wall has hydroxyapatite applied, with later versions of the implant incorporating a thin microporous coat of titanium to further aid bone growth and fixation [75] – such ingrowth achieves secondary (post-remodelling) fixation.

The bearing is fully mobile, restricted laterally by the tibial component wall. Its motion is dependent on the relative position of the distal femur to the proximal tibia. As loads across the knee are predominantly compressive, there is minimal risk of bearing dislocation [75]. Bearing mobility allows the bearing to be fully congruent with both the femoral and tibial components across the full range of motion of the knee. In contrast, non-congruent components will only interface a portion of the bearing at any one time. In addition, the femoral component is spherical, and the superior surface of the bearing which interfaces with the femoral component is fully congruent to this spherical surface. This ensures that contact area between the bearing and femoral component is constant across full range of motion. In contrast, femoral components with poly-radial designs would have reduced contact area in flexion than in extension. These two features ensure that, through the full range of motion, the contact area between the components is maximised and that loads are transmitted evenly across the femur-bearing and tibia-bearing interfaces [75]. This reduces bearing linear wear rates to below those of non-

congruent designs reported in literature [88]. Excess linear wear can predispose bearing dislocation and bearing fracture, which are sources of revision [89].

1.7.3 Specific indications for Oxford Medial UKR

Oxford Medial UKR is indicated in end-stage anteromedial osteoarthritis, which requires bone-on-bone medial osteoarthritis, a functional ACL and MCL, and full cartilage thickness in the lateral compartment [75]. These remain the key criteria for Oxford UKR use today [64].

In 1989, contraindications for UKR surgery were developed based on fixed bearing implants, and advised that UKR should be restricted by age (over 60), weight (under 82kg), profession (to exclude heavy labourers), and full-thickness patellofemoral cartilage loss [90]. However, a concurrent study suggested that these restrictions were not applicable to mobile bearing UKR [91]. Later studies validated this suggestion and found that age, weight, profession, and patellofemoral cartilage loss are not contraindications for the use of mobile bearing implants for UKR [92-95].

1.7.4 Outcomes following Cementless Oxford UKR

The Cementless Oxford UKR was introduced in 2004 and has excellent mid-to-long term clinical results [96]. The revision rate of Cementless UKR reported in national registries is about 25-50% less than that of the Cemented UKR [97], though the reasons for these are unclear. This difference has been attributed mainly to a reduction in revisions for aseptic loosening and pain. Other rarer reasons for revision include the development of

osteoarthritis in the lateral component, bearing wear / dislocation, unexplained pain, and instability [98, 99]. In the short-term after surgery, medical complication rates with UKR are lower than with TKR [73], and cementless UKR are lower than cemented UKR [100].

There has been no detailed mid-to-long term assessment of patient-reported outcomes on pain and function performed on the Cementless Oxford UKR. Randomised control trials comparing the Cementless Oxford UKR with the Phase 3 Cemented Oxford UKR found no notable difference in pain and function at 5 years, but had small sample sizes and were therefore underpowered [98, 99]. Addressing this will be one of the objectives of this thesis.

Peri-prosthetic fractures are a rare but serious complication following Cementless Oxford UKR. Reports of such fractures [101] characterise them as peri-prosthetic tibial fractures that occur in the early post-operative period. There is approximately 0.2% incidence of peri-prosthetic fractures resulting in revision reported in most studies [96, 102-104], and the true incidence of such fracture (including those managed without revision) is unknown. However, a high seven-fold odds of such fractures are reported in Size 'AA' and 'A' (i.e., very small) tibias compared to larger sizes [105]. The use of a cemented tibial component is now recommended if a patient is deemed to be at high risk of peri-prosthetic tibial fractures i.e., the Cementless Oxford UKR tibial component is contra-indicated in very small tibias. Fractures are also associated with sagittal keel cuts that are excessively extended posteriorly [106]. These risk factors are explored in **Chapter 7.**

Subsidence of the cementless tibial component has been reported in a small proportion of procedures [107], where the tibial component subsides posteriorly and laterally, and is related to knee stiffness, flexion deformity, and pain. However, the underlying cause of such subsidence is not well understood. This is explored in more detail in **Chapter 8**.

1.8 Thesis Objectives

This thesis aims to perform a detailed study of patient-reported outcomes of the Cementless Oxford UKR, and to address its high fracture incidence reported particularly in very small tibias.

To achieve this, this thesis sets out to complete three objectives:

1. Perform a detailed assessment and comparison of patient-reported outcomes of the Cementless and Cemented Oxford UKR, relating findings to fixation and remodelling.
2. Propose design changes to address fracture risk in the Cementless Oxford UKR tibial component. Two degrees of design changes will be explored:
    a. an easily deployable redesign of the tibial component keel, and
    b. a fundamental redesign of tibial fixation to address limitations of a keel design.
3. Develop appropriate mechanical tests to evaluate fracture and primary fixation in a very small tibia, and apply tests to validate existing keel designs and explore proposed design changes.

1.9 Structure of Thesis

Chapter 1 introduces the role of Unicompartmental Knee Replacement in elective orthopaedic care, and the use of Cementless Oxford UKR.

In **Chapter 2**, a detailed analysis of 5-year patient-reported outcomes between Cementless and Phase 3 Cemented Oxford UKR will be performed. This study will assess metrics relating to varying facets of pain, function, wellness, activity, co-morbidity, and neuropathy. The key finding is that 42% more patients with the Cementless Oxford UKR report having no pain at all compared to cemented. It is likely that this benefit arises from differences in fixation between cemented and cementless UKR. However, early studies do not show a relationship between radiolucency and pain. Therefore, in **Chapter 3**, a detailed assessment of fixation is performed, and the relationship between radiolucency and pain was explored. Extending radiographic analyses beyond the bone-implant interface, **Chapter 4** proposes a new technique for assessing bone density using plain film radiographs, to assess if bone remodelling and associated density changes around the keel are related to patient-reported outcomes.

The remainder of the thesis explores tibial component fracture, which is a serious complication of the Cementless Oxford UKR. **Chapter 5** and **Chapter 6** explore changes to the existing keel design to reduce the risk of fracture without compromising primary fixation. This was performed using *in-vitro* push-in and pull-out tests, which were used as metrics related to risk of fracture and primary fixation respectively. Two easily implementable changes to the current keel design are proposed, and a more profound change to the tibial component, which addresses fundamental limitations of a keel structure, is proposed. **Chapter 7** and **Chapter 8** propose and implement tests which evaluate fracture and fixation of tibial components in very small tibias, where load-to-

fracture is used to assess fracture risk, and anterior lift-off is used to assess primary fixation. These methods are then used to assess the effect of key mechanical properties of the existing keel design on fracture and fixation, and the performance of proposed new designs compared to existing designs.

Chapter 9 summarises the key findings and design changes proposed to the existing tibial component, and explores the next steps needed to bring these design changes to clinical use.

2 Mid-Term Patient Reported Outcomes of Cementless and Cemented Oxford UKR

2.1 Motivation for Chapter

There is extensive reporting of outcomes following the Cementless Oxford UKR in literature, analysing data from patient cohorts or national registry data [56, 59, 73, 85, 100, 108-113]. A 2017 systematic review summarised all non-registry studies [72]. These studies assessed clinical outcomes and selected Patient-Reported Outcomes (PROMs), such as the Oxford Knee Score (OKS), Western Ontario and McMaster Osteoarthritis Index (WOMAC), American Knee Society Score (AKSS), Hospital for Special Surgery Score (HSS), and Tegner Activity Score (TAS). Registry studies generally include a subset of these scores [52, 97, 109, 111, 114-116].

However, several outcomes remain unknown. There is limited reporting of detailed pain-related outcomes in Cementless Oxford UKR, and do not explore the origin of the pain. The work performed in this chapter hopes to contribute evidence towards these unmet areas.

2.2 Introduction and Study Aims

The two main options for anteromedial knee replacement are total (TKR) and unicompartmental knee replacement (UKR) (**Section 1.5.2**). UKR provides faster recovery, better function, lower cost, and fewer and less severe complications [58-60] but has higher revision rates in national registries [117]. Aseptic loosening is a common reason for such revisions [100, 111]. In an attempt to address this, the Cementless Oxford UKR was developed.

The Cementless medial, mobile bearing Oxford UKR is identical to the Phase 3 cemented version except for its fixation surfaces. The main differences are that the cementless has hydroxyapatite-coated porous titanium surfaces for bone attachment, a parallel-sided rather than a tapered femoral peg, and an additional anterior peg to improve primary stability (**Figure 2.1**). The later twin-peg cemented Oxford UKR incorporated some of these design elements but is not within the scope of this study. These implants are referred to as Cementless UKR and Cemented UKR for the remainder of this Chapter.

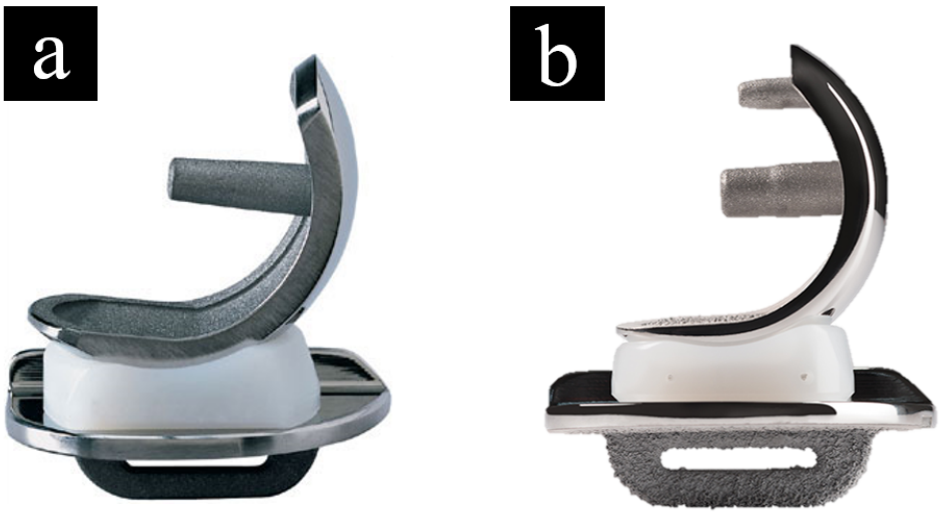


Figure 2.1: *Implants assessed in this study.* ***(a)*** *Cemented Phase 3 Oxford UKR.* ***(b)*** *Cementless Oxford UKR. Photos from Zimmer Biomet.*

The surgical technique and instrumentation for both implants are identical, except for the final stages of fixation; the slot in the tibia for the implant keel is narrower in the Cementless UKR so as to achieve a press fit, and wider with a cement mantle in the Cemented UKR. The cementless components are impacted until fully seated and achieve an interference fit [118, 119]. The overall time of procedure varies with surgeon and patient factors, but Cementless UKR is 20% quicker on average [120], which can be attributed to avoiding cementing the implants.

The revision rate of Cementless UKR reported in national registries is about half that of equivalent Cemented UKR [97]. This may partly be due to experienced surgeons disproportionately using the Cementless UKR. These surgeons have lower revision rates because they tend to do larger numbers, have better surgical techniques, and adhere to recommended indications [56]. Nonetheless, a matched study based on 10-year national registry data correcting for confounding factors, such as surgeon caseload, has shown that the revision rate of Cementless UKR is still 25% less than that of the Cemented UKR [100]. This difference was attributed mainly to a halving of revision for aseptic loosening and pain.

Two small, randomised studies, done as part of the early assessment of the Cementless UKR, showed that the incidence of radiolucent lines was much lower with cementless compared to cemented components, suggesting that cementless fixation was better [98, 99]. This likely explains the decrease in revisions for aseptic loosening. The decrease in revision for pain is less well understood. In these randomised trials, there was some evidence of improved outcome scores with the cementless components, but the differences were not statistically significant. This may be because these studies, designed

for radiographic outcome measures, were statistically under-powered to assess patient-reported outcome scores.

The aim of this study was to compare clinical outcomes for Cementless and Cemented medial UKR with an appropriately powered study. The Cementless and Phase 3 cemented Oxford UKR, which have near-identical cemented and cementless components, were studied.

2.3 Design of Study

A longitudinal cohort study comparing the 5-year outcomes of Cementless and Phase 3 Cemented medial Oxford UKR implanted between 2006 and 2012 by four high-volume knee surgeons [108] was performed. During this period, the surgeons transitioned from implanting the cemented to the cementless components. The indications and contraindications [121, 122], pre-operative care, and post-operative care, were identical for both procedures. Surgical technique was identical [86], with the exception of method of fixation. Hybrid implants, using both cemented and cementless components, were excluded from the study. Patients were reviewed by independent research physiotherapists pre-operatively, and 5 years post-operatively. Patients who could not be reviewed in clinic were contacted by post or telephone.

Information about post-operative revisions, re-operations, and complications occurring within the 5-year follow-up period were obtained from patients and their records. Revision was defined as the removal, exchange, or addition of any component [113]. This includes conversions to TKR, bearing exchange for dislocation during debridement and washout, and the addition of a lateral UKR for progression of osteoarthritis to the lateral compartment. Re-operation was defined as any knee-related procedure where the patient required anaesthesia, including manipulation under anaesthesia and diagnostic/therapeutic arthroscopies. Any complications relating to the knee, or the operation, were recorded.

Patients were assessed using the following outcome measures: Oxford Knee Score (OKS), American Knee Society Score (AKSS), EQ-5D-5L, Intermittent and Constant Osteoarthritis Pain (ICOAP), painDETECT, as well as Charnley classification.

The OKS is a knee-specific Patient Reported Outcome Measures (PROM) designed to assess the outcome of knee replacement [123]. The OKS includes two components encompassing pain (Questions 1,4,5,8,9) and function (Questions 2,3,6,7,10,11,12) [124]. The 12 questions generate a total score between 0 and 48, where higher is better. Scores can be categorised according to Kalairajah classification: 'Excellent' (42-48), 'Good' (34-41), 'Fair' (27-33), and 'Poor' (0-26) [125-127].

The AKSS is a knee-specific score designed to assess the outcome of knee replacement. It includes patient-response questions and objective measurements. It consists of an objective (AKSS-O), and a functional (AKSS-F) component, each scoring between 0 and 100, where higher is better [128]. A subset of the AKSS-O addresses pain, scoring between 0 and 50. The AKSS was created to assess TKR (at a time when optimal alignment was considered to be neutral) and points were deducted for varus and valgus mal-alignment. However, these deductions are not appropriate for the Oxford UKR, where the aim is to restore pre-arthritic alignment of the knee, which is commonly varus [129]. Hence, the measure used in this study excludes these deductions, and is termed 'AKSS-UKR variant'.

The EQ-5D-5L is a generic health status PROM. It has five domains (Mobility, Self-Care, Usual Activities, Pain/Discomfort, and Anxiety/Depression), each scored from 0 to 5, where lower is better [130]. An overall index score is calculated as a weighted average of the scores from the five domains scored from -0.285 to 1, using a reference UK population of 996 healthy individuals [131]. In addition, there is a Visual Analogue Scale (VAS), scored from 0 to 100, where higher is better.

The knee-specific ICOAP (Intermittent and Constant Osteoarthritis Pain) score quantifies the magnitude and nature of knee pain [6]. ICOAP 'A' assesses constant pain, and

ICOAP ‘B’ assesses intermittent pain i.e., pain that “comes and goes”. ICOAP ‘A’ is the total score from five questions, and ICOAP ‘B’ from six questions. Each question is equally weighted, and scores pain in different contexts from 0 (‘no pain at all’) to 4 (‘extreme’). ICOAP ‘Total’ is the sum of both ‘A’ and ‘B’ scores. ICOAP ‘A’, ‘B’, and ‘Total’ are scaled and scored between 0-100, with a higher score indicating worse pain.

The painDETECT instrument includes three visual analogue scales (PD-VAS) assessing ‘Now’, ‘Average’, and ‘Strongest’ pain experienced over the preceding four weeks, and a separate ‘PD-Q’ score to assess likelihood of neuropathy in pain. The VAS are scored between 0-10 (increasing with magnitude of pain), and PD-Q is between 0-38, where PD-Q≤12 is negative, 13≤PD-Q≤18 is unclear, and PD-Q≥19 is positive for a neuropathic pain component [7].

The Tegner Activity Score (TAS) is a single score of the level of activity a patient engages in, from 0 to 10. A score of 0 represents disability or sick leave due to ‘knee problems’ and 10 represents participation in sports at a national level or above [132].

Patients were also classified into Charnley classification [10]: a 3-point classification of disease comorbidity – ‘A’: single knee affected, ‘B’: both knees affected, and ‘C’: multiple arthritis or medical infirmity.

545 knees (267 cemented, 278 cementless) in 441 patients were consented and recruited to this study. These knees were assessed for revisions, re-operations, and complications. Four knees (0.7%) were lost to follow-up, for which outcomes are not known; however, they were not recorded as revisions in the UK National Joint Registry. At 5 years, an additional 14 knees could not be reviewed due to death from unrelated reasons (n=6) or serious illness (n=8). During the 5 years, three UKR had been converted to TKR. The

final Cemented and Cementless UKR cohorts that were assessed clinically at 5 years consisted of 524 knees (262 cemented, 262 cementless). Although these knees were all assessed with the primary outcome measure, the OKS, at 5 years, all scores were not available from all knees at all time points.

The change in implantation of Cemented UKRs to Cementless UKRs was done progressively across the middle of the study period, with the cemented generally implanted before the cementless. Differences between cohorts may hence be affected by other factors that progressively changed across the study period, such as improvements to surgical technique. To assess the likelihood of this occurrence, both cemented and cementless cohorts were split into 'early' and 'late' halves. If differences are found between the 'early-cemented' and 'late-cemented', or 'early-cementless' and 'late-cementless' groups, then the differences are likely to be due to confounding factors that change with time. In contrast, if differences are found between the 'late-cemented' and 'early-cementless' groups, which were implanted at a similar time, then the difference are likely to be due to fixation.

All data is classified by knee. 98 patients consented to the study of both their knees (196 knees), of which 38 patients (76 knees) had one cemented and one cementless UKR. In these bilateral cases, each knee was assessed independently. Continuous values were tested using the unpaired Student *t*-test for parametric (Shapiro-Wilk $p>0.05$), and the Mann-Whitney U-test for non-parametric (Shapiro-Wilk $p<0.05$) distributions. Discrete categories were assessed with the chi-square test or Fisher's exact test, as appropriate. Statistical significance is defined by p-values of <0.05 for all tests. Data was analysed and visualised using GraphPad Prism (GraphPad Software, San Diego, California, USA) and Excel (Microsoft, Redmond, Washington, USA).

A power calculation based on OKS data was performed. Data from a randomised controlled trial of cementless versus cemented UKRs provided baseline OKS data: at one year the cemented arm had OKS of 39.0 (SD 9.2) and the cementless arm had OKS 41.7 (SD 5.3) [133]. With a standardised difference 0.3, a power of 0.9, and a significance level of 0.05, a minimum of 500 patients (250 cementless, 250 cemented) would be required for this study (following Altman's Nomogram [134]).

2.4 Pre-Operative Results

Pre-operatively, there was no statistically significant difference between cemented and cementless groups in age, gender, height, weight, and Body Mass Index (BMI) (**Table 2.1**). There was also no significant difference in pre-operative OKS and AKSS.

Table 2.1: *Pre-operative characteristics of cemented and cementless cohorts.*

	Cemented (n=267)		**Cementless (n=278)**		
	No of values	Mean (SD)	No of values	Mean (SD)	p value
Age (years)	267	65.6 (9.8)	278	65.5 (11.7)	0.935[1]
Height (cm)		169.0 (10.3)		171.0 (9.7)	0.118[1]
Weight (kg)		85.4 (16.9)		85.8 (15.5)	0.787[1]
BMI		29.8 (5.2)		29.43 (4.3)	0.379[1]
Sex		57.7% male 42.3% female		62.7% male 37.1% female	0.209[2]
OKS	175	26.1 (9.0)	191	26.4 (8.3)	0.871[1]
AKSS-F[3]	165	71.3 (19.2)	178	71.4 (16.1)	0.564[1]
AKSS-O[3]	165	45.5 (21.9)	178	44.9 (24.0)	0.800[1]

All distributions were determined to be non-parametric (Shapiro-Wilk $p<0.05$).
[1]Mann-Whitley U Test, [2]Chi-Square Test. [3]AKSS-UKA Variant used.

2.5 Post-Operative Clinical Outcomes

There were 2 revisions in the cemented cohort (1 insertion of a new bearing for bearing dislocation and 1 conversion to TKR for lateral compartment arthritis) and 2 revisions in the cementless cohort (2 conversions to TKR for lateral compartment arthritis) (**Table 2.2**). The knee with revision for bearing insertion remained a UKR and was included in further analysis, while the knees with revisions to TKR were excluded from further analysis. The 5-year survival was 99.3% in both cemented and cementless cohorts.

Table 2.2: *Post-operative revision, re-operation, and complication rates.*

		Cemented (n=267)		**Cementless (n=278)**		**p-value**[1]
		Total	% of cohort	Total	% of cohort	
Revision Surgeries	Conversion to TKR	1	0.37%	2	0.72%	0.59
	Bearing insertion	1	0.37%	0	0%	0.31
	Subtotal	**2**	**0.75%**	**2**	**0.72%**	0.97
Re-operations	Arthroscopy	3	1.12%	2	0.72%	0.62
	Washout	1	0.37%	1	0.36%	0.98
	Manipulation Under Anaesthetic	0	0%	1	0.36%	0.32
	Subtotal	**4**	**1.50%**	**4**	**1.44%**	0.95
Complications	Heart attack	1	0.37%	3	1.08%	0.34
	PE	1	0.37%	2	0.72%	0.59
	DVT	0	0%	2	0.72%	0.17
	Stroke	0	0%	2	0.72%	0.17
	Transfusion	1	0.37%	0	0%	0.31
	Superficial wound infection	9	3.37%	3	1.08%	0.07
	Deep infection	0	0%	1	0.36%	0.33
	Chest infection	0	0%	0	0%	>0.99
	Subtotal	**12**	**4.49%**	**13**	**4.68%**	**0.92**
	Total	**18**	**6.74%**	**19**	**6.83%**	**0.97**

Incidence of revision surgeries, re-operations and post-operative complications within the cemented and cementless cohorts.
[1]Chi-square tests were used in comparing the incidence between cohorts.

There were 4 (1.4%) non-revision re-operations in both cohorts, consisting of arthroscopies, washouts, and manipulation-under-anaesthetic (**Table 2.2**). There were 12 recorded medical complications in the cemented cohort and 13 in the cementless cohort. No patients died for reasons relating to their knee replacement.

2.6 Post-Operative Patient-Reported Outcomes (PROMs)

2.6.1 General PROMs

OKS was significantly better in the cementless cohort than cemented (43.3 vs 41.2, p=0.008), and this stemmed mainly from better pain scores (18.2 vs 17.0, p<0.0001) rather than function scores (25.1 vs 24.2, p=0.01) (**Table 2.3, Figure 2.2**). The cementless cohort had significantly more 'Excellent' outcomes than the cemented cohort (75.1% vs 64.9%, p=0.01), and less than half the number of 'Poor' (2.67% vs 6.49%) or 'Fair' outcomes (5.34% vs 10.3%), as per Kalairajah classification (**Figure 2.3**).

AKSS-O was significantly better for the cementless cohort (93.5 vs 90.4, p=0.049). The pain subscale which contributes to the AKSS-O was also significantly better (46.2 vs 43.1, p=0.0046), whereas there was no significant difference in the non-pain related part of the AKSS-O (47.4 vs 47.3, p=0.98) (**Table 2.3, Figure 2.2**). AKSS-F was not significantly different (p>0.05).

Table 2.3: *5-year response rates and responses for Oxford Knee Score and American Knee Society Score.*

		Cemented		Cemented		
		No of values	Mean (SD)	No of values	Mean (SD)	p-value[1]
Oxford Knee Score (OKS)	**Total Score**	262	41.2 (7.9)	262	43.3 (5.9)	**0.008**
	of which Pain		17.0 (3.8)		18.2 (2.7)	**<0.0001**
	of which Function		24.2 (4.5)		25.1 (3.6)	**0.010**
American Knee Society Score (AKSS)[2]	**Objective Knee Score (AKSS-O)**	224	90.4 (13.5)	195	93.5 (9.6)	**0.049**
	of which Pain		43.1 (11.9)		46.2 (8.2)	**0.005**
	of which non-pain		47.4 (12.3)		47.3 (10.4)	0.98
	Functional Knee Score (AKSS-F)	245	84.4 (16.6)	209	85.2 (16.9)	0.45

All distributions were determined to be non-parametric (Shapiro-Wilk p<0.05).
[1]Mann-Whitley U Test used in comparing scores between cohorts.
[2]AKSS-UKR variant used.

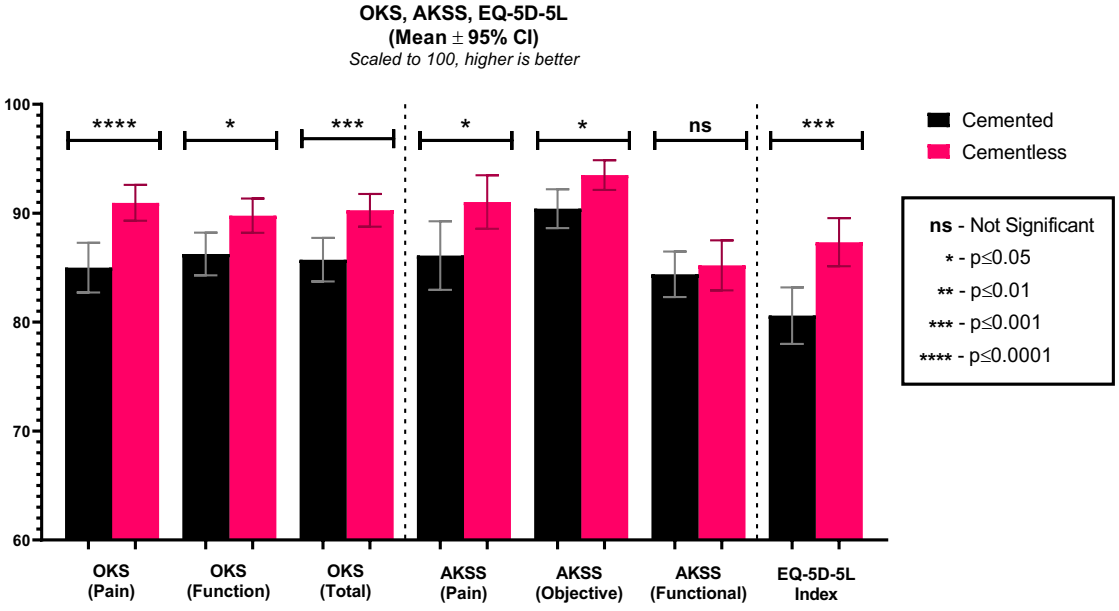


Figure 2.2: *5-year Oxford Knee Score, American Knee Society Score and EQ-5D Index, scaled to 100, for cemented and cementless cohorts.*

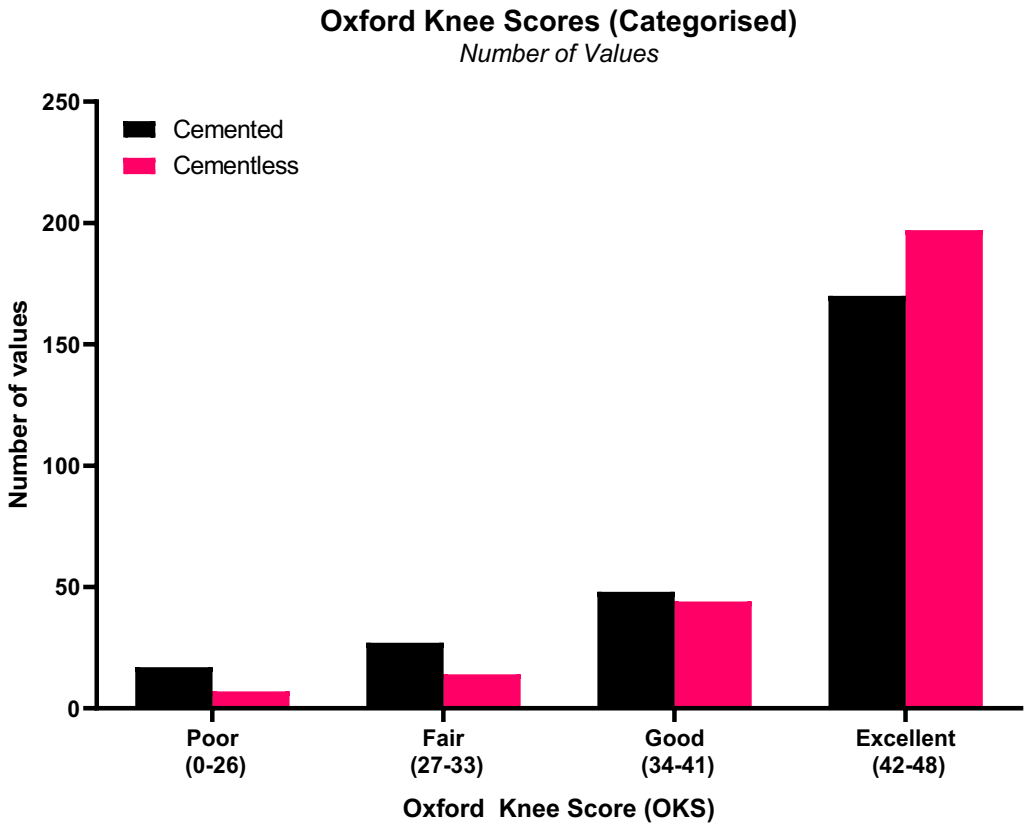


Figure 2.3: *5-year OKS for cemented and cementless cohorts, categorised into Kalairajah categories*

The cementless cohort had a significantly better EQ-5D-5L Index (0.87 vs 0.81, p=0.0001) (**Figure 2.2**). This difference stems primarily from a significantly better mean score in the 'Pain/Discomfort' domain (0.49 vs 0.79, p=0.0001, lower is better). There were also significantly better scores in the 'Usual Activities' (0.55 vs 0.42, p=0.017) and 'Mobility' (0.57 vs 0.43, p=0.025) domains, but the differences were smaller. There were no significant differences in the 'Self-Care' and 'Anxiety/Depression' domains. (**Figure 2.4**). There was no significant difference in the VAS (p=0.90).

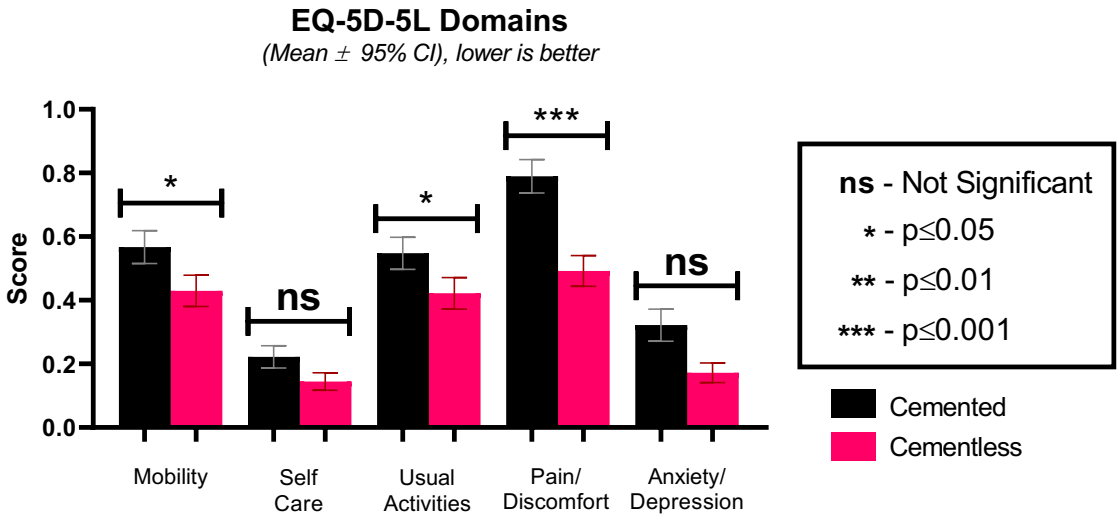


Figure 2.4: *5-year EQ-5D-5L domain scores for cemented and cementless cohorts.*

Both cemented and cementless cohorts reported a near identical TAS of 3 (p=0.642) (**Figure 2.5**). 1 in 10 patients from both cohorts had a TAS exceeding 5 (cemented 11%, cementless 12%).

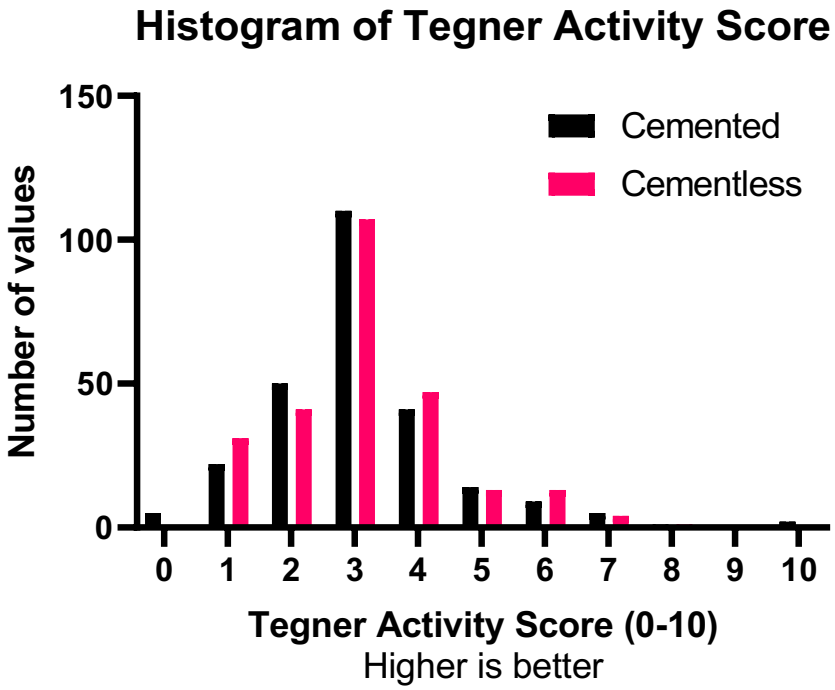


Figure 2.5: *Histogram of Tegner Activity Score in cemented and cementless cohorts.*

2.6.2 Pain-Specific PROMs

Both cemented and cementless cohorts reported low pain in nearly all measures. The cementless cohort demonstrates relatively lower pain in all pain measures assessed in this study, albeit to different magnitudes. Cementless reported lower in ICOAP Total (5.4 vs 10.8, p<0.0001, lower is better) scores, stemming from lower ICOAP 'A' Constant and ICOAP 'B' Intermittent pain scores (2.98 vs 7.60, p=0.0014 and 7.58 vs 14.0, p<0.0001 respectively). For PainDETECT Visual Analogue Scales (PDVAS), cementless reported lower PDVAS Average and PDVAS Strong but similar PDVAS Now pain (1.00 vs 1.50 p=0.0011, 1.62 vs 2.34 p=0.0022, 0.51 vs 0.74 p=0.1219). OKS Pain and AKSS Pain were lower in the cementless cohort as well (18.2 vs 17 p<0.0001, 46.2 vs 43.1 p=0.0046, higher is better) (**Figure 2.6**).

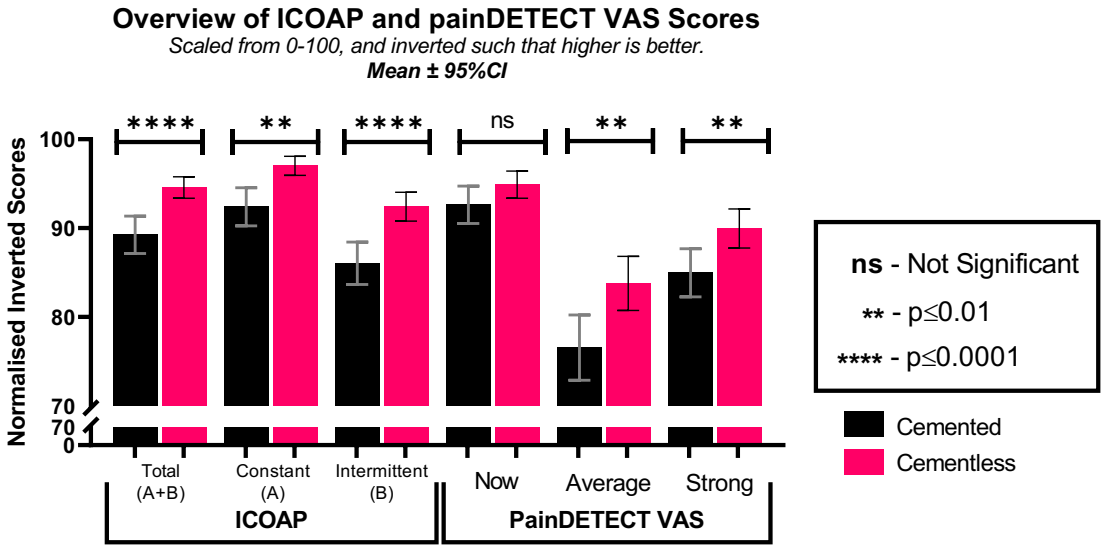


Figure 2.6: *Mean ± 95% CI scores for ICOAP and PainDETECT for cemented and cementless cohorts. All scores scaled from 0-100 and inverted where necessary such that higher is better (ICOAP A and B inverted, painDETECT multiplied by a factor of 10 from 0-10 to 0-100 and inverted).*

ICOAP Total scores were categorised into increasing magnitudes of pain from None at all to Extreme. ICOAP Total = 0 indicates the patient reported 'none at all' in all questions. The cementless cohort had a greater proportion of scores in this 'no pain at all' category and the cemented had a greater proportion in all other categories (Chi-Square, p=0.0006). 42% more of the cementless cohort cemented cohort reported 'none at all' (61% of cementless vs 43% of cemented, p<0.0001). 7 (2.9%) of the cemented cohort had Severe or Extreme pain, whereas none of the cementless did (**Figure 2.7**).

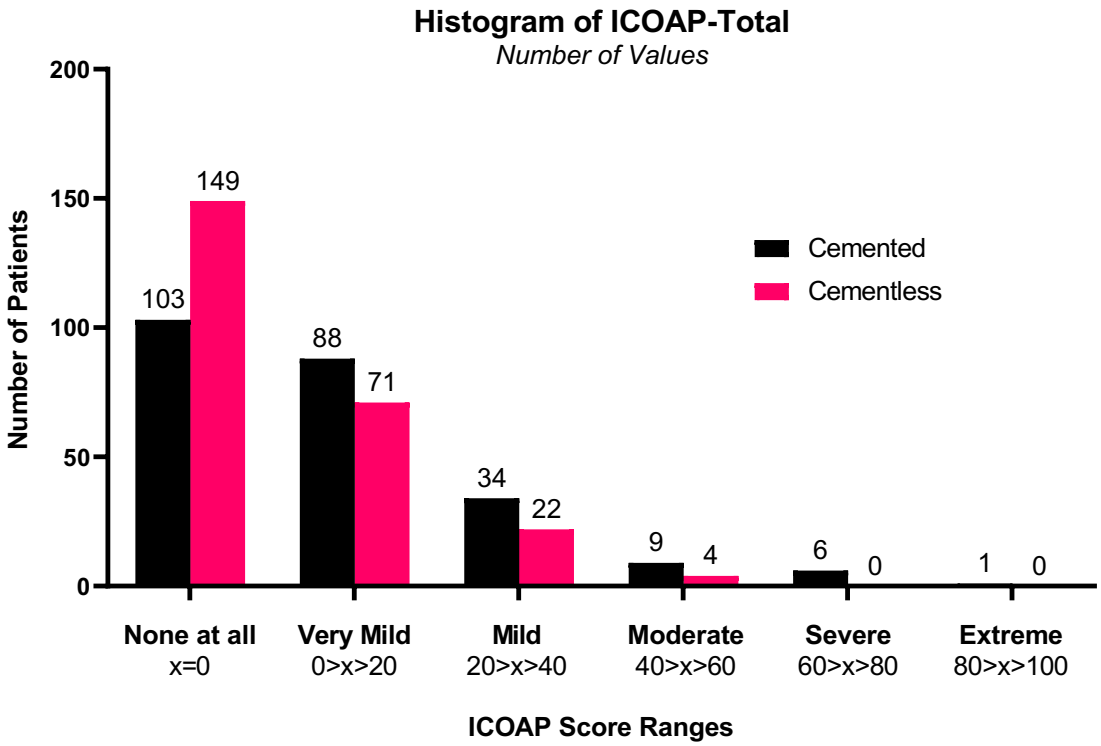


Figure 2.7: *Histogram of 5-year ICOAP (Total) score, for cemented and cementless cohorts. 2-sided Chi-Square Test across all categories had a significant difference to p=0.0006. 2-sided Chi-Square Test between 'x=0' and other categories had a significant difference to p<0.0001.*

Patients who scored ICOAP Total = 0 reported no constant or intermittent pain (ICOAP 'A' + ICOAP 'B' = 0). A significantly greater proportion of the cementless cohort reported having 'no constant pain at all' compared to the cemented cohort (84% vs 73%, p=0.003), and 'no intermittent pain at all' (63.1% vs 43.8%, p<0.0001); the difference was greater for intermittent than constant pain.

In both cohorts, the proportion of patients having 'no intermittent pain at all' was near-identical to those having 'no pain at all' (ICOAP 'B' = 0, 43.8% vs 63.1%, ICOAP Total = 0, 42.7% vs 60.6%), suggesting that if any patient experienced constant pain, they would also experience intermittent pain (**Figure 2.8**).

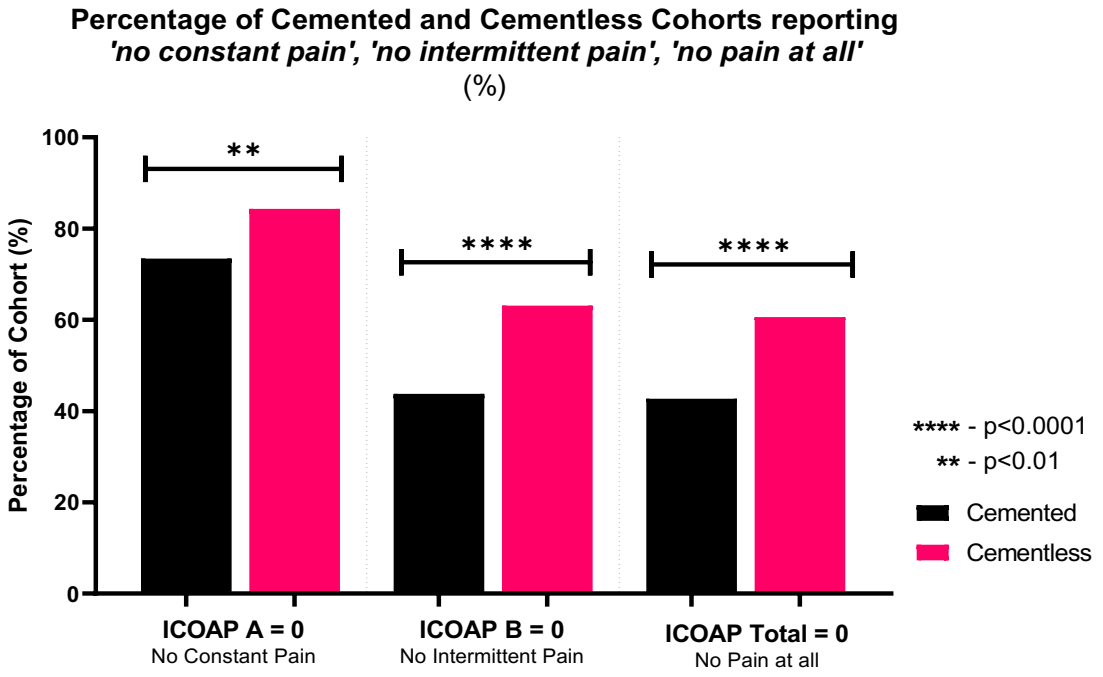


Figure 2.8: *Percentage of 5-year ICOAP 'A', 'B', and Total scores with score 0 of 100, in cemented, cementless, and combined cohorts.*

In the PainDETECT VAS, 0 (indicating no pain) was the most frequently selected score in all scales for both cohorts (**Figure 2.9**). 'Average' and 'Strongest' pain scores were significantly lower in the cementless cohorts ('Average' 1.00 vs 1.50, p=0.0011, 'Strongest' 1.62 vs 2.34, p=0.0022), but not significantly different in the 'Now' scale (0.510 vs 0.738, p=0.1219).

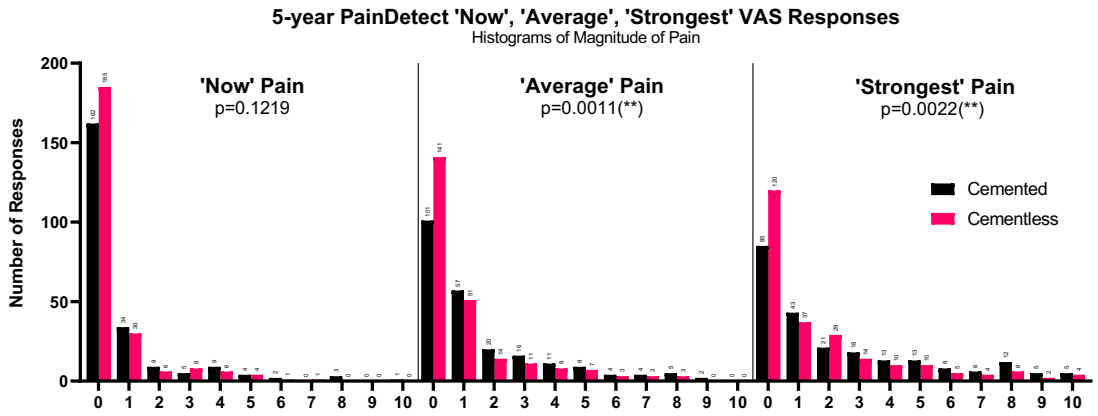


Figure 2.9: *Histograms of 5-year painDETECT Scales scores. p-values given for Mann-Whitley U-Tests performed between scores for cemented and cementless cohorts.*

2.6.3 Neuropathy and Pain

The painDETECT PD-Q score screens for the presence of a neuropathic component to pain. PD-Q≤12 is considered negative with patient unlikely (<15%) to be neuropathic, while PD-Q≥19 is considered positive with >90% likelihood of neuropathy [7]. Patients were categorised into pain categories based on PDVAS-Strongest scale response, from No to Extreme pain. Across both cohorts, where there is pain, it is highly likely to be nociceptive (painDETECT PD-Q≤12 in 87.8%). None of the patients experiencing no pain (PDVAS-Strongest=0/10) scored positive for neuropathy (cemented + cementless, 0% PD-Q≥19). Patients experiencing Severe/Extreme pain (PDVAS-Strongest≥7/10)

were 3.5-3.8 times more likely to be neuropathic (% of cohort with PD-Q≥19 in PDVAS-Str '7-10' vs '1-6') (**Table 2.4**).

Table 2.4: *Likelihood of having a neuropathic component to pain (based on PainDETECT PD-Q score) at different pain levels, scored on the PainDETECT VAS Strongest (Str) scale. Results (n and %) from cemented and cementless cohorts.*

		Cemented			**Cementless**		
		PDVAS-Str = 0	**PDVAS-Str = 1-6**	**PDVAS-Str = 7-10**	**PDVAS-Str = 0**	**PDVAS-Str = 1-6**	**PDVAS-Str = 7-10**
		No Pain	V Mild to Moderate	Severe to Extreme	No Pain	V Mild to Moderate	Severe to Extreme
PD-Q negative (≤12)	n	49	14	0	75	10	0
	%	71.0	13.9	0.0	77.3	10.9	0.0
PD-Q unclear (13-18)	n	20	82	19	22	80	11
	%	29.0	81.2	82.6	22.7	87.0	91.7
PD-Q positive (≥19)	n	0	5	4	0	2	1
	%	0.0	5.0	17.4	0.0	2.2	8.3
Total	n	69	101	23	97	92	12
	%	100.0	100.0	100.0	100.0	100.0	100.0

2.6.4 Co-Morbidity and Pain

Charnley 'A/B' indicates presence of arthritis in either/both knees, while Charnley 'C' indicates morbidity beyond knee arthritis. Cohorts were subdivided into Charnley 'A+B' and Charnley 'C', and compared.

In both cohorts, the patients with non-knee morbidities (Charnley 'C') report greater pain (ICOAP Total) than patients with knee arthritis only (Charnley 'A+B'), with approximately double the proportion of Charnley 'C' patients experiencing Mild or greater pain than Charnley 'A+B' patients (ICOAP Total>20 in Charnley 'A+B' vs 'C', 12.4 vs 24.8 in cemented, 4.9 vs 11.1 in cementless). This trend was significant in the cementless cohort (Chi-Square p=0.0092), but not in cemented (p=0.1902) (**Figure 2.10**).

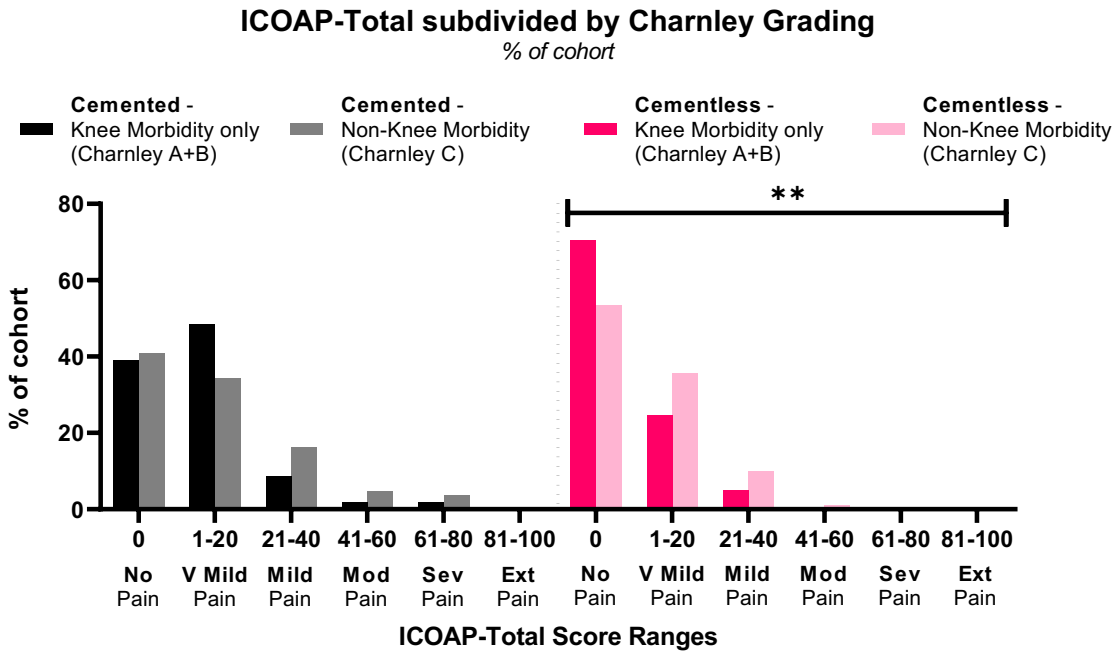


Figure 2.10: *ICOAP 'Total' scores in cemented and cementless cohorts, split by Charnley grades A+B (knee arthritis only) and Charnley C (non-knee arthritis or external morbidity). V Mild: Very Mild, Mod: Moderate, Sev: Severe, Ext: Extreme. ** - p<0.001.*

These differences are consistent with comparisons of mean scores between the cemented and cementless cohorts across ICOAP, PainDETECT, OKS 'Pain', and AKSS 'Pain' scores (**Figure 2.11**).

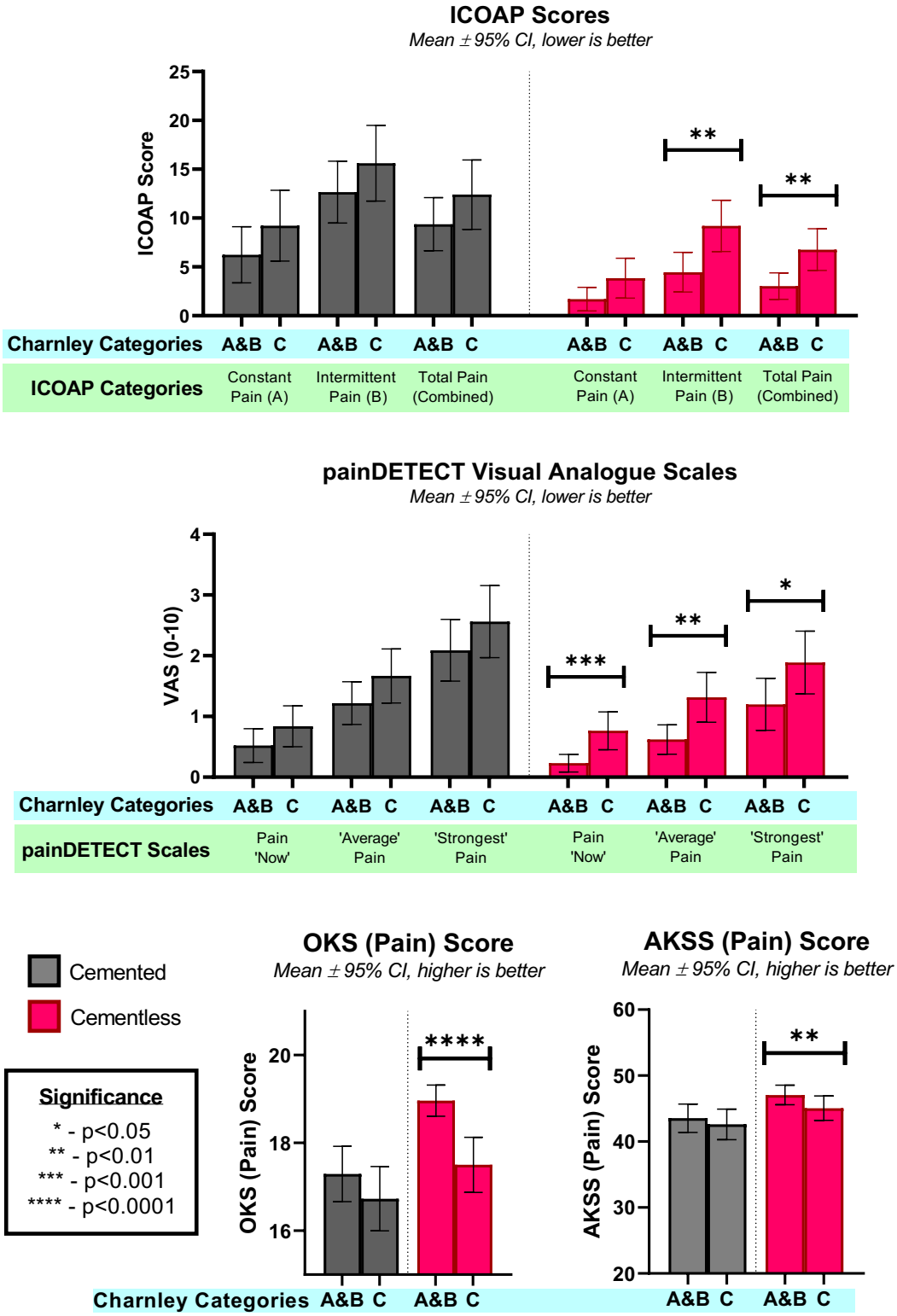


Figure 2.11: *Mean (± 95% CI) responses to ICOAP, painDETECT VAS, OKS (Pain), and AKSS (Pain) categorised into Charnley scores. All distributions are non-parametric (Shapiro-Wilk $p<0.05$), and differences tested with Mann-Whitley U test.*

2.7 Impact of Non-Contemporaneity

The cemented procedures were performed on average three years earlier than the cementless procedures, with substantial overlap (**Figure 2.12**).

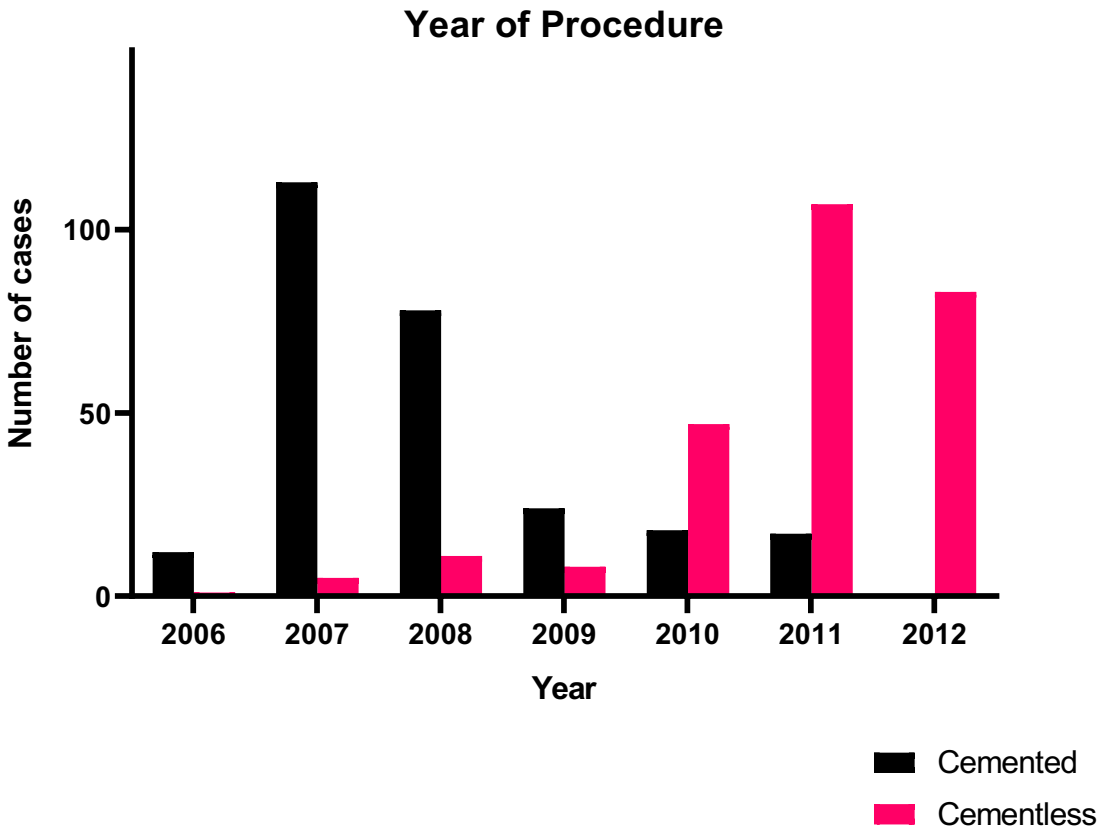


Figure 2.12: *Histogram of Years of Study and corresponding number of cemented and cementless procedures performed in each year for recruited participants.*

To assess if differences were due to non-contemporaneity, each cohort was divided into early and late subgroups by splitting at their respective medians (cemented: 22/01/2008, cementless: 24/07/2011)**.** There was no significant improvement in any scores between the early and late cemented subgroups or the early and late cementless subgroups**,** demonstrating that there was no significant improvement in the scores with time. In

contrast, compared to the late-cemented, the contemporaneous early-cementless subgroup report differences consistent with overall cohort differences **(Figure 2.13, Figure 2.14, Table 2.5)**. One exception was AKSS-O which was not significantly different between late-cemented and early-cementless subgroups. However, the magnitude of its difference between late-cemented and early-cementless subgroups was similar to the whole cohorts; the lack of significance is likely due to having half the numbers in the comparison. Furthermore, AKSS-O's pain scores in these subgroups were significantly different, and thus consistent with the whole cohorts **(Table 2.5)**.

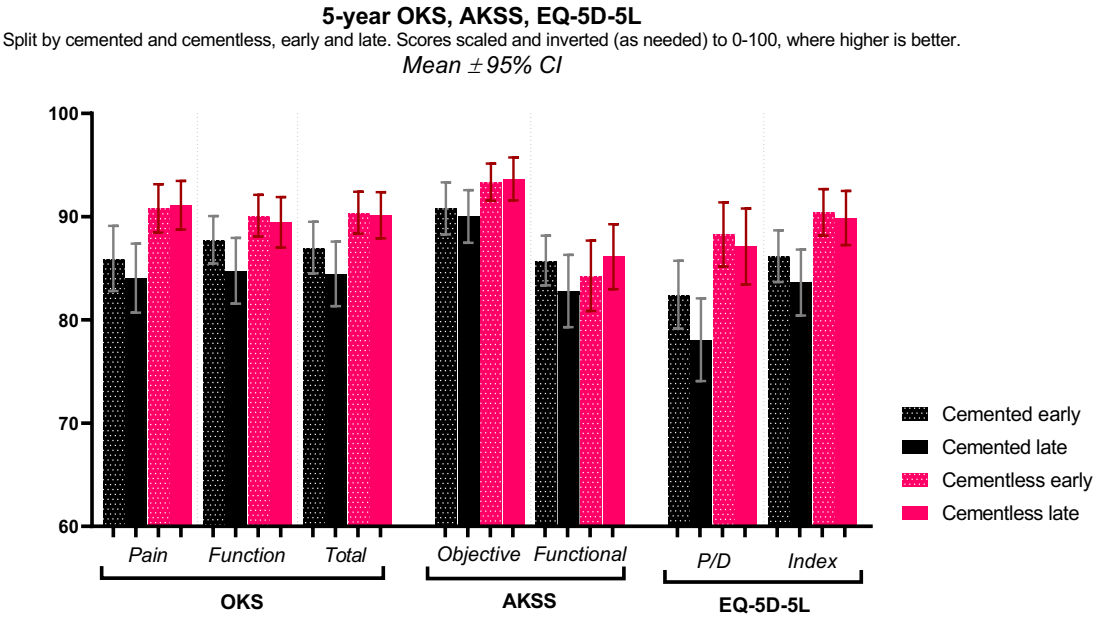


Figure 2.13: *Mean ± 95% CI values for OKS, AKSS (UKR Variant), and EQ-5D (Pain/Discomfort domain and Index score), for cemented and cementless cohorts, further classified into early and late subgroups.*

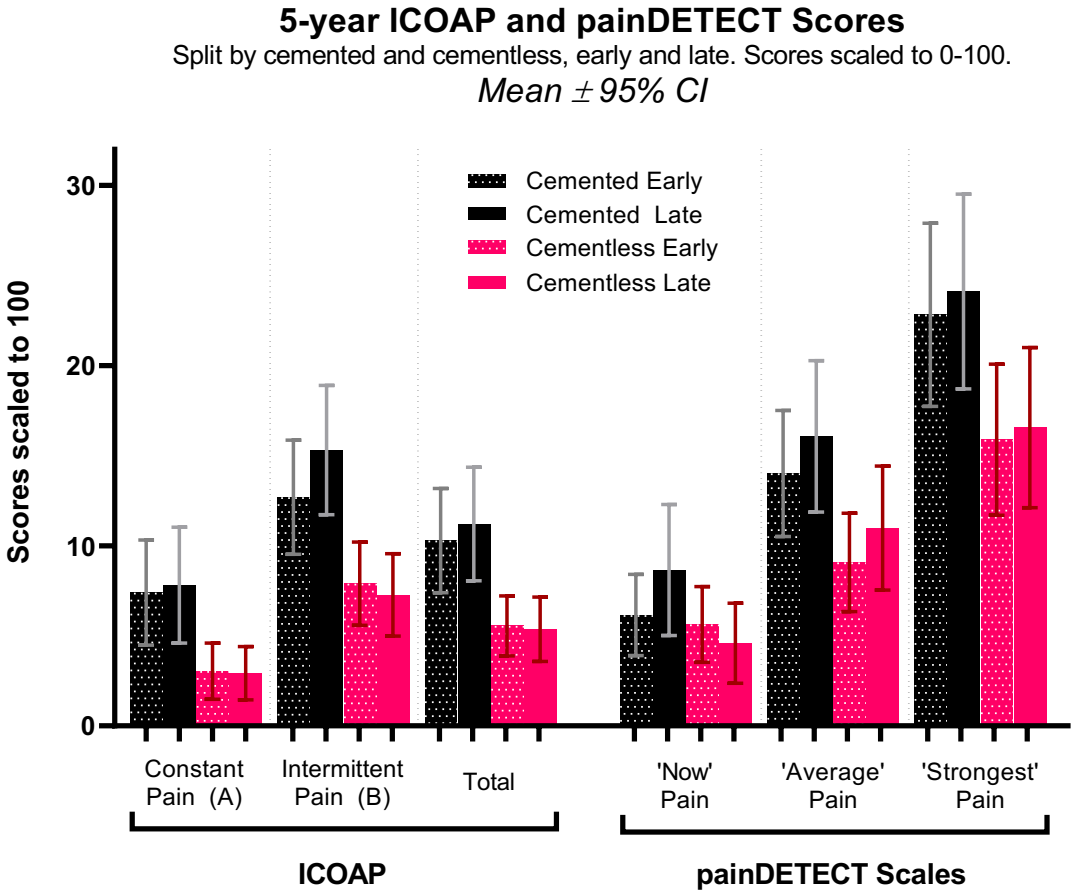


Figure 2.14: *Mean ± 95% CI scores for ICOAP and painDETECT scales, for cemented and cementless cohorts, further classified into early and late subgroups. All scores scaled from 0-100 (ICOAP already 0-100, painDETECT scales multiplied by a factor of 10 from 0-10 to 0-100).*

Table 2.5: *Comparison early and late cemented and cementless cohorts.*

p-values for groups compared	Test	Early Cemented	Early Cementless	Late Cemented	Cemented
		Late Cemented	Late Cementless	Early Cementless	Cementless
OKS Pain (mean scores)	U	0.35	0.89	**0.0012**	**<0.0001**
OKS Function (mean scores)	U	0.57	0.88	**0.048**	**0.010**
OKS Total (mean scores)	U	0.52	0.99	**0.0098**	**0.0080**
AKSS Objective (mean scores)[1]		0.90	0.53	0.27	**0.049**
of which pain (mean scores) [1]	U	0.69	0.91	**0.033**	**0.0046**
of which non-pain (mean scores) [1]	U	0.45	0.81	0.81	0.98
AKSS Functional (mean scores) [1]	U	0.55	0.46	0.65	0.45
EQ-5D Pain/Discomfort Domain (mean scores)	U	0.19	0.96	**<0.0001**	**<0.0001**
EQ-5D Index (mean scores)	U	0.51	0.96	**0.0008**	**0.0001**
ICOAP Total, mean scores	U	0.65	0.90	**0.0028**	**<0.0001**
ICOAP A, mean scores	U	0.97	0.86	**0.022**	**0.0014**
ICOAP B, mean scores	U	0.27	0.81	**0.0006**	**<0.0001**
ICOAP Total, pain categories	Chi-Square	0.67	0.90	**0.0011**	**0.0006**
ICOAP Total, pain vs no pain (0 vs non-0)	Chi-Square	0.87	0.96	**0.0048**	**<0.0001**
ICOAP A, pain vs no pain (0 vs non-0)	Chi-Square	0.95	0.82	**0.030**	**0.0030**
ICOAP B, pain vs no pain (0 vs non-0)	Chi-Square	0.52	0.96	**0.0009**	**0.0001**
painDETECT 'now' scale, mean scores	U	0.71	0.13	0.87	0.12
painDETECT 'average' scale, mean scores	U	>0.99	0.85	**0.022**	**0.0011**
painDETECT 'strongest' scale, mean scores	U	0.97	0.85	**0.039**	**0.0022**
painDETECT PD-Q score, positive vs negative	Chi-Square	0.23	0.99	0.079	0.16

U*: Mann-Whitley U Test.* Distributions tested were non-parametric (Shapiro-Wilk p<0.05). ***Chi-Square****: 2-tailed Chi-Square Test.* [1]*AKSS-UKR variant used. See* ***Methods*** *for details. All values shown rounded to two significant figures.*

2.8 Discussion of Findings

This study demonstrated that patients experience low levels of pain, and very low rates of revision, re-operation, and complication rates in both cemented and cementless cohorts. The amount of pain following Cemented or Cementless UKR was consistent with similar scores reported in literature, which are markedly less than that pain reported following TKR [63, 73, 135-137]. In cases with more serious pain, patients neuropathy and co-morbidity results show that pain was less likely to arise from knee pathology. The Cementless UKR provides better outcomes than Cemented UKR, most notably a 42% increase in the likelihood that a patient reports not experiencing any pain at all.

The knee-specific PROM OKS was 2.1 points (out of 48, p=0.008) higher for the cementless group. When categorised, cementless achieved significantly more 'Excellent' (75% vs 65%), and half the number of 'Poor' (3% vs 6%) or 'Fair' (6% vs 10%) results.

The general quality-of-life PROM used was the EQ-5D-5L. The EQ-5D-5L Index score was significantly (p=0.0001) better for patients with Cementless UKR. Of the domains, 'Pain/Discomfort', 'Mobility', and 'Usual Activities', were significantly better for cementless cohort (difference in score of 30% p=0.0001, 14% p=0.025, 12.6% p=0.017 respectively). The 'Pain/Discomfort' had the largest, as a proportion of the scale, and the most significant difference. There was no difference in the 'Self-Care' and 'Anxiety/Depression' domains, indicating that implant differences have no effect on these domains.

Pain was assessed at 5 years using four different scores: ICOAP, a PROM designed to assess pain in knee osteoarthritis; OKS 'Pain', a subset of the OKS for assessing knee replacement; AKSS 'Pain', a subset of the observer-reported AKSS for assessing knee

replacement; and painDETECT, a PROM designed to assess likelihood of neuropathic pain, originally in the spine, that includes VAS. Each measure had different sets of questions exploring pain, while each VAS referred to different elements of pain. All scores/scales showed that both the cemented and cementless UKR cohorts reported, on average, little pain. Despite floor/ceiling effects, the cementless cohorts reported significantly less pain than the cemented, providing compelling evidence for a true difference in pain (**Figures 2.3, 2.6**).

As mean pain scores were low for both cohorts, scores distributions offered greater insight. When compared to cemented UKR, patients with the cementless UKR were 42% more likely to have *No pain at all* (43% vs 61%). No cementless cases had Severe or Extreme pain whereas 2.9% of the cemented did. As a result, the vast majority of cases had No, Very Mild, or Mild pain (cementless 98%, cemented 93%). This is corroborated by the revision rate of 0.76% in both cohorts, where there were no revisions for unexplained pain.

Scores also give insight into differences in the nature of pain. Pain was twice as likely to be intermittent than constant in both cohorts (ICOAP 'B'>0 46.6% vs ICOAP 'A'>0 21.1%), a trend corroborated in literature [11-14]. In general, patients reporting constant pain, also reported intermittent pain. Both pain scores were significantly, but proportionally, lower for the cementless cohort. The painDETECT VAS results followed the expected trend - 'Strongest' pain was worse than the 'Average' which was worse than pain 'Now' (1.97 vs 1.25 vs 0.621, out of 10). The cementless cohort reported less pain across the three groups than the cemented. The difference was statistically significant for 'Strongest' and 'Average', but not for 'Now' Pain VAS, which may be explained by the especially strong floor effect in the 'Now' scale (**Figure 2.8**).

Across both cohorts, where there is pain, it is highly likely to be nociceptive (pain DETECT PD-Q≤12 in 87.8%) i.e., with a physiological origin. However, if the worst pain that patient experienced was Severe/Extreme (PDVAS-Strongest≥7/10) rather than Very Mild/Mild/Moderate (PDVAS-Strongest≥1-6), such a patient was 3.5-3.8 times more likely to have a neuropathic element to their pain (**Figure 2.9**). This is corroborated by the unexpected influence of Charnley grades on pain scores; despite all scores being knee-specific, patients with multiple arthritis or medical infirmity (Charnley 'C') consistently scored poorer than those with only arthritis in the knees (Charnley 'A'/'B') (**Figure 2.10**). More importantly, patients reporting higher levels of pain in ICOAP are more likely to be Charnley 'C' patients (**Figure 2.9**). Interestingly, these differences were statistically significant in the cementless, but not cemented, cohort. This may be due to the greater "knee origin" pain with the cemented cohort masking "other origin" pain, while the cementless cohort experience weaker "knee origin" pain, thereby allowing a relatively stronger influence of "other origin" pain to increase scores in Charnley 'C' patients.

These correlations with neuropathy and non-knee morbidity suggest that pain perceived by patients to be knee-specific may not necessarily be caused by knee pathology, but instead be of external origin, be it biological, neuropathic, or psychosocial [15]. These external causes appear to be most likely in patients experiencing higher levels of pain, whilst "knee origin" pain appears in most cases to be mild.

The origin of pain in UKR, and the cause of the differences in pain between cemented and cementless implants, remain unclear. The main difference between the implants is the bone-implant interface, which is likely to be responsible for the difference in pain. There are fewer radiolucencies with cementless than cemented tibial components [16-

18]. Existing studies suggest that there is no relationship between pain and radiolucency following cemented fixation [19]. The radiolucencies assessed in this study were under the tibial component in the implant studied (Phase 3 Cemented Oxford UKR), where a predominantly compressive load is transmitted to the bone in this region. The tibial wall experiences different mechanics. Following the resection of the subchondral bone plate at the medial tibia, the cortical "tension band" supporting the medial condyle is lost. If tension was transmitted between the wall and tibial eminence, this tension band would be restored, and may contribute to less pain [21]. More detailed study of fixation around the tibial component including the tibial wall, needs to be performed and correlated with pain to assess if there is any relationship.

Scores from both Cemented and Cementless UKR cohorts are better than TKR scores in the literature. OKS 'Pain' in TKR at 5 years is reported to be 15.9 out of 20 [23], which is worse than Cemented and Cementless UKR in this study (17.0, 18.2 out of 20). The differences are greater with the pain-specific score ICOAP and exceed minimally important clinical difference (MCID 18 of 100) [24]: UKR patients experience 8 times less constant pain (ICOAP 'A' 5.3 vs 42.3), 5 times less intermittent pain (ICOAP 'B' 10.8 vs 52.3), and 6 times less total pain (ICOAP 'Total' 8.1 vs 47.7) than TKR [25]. These studies are not matched and have different lengths of follow up. Nonetheless, TKR scores are consistent in literature [13, 24] do not change substantially after 6 months [15, 16], and any changes that do occur would likely be small relative to the differences noted.

Score differences between cemented and cementless cohorts in this study are not greater than published MCIDs: ICOAP 'Total' 18/100 [24], PD-VAS 0.9/10 [26], OKS 'Pain' 5/20 [138]. However, these MCIDs were developed based on TKRs, where scores are more normally distributed than the UKR scores encountered in this study. Due to strong

floor/ceiling effects, it is unfeasible to apply them to this study: for example, the cemented ICOAP 'Total' was 10.8, which cannot be decreased by 18 points (the MCID). MCID for AKSS 'Pain' was not found in literature.

More generally, the outcome measures included in this study consistently experienced strong floor and ceiling effects in both cemented and cementless Oxford UKR. A non-negligible 1 in 10 patients with implants perform high levels of activity, with TAS≥5. Therefore, scores could be expanded to incorporate pain and function in high activity levels, to mitigate floor/ceiling effects.

There were no significant differences between the cemented and cementless UKR in revision, re-operation and complication rates, demonstrating that the procedures are equally safe. Registry studies have shown that the revision rate of the cementless Oxford UKR is lower than the cemented [100], but is not necessarily inconsistent with this study; with two revisions in each cohort, this study is too underpowered to show a difference. The survival rate of both cemented and cementless UKR was 99% at 5 years, which is similar to that of the best TKR, but the revisions are more minor (being conversions to primary TKR or bearing exchange). Furthermore, the re-operation and complication rates are substantially lower than those of TKR.

The main limitation of the study is that it is not randomised. Although the cohorts are well matched for demographics and pre-operative scores (**Table 2.1**), the cementless cases were implanted on average three years after the cemented, introducing the possibility of confounding due to differences associated with the date of operation, such as progressive improvements in surgical technique with time. However, when comparing the early and late sub-groups within the cemented and cementless cohorts, there was no significant improvement in outcomes. In contrast, when comparing the late-cemented

and early-cementless sub-groups, which were approximately contemporaneous, there were significant differences in scores, and patterns were similar to those in the overall comparison (**Figure 2.12, Figure 2.13, Table 2.5**). As the early-cementless cases were done at about the same time as the late-cemented cases, this strongly suggests the differences are due to fixation and not improvements in technique with time. Furthermore, differences in outcome scores in this study were similar to those found in previous randomised trials that were underpowered for clinical outcomes [98, 99, 133], further supporting these findings.

The procedures in this study were performed by high volume surgeons, which limits its generalisability. However, evidence suggests that if surgeons adhere to the recommended indications and surgical techniques, they get similar results [139-141]. Therefore, the conclusions of this study should relate to all surgeons using the recommended indications and techniques.

2.9 Chapter Summary

This study demonstrates that at 5 years, both cemented and cementless Oxford UKR are safe with implant survival of 99.2%, non-revision re-operation rates of 2%, and complication rates of 5%. Although both devices had excellent PROMs, the cementless had significantly better PROMs than the cemented. The differences were most marked in the pain scores, and the other functional advantages seen may be due to decreased pain. Most notably, 42% more patients with cementless UKR reported having no pain compared to cemented UKR. If pain was experienced, it was likely to be mild. Most PROMs experienced strong floor/ceiling effects, and this could be mitigated by expanding scores to score pain and function during higher levels of physical activity.

In all, this study suggests that surgeons using the recommended indications and techniques should consider using Cementless rather than Cemented Oxford UKR where possible. However, the underlying reasons for this difference are not clear. This will be explored in the next chapter.

3 Tibial Component Fixation and Pain

3.1 Motivation for Chapter

In **Chapter 2**, it was shown that patients report a reduced incidence of mild pain arising from the knee if they had a Cementless Oxford UKR implant instead of the Phase 3 Cemented Oxford UKR. The reasons for this difference are not clear, especially given the identical indications, and highly similar implant designs and surgical technique. Therefore, the main difference between the implants – fixation at the bone-implant interfaces – was explored.

3.2 Bone-Implant Interfaces of the Tibial Component

When the tibia is prepared for implanting the tibial component of the Oxford UKR, sagittal and transverse saw cuts, as well as a slot cut, are made (**Figure 3.1b**). The tibial component is then press-fit into the slot [86].

The sagittal bone cut interfaces with the tibial component wall, but it is believed that no load is transmitted through this surface. The transverse cut interfaces with the tibial component floor, which experiences compression when a load travels through the medial knee joint. The keel interfaces with the slot, and due to its interference fit, is under constant compression during primary fixation.

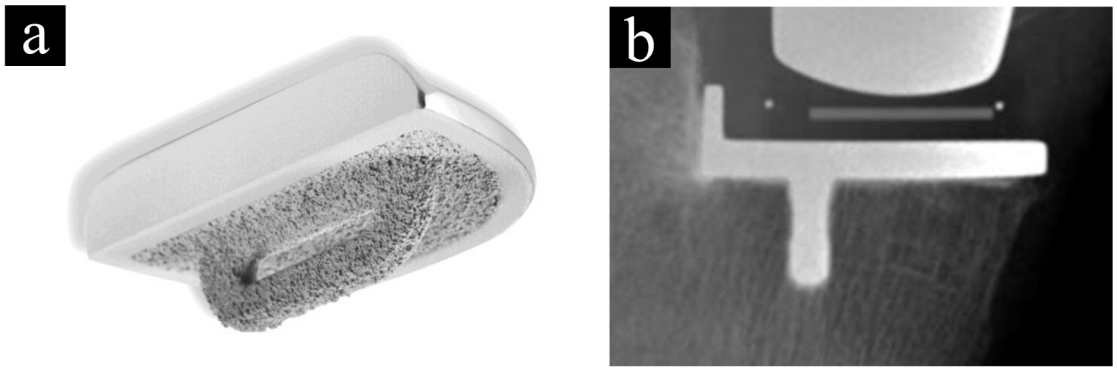


Figure 3.1: (a) *The Tibial Component of the Cementless Oxford UKR showing porous transverse surface and smooth wall surface. Image adapted from Campi et al [142].* ***(b)*** *An AP radiograph of a Cementless Oxford UKR, demonstrating the transverse/horizontal cut, sagittal/vertical wall cut, and slot cut.*

3.3 Current Knowledge and Chapter Aims

In **Chapter 2**, it was shown that there was a notable difference in the incidence of pain reported by patients with the Phase 3 Cemented, and Cementless, Oxford UKR. Such pain generally arises in the medial aspect of the anterior proximal tibia [75]; hypotheses for the source of this pain are further discussed in **Section 3.4**.

The only difference between these implants is fixation. In the tibial component, the Cemented UKR is inserted with space-filling cement and no interference fit. In contrast, the Cementless UKR has a porous bottom surface with hydroxyapatite, with the keel component being inserted with an interference fit – no cement is used.

Small, randomised studies comparing Cemented and Cementless Oxford UKR found that there were fewer radiolucencies with the cementless implant, but no relationship between radiolucencies and pain were identified [98, 99]. These findings were corroborated by another study of only Cementless Oxford UKR [144]. However, there are several limitations with these studies, namely that the incidence of pain and radiolucencies at the tibial component wall were not studied. Limitations will be discussed in further detail in **Chapter 3.5**.

The work in this chapter aims to perform an assessment of tibial component fixation that addresses these limitations. First, fixation at the tibial component wall will be assessed. Second, the effect of fixation on pain will be assessed.

3.4 Surface Microstructure of Bone-Facing Surfaces of the Oxford UKR Tibial Component

To better understand the surfaces being assessed, the surface microstructure of the bone-facing Cobalt-Chrome (CoCr) surfaces on the Oxford UKR tibial component were imaged using Scanning Electron Microscopy (SEM). Images were acquired with a Field-Emission Gun SEM instrument (TESCAN© MIRA3, Kohoutovice, Czech Republic) at an acceleration voltage of 5.0 kV[1].

The Cemented Oxford UKR has a smooth surface on all bone-facing surfaces (**Figure 3.2a**). This surface is shot-blasted to provide a slightly rough surface for cement adhesion, but was not porous (**Figure 3.2f**). With cemented fixation, usually no attempt is made to put cement at this wall interface. However, when the cement is pressurised during implantation, some cement may extrude up beside the wall. Therefore, in this wall region, the bone interfaces with either the CoCr implant surface, or bone cement.

The Cementless Oxford UKR keel and most of the inferior surface of the component (hereafter termed 'tibial floor') have a porous surface applied using plasma-sprayed titanium (**Figure 3.2d**). The porous surface provides a surface for bone ingrowth during remodelling, which can improve implant fixation into bone [145]. This bone growth is further induced by a coat of hydroxyapatite (**Figure 3.2f**) to the surface, which induces osteogenesis and bone adhesion [87]. The early version of the cementless implant wall was identical to that of the cemented, except for the addition of a hydroxyapatite coat (**Figure 3.2b**), and was not designed to achieve fixation with adjacent bone.

[1] Microscope operation and image acquisition was arranged for with a collaborator (Department of Materials, University of Oxford, UK).

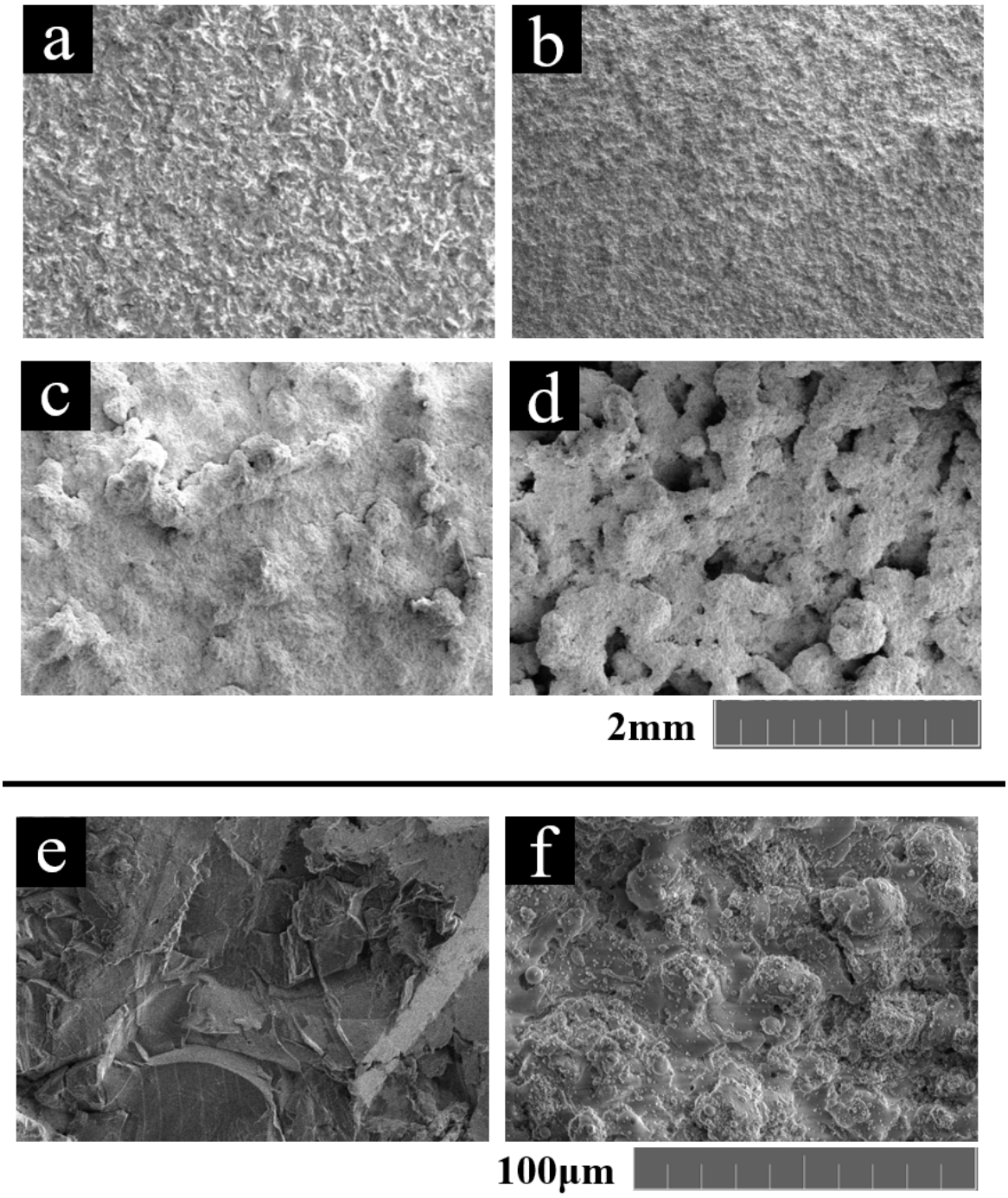


Figure 3.2: *Scanning Electron Micrographs of Bone Contact Surfaces in Oxford UKR tibial components. (**a**) Tibial Wall/Floor/Keel in Cemented UKR, without hydroxyapatite. (**b**) Tibial Wall in Early Cementless UKR, with hydroxyapatite. (**c**) Tibial Wall in Later Cementless UKR, with microporous titanium and hydroxyapatite. (**d**) Tibial Floor/Keel in cementless UKR, with porous titanium and hydroxyapatite. (**e**) Close-up view of Cemented UKR surface showing absence of hydroxyapatite. (f) Close-up view of Cementless UKR surface showing hydroxyapatite coating.*

After the introduction of this early cementless wall design, Small et al studied the load distribution after UKR in cadaveric bones and found that the stress in the cortex in the region inferomedial to the component (where pain is experienced) increased following UKR [146]. Simpson et al did a similar computational study and showed that, in this region, the strain in the bone increased by 40% when a UKR was implanted [147]. In most cases, it is likely that, with time, the bone remodels in response to the increased strain and residual strain returns to normal levels [148], causing the bone-related pain to settle. Where pain persists, it can be hypothesised that the strain remains abnormally high. Using a computational model, Simpson et al investigated approaches to minimise the increase in strain and found that the most effective method was to achieve a mechanical link between the vertical wall of the tibial component and tibial eminence. It was therefore suggested that if a mechanical link could be achieved, the incidence of pain would be reduced.

Based on this analysis, the design of the Cementless Oxford UKR tibial component was modified. A micro-porous titanium coat (MPC) layer was applied to the tibial wall and margin surrounding the porous coat on the tibial floor before the hydroxyapatite coating, in an attempt to enhance fixation (**Figure 3.2c**).

3.5 Assessing Tibial Wall Fixation

Tibial wall fixation has not been assessed in literature. Therefore, a novel approach using antero-posterior (AP) radiographs is proposed. This approach looks at the proportion of the component wall or cement which is radiographically in contact with adjacent bone.

3.5.1 Collecting Radiographs

Horizontally rotated radiographs can mask radiolucencies at the tibial wall. Similarly, vertically rotated radiographs can mask radiolucencies at the tibial floor. Therefore, AP radiographs of knees used in this study were collected from one centre in the United Kingdom where consideration was given to radiographic alignment at time of acquisition. Radiographs were aligned clinically with fluoroscopic guidance, with the patients in a supine position. Beam direction was finely adjusted until the tibial wall and tibial floor were as narrow as possible in the clinical setting. Radiographs were then digitally encoded into a DICOM format (DICOM Standard, ISO 12052:2017) and later to a JPEG format (JPEG Standard, ISO / IEC 10918) for further assessment.

3.5.2 Quantifying Horizontal Alignment in Radiographs

Further to clinical alignment of radiographs, further filtering was necessary to ensure that only aligned radiographs are studied; radiolucencies may otherwise be underreported, as wall masking will result in false negative results. Such masking will occur only if the beam direction was internally or externally rotated relative to the tibial component wall (**Figure 3.3**).

To assess the amount of horizontal internal/external malalignment in a radiograph, a Horizontal Rotation Ratio (HRR) was defined using the equation below.

$$\boldsymbol{HRR} = \frac{Tibial\ Wall\ Width\ (W_{wall})}{Internal\ Tibial\ Wall\ \ Height\ (H_{wall-I})} \times 100\%$$

In an AP radiographic projection, horizontal rotation would increase W_{wall} rapidly, while $H_{wall\text{-}I}$ remains relatively constant, allowing these values to be suitable constituents of the HRR measurement.

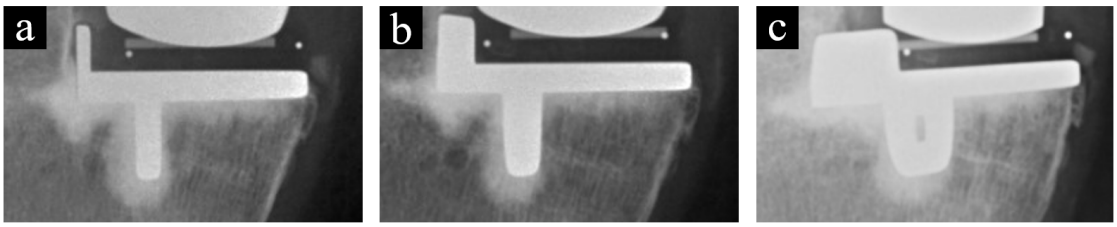


Figure 3.3: *Three progressively rotated AP knee radiographs from a patient, demonstrating how rotation can cause masking of a radiolucency adjacent to the tibial wall. Horizontal Rotation Ratios for each radiograph were* ***(a)*** *32%,* ***(b)*** *82%,* ***(c)*** *223%.*

In all tibial component sizes, the W_{wall} is manufactured to be 1.6 mm wide and the H_{wall-I} is manufactured to be 5.3 mm. Therefore, a perfectly aligned radiograph would have a HRR of 30%. There is no upper limit to HRR; HRR = 100% arbitrarily indicates that the wall thickness (W_{wall}) was equal to the internal height (H_{wall-I}). A HRR threshold of 50% was set for analyses performed in this thesis, which equates to an apparent W_{wall} of 2.6 mm, which is 1 mm wider than true W_{wall}. Therefore, all tibial wall radiolucencies greater than 1 mm thick will be visible in the radiographs included in this study.

3.5.3 Quantifying Wall Fixation in Radiographs

It was observed that, where there is incomplete fixation of the bone to the tibial wall, the radiolucency appear at the top, and direct apposition of bone to the implant wall is at the bottom. Therefore, the wall fixation was assessed using a Wall Fixation Ratio (WFR), defined as follows:

$$\boldsymbol{WFR} = \frac{External\ Tibial\ Wall\ \ Height\ (H_{Wall-E}) - Radiolucency\ Height\ (RLH)}{External\ Tibial\ Wall\ \ Height\ (H_{Wall-E})} \times 100\%$$

WFR represents the proportion of the wall where there is bone contact, seen on the AP radiograph i.e., on the coronal plane. WFR = 0% indicates no direct contact between bone and the full height of the implant wall, and WFR = 100% indicates bone appears to be in direct contact with the full height of the wall.

3.6 Tibial Wall Fixation in variants of Oxford UKR

3.6.1 Study Aims and Method

To understand the effect of the tibial wall surfaces variants on fixation, a radiographic study was performed. The aim of the study was to compare the radiolucencies by the wall of Oxford UKR tibial components with three clinically used variants of the tibial component wall: no coat or bone cement (Cemented), hydroxyapatite (HA), and hydroxyapatite on a microporous titanium coat (HA+MPC).

Clinical AP radiographs were obtained 1-2 years after surgery. Alignment was assessed using the Horizontal Rotation Ratio (HRR). An upper threshold of HRR = 50% was used to ensure all radiolucencies wider than 1 mm would be included (see **Section 3.3.2** for more details). Tibial wall fixation was assessed in radiographs passing this requirement, using Wall Fixation Ratio (WFR).

The presence of any radiological features or patterns observed during radiograph analysis by operators was noted. A key feature sometimes seen was two parallel radiolucent zones between the component wall and tibial eminence, between which appeared to be bone with a characteristic hemi-lenticular shape (**Figure 3.7**). All radiographs were assessed to see if this hemi-lenticular sign was present.

3.6.2 Study Cohort

Three separate consecutive cohorts were retrospectively identified (n = 221 cemented in 2005-2007, n = 118 HA in 2014-2015, n = 125 HA+MPC in 2016-2017) from one centre in the United Kingdom. Cohort dates were determined by periods where the respective

surface variants were predominantly used. The cemented cohort was initially 2006-2007, but was expanded to 2005-2007 to ensure a minimum of 30 sufficiently aligned radiographs were included in the study.

AP knee radiographs taken for routine clinical follow-up, between 1-2 years (10-26 months) post-operatively, were collected. Measurements to calculate HRR were made for all radiographs. Radiographs with HRR≤50% (i.e., adequately aligned) were obtained in 33 knees with 'Cemented', 37 knees with 'HA', and 57 knees with 'HA+MPC'. The average time between the operation and the radiograph was 13.9, 16.7, and 15.5 months respectively. There was no significant difference in the time between surgery and radiography across the three cohorts (One-way ANOVA, p=0.084).

Adequately aligned radiographs were assessed by two independent observers to calculate WFR. Inter-observer correlation was assessed, and the average WFR of both observers were used for each radiograph. Observers were blinded to implant type, though the presence of bone cement can be seen in radiographs.

3.6.3 Software and Statistics

Radiograph measurements were made using ImageJ (National Institutes of Health, Bethesda, Maryland, USA) based on measurement protocols detailed in **Section 3.5**. Inter-observer correlation was performed using SPSS (IBM Corporation, Armonk, New York, USA). Data was analysed and visualised using GraphPad Prism (GraphPad Software, San Diego, California, USA) and Excel (Microsoft, Redmond, Washington, USA).

All data was classified by knee. Radiographic measurements were compared between cohorts using the unpaired Student t-test for parametric (Shapiro-Wilk $p>0.05$), and the Mann-Whitney U-test for non-parametric (Shapiro-Wilk $p<0.05$) distributions. Other statistical tests, where performed, are described in the relevant sections.

3.6.4 Results

WFR from the two independent observers were compared (**Figure 3.4**). Intraclass Correlation Coefficient (ICC) was calculated using a two-way mixed effects model for average measures. ICC for all cohorts separate and combined, were excellent (cemented 0.959, HA 0.982, HA+MPC 0.972, all 0.985).

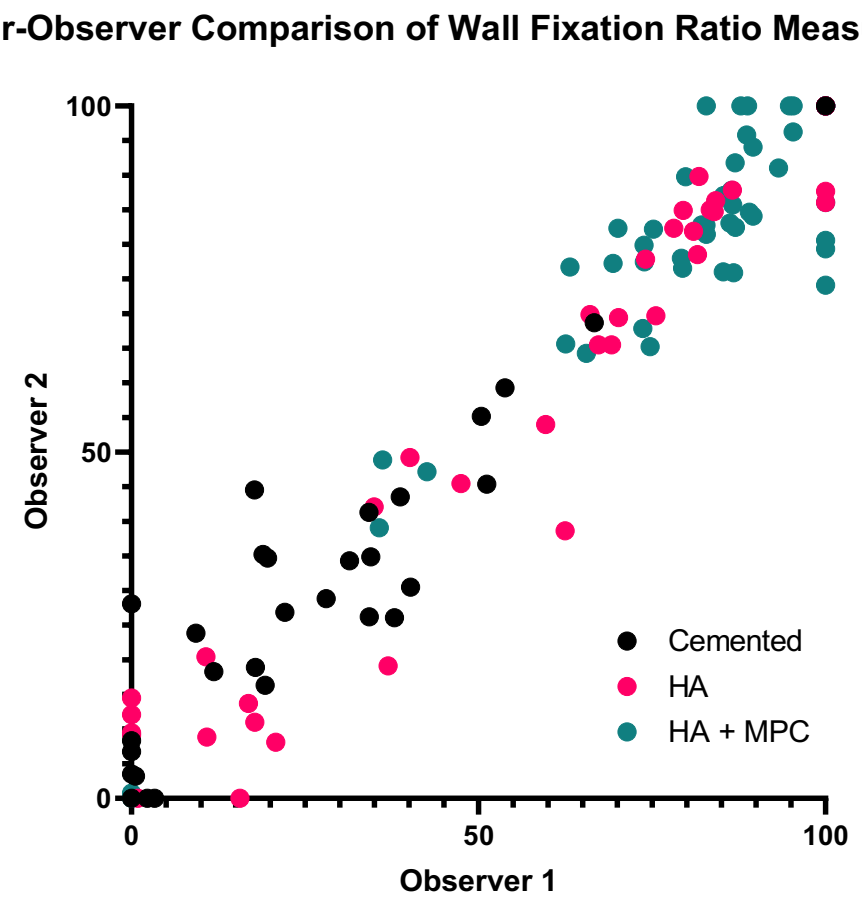


Figure 3.4: *Comparison of Wall Fixation Ratio (WFR) measured by both observers, separated by coating type.*

Fixation was significantly better in HA group compared to Cemented (mean WFR 55% vs 25%, p=0.0016). The added microporous coat (HA+MPC) further significantly improved fixation compared to the HA only group (mean FR 81% vs 55%, p<0.0001) (**Figure 3.5**). FR>80% was achieved in 3% of the cemented implants, 32% of HA implants, and 68% of HA+MPC implants (**Figure 3.6, Table 3.1**).

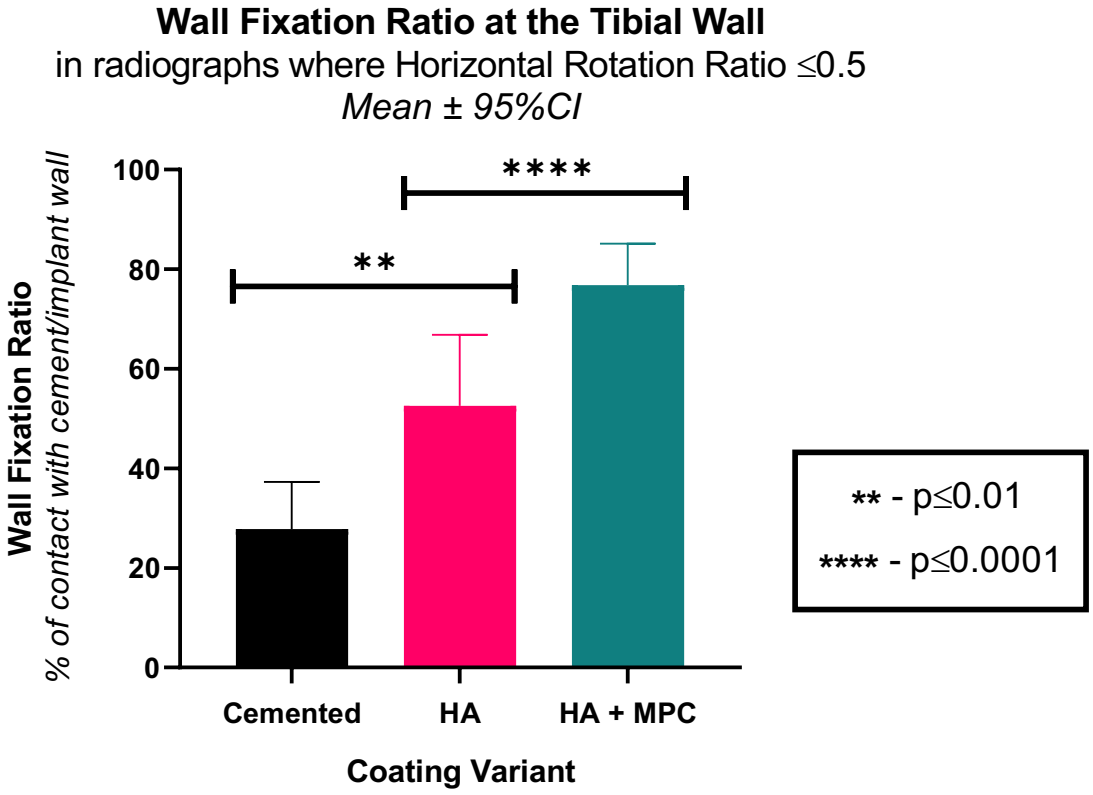


Figure 3.5: *Mean Wall Fixation Ratio at the tibial wall in all aligned radiographs, separated by coating at tibial wall.*

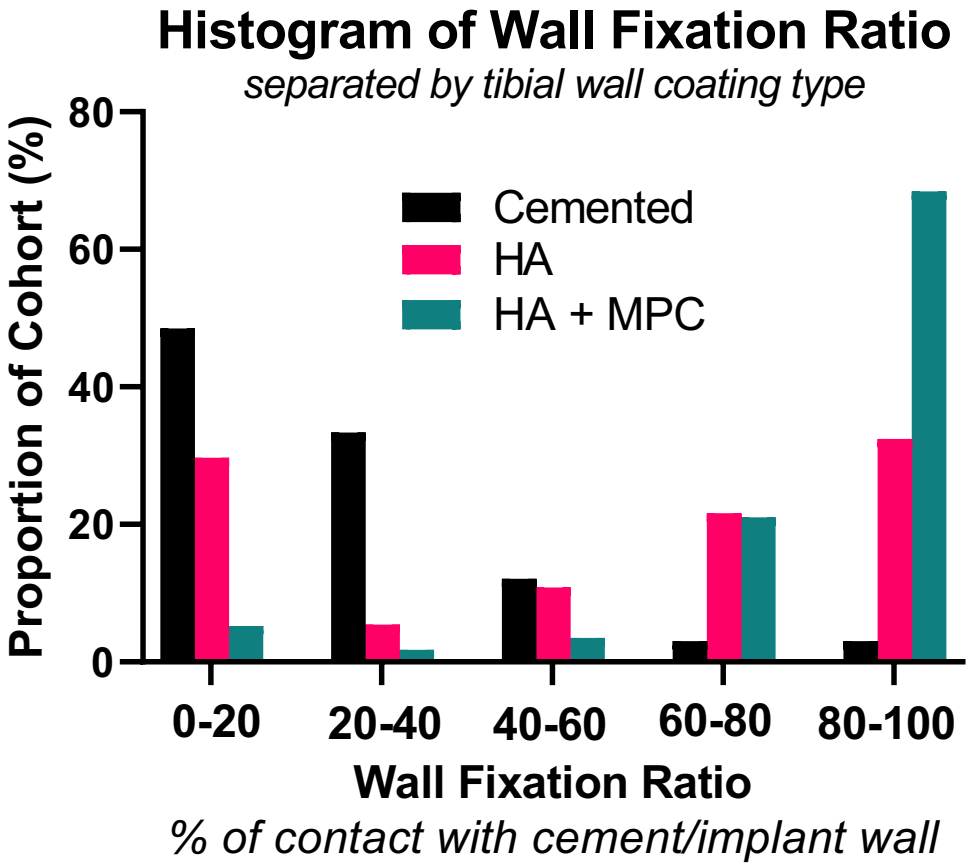
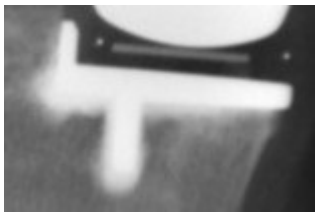
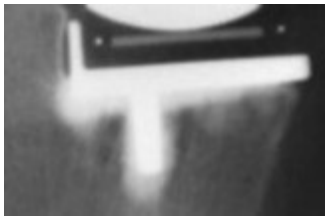
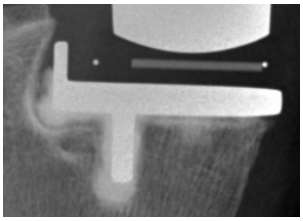
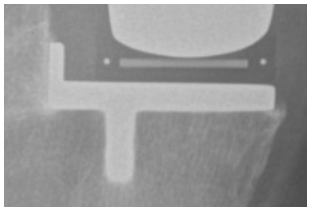
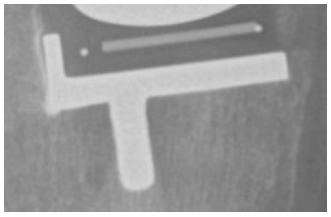
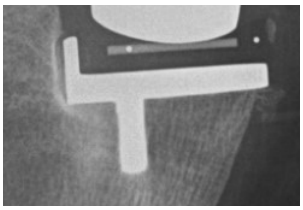
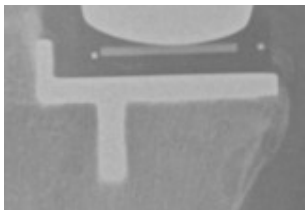
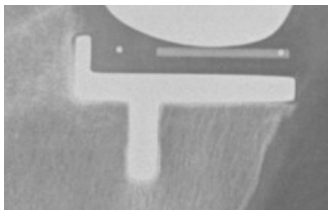
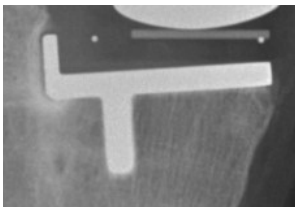


Figure 3.6: *Histogram of Wall Fixation Ratio at the tibial wall in all aligned radiographs, separated by coating at tibial wall. FR is split into 20% groups from poor fixation (FR = 0-20%) to excellent fixation (FR = 81-100%).*

Table 3.1: *Representative images of Oxford UKR tibial components and bone-implant interfaces at the tibial wall, separated by coating type. Note that the mean WFR progressively increases from the Cemented, to the HA, to the HA+MPC variants.*

	Highest WFR	**Mean WFR**	**Lowest WFR**
	Image and Wall Fixation Ratio (nearest 10%)		
Cemented	 **100%**	 **30%**	 **0%**
Hydroxyapatite	 **100%**	 **50%**	 **0%**
Hydroxyapatite on Microporous Coat	 **100%**	 **80%**	 **0%**

All radiographs were assessed for the presence of a hemi-lenticular bone growth. These structures were only observed where WFR<20%. Of these, 0 of 16 (0%) cemented, 8 of 12 (67%) knees in the HA cohort, and 3 of 3 (100%) of knees in the HA+MPC cohort had this hemi-lenticular feature (**Figure 3.7, Table 3.2**). The thickness, height, and distance from adjacent surfaces of this hemi-lenticular feature varied between cases.

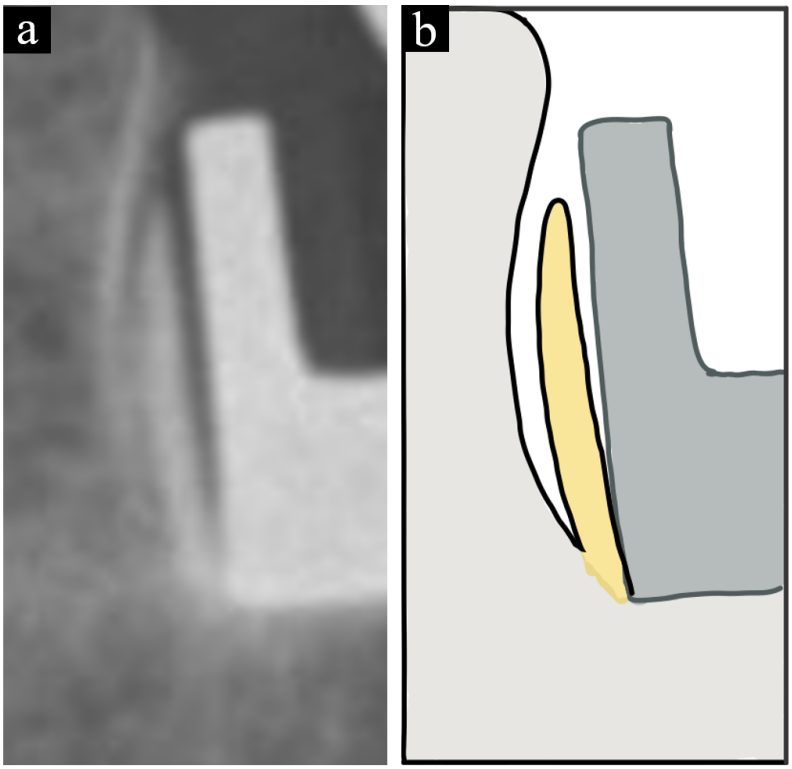
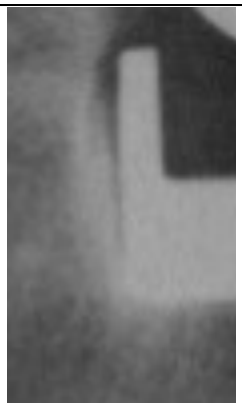
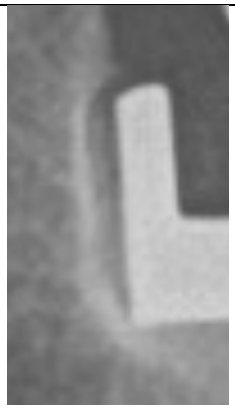
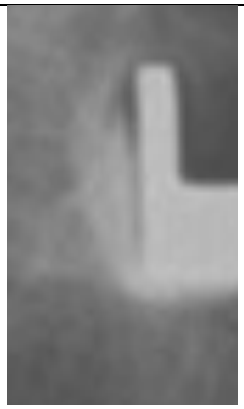
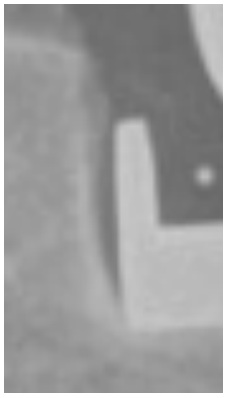
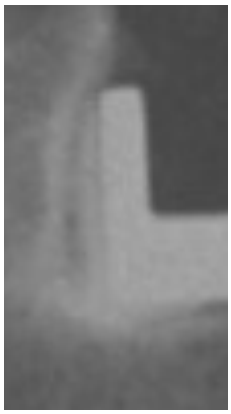
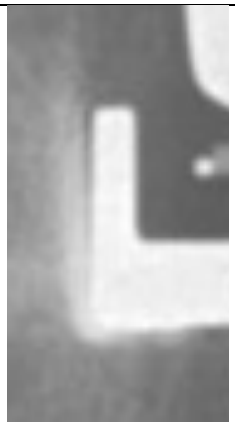
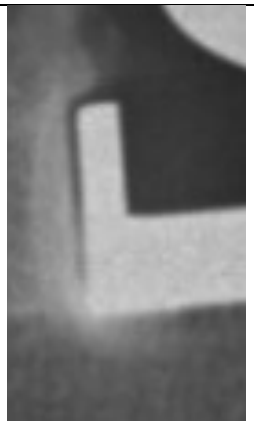
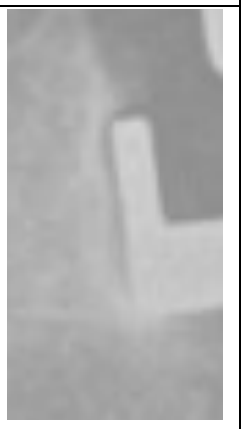
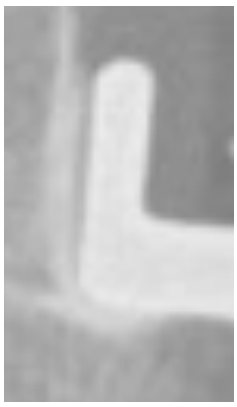


Figure 3.7: *Bone growth found in some radiographs where fixation to the tibial wall is poor (FR<20%). Feature is radiographically characterised as a generally hemi-lenticular opacity between implant and sclerosed vertical bone surface. (**a**) Radiograph of a cementless implant, (**b**) Graphical representation with hemi-lenticular opacity highlighted in yellow.*

Table 3.2: *HA and HA+MPC cohort radiographs with features of delaminated bone growth*

HA				
				
HA+MPC				

3.6.5 Discussion of Findings

Cementless Oxford UKR has substantially better fixation at the tibial wall than Cemented Oxford UKR. A cemented implant fixes to, on average, 25% of the wall. A cementless implant with a hydroxyapatite coat (HA) significantly increases wall fixation to 55%, and a microporous titanium coat with HA (HA+MPC) increases fixation significantly more to 80%. Both cemented and cementless fixation are considered to provide good patient outcomes when the interface is loaded in compression [149]. The interface by the vertical wall is not loaded in compression. Therefore this study highlights the differences between the methods of fixation in a mechanical environment less conducive to bone formation [150].

In **Chapter 2**, it has been shown that there is less pain at five years following Cementless compared to Cemented Oxford UKR. This pain is typically antero-medial below the tibial component. A computational study of the implant found that the strain in the bone in this area increased substantially post-operatively, and suggested that this might contribute to the pain [147]. Further analysis suggested that if a bond that could transmit tension could be achieved between the wall and the tibial eminence, the bone strain in the painful area would decrease. It therefore seems likely that the improved fixation in the region of the wall with cementless components may have resulted in the improvement in the pain.

In the cemented cohort, the amount of cement covering the wall was variable. When it only partially covered the wall, it tended to be at the bottom, with exposed cobalt-chrome (CoCr) at the top. It was generally observed that the bone was hardly ever in direct contact with the CoCr, but was sometimes in direct contact with the cement (**Table 3.1**). Cement is placed between the transverse cut and floor of the component. When pressured during implantation, it can be forced up between the CoCr wall and the vertical cut bone, and

into adjacent trabecular bone. This bone may resorb, causing a radiolucency to form around the cement. The uncoated CoCr wall abutting the sagittal bone cut has no mechanical interaction with the bone and does not have a surface that stimulates bone formation [148].

In implants with the HA coating only, the tibial wall fixation was bimodal – bone was either likely to have near complete fixation at the implant wall (FR>80% in 1/3 of cohort), or if not, poor fixation (FR<20% in 1/3 of cohort). This may be indicative of the variability in benefit provided by hydroxyapatite signalling. Osseous interfacing has been shown to occur in gaps of up to 1 mm between bone and hydroxyapatite, but this does not occur in all patients [151]. This seems to depend on how successful hydroxyapatite signalling and osteoblast activation is [152-154]. However, even if bone grows up to the surface, as the surface is smooth, it is unclear how strong the attachment would be, and can be expected to be limited.

The HA+MPC cohort (where hydroxyapatite is applied over a microporous titanium coat at the tibial wall) showed the best wall fixation of all three groups, with over 60% of all radiographs showing near complete tibial wall fixation (FR>80%). The addition of the MPC provides a coarser surface. A coarse surface has been shown to increase release of prostaglandin E_2 (PGE_2) and transforming growth factor-β1 (TGF-β1) which induce osteoblast differentiation [155]. The combination of HA+MPC has been further shown to benefit cell proliferation and provide a more favourable biomimetic microenvironment for osseointegration [156]. In addition, the bone can potentially grow into the microporous surface providing strong fixation which may be able to transmit tension.

The appearance of a hemi-lenticular structure (**Figure 3.7, Table 3.2**) usually with a radiolucency on either side is seen in 8-of-12 HA-coated tibial walls, where fixation was

measured to be low (FR<20%). The medial side of the structure facing the implant is flat but angled away from the implant wall. This structure is suggestive of initial bone growth on the surface of the implant wall, which had later delaminated from the implant wall surface. Such delamination may explain the bimodal nature of radiographs, where poor tibial wall fixation is seen in the HA cohort (**Figure 3.6**). With the HA+MPC cohort, stronger mechanical fixation at the implant wall may have reduced such delamination, with bone growth less likely to be sheared off the wall, explaining the reduced incidence of the hemi-lenticular structure (**Table 3.2**) and improved tibial wall fixation (**Figure 3.6**). In contrast, none of the uncoated cemented tibial walls demonstrated this sign, likely because bone never grew against the wall surface.

All radiographs assessed in this study had fixation at the superior aspects of the tibial wall only if the inferior aspects of the tibial wall were also fixed. No radiographs were found to have fixation at a superior aspect of the wall if a more inferior aspect was not fixed. It is not clear why this happens. It may relate to the amount of micromotion occurring at the interface, with more micromotion at the top rather than the bottom. Alternatively, cancellous bone may be more likely to fix to the implant than cortical bone and the lower part of the wall is in contact primarily with cancellous bone and the upper part with cortical bone.

One limitation of this study is that it was conducted on radiographs collected from three separate (though each consecutive) cohorts from 2005-2007, 2014-2015, and 2016-2017 so other factors that changed with time may have influenced the outcomes assessed. However, identical indications were used for all cohorts and identical techniques were used for the two cementless cohorts. With cemented fixation, the technique was the same as the cementless (apart from a narrower keel slot preparation), and it is unlikely this

would have influenced wall fixation. A novel finding of the study was the hemi-lenticular structure at the interface that was most common in the HA-only walls. It is postulated that this was caused by bone forming on the wall and then delaminating. To determine how it formed would require a time-course analysis of serial radiographs.

3.6.6 Conclusion

This study has shown that tibial wall fixation in the Phase 3 cemented Oxford UKR is poor. It improves with a hydroxyapatite coating and improves further with a microporous titanium coating, found in the Cementless Oxford UKR. Fixation at the wall is consistently ‘bottom-up’, with fixation at the superior aspect of the wall present only when the inferior aspect is fixed. The implications of radiographic fixation to load transmission across the wall requires further assessment. Nonetheless, improved tibial wall fixation may explain the lower levels of in pain observed with cementless rather than cemented fixation.

3.7 The Effect of Tibial Component Fixation on Pain

3.7.1 Limitations in Current Knowledge

A small randomised study by Gulati et al of 161 knees found fixation to be unrelated to patient reported pain and function based on the OKS, AKSS, and TAS [157]. A similar study by Panzram et al in a different centre using OKS, AKSS, and a VAS, found similar results [158]. The method for identifying radiolucencies was identical in both studies. The tibial floor and keel were divided into six zones, and presence of radiolucency in each zone was scored with a binary yes/no outcome. Gulati et al then categorised results into total radiolucencies (if all zones were scored 'yes'), partial radiolucencies (if some but not all zones were scored 'yes'), and no radiolucencies (if no zones were scored 'yes'). Panzram et al split the cohort into cohorts with and without radiolucencies. In both cohorts, PROM scores within each group were statistically compared and found no difference.

There are limitations with these studies. First, they assessed only the regions directly below the component, and did not assess the tibial wall interface. Second, they did not analyse the keel and floor regions separately. As these regions would likely experience different loading characteristics, the analyses provide limited insight to the effect of no compression (beside the wall), intermittent compression (below the floor), and constant compression (around the keel) on bone.

Furthermore, these studies only assessed the relationship of fixation to magnitude of pain reported, instead of the incidence of pain. The results presented in **Chapter 2** demonstrate that pain scores experience strong floor/ceiling effects in both Cemented and Cementless Oxford UKR, and that the greatest difference observed was in the actual

incidence of pain with 61% cementless compared to 43% cemented patients stating that they have no pain at all. This difference is highly clinically relevant to patients. Finally, based on calculations of statistical power performed in **Section 2.2**, the cohort size would be underpowered to show statistical differences, at least with the Oxford Knee Score.

Therefore, a comprehensive radiographic study measuring radiolucencies at the tibial wall, floor, and keel, and their effects on different measures of pain, does not exist. To reliably assess the relationship between pain and tibial component fixation, such a study needs to be performed.

3.7.2 A Protocol to Assess Radiolucencies around the Tibial Component

The studies performed by Gulati et al [157] and Panzram et al [158] outline methods to assess tibial floor fixation. However, they have two limitations.

First, there was no post-acquisition measurement of radiographic alignment – poorly aligned radiographs will result in the implant masking adjacent radiolucencies. For assessment of the tibial wall (in **Section 3.6**), this was resolved using a Horizontal Rotation Ratio (HRR). A similar Vertical Rotation Ratio (VRR) can be measured for assessing radiolucencies at the tibial floor. The second limitation was that floor radiolucency was scored using a binary yes/no measurement for each of the 6 regions studied, and consolidated into two or three groups: complete or no radiolucency (or partial). This limits assessment to fixation as a whole, without assessment of individual regions. Therefore, a modified protocol which addresses these limitations was proposed.

First, all radiographs were assessed for vertical rotation using the following method.

$$\textbf{\textit{Vertical Rotation Ratio}}\ (\boldsymbol{VRR}) = \frac{Tibial\ Floor\ Height\ (H_{floor})}{Internal\ Tibial\ Wall\ \ Height\ (H_{wall-I})} \times 100\%$$

With small changes in upward and downward vertical rotation, radiographic H_{floor} will increase rapidly while $H_{wall\text{-}I}$ will be relatively constant. Manufacturing dimensions for H_{floor} is 3.3 mm and $H_{wall\text{-}I}$ is 5.3 mm in all implant sizes. True VRR would be 60%. With the same 1 mm radiolucency threshold as the Horizontal Rotation Ratio (HRR), an upper limit for VRR of 80% will be used.

HRR and VRR were assessed in all radiographs. Thresholds of HRR<50% and VRR<80% were used to select radiographs where all radiolucencies around the tibial component larger than 1 mm will be visible.

Radiographs passing rotation thresholds were assessed for radiolucencies around the component, split into 7 regions. For each region, a score of 0, 1, or 2 was given: 0 indicating no radiolucency, 1 indicating a partial or unclear radiolucency, and 2 indicating a complete radiolucency. Scores for each region were then scaled between 0 and 100, where 100 indicates a complete radiolucency. Three further scores, Tibial Wall Fixation (TWF), Tibial Floor Fixation (TFF), and Tibial Keel Fixation (TKF) were calculated, averaging the radiolucency scores from their constituent regions (**Figure 3.8**).

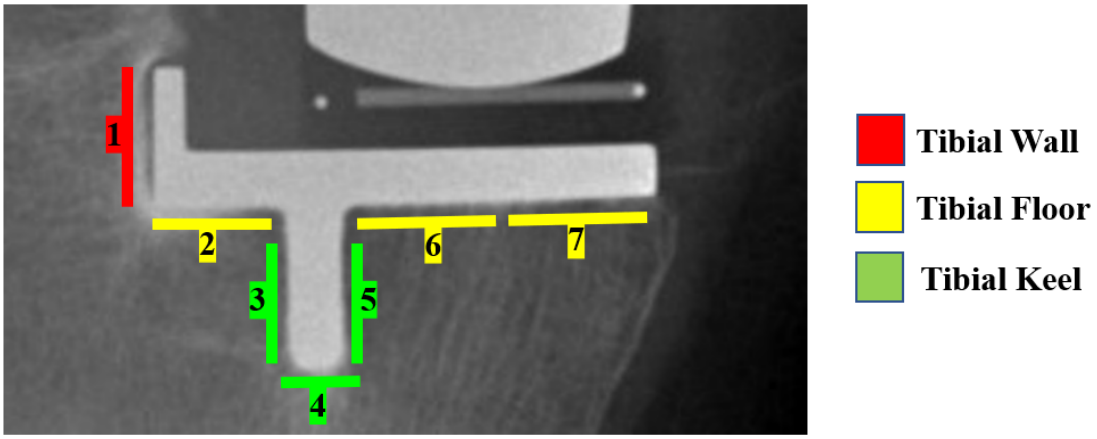


Figure 3.8: *Regions assessed and region grouping used to assess presence of radiolucencies in 5-year study cohort.*

All adequately aligned radiographs were assessed by one observer, and 20% of these radiographs were assessed by a second observer. Inter-observer correlation was assessed to verify reliability of measurement method. Observers were blinded to implant type, though the presence of bone cement can be seen in radiographs.

3.7.3 Software and Statistics

Radiograph measurements were made using ImageJ (National Institutes of Health, Bethesda, Maryland, USA) based on measurement protocols detailed in **Section 3.5**. Inter-observer correlation was performed using SPSS (IBM Corporation, Armonk, New York, USA). Data was analysed and visualised using GraphPad Prism (GraphPad Software, San Diego, California, USA) and Excel (Microsoft, Redmond, Washington, USA).

All data was classified by knee. Radiographic measurements were compared between cohorts using the unpaired Student t-test for parametric (Shapiro-Wilk $p>0.05$), and the Mann-Whitney U-test for non-parametric (Shapiro-Wilk $p<0.05$) distributions. Other statistical tests, where performed, are described in the relevant sections.

3.7.4 Tibial Wall Fixation in 5-year cohort

The 5-year cohort studied in **Chapter 2** was retrospectively reviewed for clinical radiographs at 5 years. Of the 262 cemented patients, 237 had 5-year radiographs. Of the 262 cementless patients, 191 had 5-year radiographs. Of these, 100 cemented and 93 cementless had radiographs which had horizontally aligned radiographs (HRR<50%), and 58 cemented and 46 cementless had both horizontally and vertically aligned radiographs (HRR<50% and VRR<80%).

To validate findings in **Section 3.6**, the Wall Fixation Ratio (WFR) of cemented and cementless knees was first assessed in all horizontally aligned radiographs, using the protocol outlined in **Section 3.5**. The cementless implants in the 5-year cohort were recruited between 2008-2012, prior to the introduction of the microporous coat at the cementless implant wall in 2015. Therefore, all cementless implants in this 5-year cohort have only a hydroxyapatite coating.

Results are consistent between this analysis and analysis performed in **Section 3.6**, with less than 10% differences between study cohorts (**Figure 3.9**, **Table 3.3:** Fixation Ratio in studies performed.). Difference in TWF between cemented and cementless cohorts is highly statistically significant (cemented 19% vs cementless 54%, $p<0.0001$). This validates the findings of both studies.

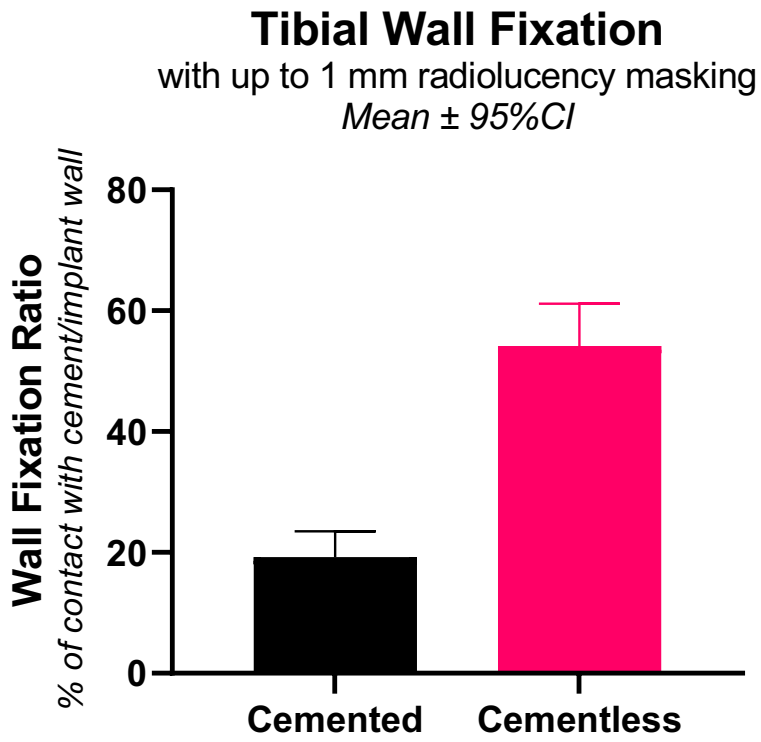


Figure 3.9: *Fixation Ratio at Tibial Wall in 5-year Cemented and Cementless Oxford UKR cohorts.*

Table 3.3: *Fixation Ratio in studies performed.*

Wall Fixation Ratio (%) in horizontally aligned radiographs	**Study of three 1-2 year consecutive cohorts (Section 3.4)**	**Study of 5-year cohort (Section 2)**
Cemented	28	19
Cementless (HA)	53	54
Cementless (HA+MPC)	77	

3.7.5 Tibial Radiolucencies and the Incidence of Pain in 5-year cohort

The protocol outlined in **Section 3.5.2** was used to assess radiolucencies around the tibial component in horizontally and vertically aligned radiographs. Intraclass Correlation Coefficient (ICC) was calculated using a two-way mixed effects model for single measures. ICC for all cohorts separate and combined, were excellent (cemented 0.930, cementless 0976, all 0.941).

Comparing the regions assessed, both cemented and cementless cohorts had most radiolucency at the tibial wall (Region 1), followed by the medial-most aspect of the tibial floor (Region 7), followed by the lateral-most aspect of the tibial floor (Region 2) (**Figure 3.9, Table 3.3**).

Comparing between cemented and cementless cohorts, radiolucencies were significantly greater in the cemented cohort across all regions (**Figure 3.9, Table 3.3**). An overall difference between cemented and cementless components was found across Tibial Wall, Tibial Floor, and Tibial Keel as well (Chi-Square Test, p=0.0466).

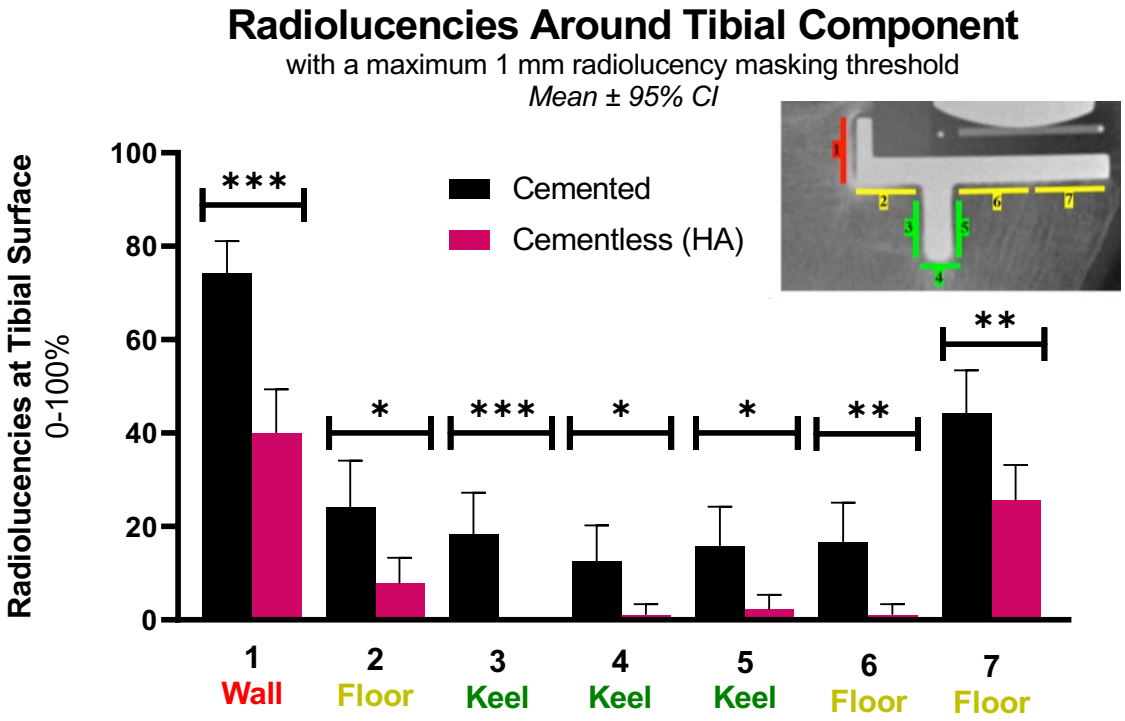


Figure 3.10: *Radiolucencies around the tibial component in 5-year Cemented and Cementless (HA) Oxford UKR cohorts. *: p<0.05. **: p<0.01. ***: p<0.001.*

Table 3.4: *Comparison of Radiolucency Score in Specific Regions and Combined Scores in 5-year Cemented and Cementless (HA) Oxford UKR cohorts. Difference between cohorts across regions is visualised using a colour scale, where red indicates a relatively greater difference.*

Radiolucency Score	Cemented	Cementless (HA)	Difference between cohort	p value
Region 1/Tibial Wall	74.2	40.0	34.2	<0.0001 (****)
Region 2	24.2	7.78	16.4	0.0334 (*)
Region 3	18.3	0.00	18.3	0.0003 (***)
Region 4	12.5	1.11	11.4	0.0159 (*)
Region 5	15.8	2.22	13.6	0.0108 (*)
Region 6	16.7	1.11	15.6	0.0024 (**)
Region 7	44.2	25.6	18.6	0.0070 (**)
Average of Regions 2,6,7 (Tibial Floor)	28.3	11.5	16.8	0.0007 (***)
Average of Regions 3,4,5 (Tibial Keel)	15.6	1.11	14.5	0.0008 (***)

All scores are non-parametric (Shapiro-Wilk $p<0.05$). Mann-Whitley U-test performed in all cases. *: $p<0.05$. **:$p<0.01$. ***:$p<0.001$. ****:$p<0.0001$.

Of the PROMs studied in the 5-year cohort (covered in **Chapter 2**), this section will focus on results from the Intermittent and Constant Osteoarthritis Pain (ICOAP) Total score. The score covers pain intensity and the pain's effect on sleep, social, and emotional factors. An important feature of the ICOAP (Total) score is that all 11 questions give a score between 0 and 4, where 0 refers to 'no pain at all'. Therefore, a patient scoring 0 across all ICOAP questions indicates that they have no pain or pain-related concerns about their knee.

Therefore, patients scoring ICOAP (Total) = 0 were grouped into 'No Pain' and patients scoring ICOAP (Total) ≠ 0 were grouped into 'Pain', allowing for a comparison of incidence of pain. These groups were used to compare the relationship between radiolucency and incidence of pain in the 5-year cohort (**Figure 3.10)**.

Radiolucency was associated with incidence of pain in all regions of the tibial component (wall, floor, keel) in cemented and cementless cohorts. This was statistically significant in the floor in cemented ($p=0.046$) and cementless ($p=0.033$) cohorts, and keel in the cemented cohort ($p=0.022$). However, where differences were not statistically significant, scores were very low (keel in cementless cohort) or had relatively large variability (wall in cemented and cementless cohorts), rendering the study potentially underpowered to detect differences in these regions.

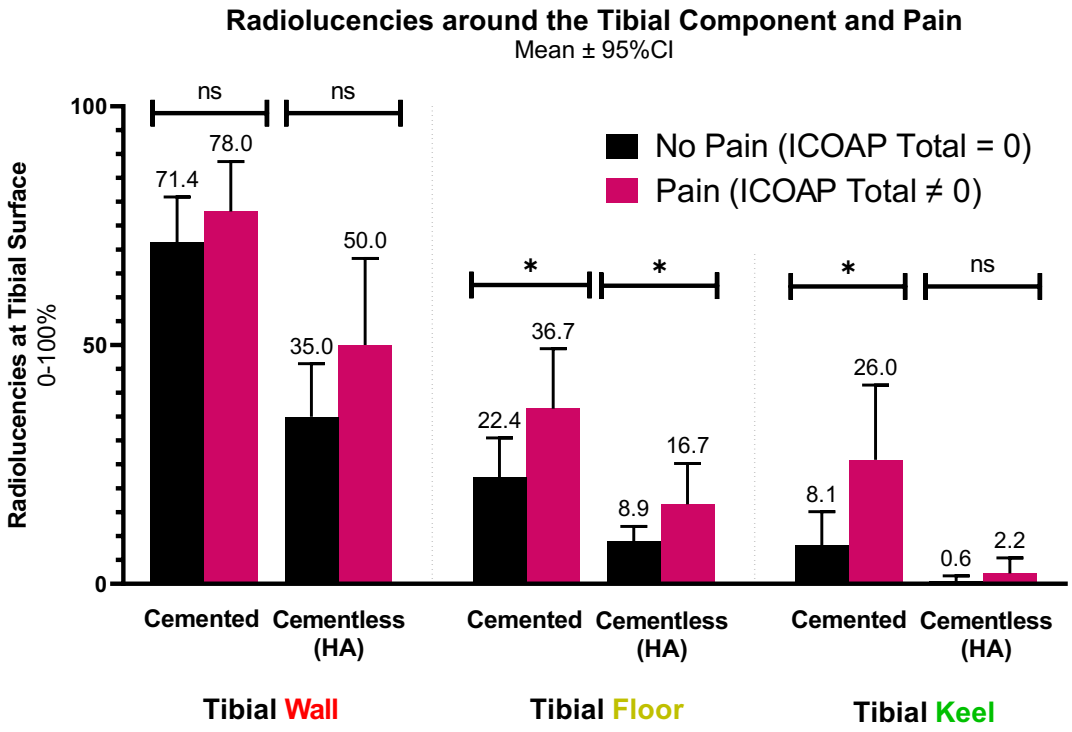


Figure 3.11: *Radiolucencies at the Tibial Wall/Floor/Keel and Incidence of Pain in 5-year Cemented and Cementless (HA) Oxford UKR cohorts. ns: p≥0.05. *: p<0.05.*

To assess if there was a further relationship between radiolucency and the magnitude of pain, linear regression analysis was performed, assessing correlation between radiolucencies at the tibial component wall/floor/keel and ICOAP (Total) (**Figure 3.11**). Variables were largely unrelated; the only statistically significant correlation is at the cemented component keel (**Figure 3.11e**). Further analysis shows that radiolucency at the tibial keel in cemented components is bimodal - there is likely to be either no radiolucency or full radiolucency. If there is full radiolucency, it is significantly correlated with pain. Radiolucencies at the cementless tibial keel are effectively non-existent.

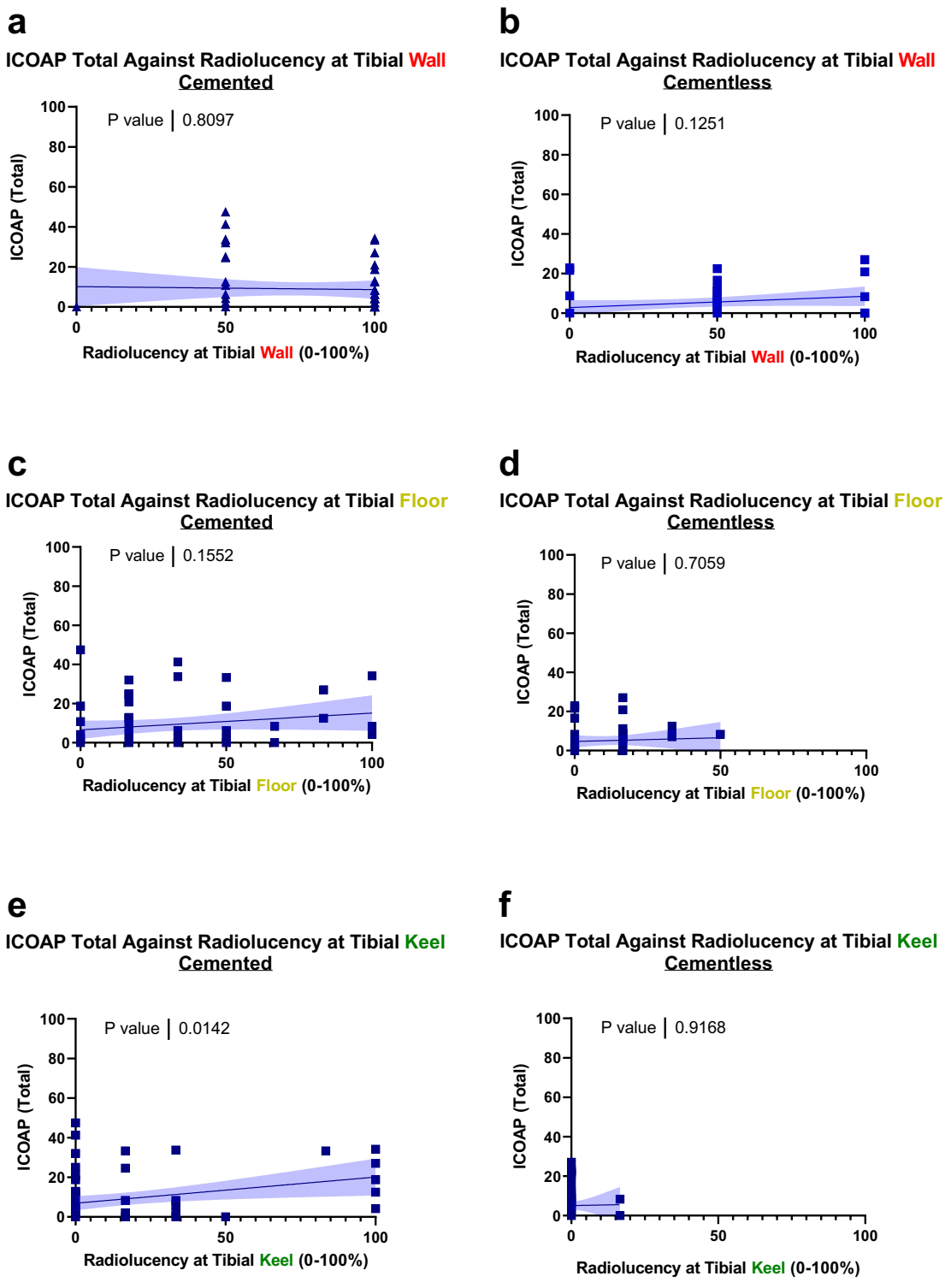


Figure 3.12: *ICOAP (Total) scores against Radiolucency at the Tibial Wall/Floor/Keel in Cemented and Cementless cohorts.*

Similar correlations were performed between radiolucency at wall/floor/keel and Oxford Knee Score (OKS) Pain, Function, and Total Scores, ICOAP 'A' (Constant Pain), ICOAP 'B' (Intermittent Pain), and Tegner Activity Score. Results are included in **Appendix B**. The only correlations were with ICOAP 'B' (intermittent pain) a constituent of ICOAP 'Total'. There was no correlation with ICOAP 'A' (constant pain) scores.

3.7.6 Discussion of Findings

Radiolucencies were more likely in patients who report experiencing pain in both cemented and cementless Oxford UKR cohorts. This is a new and important finding not reported in literature. However, there is no reliable relationship between radiolucency and magnitude of pain, consistent with the findings of Gulati et al [157] and Pazram et al [158]. The difference in relationship with incidence and magnitude of pain appears to be conflicting. The lack of a relationship between radiolucency and magnitude of pain may arise from the strong floor and ceiling effects seen in the scores studied (discussed in **Section 2.8**). These effects minimise differences in magnitude of pain, and would mask any relationship if there were present. Therefore, we cannot reliably exclude a relationship between radiolucency and pain magnitude with existing data.

ICOAP 'Total' pain scores in this study appears to stem from differences in intermittent pain (ICOAP 'B'), while there is no relationship to constant pain (ICOAP 'A') or other pain scores (OKS 'Pain'). Intermittent pain is still an important clinical consideration, due to the pain itself and its relationship to reduced function [159].

As radiolucencies have been linked to pain, a first step would be to identify the source of radiolucencies in the cementless cohort. Within the cementless cohort, there are virtually

no radiolucencies in any areas which interface with the porous regions of the tibial component (Radiolucency Score ≤ 2% in Regions 3,4,5,6). In contrast, radiolucencies are greatest at the tibial wall (40%), consistent with the findings of the more precise Wall Fixation Ratio measurements made in **Chapter 3.5** (47%) and **Chapter 3.6.4** (46%). There are intermediate radiolucencies in Zones 2 (8%) and 7 (26%) of the cementless cohort; these are regions which partly interface with the porous coat and partly with a smooth surface coated in hydroxyapatite (see **Figure 3.1a**). The alignment of the radiolucencies generally seen at the tibial floor and the smooth border of the tibial floor, is shown in a sample radiograph in **Figure 3.13**.

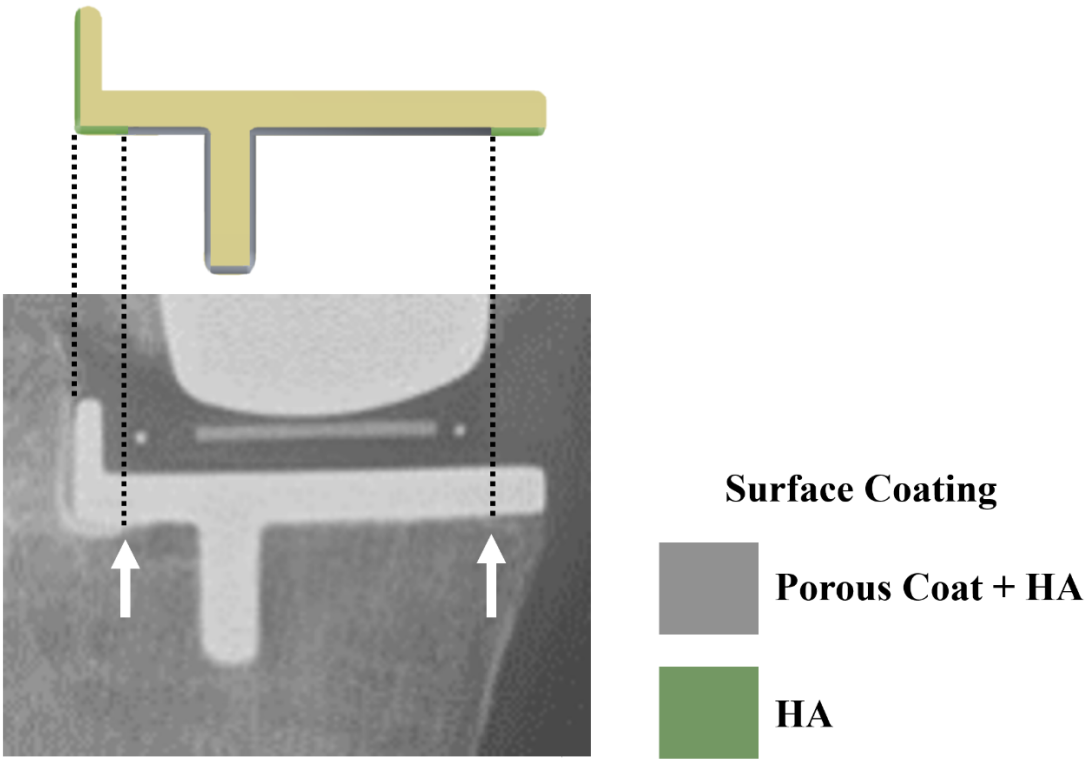


Figure 3.13: *Overlay of an AP radiograph of a Cementless Oxford UKR assessed in this study, against a model of a tibial component and it is bone-facing surfaces. Overlay demonstrates the alignment of the radiolucency locations at the tibial floor with the regions where porous coat is absent. White arrows indicate transition points where radiolucencies begin/end.*

The relationship between pain and tibial wall radiolucency has previously been explored (**Section 3.6**), but its relationship to tibial floor and keel radiolucency has not. Though it is generally believed in knee arthroplasty that micromotion is associated with pain [160, 161], a mechanism relating fixation and intermittent pain is not immediately clear. Radiostereometric analyses in literature demonstrate that there is virtually no implant migration after remodelling in the Cementless Oxford UKR [149]. However, Horsager et al have shown that cemented UKR experience micromotion when loaded in a step-up/down motion, and that micromotion is greater when radiolucencies are present [162]. This can be extended to hypothesise that radiolucencies are linked to increased implant micromotion, which can explain the intermittent pain experienced by patients. Therefore, efforts to reduce radiolucencies at not just the wall, but across all bone-implant interfaces, may therefore help to reduce intermittent pain in the Cementless Oxford UKR. Based on the findings of this study, replacing the non-porous surfaces of the tibial floor and tibial wall with a porous surface may help to improve fixation, thereby reducing pain.

This study only assessed Cementless Oxford UKR tibial components which had hydroxyapatite applied at the tibial wall and floor border. The later version of the cementless tibial component also had a microporous titanium coat also applied to these surfaces. The microporous coat has demonstrated even better fixation, at least at the tibial wall (see **Section 3.5.4**), and its rougher surface would more likely allow both ingrowth and therefore stronger fixation. Further assessment of fixation and pain in this implant would help to test the radiolucency–pain hypotheses discussed above and in **Section 3.6**.

This study has one key limitation. Radiolucency within each region was scored on a 3-point scale, which provides substantially less precision than the Wall Fixation Ratio score. However, a similar approach to the Wall Fixation Ratio score was not possible as

radiolucencies were not as discrete and clear around the floor and keel. Nonetheless, there was adequate granularity to determine patterns in radiolucency in different regions around the component (**Figure 3.9**).

3.7.7 Conclusion

Radiolucencies around the Oxford UKR tibial component are related to the incidence of pain, but not the magnitude of pain. The disparity between incidence and magnitude is likely due to the strong floor/ceiling effects seen in pain scores of most PROMS. Cementless tibial components have significantly reduced radiolucencies than cemented, but radiolucencies were still present in them. These radiolucencies occur almost exclusively at the non-porous regions of the bone-facing implant surfaces, while porous interfaces had virtually no radiolucency. Applying a porous coat onto these additional surfaces may further reduce radiolucency, and pain.

3.8 Chapter Summary

Tibial wall fixation in the Phase 3 cemented is poor, and better in the early Cementless, likely due to the addition of hydroxyapatite. Absence of pain reported by patients with the early Cementless Oxford UKR can be attributed, at least in part, to better fixation at bone-implant interfaces of the tibial component, compared to Cemented Oxford UKR. However, radiolucencies are still present in the cementless tibial component at non-porous surfaces, namely the wall and the border of the tibial floor; these radiolucencies are associated with patients reporting intermittent pain. Furthermore, stronger fixation at the tibial wall surface is likely to transmit tension, restore the "tension band", and may help reduce pain (**Section 3.4**). Therefore, replacing these surfaces with a porous coat may further reduce radiolucencies in these regions and reduce pain. An assessment of radiolucency and pain in the later cementless tibial components with the microporous titanium coat may help to preliminarily validate this.

4 Peri-Keel Bone Density and Pain

4.1 Motivation for Chapter

In **Chapter 2**, the incidence and magnitude of pain in Cementless Oxford UKR were explored. While pain scores were better than Cemented Oxford UKR, a substantial proportion of the cohort still report having some pain arising from the knee. In **Chapter 3**, presence of pain was attributed to greater radiolucencies at the bone-implant interfaces of the tibial component. Radiolucencies were virtually non-existent around the keel of the Cementless Oxford UKR. However, the effect of the keel on bone beyond the bone-implant interface has not been explored in literature.

Therefore, this chapter seeks to explore the changes in bone density around the keel of the tibial component, and the effect of these changes on patient-reported outcomes.

4.2 Peri-Prosthetic Effects of Inserting a Cementless Keel

In the Cementless Oxford UKR, the keel is the main fixation element of the tibial component. It is a vertical protrusion at the base of the tibial component and is inserted with an interference fit into a slot in the tibia. This interference fit, along with compressive forces through the knee joint, are responsible for ensuring the tibial component does not loosen [75]. In the previous chapter, it was shown that the bone around the keel also had a nearly no radiolucencies, demonstrating its benefits to long-term fixation after bone remodelling (**Section 3.7.5**). However, the effect of this keel structure on the density of surrounding bone mass is not well understood.

Bone is living tissue which remodels to support loads it experiences. Remodelling patterns are classically described by Wolff's Law [163], where increased bone usage (i.e. loading) conserves and increases bone density, while disuse (i.e. lack of loading) results in bone resorption and reduced bone density. After a UKR procedure, bone can be expected to remodel due to three reasons. First is the introduction of interference-induced compressive forces at the keel. Second, the replacement implant does not have identical joint mechanics to the joint tissue it replaces, resulting in differing loading of the underlying bone. Third, the introduction of a bone-implant interface where the metal alloy is significantly stiffer than its surrounding bone. This introduces the possibility of peri-prosthetic zones of load concentrations and isolations developing in the bone surrounding the implant.

Bone around the tibial component can be expected to adapt to the new loading patterns experienced. Based on Wolff's Law and further physiological understanding of bone growth, bone which experiences increased load can be expected to increase in its bone mineral density [163]. These may be a product of internal loads (e.g., when tibial

component is inserted with a press-fit) or applied loads (e.g., transferred from the femur to the tibia when joint is loaded during walking). However, the actual mechanical patterns of bone response to internal and applied loads in the tibia are not well characterised. It is not clear if remodelling reduces internal loads and fortifies against applied loads in peri-prosthetic bone. It is also unclear these changes affect patient outcomes.

4.3 Concerns about varying Bone Radio-Opacity around the Tibial Keel

It was observed that there is sometimes varying bone radio-opacity around the keel of cementless UKR tibial components. This may be a cause of clinical concern. Three randomly selected clinical AP radiographs have been included below, which demonstrate patterns of varying bone radio-opacity around the keel (**Figure 4.1**).

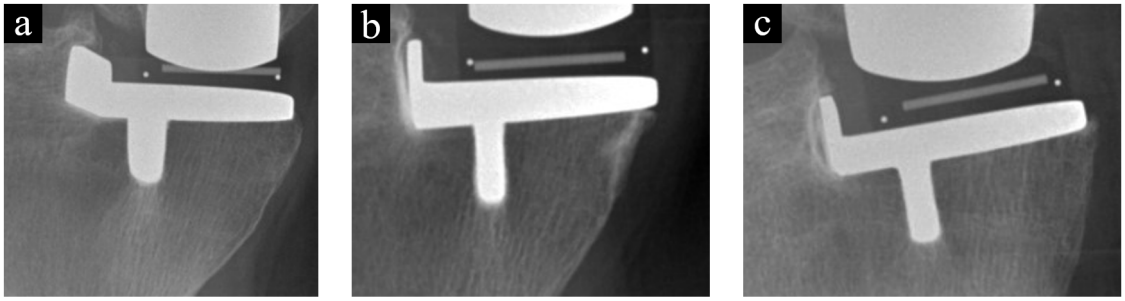


Figure 4.1: *Three 5-year AP radiographs demonstrating consistent patterns of varying radio-opacity in bone.*

It is not known if the presence, or magnitude, of increases and decreases in bone radio-opacity around the keel, are relevant to patient outcomes. Radio-opacity is influenced by a number of factors, and changes in radio-opacity cannot be assumed to be due to bone mineral density without addressing these other factors (discussed in **Section 4.5**).

Nonetheless, it is generally understood that bone mineral density is relevant to bone strength, and that loss in bone mineral density and associated loss in bone strength can increase fracture risk [164]. Low bone mineral density is also associated with implant migration [165]. Subchondral cortical bone thickness and trabecular bone loss is deemed to be clinically relevant to surgical outcomes [166].

4.4 Chapter Aims

The overall aim of this chapter is to quantify and address the potential clinical concerns raised in **Section 4.3** – is there variability in bone density observed around the cementless tibial keel, and if so, is it of clinical concern?

This will be achieved by performing an objective assessment of bone density around the keel to determine if there is a true pattern, and later, using this measure to assess the relationship between bone density changes and clinical outcomes.

First, a novel protocol was developed to measure radio-opacity around the keel and process the data to quantify bone density changes around the keel. This will be performed in clinical radiographs.

Second, the relationship between bone density around the keel, and relevant characteristics and patient-reported outcomes, particularly pain, will be analysed.

4.5 A Protocol to Assess Bone Density in Plain-Film Radiographs

Plain-film radiographs are generally not used to assess bone mineral density. This is due to noise introduced by soft tissue and other non-bone substances. Therefore, bone density is more commonly assessed using Dual-Energy X-ray Absorptiometry (DEXA) scans [167, 168], a technique involving the imaging using x-rays of two different energy levels – the higher energy x-rays penetrate soft tissue, while the lower energy x-rays are attenuated by soft tissue. Information from the lower energy scan is subtracted from the higher energy scan, giving bone mineral density.

Despite lacking this subtraction, it has been shown that there are significant correlations between bone mineral density and radio-opacity in plain-film AP radiographs, in subchondral trabecular bone [169]. However, there are challenges in attempting to assess bone density in these radiographs. X-rays of only one energy level are used, which are attenuated not only by bone but also soft tissue (albeit to a lesser extent). This results in signals on a radiograph arising from both bone and soft tissue. Furthermore, plain-film AP radiographs are two-dimensional images which summate the three-dimensional thickness of bone to a single plane, resulting in bone thickness confounding density information.

To assess bone density around the keel using standard radiographs while mitigating the abovementioned challenges, a novel method utilising ImageJ (National Institutes of Health, Bethesda, Maryland, USA) was proposed.

1. Digitised AP radiographs in DICOM format (DICOM Standard, ISO 12052:2017) were encoded to JPEG format (JPEG standard, ISO / IEC 10918), and imported into ImageJ software.
2. Within ImageJ:
    a. The shape and size of the keel in the radiograph was measured.
    b. The average grey value of the pixel within 9 keel-sized regions (U1, U2, U4, U5, L1, L2, L3, L4, L5) directly adjacent and below the keel are measured, as per the **Figure 4.2**, and recorded. The grey value of each pixel in the JPEG format a value between 0-255, where 0 is black and 256 is white (JPEG standard, ISO / IEC 10918).

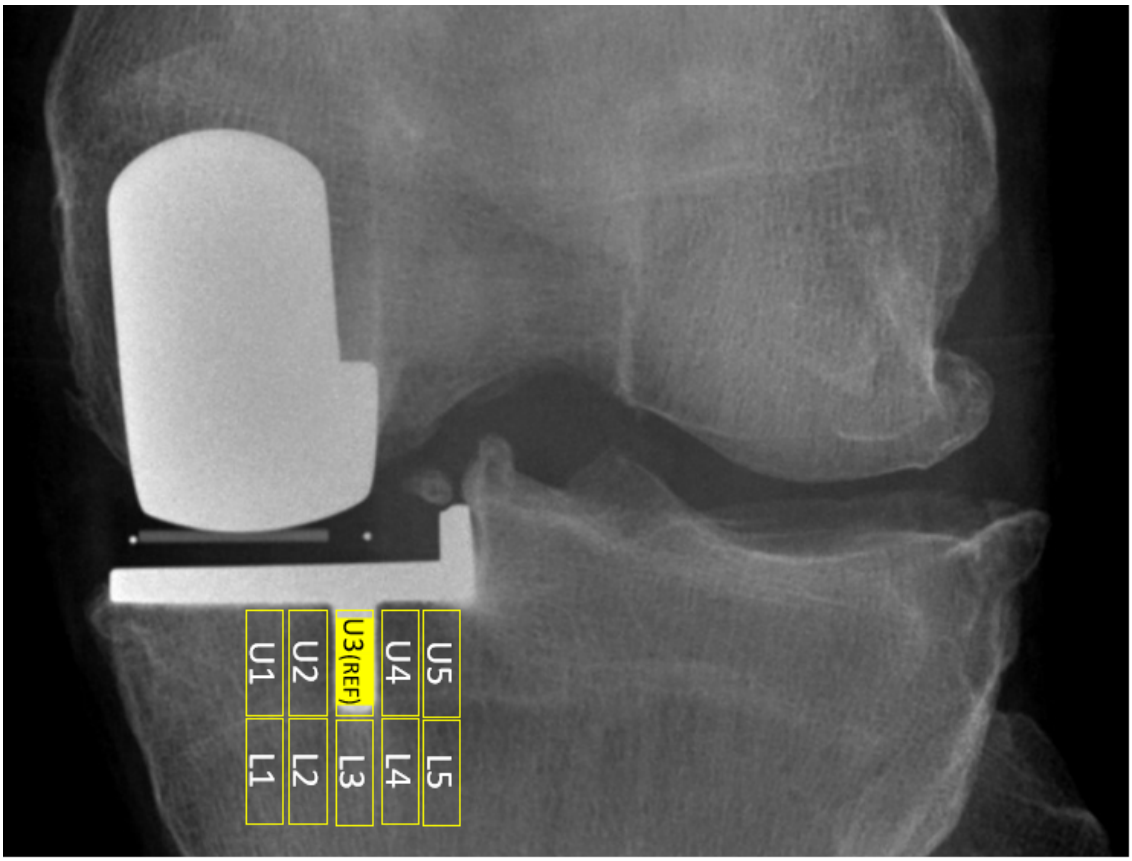


Figure 4.2: *Regions assessed in study. Size of keel, which is constant for all implant sizes, was used as a reference for region size. Regions were termed U1-U5 at the level of the keel and L1-L5 at the level immediately below the keel, where '1' referred to the most medial region. U3 was the keel itself and was left out of analyses.*

3. The average grey value across all nine regions in each radiograph was calculated.
4. A Standardised Opacity Value (SOV) was calculated based on Grey Values (GV), defined as:

$$SOV_{Region\ X} = \frac{GV_{Region\ X} - \overline{\sum GV}}{\overline{\sum GV}} \times 100\%$$

5. Change in SOV (ΔSOV) was calculated as the difference in SOV between two time points.

$$\Delta\text{SOV} = SOV_{5-year\ radiograph} - SOV_{post-operative\ radiograph}$$

6. A composite score was generated to represent the magnitude of bone remodelling in regions directly interfacing with the keel component. This peri-keel composite remodelling score takes the average magnitude of SOV change in U2, U4, and L3.

$$\text{Perikeel Composite Remodelling Score} = \frac{|\Delta\text{SOV}_{U2}| + |\Delta\text{SOV}_{U4}| + |\Delta\text{SOV}_{L3}|}{3}$$

The SOV provides a percentage value representing the relative opacity of a region compared to all other regions, which allows for comparisons between radiographs to be performed. If time-course radiographs were available for the same implanted knee, ΔSOV can be calculated for each region. Cohort analysis and statistical comparisons were performed on radiograph measurements, patient demographics, and PROMS.

ΔSOV provides a percentage value that represents the change in radio-opacity within a peri-keel region between two timepoints. Assuming no heterogenous osteoporotic patterns, no heterogenous soft tissue changes, and no changes in bone anatomy, ΔSOV would be affected primarily by changes in bone density within each region.

Continuous values were tested using the unpaired Student t-test for parametric (Shapiro-Wilk $p>0.05$), and the Mann-Whitney U-test for non-parametric (Shapiro-Wilk $p<0.05$) distributions. Discrete categories were assessed with the chi-square test. Data was analysed and visualised using GraphPad Prism (GraphPad Software, San Diego, California, USA) and Excel (Microsoft, Redmond, Washington, USA). Inter-observer correlation was performed using SPSS (IBM Corporation, Armonk, New York, USA).

4.6 Study Cohort and Method

This study aimed to assess the effect of Cementless Oxford UKR implantation on tibial bone remodelling (i.e., increases and decreases in bone density) at 5 years, and to explore the relationship of this remodelling to underlying patient attributes and patient-reported outcomes (PROMs).

Post-operative and 5-year radiograph AP radiographs were obtained from the follow-up of knees implanted with a medial Cementless Oxford UKR in the 5-year outcome cohort discussed in **Chapter 2**. Patient demographics and patient-reported outcome scores were collected as well, as reported in **Chapter 2.**

The mean age at surgery was 65 years old. The overall cohort was 58% male, with 51% of implants in the right knee. The most common size of tibial component used was 'C'.

Table 4.1: *Cohort characteristics.*

Property	Proportion of cohort
Age at surgery	Mean 64.9, SD 12.6 (years)
Gender	58.2% male, 41.8% female
Knee	50.8% right, 49.2% left
Tibial Component Size	AA: 0% A: 1.1% (100% female) B:10.6% 100% female) C: 27.5% (81% female, 19% male) D: 20.6% (30% female, 70% male) E: 22.2% (100% male) F: 16.9% (100% male)

115 knees were identified which had both post-operative and 5-year AP knee radiographs. Post-operative radiographs were defined as any radiograph taken after surgery while staples were still present. Radiographs performed between 4-6 years after surgery (mean 4.95, SD 0.29) were considered 5-year radiographs.

At 5 years after surgery, patients also completed the Oxford Knee Score (OKS), Intermittent and Constant Osteoarthritis Pain (ICOAP) score, and Tegner Activity Score (TAS). Scores were scaled from 0-100, where 100 is better. These scores are described in **Chapter 2**.

Radiographic assessment was performed on all radiographs as per the protocol outlined **in Section 4.5**. One operator performed measurements in radiographs from all cases, and an independent second operator performed measurements on a random selection of 20% of cases. Inter-operator correlation was assessed.

4.7 Bone Density Changes around the Cementless Keel

All raw grey value measurements performed by both observers were compared using Intraclass Correlation Coefficient (ICC) for validation of method. ICC was calculated using a two-way mixed effects model for single measures. ICC was 0.999 – excellent (**Figure 4.3**).

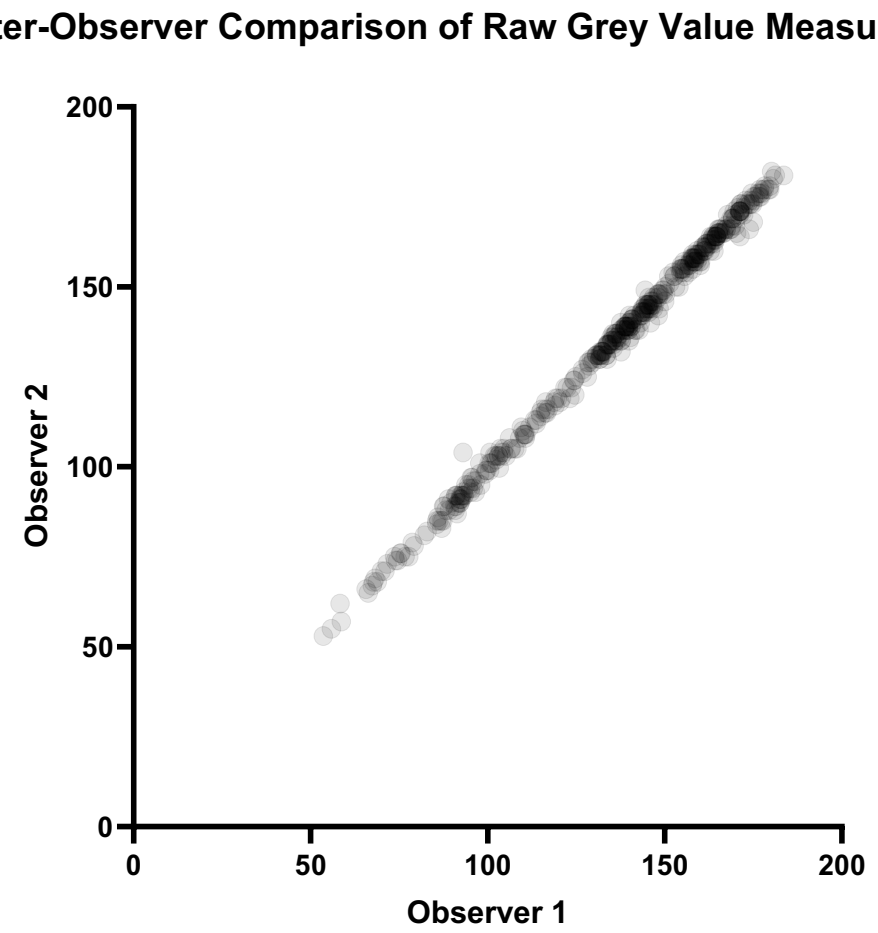


Figure 4.3: *Comparison of raw grey values measured by both observers.*

Post-operatively, the SOV of the L1/L2 region was lower than other lower regions, while U4 was greater than other higher regions (black bars in **Figure 4.4**).

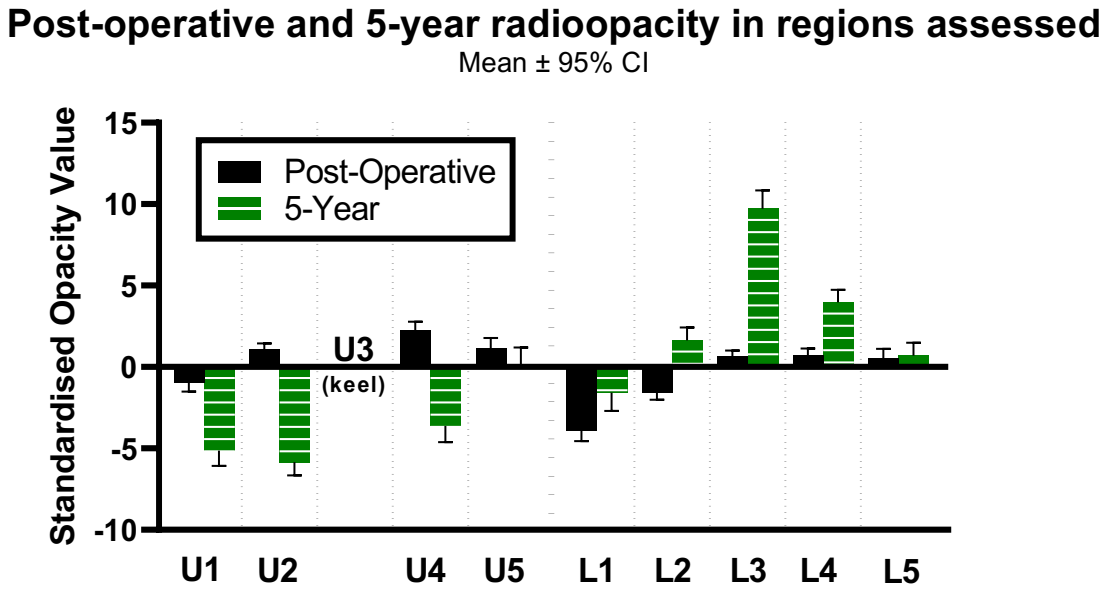


Figure 4.4: *Post-operative (black) and 5-year (green) Standardised Opacity Values in regions assessed.*

The change in SOV between the 5-year and post-operative radiographs was calculated for each region in all radiographs (**Figure 4.5**). Change in SOV would represent bone densification (if positive) and resorption (if negative), due to bone remodelling between the post-operative and 5-year timepoints after surgery. The results show a significant increase in density in the area directly below the keel compared to the next highest region (L3 vs L4, 9.1% vs 3.3%: $p<0.0001$), and a significant reduction in density in the regions beside the keel compared to respective adjacent regions (U2 vs U1, -6.2% vs -4.9%, $p<0.0001$ and U4 vs U5, -5.9% vs -1.0%, $p<0.0001$).

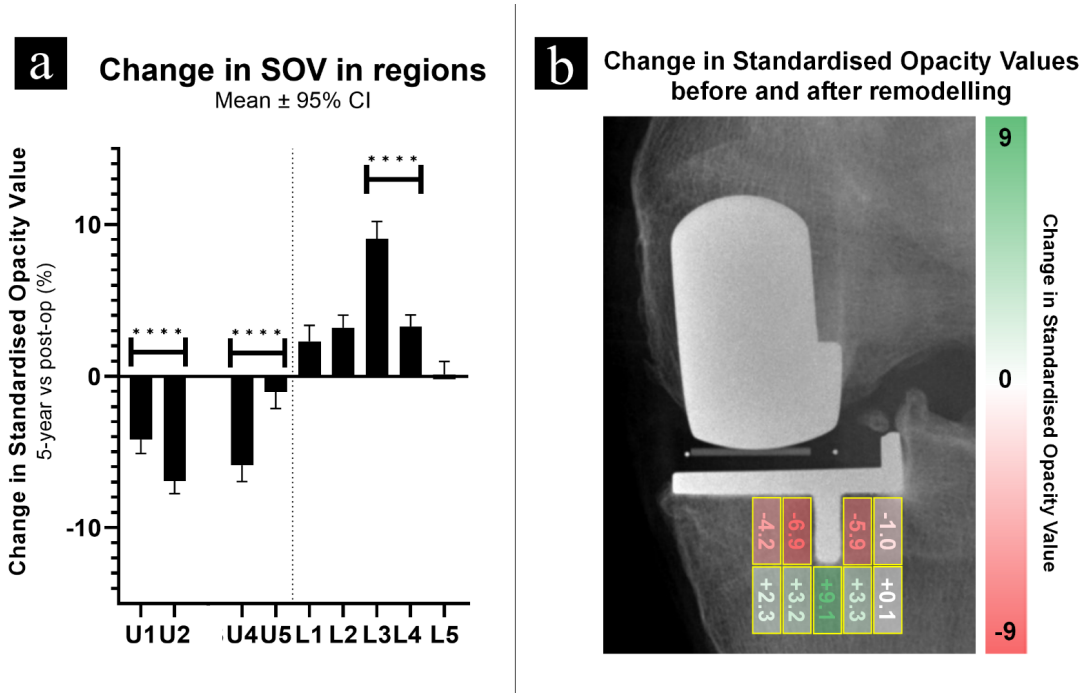


Figure 4.5: *Change in Standardised Opacity Values for each region between postoperative and 5-year radiographs, indicating relative changes in bone density for each region.* ***(a)*** *Change in Standardised Opacity Values for each region, with significant differences shown ****: p<0.0001.* ***(b)*** *Mean changes in Standardised Opacity Values overlayed on a radiograph to demonstrate average change in each region.*

Peri-keel composite remodelling score found that more remodelling occurred in anatomically smaller tibias, which require smaller tibial components (One-way ANOVA, p=0.0149) (**Figure 4.6**). Post-operative and 5-year radiographs for the smallest tibial component (A), and one of the largest (F) in the study are shown in **Figure 4.7** and demonstrate the differences in remodelling.

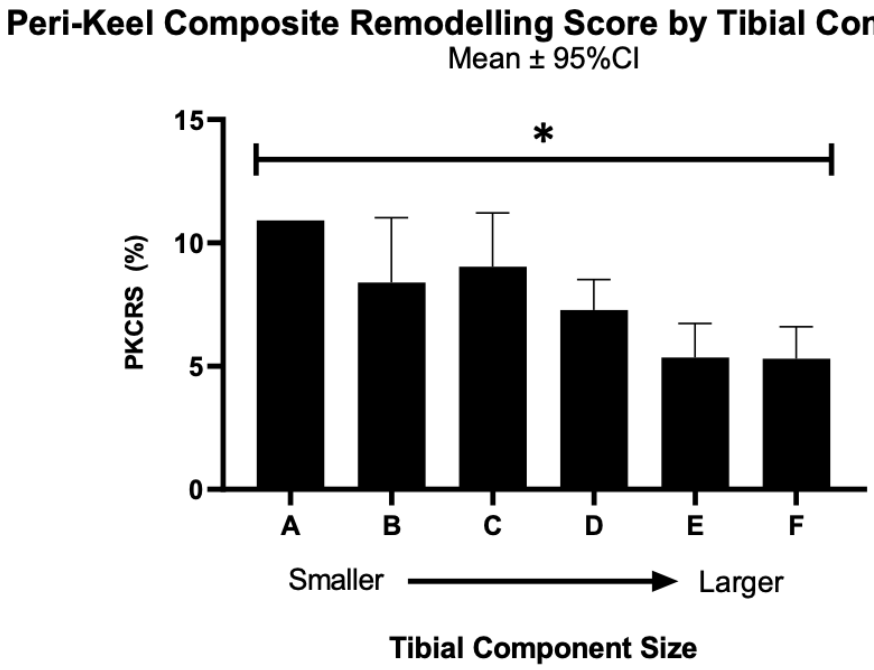


Figure 4.6: *Peri-keel Composite Remodelling Score by Tibial Component Size. Effect of size significantly related to remodelling. **: p<0.01.*

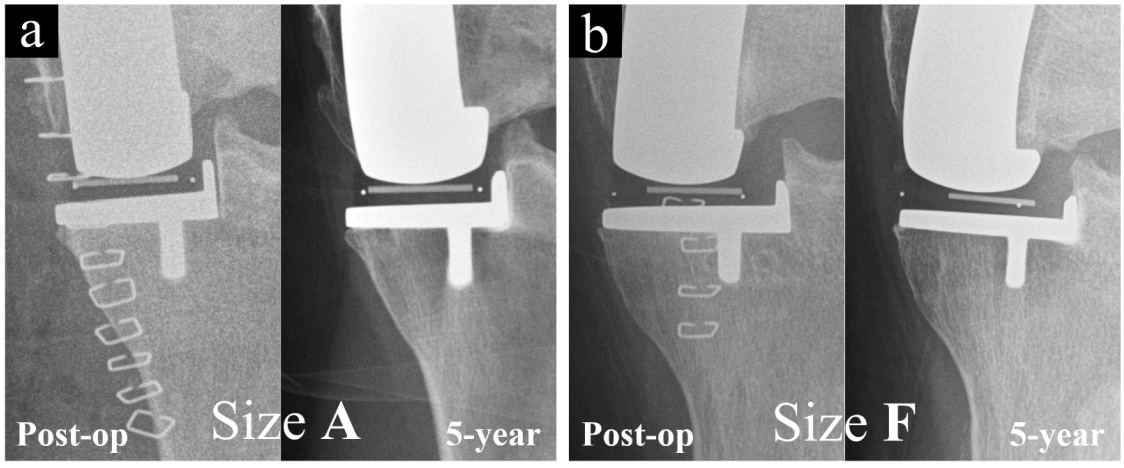


Figure 4.7: *Post-operative and 5-year radiographs for Size A and one Size F patient included in study. Post-operative radiographs in both knees indicate similar bone density around keel. 5-year radiographs indicate greater remodelling around keel in Size A than Size F, consistent with study findings.*

A direct comparison of males and females was not appropriate as females were more likely to have a smaller implant size (**Table 4.1, Figure 4.8a**) – size may be a confounding factor. Therefore, a matched comparison of cases by implant size was performed. Matching produced a comparison of 14 females and 14 males (implants in females: 43% 'C', 57% 'D', implants in males: 43% 'C', 57% 'D', randomly chosen). Remodelling was found to be significantly greater in females than males (females 10.7 vs males 5.9, p=0.0106) (**Figure 4.8b**). There was no relationship between the peri-keel composite remodelling score and age (R^2=0.001) and BMI (R^2=0.002).

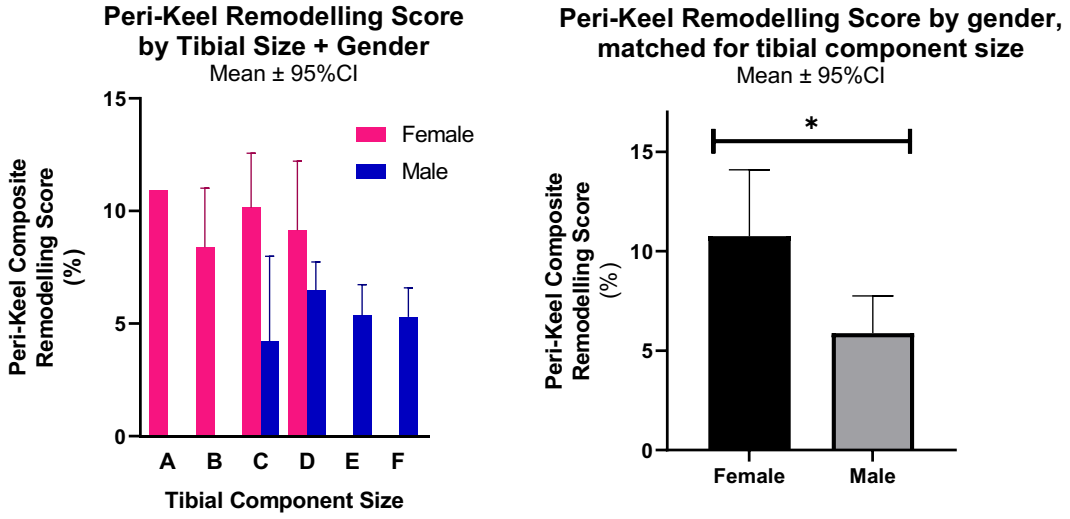


Figure 4.8: (a, left) *Peri-keel Composite Remodelling Score for each tibial component size from Size A to Size F (no patients in study had a size AA implant), split by female (pink) and male (blue).* ***(b, right)*** *A size-matched comparison of Peri-keel composite remodelling score by sex. *:p<0.05.*

There was no statistically significant relationship between magnitude of remodelling and patient outcomes at 5-years: OKS Pain (R^2=0.017, p=0.168), OKS Function (R^2=0.030, p=0.068), OKS Total (R^2=0.028, p=0.074), ICOAP 'A' (constant pain, R^2=0.009, p=0.327), ICOAP 'B' (intermittent pain, R^2 =0.007, p=0.363), ICOAP Total (R^2 =0.011, p=0.258), TAS (R^2 =0.020, p=0.135), incidence of pain (p=0.343). (**Figure 4.9**).

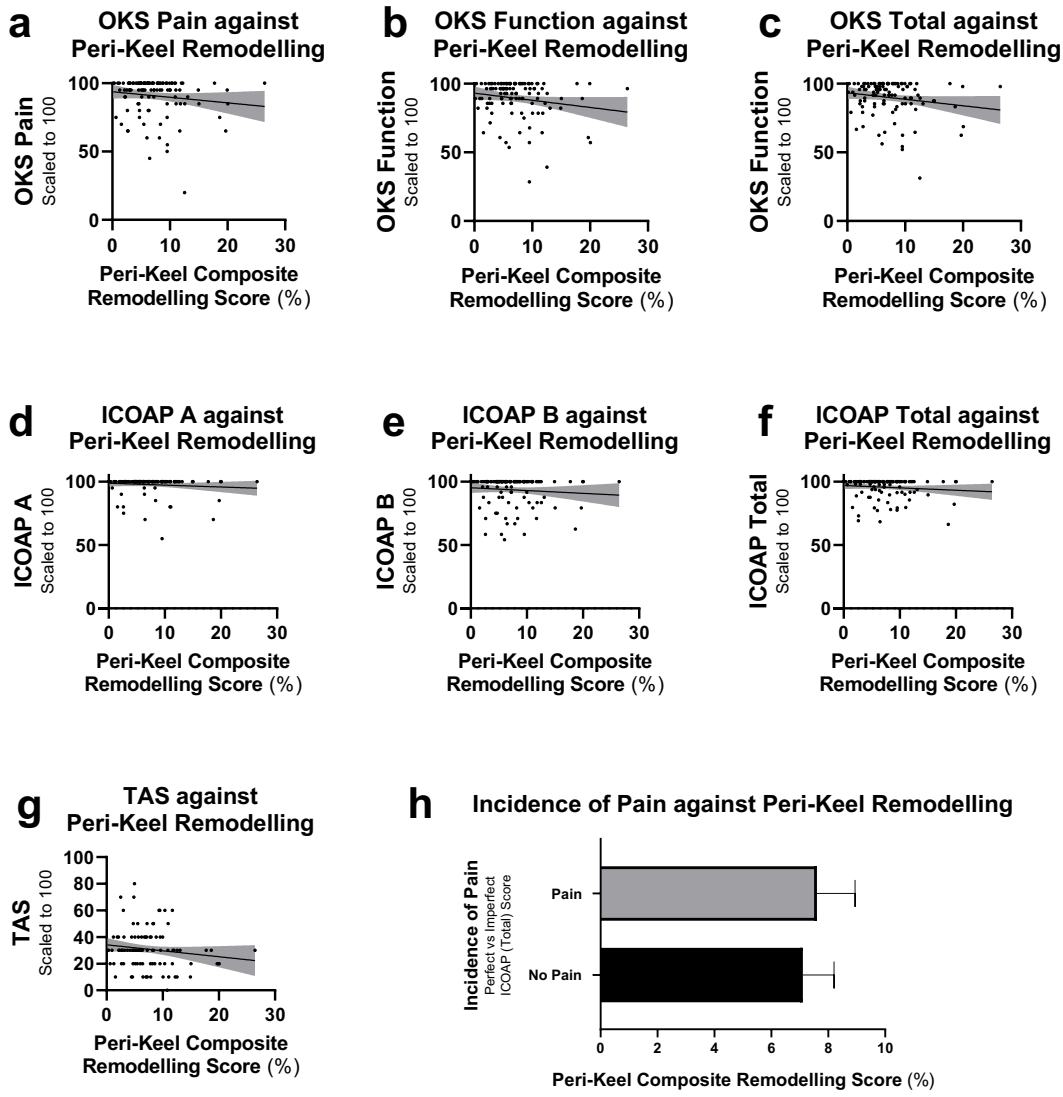


Figure 4.9: *The relationship between patient-reported pain and function outcomes and the remodelling observed in their keel. Peri-keel composite remodelling score represents magnitude of remodelling. Patient-reported outcomes all scaled from 0-100, and higher is better. Individual values shown as dots, linear regressions shown as solid black lines, 95% confidence intervals for linear regressions shown as in grey.* ***(a)*** *Oxford Knee Score (Pain sub-score).* ***(b)*** *Oxford Knee Score (Function sub-score).* ***(c)*** *Oxford Knee Score (Total score).* ***(d)*** *Intermittent and Constant Osteoarthritis Pain Score ('A' Constant Pain score).* ***(e)*** *Intermittent and Constant Osteoarthritis Pain Score ('B' Intermittent Pain score).* ***(f)*** *Intermittent and Constant Osteoarthritis Pain Score (Combined Pain score).* ***(g)*** *Tegner Activity Score against peri-keel remodelling.* ***(h)*** *Remodelling in patients split into those who experienced pain vs no pain based on ICOAP Total scores.*

4.8 Discussion of Findings

A method to discern changes in bone density around the keel of the Cementless Oxford UKR tibial component using plain film AP radiographs is proposed. With this method, distinct remodelling patterns have been noted around the keel. Remodelling is greatest at the regions directly adjacent to the keel, with substantial densification of bone below the keel, and substantial resorption adjacent to the keel. These remodelling patterns occur consistently in knees of all sizes. Remodelling is significantly greater in smaller knees and in females more than males, although the relative importance of size and gender is not clear as these are related. The extent of remodelling is not related to pain and function reported by patients at 5 years.

At 5 years, it can be expected that bone remodelling around the tibial component would be affected by applied loads experienced in medial tibial condyle. In cementless press-fit total hip stems, surrounding bone has been found to maintain or lower in density within 3 months after implantation [13]. In this study (UKR tibias), the increased density below the keel (L3) suggests that loads transmitted through the implant to the tibia travel disproportionately through the bottom of the keel rather than the rest of the tibial plateau. In contrast, the regions directly adjacent to the keel (U2 and U4) are mechanically isolated/shielded from loads, as they pass through the relatively stiffer keel, resulting in significant bone resorption. The effect of latent loads, such as those introduced by press-fit of the keel into the tibia are not well described in literature, but can be expected to be mitigated in the early remodelling period and are unlikely to play at role at 5 years after surgery.

Patient-reported pain or function did not significantly correlate with remodelling around the keel at 5 years, though there appears to be a downward trend. Pain is known to occur

when loads are transmitted through bone which is insufficiently dense to support the load which results in abnormally high bone strain [170, 171]. It has been suggested that the pain that sometimes occurs early after implantation antero-medially in the proximal tibia is due to elevated levels of strain [75, 172] (discussed in **Section 3.4**). However, after 5 years of remodelling, there was no relationship between remodelling and pain or function. Therefore, it appears that, after remodelling, the medial tibial condyle and surrounding anatomy adapts to the new loading patterns it experiences, and the strain in the bone has returned to normal levels, negating it as a source of bone pain.

The extent of remodelling around the tibial component, and particularly around the tibial keel, varies between knee size. Remodelling was found to be significantly greater in smaller tibial components. The depth of the keel is the same in all sizes of tibial components. Therefore, relative to the size of the component and thus the patient, the depth of the keel increases in smaller sizes, resulting in less bone mass supporting loads transmitted through the keel. As a result, in smaller patients, the distance between the medial cortex and the bottom of the keel decreases. This can be expected to increase the stress in surrounding bone. This likely explains why the remodelling is higher with smaller sized components. Furthermore, it would suggest that if depth of the keel decreased in smaller sizes, the remodelling in smaller sizes would be reduced. The greater remodelling in smaller keels is suggestive of higher stresses below the keel, which may play a role in early peri-prosthetic tibial fractures. These tend to be more common in smaller tibial components (Size AA and A) [100, 105]; this will be further discussed in **Section 5.2.1**. A better understanding of physiology underlying the patterns of load distributions, and remodelling observed, may give insights into the aetiology of these fractures.

Remodelling was found to be significantly greater in females over males, independent of size. This difference between sexes has been described in literature and linked to endocrine signalling, though underlying reasons are not clear [173].

The use of plain film radiography to perform a longitudinal, comparative assessment of bone density is novel. While bone density assessments traditionally require the use of dual-energy X-ray absorptiometry (DEXA), it was possible to use plain films as the radiographs were aligned on the components so they were taken in an identical direction and as areas of interest could be accurately defined. Furthermore, as the opacity was adjusted to average baseline values, the method allowed for compensation of differences between radiographs such as the radiographic exposure and varying patient bone density. The time-course comparison between radiographic regions in the same knee accounted for variable bone thickness across the proximal tibia.

There are some limitations to this study. The change in SOV method is unable to account for differences in opacity induced by time-course changes to soft tissue and bone which are not due to keel-related effects (such as changes in soft tissue mass and osteoporosis). Nonetheless, such differences are unlikely to follow the defined opacity patterns seen in this study, and would more likely present as noise. Opacity and density of bone were discretised into keel-sized regions, and therefore possible patterns finer than the size of the keel were lost. While the resolution used was able to identify the remodelling patterns found around the keel, higher-resolution measurements may be able to distinguish finer remodelling patterns not seen with this method. Finally, the study compared radiographs between two timepoints that were 5 years apart, and differences noted represent the total sum of remodelling that occurred between the radiographs. As it is known that most implant remodelling occurs within 3-12 months after surgery [174], and as remodelling

response to the press-fit is likely to occur in a subset of that timeframe, more frequent comparisons could have been performed to better assess the actual time-course of remodelling. However, this was limited due to the use of clinical radiography performed within 12 months following surgery.

4.9 Chapter Summary

Remodelling of trabecular bone around the tibial keel results in increased density in the region below the keel, suggesting increased loads transmitted vertically by the keel, and reduced density in regions directly adjacent to the keel, suggesting shielding from loads as they pass through the relatively stiffer keel. This remodelling is greater in smaller tibial components and in females. Remodelling is not related to patient-reported pain or function five years after surgery, suggesting that bone adapts to the new loading patterns induced by the implant. Therefore, if radiographs show decreased bone density beside the keel and increased density below the keel, this can be ignored at five years after surgery, as it is unlikely to be a source of pain. However, disproportional loading through the keel may play a role in the increased early fracture risk seen in smaller tibias, suggesting that components implanted into such tibias should have smaller keels. This will be explored in the following chapter.

5 Reducing Keel Size in the Cementless Oxford UKR Tibial Component

5.1 Motivation for Chapter

In **Chapter 2**, the Cementless Oxford UKR was shown to result in better pain and function outcomes, and in **Chapter 3**, this was attributed to better fixation at the tibial component. Bone density changes around the keel were found not to adversely affect outcomes in the implant (**Chapter 4**). In literature, the implant is shown to have the lowest revision rate of all commonly used UKR at 10 years [52, 100, 175]. These results suggest that Cementless Oxford UKR should be used when indicated.

Despite these benefits, approximately 7% patients in the UK who fall within the indications for Cementless Oxford UKR are not given the implant, in part due to concerns about the relatively higher incidence of peri-prosthetic tibial fractures in very small (Size 'AA' or 'A') tibias [52]. In Asia Pacific populations, this is estimated to be around 17% of the population [105]. More generally, the Cementless Oxford UKR has approximately two to three times the incidence of fractures compared to the Phase 3 Cemented [100, 175, 176]. These are discussed in detail in **Section 5.2**. The keel is implicated in this increased risk.

Therefore, this chapter aims to assess design changes to the keel in an attempt to address this fracture risk.

5.2 The Nature and Risk of Fracture in the Cementless Oxford UKR

Peri-prosthetic fracture as a cause for revision is approximately 0.2-0.3% [100, 176]. This constitutes 2% of all causes of cementless UKR revision [177]. The true incidence of fracture may be greater, as most studies and registries do not record fractures if they do not result in revision (e.g., if they are treated conservatively, or with procedures circumventing revision such as open reduction and internal fixation).

Fractures involving cementless UKR are overwhelmingly peri-prosthetic medial tibial plateau fractures. 84% of these fractures had no precipitating patient trauma (e.g., a fall). 87% occur within a year of surgery, of which 20% were intraoperative and 62% occurred within 3 months after surgery [178, 179]. Therefore, fractures in the Cementless Oxford UKR can be described as early peri-prosthetic tibial stress fractures.

5.2.1 Fractures in Smaller Tibial Components

There are currently nine studies in literature which assess the incidence of fracture in the Cementless Oxford UKR, identified in a systematic review performed by Burger et al [179]. Two studies, Yoshikawa et al [180] and Leenders et al [181] demonstrated a significantly higher incidence of fractures than the remaining seven studies.

A further study of the Yoshikawa cohort by Hiranaka et al [105] found that there was a seven-fold increase in fracture incidence in very small tibial components (Size ‘AA’ and Size ‘A’) compared to larger ones. The Yoshikawa study was the only Asia Pacific study across the nine studies, performed in Japan [179]. The study by Leenders et al was on a

Dutch cohort, and was likely underpowered (i.e., had insufficient very small tibias) to identify a relationship between tibial component size and fracture incidence [181].

There is limited reporting of the size of tibial components used in literature. In the 5-year cohort presented in **Chapter 2**, only four of the 278 (1.4%) cementless tibias were 'very small' – all four were size 'A' and none were size 'AA'. In an anthropometric study, Yue et al found that tibias were significantly smaller in the 'Asia Pacific' vs 'White' populations [182]. In particular, very small tibias are more common in the Japanese population, reported at 17% in the Hiranaka / Yoshikawa cohort [105].

These findings can be generalised to assert that the risk of fracture risk is highly likely to be greater in very small tibias. Such tibias are rare in 'White' populations, but are significantly more common in 'Asia Pacific' populations.

Presently, surgeons operating on very small tibias (Size 'AA' or 'A') are advised to replace the cementless tibial component with a cemented tibial component, which has a lower fracture incidence of 0.09% [100, 175]. Despite the very low incidence of fracture in very small tibias, UK registry data shows that in 7% of cementless Oxford UKR, the cementless tibial component is swapped for a cemented component (1895 of 26870) [52]. There are very limited indications for use of cemented Oxford UKR tibial component over cementless, such as if the cementless component is peri-operatively assessed to be insecure [75]. Approximately 1.4% patients receiving the implant have very small tibias (based on 5-year cohort studied in **Chapter 2**), compared to the 7% receiving the cemented tibia in place of the cementless – this substantial difference may be an overcorrection due to concerns over peri-prosthetic tibial fracture.

The specific mechanism of fracture in the cementless tibial component has not yet been explored in detail. Literature presenting radiographic evidence of fractures were systematically identified by Burger et al [179], and further identified in other papers discussed in earlier paragraphs. All such evidence was collated and reviewed. Two papers present radiographic evidence of fracture in Cementless Oxford UKR [105, 183] – in both, fractures can be seen to follow the path of the keel in anatomically small tibias, and were described to occur in the early post-operative period (approximately one month postoperatively). Of peri-prosthetic fractures in other keel-based components reported with radiographic imaging, five of six fractures in Cemented Oxford UKR can be seen to follow the path of the keel [184-188], and all six fractures in non-Oxford UKR which had keels were seen or reported follow the path of the keel (four AMC UKR [189] and two Sigma HP UKR [190]) – AMC UKR (Alphanorm Medizintechnik, Quierschied, Germany) and Sigma HP UKR (DePuy Synthes, Indiana, USA). This suggests that the keel has a role to play in peri-prosthetic tibial fractures. This will be studied in more detail in **Chapter 7**.

5.2.2 Fractures in Extended Keel Cuts

A key step in preparing the tibia during UKR is the cutting of a vertical slot for the keel. The slot position is determined using a template which is held with a pin, and a reciprocating keel cut saw is used to make the cut. The blade is sunk to its shoulder, and advanced posteriorly with up and down movement. The pin is held to secure the template and for the surgeon to feel if the saw hits the anterior and posterior borders of the template (**Figure 5.1**).

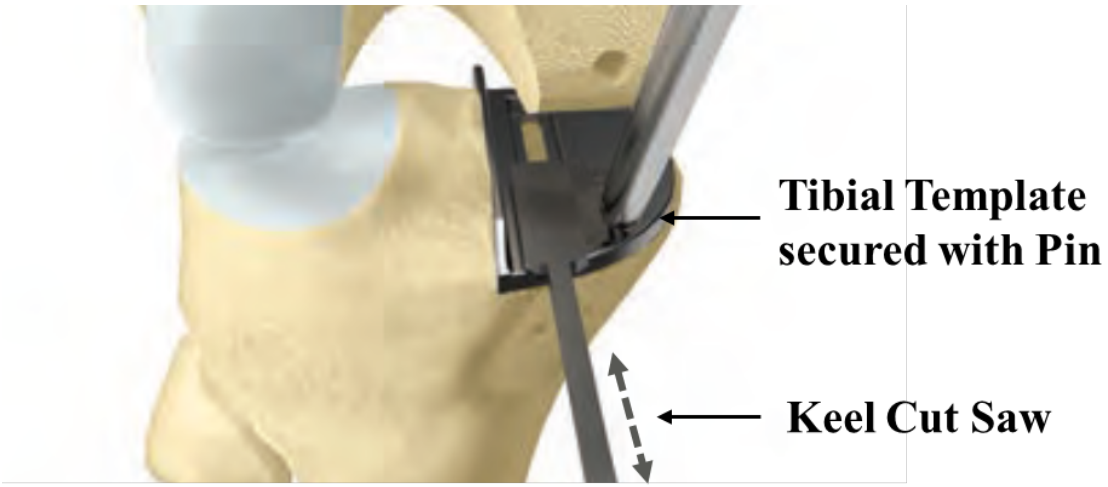


Figure 5.1: *Preparing the keel slot using a reciprocating keel-cut guided by a template held with a pin, placed on a prepared tibial floor. Image adapted from [86].*

The tibial component is positioned with its posterior margin flush with the posterior tibial cortex. This is done to ensure optimal load transfer to posterior cortical bone and surrounding trabecular bone [191].

The posterior edge of the keel slot is 7-9 mm from the posterior border of the tibia, varying with tibial component size. Intra-operative complications, such as loosening of the tibial template, can result this keel cut extending posteriorly, compromising the posterior cortex [106, 186].

Slots that extend too far posterior and damage the posterior cortex have been shown to reduce the load causing fracture by more than 50% in mechanical and cadaveric studies, and have been found to be a cause of peri-operative fracture in Oxford UKR [186, 192-194]. These occur if the posterior motion of the saw blade drives the template posteriorly, thereby extending the cut posteriorly and potentially damaging the cortex [106].

Posterior cortical integrity is also shown to be important in avoiding the tibial component subsiding posteriorly, and therefore even incomplete compromise of the posterior cortex is an important complication [195].

5.3 Depth and Length of Tibial Component Keel across Implant Sizes

There are 7 tibial component sizes: AA (smallest), A, B, C, D, E, and F (largest). The tibial component is scaled across all tibial component sizes. The only exceptions to this are the width and depth of the keel, which are 3.7-3.8 mm and 9 mm respectively across all sizes. The constant width allows all procedures to use the same saw instrumentation to produce the slot, while the constant depth was designed to ensure adequate fixation across all sizes. Consequently, in smaller components, the keel is relatively deeper and more posterior (**Figure 5.2c, d**). This relatively deeper keel results in disproportionately less bone volume below the tibia and may be increasing fracture risk. The posterior edge of the keel is also closer to the edge of the component in the smallest vs largest component (7 mm vs 9 mm).

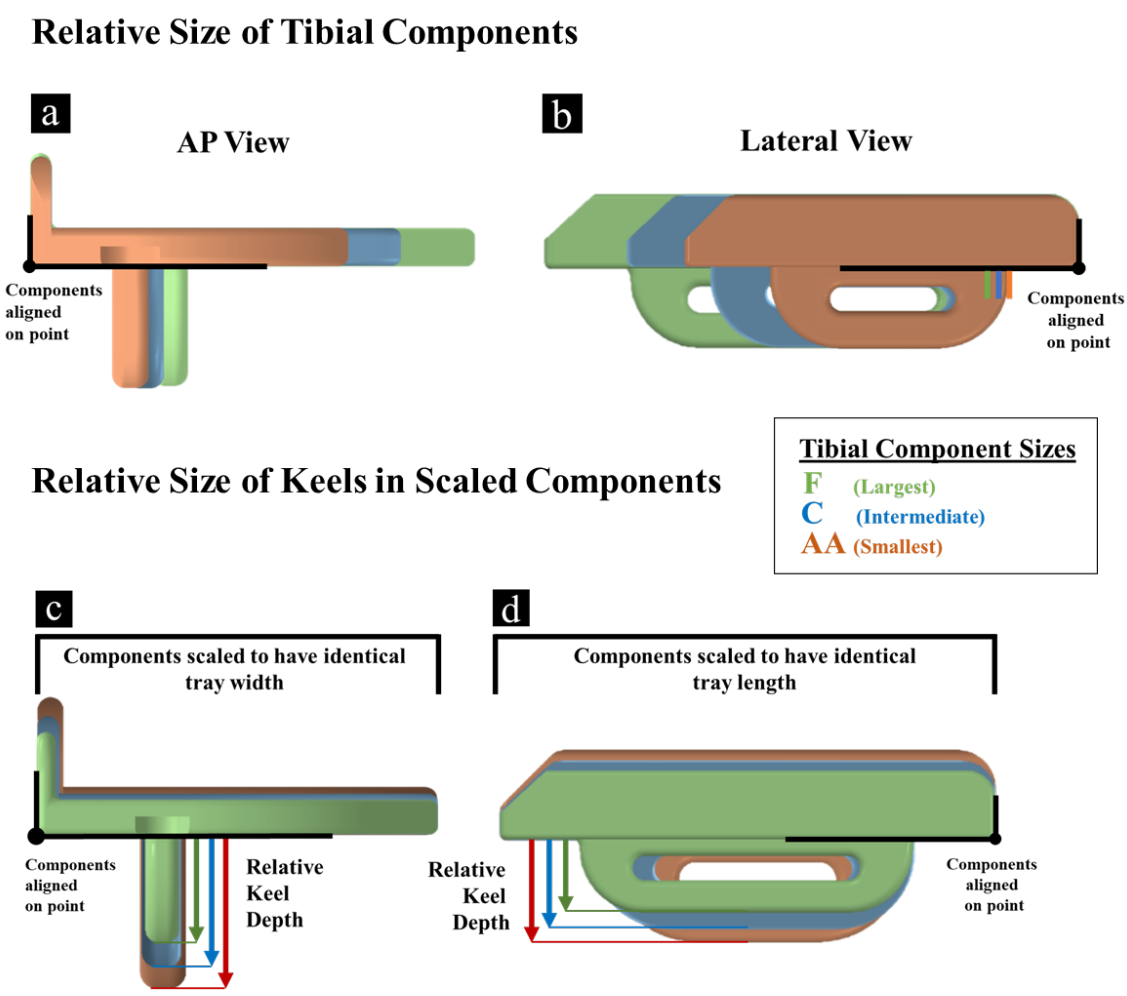


Figure 5.2: *The size of the Cementless Oxford UKR Tibial Component.* ***(a, b)*** *AP and lateral views of relative size of the smallest (AA), middle (C), and largest (F) components. Lines at the posterior aspect of keels in (b) indicate the posterior edge of Size F (green), C (blue), and AA (orange) keels.* ***(c, d)*** *AP and lateral views of the tibial components, scaled to implants.*

5.4 Designing a New Keel

5.4.1 Design Aims

The keel is implicated in fracture risk relating to both the size of the component and extended sagittal cuts. Therefore, it is a good candidate for potential design changes to reduce fracture risk.

If the size of this keel can be reduced in smaller implants, this will likely reduce fracture risk. Furthermore, if the distance of the keel from the posterior edge is increased in smaller implants, it increases the margin of safety when keel slots are cut, reducing the risk of posterior cortex compromise. However, changes to keel design should not compromise the primary role of the keel, which is implant fixation.

The overall aim of this Chapter is to propose a simple and easily implementable change to the keel in very small tibias, to address the high incidence of fracture in very small tibias.

Therefore, the design aims for a new keel are:

Aim 1. Reduce fracture risk when Cementless Oxford UKR is implanted in very small tibias.

Aim 2. Preserve tibial component fixation in very small tibias.

Aim 3. Minimise change to component design, surgical technique, and surgical instrumentation, to ensure change is easily implementable.

5.4.2 Implementing Design Aims

To achieve **Aim 1** (reduce fracture risk), changes to the keel design will be explored which incorporate a reduced keel depth and increased distance between keel and the posterior edge of component. To achieve **Aim 2** (preserve fixation), the abovementioned changes will be tested to ensure that new keel designs perform as well as or better than the current keel design in primary fixation. In addition, any new keel designs will retain the existing porous surface area of the keel in contact with the slot, to preserve secondary fixation. To achieve **Aim 3** (minimise change), the tibial component, instrumentation, and technique, should remain unchanged, with the exception of the keel design and keel/slot dimensions.

5.4.3 Testing Design Aims

In literature, the interaction between the keel and slot of the Cementless Oxford UKR has been assessed using Push-In-Pull-Out (PIPO) testing [118, 119]. This involves pushing-in then pulling-out a keel into a keel slot in a polyurethane bone analogue at a fixed rate of displacement, and measuring the forces acting on the keel during this motion. The maximum push-in force (N) is used as a measure of fracture risk, as the greater forces needed to push-in a keel would result from forces needed to deform bone in interference with the keel being inserted, inducing splitting forces along the slot which will induce fracture if bone mass is unable to resist splitting [118, 119, 196]. The maximum pull-out force (N) is used as a measure for primary fixation as it measures the force needed to overcome constraint and induce keel motion [118, 119]. These simple tests will allow rapid assessment of keel design changes.

Following this preliminary PIPO testing, promising designs can be validated by further tests which incorporate physiological loading patterns and bone anatomy (performed in **Chapters 7 and 8**) and appropriate clinical trials (discussed in **Chapter 9**).

5.5 Testing Design Changes

5.5.1 Study Design

An *in-vitro* mechanical study was performed, which involved the push-in and pull-out of 3D-printed titanium keels into slots cut into polyurethane foam. The 'standard' keel replicates the existing keel found on the smallest tibial component (Size 'AA') of the Cementless Oxford UKR. All other variants were designed for this study and described later (in **Section 5.5.3**). Solid rigid polyurethane foam (Sawbones, Malmo, Sweden) of 20 pounds per cubic feet (PCF) density was used as it has material properties similar to trabecular bone (PCF 20 foam: density 0.32 g/cm^3 and compressive modulus 210 MPa, vs trabecular bone: 0.3 g/cm^3, range 14–345 MPa) [197-199]. Printed titanium was used as it was relatively much stiffer than 20 PCF PU foam, and therefore is identical to clinically-used Cobalt-Chromium-Molybdenum components in its mechanical interactions with the foam.

Push-In and Pull-Out tests were performed using a servo-hydraulic testing machine (Dartec HC 10, Zwick Ltd, Herefordshire, UK) which measures displacement and a S-beam load cell (FSB-01, Force Logic, Berkshire, UK) which measures vertical force. The foam was immobilised to ensure only keel displacement occurred. The test involved a displacement-controlled push-in of the keel into a slot with an interference fit (**Figure 5.3**). Push-in was performed at a rate of 10 mm min^{-1}, followed by a 10s dwell, a slower pull-out at a rate of 1 mm min^{-1} until keel was unloaded, another dwell of 10s, and pull-out of the keel from the slot at a rate of 10 mm min^{-1}. The unloading phase was added to decouple the push-in phase (which has a force pushing the keel out of the slot), and the pull-out phase (which has a force pulling the keel into the slot) (**Figure 5.4**). The standard keel was inserted 9 mm, while all modified keel designs, which were 3 mm shallower,

were inserted by 6 mm. Force, displacement, and time data were collected at 250 Hz for analysis. The process was then repeated to model what would happen if the keel was partially removed. Each test was repeated three times (n=3).

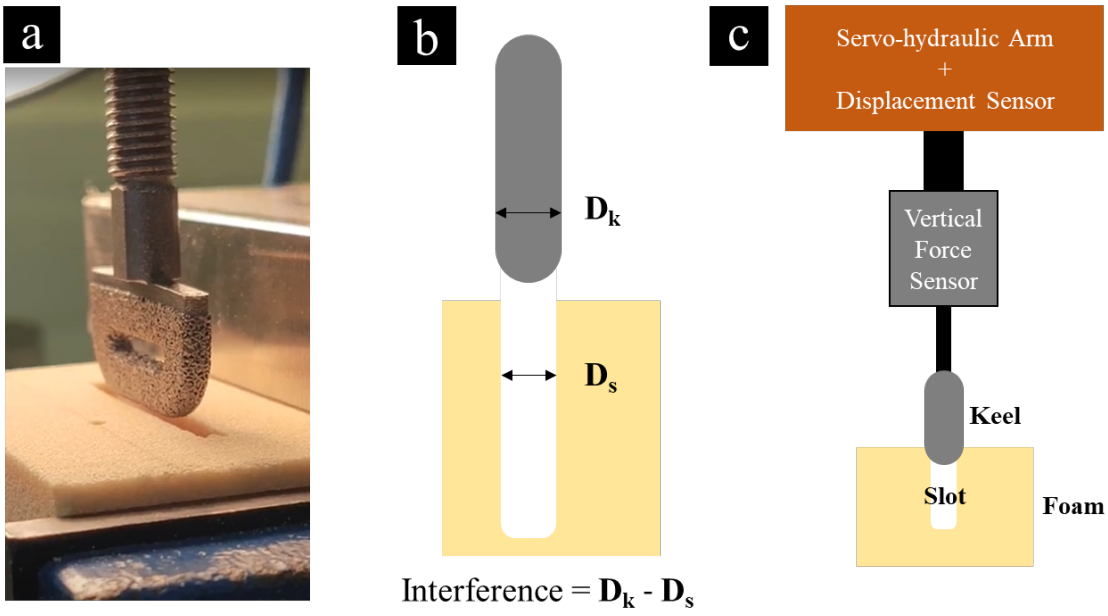


Figure 5.3: ***(a)*** *A typical keel PIPO test setup. Polyurethane foam is constrained from vertical motion,* ***(b)*** *Diagram representing interference.* ***(c)*** *Depiction of key components of keel PIPO test setup components.*

5.5.2 Data Processing

Raw data from the servo-hydraulic testing machine was processed using custom code (MATLAB, Natick, Massachusetts, USA), which identified and separated data into Push-In, Unload, and Pull-Out phases, and identified the maximum push-in ($MaxF_{in}$) and pull-out ($MaxF_{out}$) forces recorded (N) and their respective displacements (mm) to produce a calculation of total energy (N.mm) involved in the push-in and pull-out phases (**Figure 5.4**).

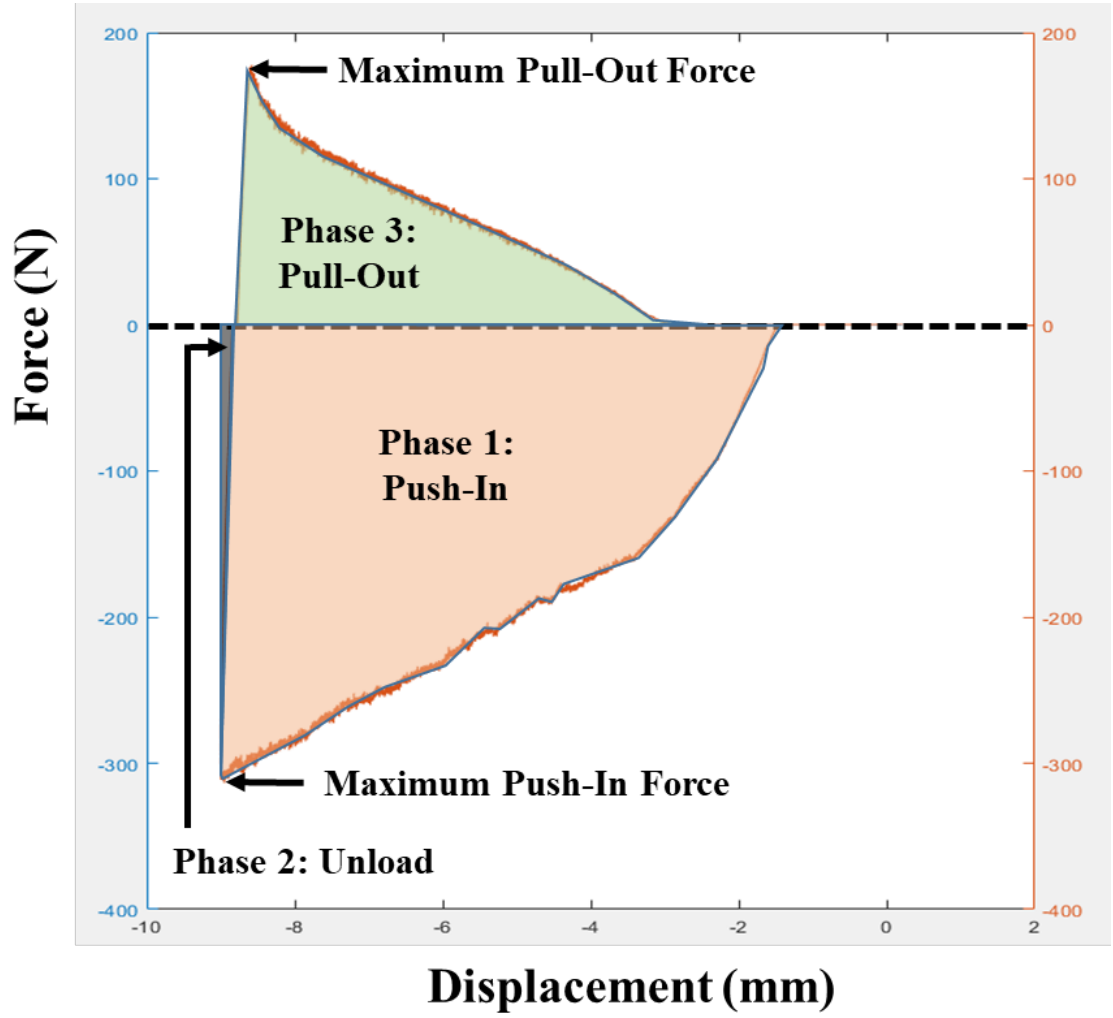


Figure 5.4: *A sample force-displacement graph from a PIPO test, indicating the Push-In, Unload, and Pull-Out phases, as well as the maximum Push-In and Pull-Out forces. Graph generated on MATLAB. The areas shaded in orange and green highlight the Push-In and Pull-Out energies respectively.*

Continuous values were tested using the unpaired Student t-test for parametric (Shapiro-Wilk $p>0.05$), and the Mann-Whitney U-test for non-parametric (Shapiro-Wilk $p<0.05$) distributions. Data was analysed and visualised using GraphPad Prism (GraphPad Software, San Diego, California, USA) and Excel (Microsoft, Redmond, Washington, USA).

5.5.3 Design Elements Tested

The effects of keel size, taper, and surface roughness were tested using a series of keel variants designed using Computer-Assisted Design (CAD) (SOLIDWORKS, Dassault Systèmes, France) by an engineer, and were additively manufactured (i.e., 3D printed) from powdered titanium (Cp-Ti Grade 2, AP&C, Saint-Eustache, Canada) with a Direct Metal Laser Melting system (Concept Laser MLAB200, General Electric, Boston, Massachusetts, USA).

The standard keel (of width 3.7 mm) was tested with standard interference using a cementless keel-cut sawblade (which produces an average slot width of 3.0 mm [119]), as well as with reduced interference by expanding the slot with a pick originally designed for Cemented Oxford UKR keel preparation (which expands slot width by 0.5 mm) [119]. This was performed for use as a control, as reduced forces for push-in and pull-out could be expected from this widened slot. In addition, some surgeons concerned about fracture widen the slot with this technique, providing anecdotal evidence that this does not compromise primary fixation. Therefore, this test will also provide an approximate reference for a lower but potentially safe maximum pull-out force.

In addition to the standard keel, which has a window (see **Section 1.7.2**), smaller keels without a window were designed and tested. These smaller keels were 3 mm shallower and 4 mm shorter than the standard keels, and had the same surface area on their sides to avoid compromising secondary fixation (**Figure 5.5a, b**). The overlay of the standard and new keel designs demonstrates the intended changes of making a shallower keel which is further from the posterior edge of the posterior tibial cortex (**Figure 5.5c**).

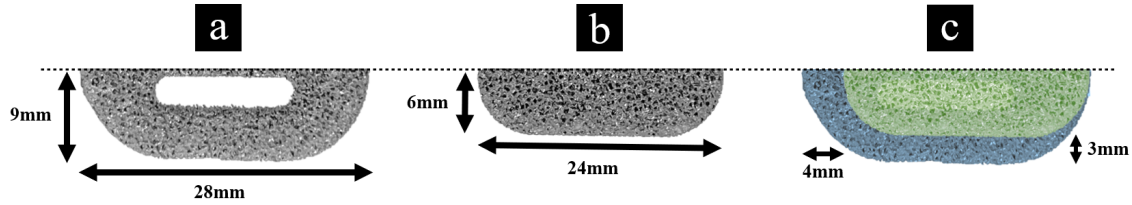


Figure 5.5: *Keel designs explored in this study.* ***(a)*** *Standard clinical keel design, and* ***(b)*** *a new smaller keel.* ***(c)*** *Overlay of standard and new keel designs, demonstrating the difference in depth and distance from posterior cortex. All keels are based on the Size 'AA' tibia of the Cementless Oxford UKR.*

Two design elements of the keel were modified for testing with this new size: the taper (non-tapered as found in the standard keel, and 2° tapered), and surface (a porous coat similar to the standard cementless keel, no coat similar to a cemented keel, and a porous coat with a smooth edge). Surfaces of the 3D-printed keels and their respective clinically-used surfaces were imaged with scanning electron microscopy (SEM) to validate surface structure (**Figure 5.6**) (TESCAN© MIRA3, Kohoutovice, Czech Republic)[2].

[2] Microscope operation and image acquisition was arranged for with a collaborator (Department of Materials, University of Oxford, UK).

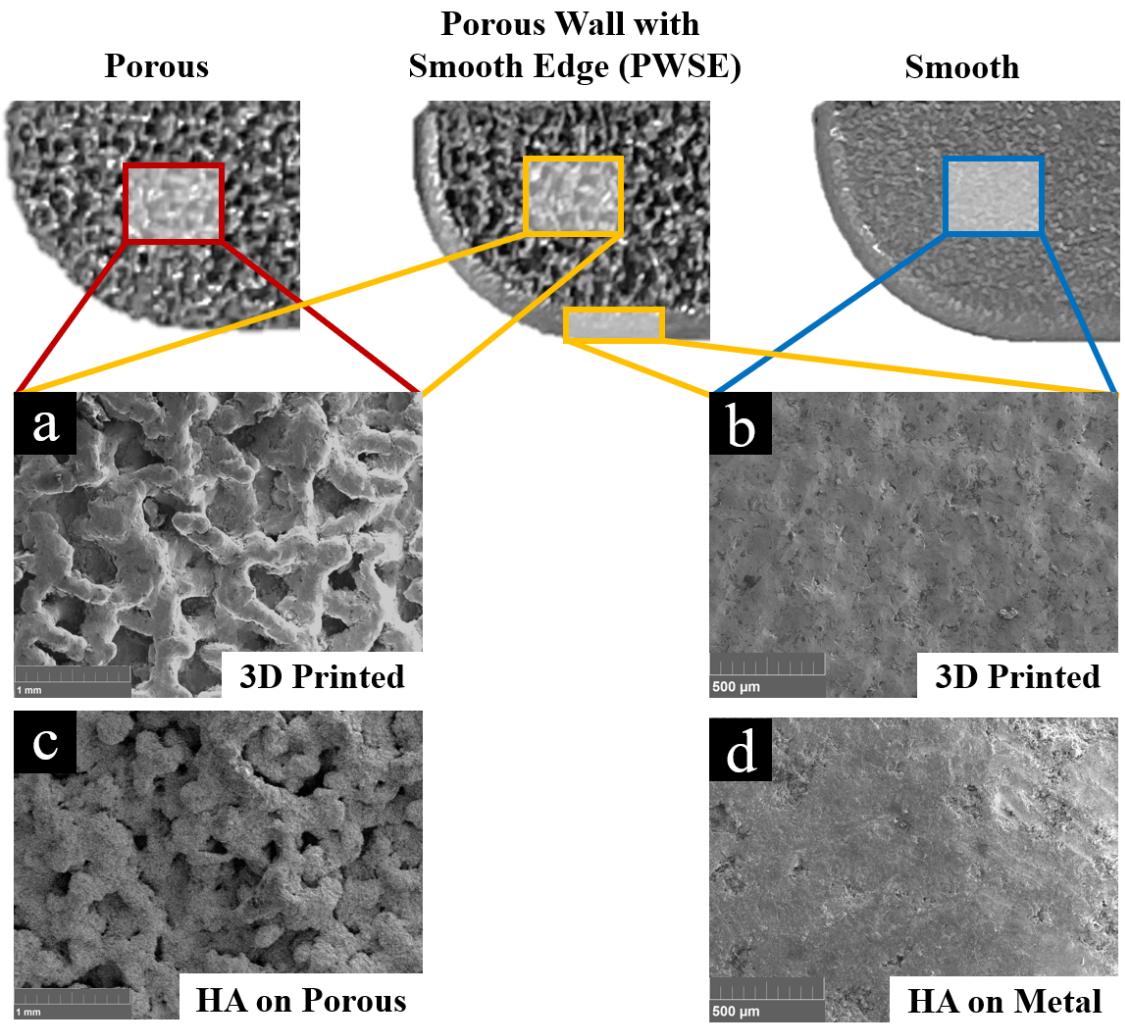


Figure 5.6: *Scanning Electron Micrographs of keel surfaces used in this study and the surfaces they are meant to represent.* ***(a)*** *Printed porous surface,* ***(b)*** *Printed smooth surface,* ***(b)*** *Clinical porous surface made with porous spray coated with hydroxyapatite,* ***(d)*** *Clinical smooth surface which is cast and coated with hydroxyapatite. Keels used in this study: Porous, Porous Walled with Smooth Edged (PWSE), and Smooth, are shown above.*

Slots for the standard keel were produced using standard clinical techniques and instruments: the use of a template and a keel-cut saw. A clip-on template riser was designed using CAD (SOLIDWORKS, Dassault Systèmes, France) and 3D-printed using a poly-lactic acid (PLA) polymer (Ultimaker 2+ Open-Filament System, Ultimaker B.V., Netherlands). The riser was used to make smaller slots for smaller keels (**Figure 5.7**).

The clearance i.e., the difference between slot and keel in depth, length, and width remained the same between standard and smaller keels.

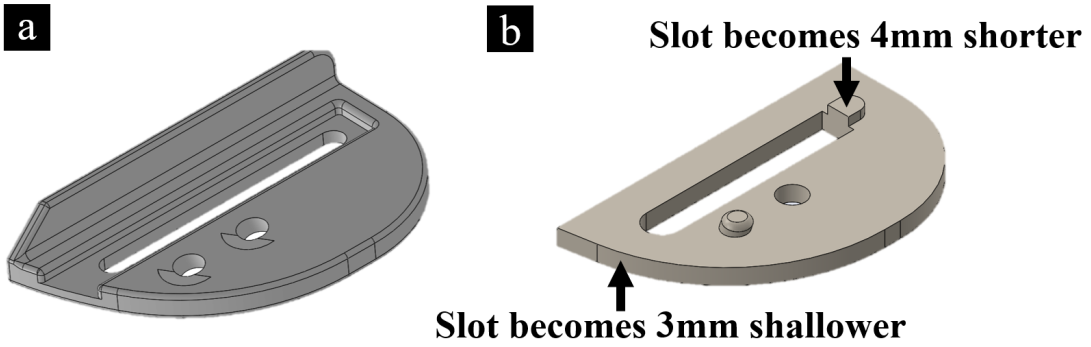


Figure 5.7: (a) *The template for a standard 'Size AA' tibial component keel cut.* ***(b)*** *A 3D-printed clip-on template riser, used to make smaller slots for smaller keels with same clearance as standard template. Riser used the posterior limiting peg and another accessory peg to secure riser to template, leaving one hole for pin insertion to secure template during keel cut (see* ***Section 5.2.2****).*

5.5.4 Results

5.5.4.1 Maximum Push-In and Pull-Out Forces

A standard keel (which has a porous surface) inserted into a standard slot reached a $MaxF_{in}$ of 738 N and $MaxF_{out}$ of 178 N. A wider slot made with a cemented pick reduced the $MaxF_{in}$ by 55% ($p=0.0026$) and $MaxF_{out}$ by 30% ($p=0.040$).

A smaller keel with the same porous surface, inserted into a slot with the same clearance as the standard keel and slot, had a small but non-significant decrease in $MaxF_{in}$ compared to the standard keel in standard slot (738 N vs 661 N, $p=0.134$), but a significantly lower $MaxF_{out}$ (178 N vs 113 N, $p=0.0003$). The same small keel but with a smooth surface had a significantly lower $MaxF_{in}$ than the small porous keel (661 N vs 536 N, $p=0.005$) and a higher $MaxF_{out}$ (113 N vs 208 N, $p<0.0001$).

Adding a 2° taper to the small porous keel does not affect $MaxF_{in}$ (661 N vs 675 N, $p=0.743$) but increases the $MaxF_{out}$ (113 N vs 161 N, $p=0.006$) relative to a non-tapered porous keel. The addition of a 2° taper in the small smooth keel results in a small non-significant reduction in $MaxF_{in}$ (536 N vs 485 N $p=0.093$) and a similar $MaxF_{out}$ (208 N vs 204 N, $p=0.543$).

A porous walled and smooth edged (PWSE) keel had the lowest $MaxF_{in}$ of all porous designs, and highest $MaxF_{out}$ of all designs tested. When compared to the standard keel in a standard slot, the PWSE keel had a 26% lower maximum $MaxF_{in}$ (738 N vs 545 N, $p=0.006$) and 31% higher $MaxF_{out}$ (178 N vs 234 N, $p=0.0004$).

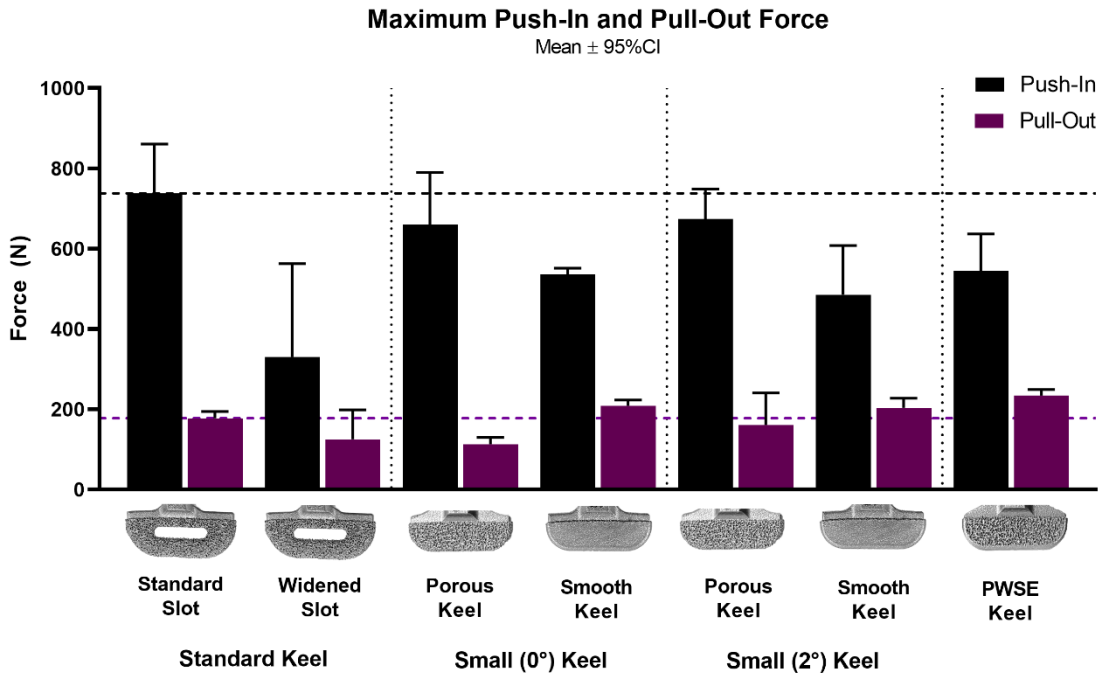


Figure 5.8: *Maximum push-in and pull-out forces for keel and slot designs. Horizontal lines are drawn at the level of the maximum push-in and pull-out forces of the standard keel in standard slot, for comparison.*

5.5.4.2 Total Push-In and Pull-Out Energies

Further to maximum push-in and pull-out forces, the total energy taken during the push-in and pull-out phases of testing were calculated, based on the area under curve of the force-distance plots of test data.

Reduced interference with the widened slot significantly reduced the total push-in energy (3508 N.mm vs 1808 N.mm, p=0.0027) and had a small but non-significant decrease in total pull-out energy (642 N.mm vs 517 N.mm, p=0.1061). Total push-in energy and pull-out energy of the standard keel in the standard slot was significantly higher than all small keels if porous or smooth ($p<0.05$ in all comparisons). The only exception was the PWSE keel, where total pull-out energy was similar to the standard keel in standard slot (642 N.mm vs 611 N.mm, p=0.2595).

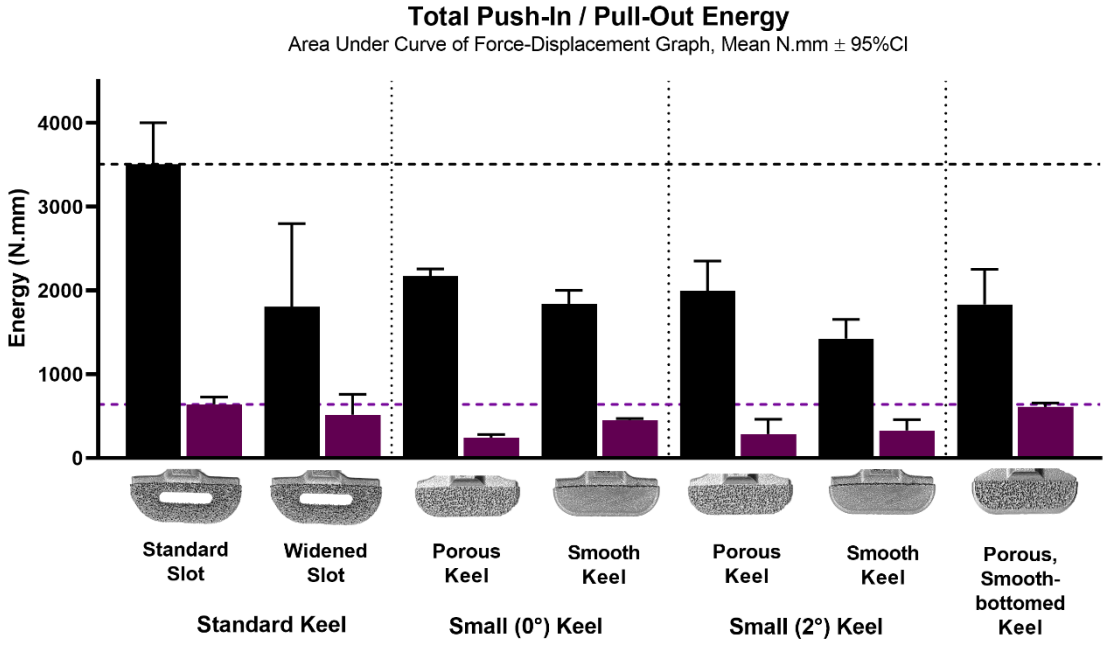


Figure 5.9: *Total Push-In and Pull-Out Energy for keel and slot designs. A horizontal line is drawn at the level of the maximum Push-In and Pull-Out forces of the standard keel in standard slot for comparison.*

5.5.4.3 Forces and Energies on Reinsertion

Push-in and pull-out tests were repeated into the same slot to assess effect of re-insertion. Re-insertion $MaxF_{out}$ forces were significantly greater with smooth keels compared to their equivalent porous keels (small 0° keel porous 55 N vs rough 196 N $p<0.0001$, small 2° keel porous 103 N vs rough 166 N $p=0.0266$). Reinsertion of the PWSE keel required greater $MaxF_{out}$ than the standard keel (152 N vs 92 N, $p=0.0005$) (**Figure 5.10**). Patterns of reinsertion energy and first insertion energy are consistent with the differences seen between first insertion force and reinsertion force (**Figure 5.11**).

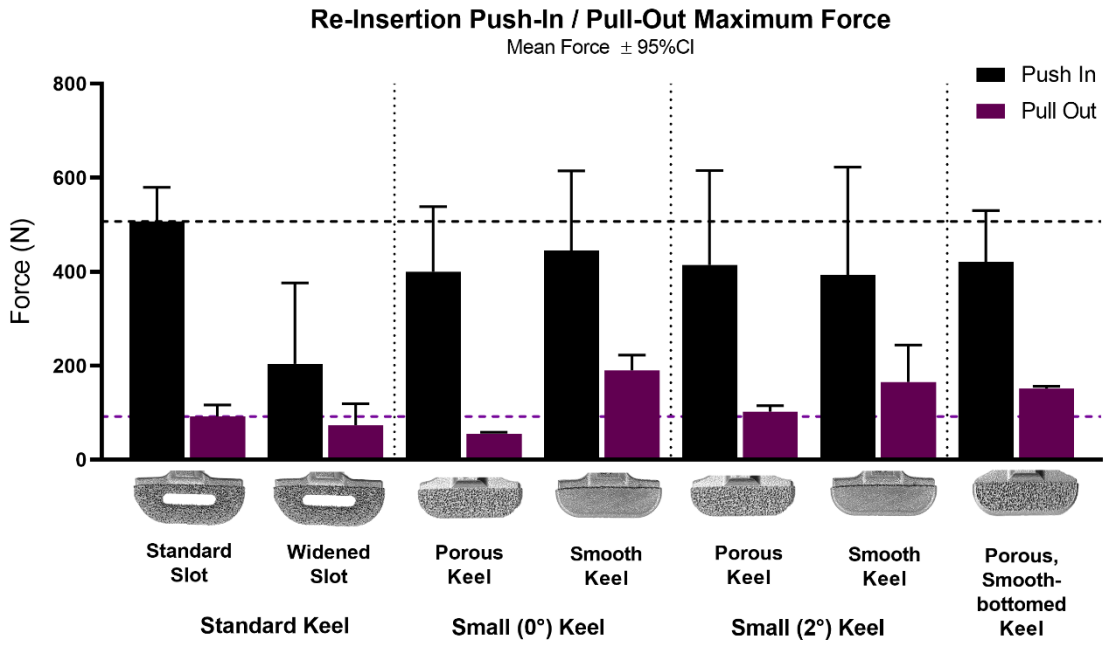


Figure 5.10: *Maximum push-in and pull-out forces for keel and slot designs on re-insertion into slots. Horizontal lines are drawn at the level of the maximum push-in and pull-out forces of the standard keel in standard slot, for comparison.*

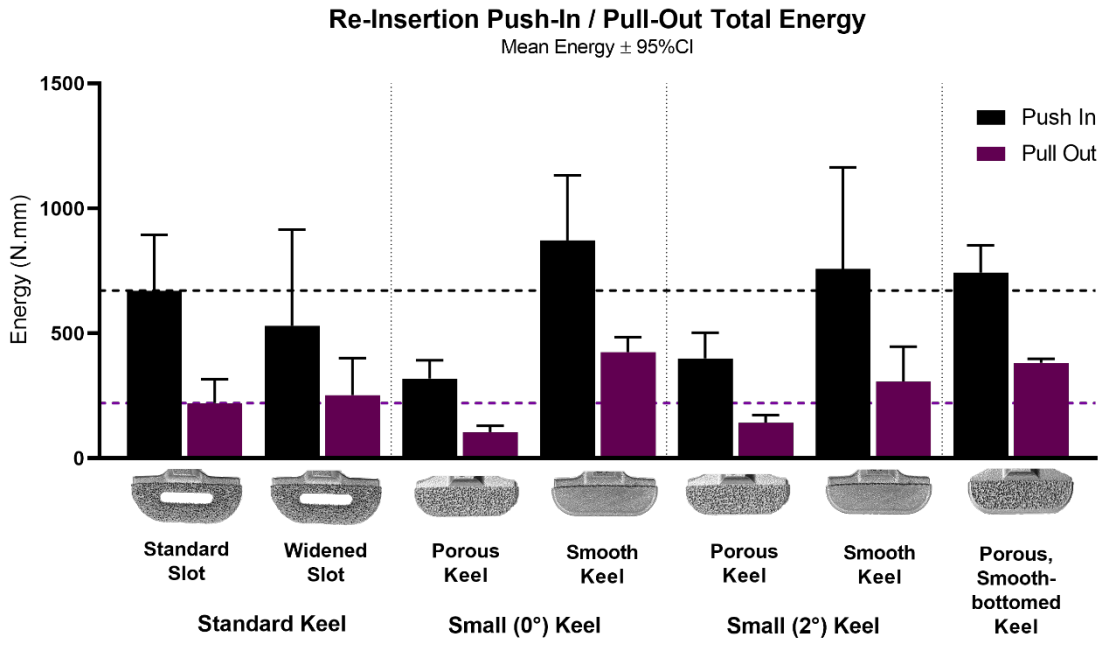


Figure 5.11: *Total push-in and pull-out energies for keel and slot designs on re-insertion into slots. Horizontal lines are drawn at the level of the total push-in and pull-out energies of the standard keel in standard slot, for comparison.*

5.5.5 Discussion of Findings

The size, porosity, taper, and interference of the keel influence the forces experienced by the keel when pushed-in and pulled-out of a slot.

Compared to the standard keel, a small porous keel requires 90% of force to push-in, but only withstands 63% of force before pulling out. As the maximum pull-out force of the small keel, which is related to primary fixation, is substantially lower than that of the standard keel, it suggests poorer primary fixation. However, the maximum pull-out force for the small keel is similar to that of the standard keel with a widened slot, which anecdotal evidence suggests is not associated with loosening. Therefore, the relatively poorer fixation with the small keel may not necessarily result in an increased incidence of loosening clinically. Despite this, it would be appropriate to consider introducing further design changes to the keel to minimise the risk of loosening.

Keels with a smooth surface have lower push-in forces, higher pull-out forces, and higher re-insertion pull-out forces than keels with a porous surface. This suggests that they would have lower fracture risk and improved primary fixation. This is likely due to less damaging during the interaction of the keel in the slot. A smooth keel displaces foam and deforms it as it enters the slot, while a porous keel rasps foam off the slot on entry and exit. However, a fully smooth surface reduces the total porous surface area of the keel and may compromise secondary fixation. With hydroxyapatite on a shot-blasted smooth surface, there will be some secondary fixation (based on **Chapter 3**), but its ability to withstand loading is unclear, and will likely not be as good as a porous surface. As there is good secondary fixation under the component the secondary fixation (shown in **Chapter 3**), a smooth keel may be adequate. However, a long-term clinical study would be needed to assess this.

Introducing a taper to the small porous keel appears to increase the force needed to pull the keel out by 42% with no change to push-in forces; this push-in/pull-out force ratio is similar to the standard keel. Tapering the keel reduces the width of the keel's leading edge and increases the width of its trailing edge, making it less likely that the leading edge will rasp and damage the slot during insertion. A smooth tapered keel has a lesser degree of improvement over a porous tapered keel than the non-tapered smooth and porous keels, further suggesting the damage at the leading edge as a viable source of improvement.

Total energy analysis provides further important information about slot-keel interaction. This is calculated as the total amount of energy (force over displacement) needed to push-in and pull-out the keel. While maximum pull-out forces were consistently higher when a smooth or tapered keel is used in place of a porous non-tapered keel, the total energy needed for the pull-out was significantly lower in both cases. This was consistently due to a rapid drop-off of the maximum force with small changes in displacement (**Figure 5.12**). In contrast, non-tapered porous keels (both standard and small) retained their maximum pull-out force for a larger displacement. These findings are consistent with the mechanical properties that can be expected of these surfaces: with smooth keels, there is less mechanical interlocking of the surface with the slot compared to the porous keel surface. Therefore, it is likely that once static friction is overcome and the keel begins moving, there is a rapid drop-off in frictional forces restricting movement of the keel, and consequently, a reduction in pull-out force. With the porous keel, the porous interface may be assisting to improve dynamic friction between surfaces, limiting the rapid drop-off of pull-out force. With tapered keels, a small pull-out displacement will fully separate the keel and slot faces, while non-tapered keels will still retain a portion of the keel-slot

interface until fully pulled out. This may account for the even more rapidly reducing friction between the surfaces and rapidly reducing the pull-out force (**Figure 5.12**).

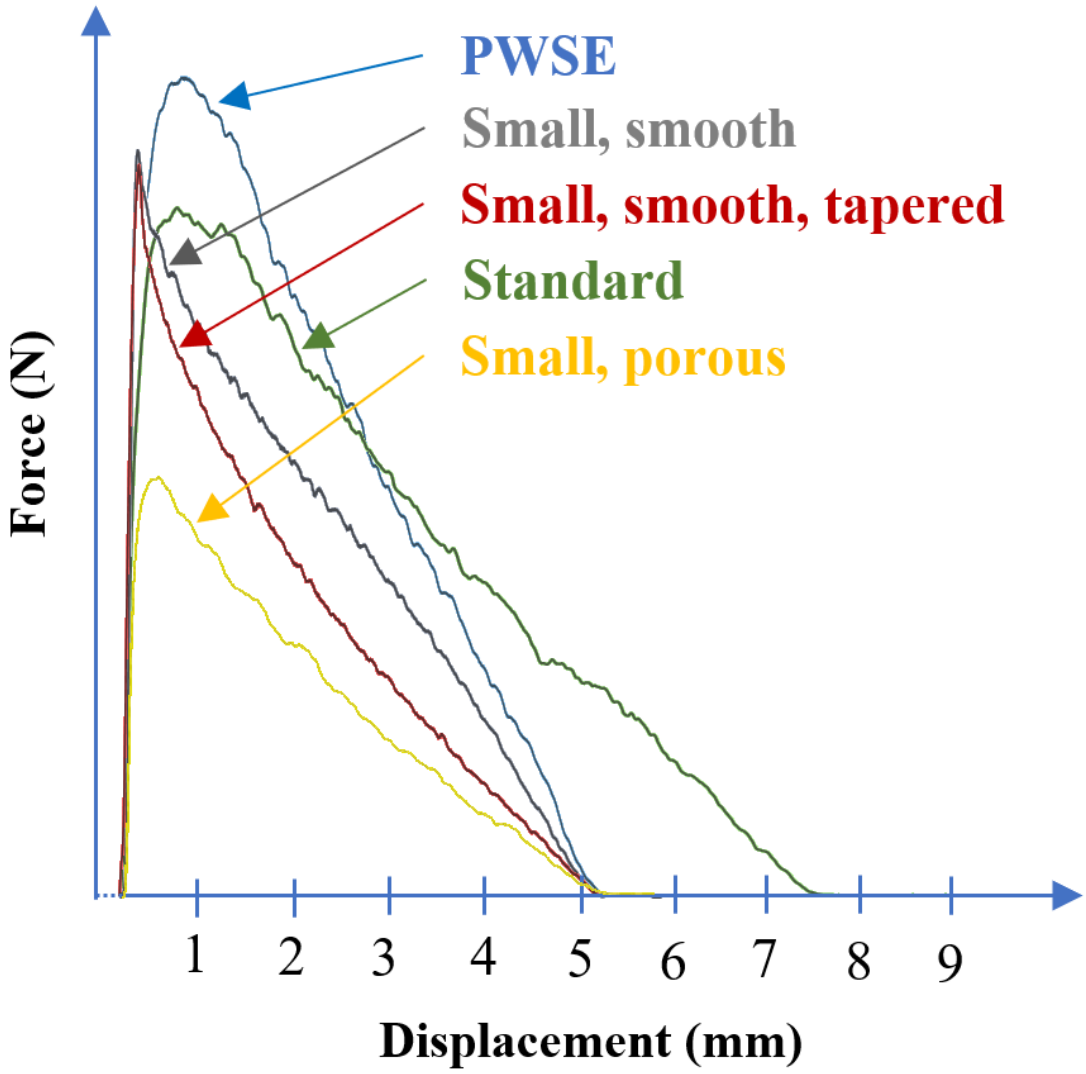


Figure 5.12: *Representative force-displacement curve profiles for the pull-out phase of testing for each sample variant, scaled to average MaxF_{out} of all repeats for each variant. Area under curve represents total energy of pull-out phase. Note the sharp drop-off with smooth keel, and further smooth tapered keel.* ***Blue:*** *Small porous-walled, smooth-edged non-tapered 6mm keel - mean $FMax_{out}$=234 N and E_{out}=611 N.mm.* ***Grey:*** *Small smooth non-tapered 6 mm keel - mean $FMax_{out}$=208 N and E_{out}=434 N.mm.* ***Red:*** *Small smooth tapered 6 mm keel - mean $FMax_{out}$=204 N and E_{out}=328 N.mm.* ***Green:*** *Standard (porous, non-tapered) 9 mm keel - mean $FMax_{out}$=178 N, mean E_{out}=642 N.mm.* **Yellow:** Small *porous, non-tapered 6 mm keel - mean $FMax_{out}$=113 N, mean E_{out}=243 N.mm.*

The improved pull-out forces with the smooth and tapered keels suggest the greatest damage to the slot by the keel occurs at the leading edge of the keel. Based on this, it can be expected that reduced damage of the slot will improve pull-out forces for the same push-in forces. Therefore, a porous keel with a smooth leading edge (PWSE) design was explored, to minimise the rasping effect on insertion whilst retaining the porous coat on the wall of the keel. This design appears to be successful in combining the beneficial effect of the smooth surface at the leading edge in limiting the rasping of the slot, with the beneficial effect of the porous surface at the wall in retaining pull-out forces despite keel motion. A PWSE keel with 6 mm insertion has a 30% reduced maximum push-in force and a 30% greater maximum pull-out force compared to a standard keel with 9 mm insertion. This design retains the same surface area of porous coat interfacing with the wall as the standard keel, so adequate secondary fixation can be expected to be retained.

While not part of standard surgical method, it is possible that a keel may need to be moved to ensure optimal positioning in the medial tibial condyle. Therefore, reinsertion of keel was assessed. Reinsertion data demonstrates that the damage linked to a porous surface is concerning, as it retains only 50% of its first insertion maximum pull-out force (178N vs 97N). A smooth keel performs significantly better in both non-tapered and tapered keels, with >90% of the maximum pull-out force retained. The PWSE keel performs only slightly better than the standard keel on reinsertion, retaining 65% of its first maximum pull-out force (234N vs 152N). However, due to its higher initial pull-out force, reinserting a PWSE keel would result in a maximum pull-out force that is higher than the reinsertion pull-out of the standard keel (152N vs 97N, $p=0.0004$) which is only 15% lower than the first insertion of the standard keel, suggesting it is a safer keel than the standard keel if mispositioned and moved.

For this study to be relevant to clinical components, the porous and smooth surfaces of the 3D-printed keels should be similar to those seen clinically. This was assessed in this study using electron microscopy. Printed and real smooth surfaces were largely identical, and had grossly similar pore sizes. However, the real porous surface had shallower pores with less consistent pore size, and a rougher microstructure than the 3D-printed porous surface. It is not clear how much these differences would affect the interaction seen in this study. Further assessment of design changes using clinical components will be necessary to validate findings. This is discussed further in **Chapter 9**.

Push-in and pull-out forces do not directly measure risk of fracture and primary fixation. However, these forces are mechanically linked to these outcomes and are a good measure for comparative analysis of fracture risk and primary fixation, particularly for keels of the same size [118, 119, 196, 200]. It is not clear how impactful the effect of keel depth will be in affecting fracture risk independent of push-in and pull-out forces. This will be assessed in **Chapter 7**.

Much of the discussion regarding the mechanisms underlying force changes with displacement, and their relationship with keel structure/surface and friction, are speculative. While a detailed understanding of these interactions is not necessary for the aims of this chapter, empirical testing of these speculated modes of interaction would be needed to validate them. This is discussed in further detail in **Chapter 6.5.4**.

Keel designs in this study were 3D-printed, but clinically used components are produced using considerably different processes and have different surface microstructure. Therefore, the new keel design will need to be re-tested with clinically manufactured surfaces. Similarly, although the polyurethane foam used has similar density and Young's Modulus to trabecular bone, the applicability of several other material properties

important to interference fit and porous surfaces (such as frictional coefficient and plastic deformation patterns) are untested. Therefore, before the introduction of a new design of keel, a clinical study of the designs should be validated *in-vivo*. These are discussed further in **Chapter 9**.

5.5.6 Conclusion

A smaller porous keel had lower maximum pull-out forces, suggesting worse primary fixation, and therefore potentially higher risk of implant loosening. However, its maximum pull-out force was similar to that of the standard keel inserted in a widened slot which some surgeons, concerned about fracture, have successfully used without an increased incidence of loosening.

A small keel with a smooth surface demonstrated lower fracture risk with better primary fixation, but at the expense of the porous surface, which is important for secondary fixation. The smaller keel with a taper had a similar maximum pull-out force but substantially lower total pull-out energy compared to the standard keel. A small porous-walled, and smooth-edged keel appears to perform superiorly to the standard keel with lower push-in and higher pull-out forces, and retains more of its pull-out force if reinserted. This suggests that the small porous-walled, smooth-bottomed keel will have a lower risk of fracture than the standard keel without increasing the risk of loosening.

5.6 Chapter Summary

The Cementless Oxford UKR has a high risk of fracture particularly in very small tibias, and a risk of intra-operative fractures due to extended keel cuts.

Reducing the size of the keel appears to reduce this risk of fracture, but may increase the risk of implant loosening. To address this, a change in the design of the smaller keel, to include a porous-walled, smooth-edged surface, is proposed. This design demonstrates a lower risk of fracture alongside a lower risk of implant loosening compared to the standard keel. It retains the same porous surface area in contact the slot as the current keel. This keel can be used with existing surgical instrumentation and technique, only requiring a new component and a new template.

These small incremental changes to keel design are unlikely to carry unforeseen risks, whilst addressing the risk of fracture due to relatively deeper keels in smaller tibias. They also increase the distance that a slipped keel-cut saw will need to travel before the posterior cortex is compromised, and therefore help to address the intraoperative fracture risk of extended keel cuts.

The viability of these new keel designs will need to be further validated using more physiologically relevant tests of fracture and fixation. These will be explored in **Chapter 7**, with load-to-fracture testing, and **Chapter 9**, with assessment of anterior lift-off.

6 Pegs as an alternative to the Keel in the Cementless Oxford UKR Tibial Component

6.1 Motivation for Chapter

In **Chapter 5**, reducing the size of the keel was shown to potentially reduce fracture risk. However, some fundamental sources of risk remain with a smaller keel, albeit with a larger margin of safety. These are: risk of excessive posterior cuts compromising the posterior cortex, introduction of splitting forces by the keel in the proximal tibia, and the reliance on friction for constraining motion in the sagittal plane.

In this chapter, tibial component fixation using pegs in place of keels will be explored, aiming to address these issues associated with a keel design.

6.2 Limitations of a Keel

Chapter 5 introduced the fracture risks associated with the existing keel design, and changes to the keel aiming to address them. Nonetheless, the use of a keel as fixation element has inherent limitations.

With a cementless keel, constraint against anterior/posterior translation, upward vertical translation, and 'pitch' rotations (i.e., on the sagittal plane) of the tibial component rely on frictional forces generated by the keel's interference fit. If this friction between the keel and the slot is unable to constrain these motions, the tibial component will move relative to interfacing bone, experiencing micromotion. This micromotion can lead to the formation of fibrous tissue, arresting or damaging bone ingrowth, and limiting secondary fixation [201]. It may also contribute to subsidence seen in some cementless patients (further discussed in **Chapter 8.2**).

The new keel designs proposed in **Chapter 5** still fundamentally rely on these frictional forces to limit implant motion. Moreover, they require appropriate sizing of the keel to avoid excessive splitting forces, and careful technique to avoid excessively posterior keel cuts perioperatively, albeit with greater margins of safety.

If tibial component fixation was to be reviewed and a new fixation element was designed, it would ideally eliminate these concerns.

6.3 Pegs as an Alternative Fixation Element

A peg can generally be described as a short pin or bolt which is used for securing something to a surface [202]. Pegs are used in a wide variety of cemented and cementless implants as fixation elements. In medial UKR, they are found in the femoral component of all commercially available components, and in some tibial components such as the Persona Partial / ZUK implants (**Section 1.6**).

The shear resistance of pegs was explored in detail by Grigori et al [203], who demonstrated multiple key principles of peg fixation in resisting shear forces:

- Multiple pegs are able to act independently in resisting shear forces if placed sufficiently far apart.
- Smaller pegs provide greater shear resistance in the direction of applied load than larger pegs, corrected for surface area.
- High aspect ratio (long and thin) pegs provide greater shear resistance than low aspect ratio (short and thick) pegs, but fail more easily in excess load.

The axial resistance of pegs was assessed by Geraldes et al using a Push-Pull protocol similar to the one used in **Chapter 5**, and found that a simple plain cylindrical peg can retain 50-80% of push-in force on pull-out [201]. This is greater than any of the keels tested in **Chapter 5** (greatest ratio in PWSE keel, where $MaxF_{in}$ 545 N and $MaxF_{out}$ 234N: 43%), suggesting pegs can have improved primary fixation without increasing risk of fracture compared to keel designs.

Cursory intraoperative assessment of 20 tibias undergoing Cementless Oxford UKR have shown that holes for pegs can be drilled on the tibial floor after the transverse cut is made using current surgical approach; this is limited to the anterior half of the tibial floor, as

the posterior half cannot be accessed as further anterior tibial draw is restricted by the anterior cruciate ligament [86, 204].

In Cementless Oxford UKR, pegs could be explored to fix the tibial component. If pegs are designed to constrain tibial component motion without relying on frictional forces at the keel-slot interface, the keel and its fracture-inducing splitting forces in the medial proximal tibia could be avoided. The use of pegs, which would require holes to be drilled rather than a slot cut with a keel saw, can also greatly limit the risk of posterior cortex compromise. Furthermore, if small, high-aspect ratio pegs can be used safely, this will reduce the amount of bone resection needed. This can make the implant safer, particularly in anatomically smaller patients.

6.4 Design Aims

The aim of this re-design of the Cementless Oxford UKR tibial component keel is to eliminate fracture-related concerns whilst offering similar or superior fixation to the existing, and new, keel designs.

The design aims for this chapter are to:

Aim 1. Remove the need for a keel and slot.

Aim 2. Provide similar or superior fixation of the tibial component.

Aim 3. Determine the optimal peg profile and position to address forces experienced by the tibial component.

Aim 4. Describe changes to surgical instrumentation and technique needed to implant this new component.

6.5 Optimising Peg Profile

6.5.1 Study Design

An *in-vitro* Push-In Pull-Out (PIPO) study based on the protocol outlined in **Section 5.5.1** was performed. It involved the push-in and pull-out of 3D-printed titanium pegs into slots cut into polyurethane (PU) foam. Mechanical properties of the foam were as described in **Chapter 5**.

Holes for pegs were made using a pillar drill (RS Pro Bench Pillar Drill, RS Components Ltd, Northants, UK) and high-speed steel drill bits (Harlingen Tools, Harlingen, Netherlands) with thickness tolerances of ±0.01 mm. Interference was defined as the difference in diameter of a peg and the hole it was inserted into. Holes were made to be 15 mm deep in all tests. Push-In and Pull-Out tests were performed using a servo-hydraulic testing machine (Dartec HC 10, Zwick Ltd, Herefordshire, UK) which measures displacement and a S-beam load cell (FSB-01, Force Logic, Berkshire, UK) which measures vertical force. Foam was immobilised to ensure only keel displacement occurred (**Figure 6.1**). The test involved a displacement-controlled push-in of the keel at a rate of 10 mm min^{-1}, followed by a 10s dwell, a slower pull-out at a rate of 1 mm min^{-1} until keel was unloaded, another dwell of 10s, and pull-out of the keel from the slot at a rate of 10 mm min^{-1}. All pegs were inserted 9 mm vertically unless otherwise stated. Force, displacement, and time data were collected at 250 Hz for analysis. Each test was repeated three times (n=3).

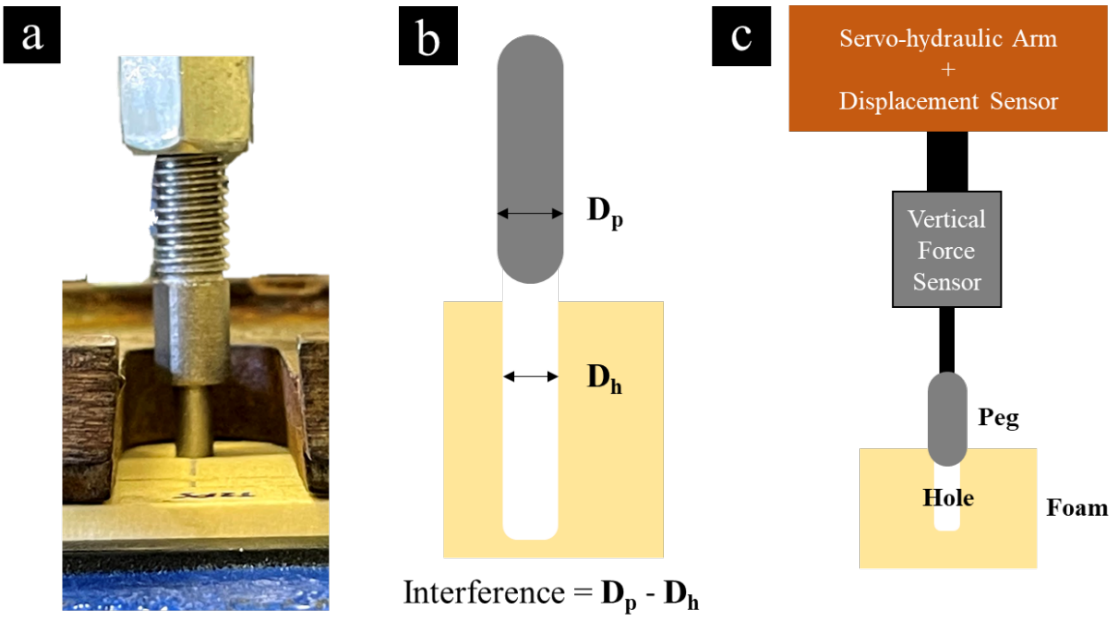


Figure 6.1: (a) *A typical peg PIPO test setup. PU foam is constrained from vertical motion,* ***(b)*** *Diagram representing interference.* ***(c)*** *Depiction of key components of PIPO test setup components.*

Raw data from the servo-hydraulic testing machine was processed using custom code (MATLAB, Natick, Massachusetts, USA), which identified and separated the Push-In, Unload, and Pull-Out phases, and identified the maximum push-in ($MaxF_{in}$) and pull-out ($MaxF_{out}$) forces recorded (**Figure 5.3**). Results from tests performed over a series of interferences, depths, or angles were fitted to appropriate regression lines. Single variable statistical comparisons were performed using Students' t-test or Mann Whitley U test, depending on parametricity, determined using Shaprio-Wilk tests. Two variable statistical comparisons were performed using extra sum-of-squares F test between regression lines. Any other tests performed are stated in-line in the respective sections. Data was analysed and visualised using GraphPad Prism (GraphPad Software, San Diego, California, USA) and Excel (Microsoft, Redmond, Washington, USA).

6.5.2 Design Elements Tested

A series of design elements were tested (**Table 6.1**) were designed using CAD (SOLIDWORKS, Dassault Systèmes, France) by an engineer, and were additively manufactured from powdered titanium (Cp-Ti Grade 2, AP&C, Saint-Eustache, Canada) with a Direct Metal Laser Melting system (Concept Laser MLAB200, General Electric, Boston, Massachusetts, USA).

All pegs were designed with a circular cross-sectional profile to maximise volume for a given surface area to reduce risk of pegs breaking, and to avoid edges which are more likely to induce edge loading and stress concentrations. All pegs unless otherwise stated also had a 2 mm radius at the tip.

Table 6.1: *Design elements and variants tested, with reasons for exploring the rationale and ideal outcome for each measurement.*

Design Element(s)	**Variants**	**Reason for testing**
Peg Diameter	3.7 mm, 4.7 mm, 5.7 mm	Compare the effect of peg diameter, taper, surface coat, and peg depth.
Peg Taper	0°, 1°, 2°, 3°	
Peg Surface Roughness	Porous, Smooth	
Peg Depth	3 mm, 6 mm, 9 mm	
Base Gap	No base gap, 2 mm base gap	Compare the effect of having no interference at the base of the peg.
Tip Profile	Round (2 mm radius), 30° 'Flat' (0.5 mm radius)	Compare the effect of a rounded vs relatively flatter, angled tip (as would be found on an angled peg).

Peg Angle	20°, 30°, 40°, all with and without constraint	Compare effect of peg angle. Pegs were tested with no constraint to determine effect of angle on axial pull-out. Tests were repeated with pegs constrained to vertical displacement to determine effect of pull-out in a vertical motion.
Tip Surface Roughness	Porous, smooth	Compare the effect of a porous vs smooth bottom on a porous peg, as done in **Chapter 5**.

Peg diameter, taper, surface coating, and depth, were tested as key properties of peg profile. Peg diameters of 3.7 mm, 4.7 mm, and 5.7 mm were chosen for testing as a clinically used porous coat is approximately 0.7 mm in thickness. For any tapered peg, the taper started from the base of the peg and descended to the tip of the peg. Smooth and porous surfaces are tested – they shared similar surface microstructure to clinically manufactured surfaces (discussed in **Section 5.5.3** and **Figure 5.5**).

Peg angle was tested with constraint to vertical motion, to simulate the presence of an angled peg on the anterior half of the tibial component. Such motion is most likely to occur in the anterior aspect of the tibial compartment when loads are transmitted through the knee (**Figure 6.2**), as large frictional forces can be expected at the posterior aspect of the tibial component which restrict sagittal motion of the component. Such loading and its implications to motion are discussed in detail in **Section 8.2.1**.

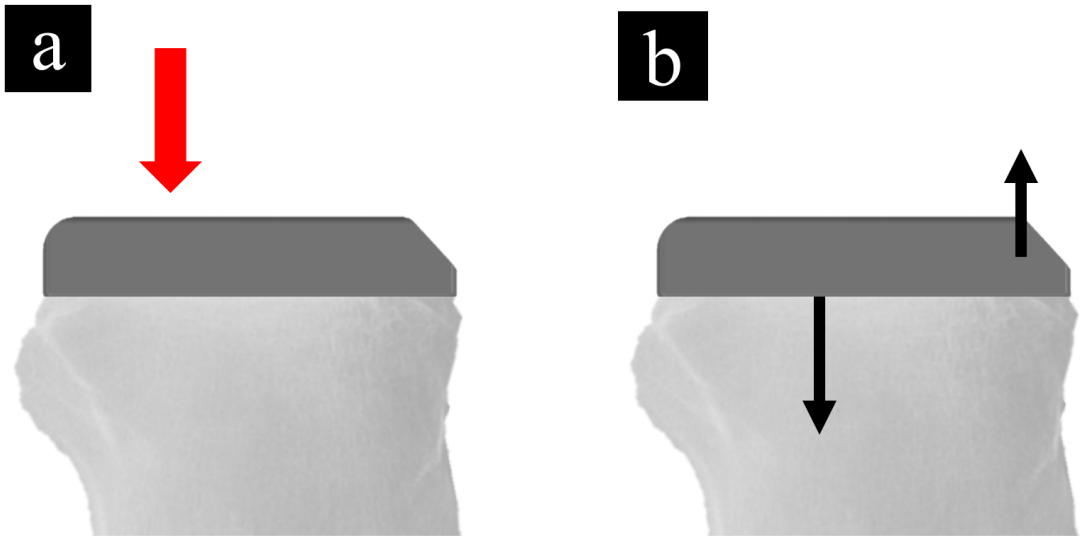


Figure 6.2: (a) *A load being applied at the location of the red arrow in the sagittal plane.* ***(b)*** *The predicted tilting implant motion that would result indicated with black arrows, demonstrating constrained vertical lift-off of the anterior aspect of the tibial component.*

Unlike all other tests where pegs were pushed in and pulled out as part of the test sequence, the angled pegs were pushed-in using a pillar drill spindle, with the foam secured to an appropriately angled worktable (RS Pro Bench Pillar Drill, RS Components Ltd, Northants, UK). Spindle position for push-in on the peg was pre-defined using a recessed area positioned superiorly and along the axis of the peg (**Figure 6.3**). Following push-in, the peg and foam specimens were secured to the materials testing machine for pull-out testing. Tests were performed with pegs constrained to vertical motion, which would be expected in the anterior aspect of the tibial component (**Figure 6.2b, 6.3**).

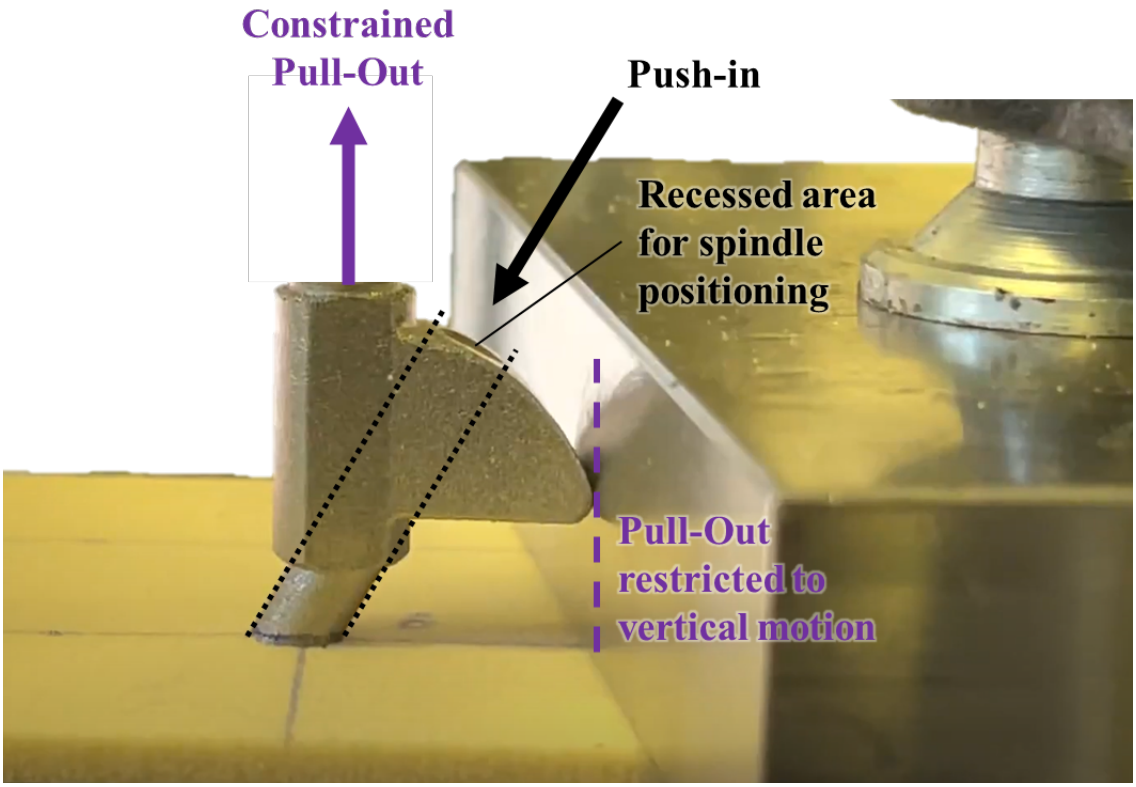


Figure 6.3: *Test setup for pull-out of an angled peg with vertical constraint, highlighting spindle position for push-in.*

The presence of a 'base gap', and varying tip profiles, were tested. In an angled peg, pull-out motions would induce edge loading at the base of the peg on the side of the acute angle (**Figure 6.4a**). A gap at the base with no interference would help to mitigate this, and was therefore explored (**Figure 6.4b**).

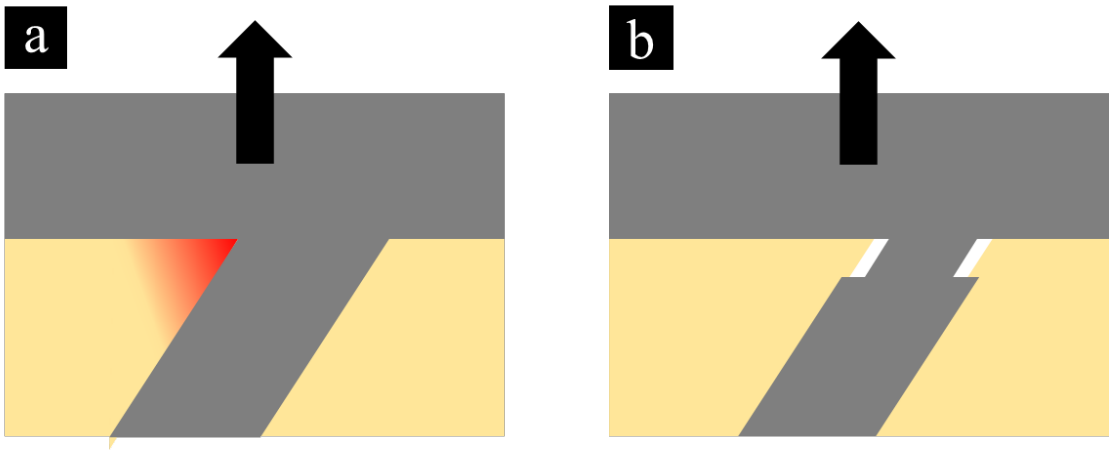


Figure 6.4: ***(a)*** *A depiction of the stress concentration resulting at the base of an angled peg of a constant diameter, indicated in red.* ***(b)*** *A depiction of a 'base gap' and how it mitigates stress concentrations.*

A flat, angled tip, when used with an angled peg, would be able to substantially increase the surface area of interaction between the peg and the superior surface of the hole, which would likely improve shear resistance [203] requiring greater force to pull out (**Figure 6.5**). However, based on discussions on taper in **Chapter 5**, a round-tipped peg can be expected present a less-sharp angle at the leading edge of the peg, and is likely to experience less rasping and therefore a higher pull-out force. To assess this, round tipped and a 30° angled flat-tipped peg were compared.

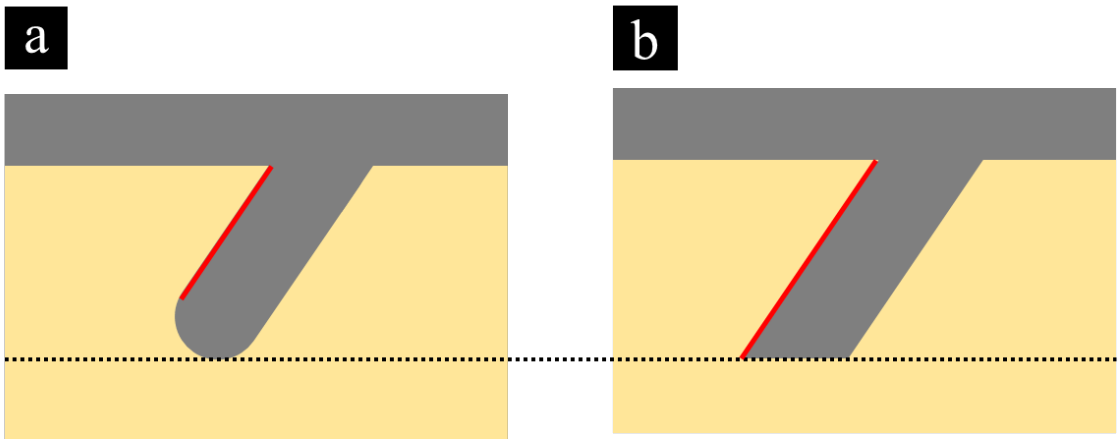


Figure 6.5: *Difference in surface area of interaction between peg and superior surface of the hole with* ***(a)*** *round-bottomed and* ***(b)*** *flat-bottomed pegs inserted the same vertical distance, demonstrated by the red line.*

Finally, following the positive findings of the porous-walled smooth-edged (PWSE) keel in **Chapter 5**, a similar design was tested with the porous-walled smooth-bottomed (PWSB) peg.

In tests where interferences were varied, interferences from 0.4 mm to 1.2 mm were tested in 0.2 mm increments, based on literature that 0.6-0.8 mm was the ideal interference for tibial subchondral trabecular bone [118].

Unless indicated, all pegs had a 2 mm radius at the tip, were not angled, had no taper, and were tested at 0.6 mm interference. Each of the three variants of tapered pegs (1°, 2°, and 3°) was tested 5 times, once at each interference, totalling n=3 at each interference. All other tests were performed in three times (n=3).

6.5.3 Results

6.5.3.1 Effect of Diameter

With greater interferences, maximum push-in force ($MaxF_{in}$) increased and maximum pull-out force ($MaxF_{out}$) had a generally parabolic trend in all peg diameters tested. With porous pegs, $MaxF_{in}$ increased with interference in all peg diameters. $MaxF_{in}$ values were similar between 4.7 mm and 5.7 mm pegs ($p=0.204$), but were significantly lower in 3.7 mm pegs compared to 4.7 mm pegs ($p<0.0001$).

$MaxF_{out}$ followed a parabolic trend across the range of interferences tested; an interference of 0.6 mm for 3.7 mm, 0.8 mm for 4.7 mm, and 1.0 mm for 5.7 mm pegs, resulted in greatest $MaxF_{out}$. $MaxF_{out}$ curves were significantly different between peg diameters (3.7 mm vs 4.7 mm, $p<0.0001$, 4.7 mm vs 5.7 mm, $p<0.0001$). Across all interferences, the highest $MaxF_{out}$ was achieved by 4.7 mm peg. At 0.8 mm, its $MaxF_{out}$ was 113 N, which was significantly higher than the 3.7 mm peg (3.7 mm vs 4.7 mm, 93 N vs 113 N, $p=0.0456$), but not the 5.7 mm peg (4.7 mm vs 5.7 mm, 113 N vs 101 N, $p=0.108$). There was little change in the $MaxF_{out}$ between 0.6-1.0 mm of interference (107 N vs 113 N vs 110 N, one-way ANOVA $p=0.317$) (**Figure 6.6**). Ratio of $MaxF_{out}$: $MaxF_{in}$ followed similar but inverse patterns to $MaxF_{in,}$ and converged at higher interferences.

Patterns were similar with smooth pegs, and results have been included in **Appendix E**.

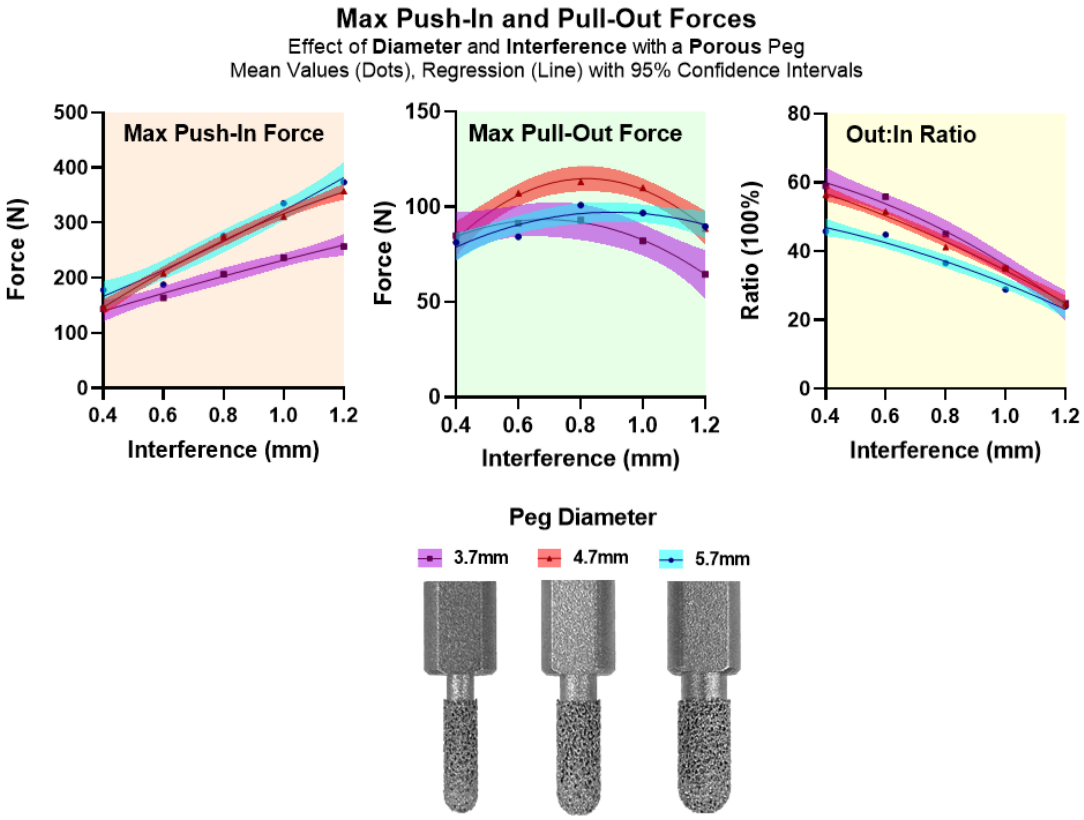


Figure 6.6: *Maximum Push-In, Pull-Out Forces, and ratio of values, with varying peg diameter and interference in a porous peg. Quadratic regression was performed for each variant across interferences.*

6.5.3.2 Effect of Taper

An increase in taper angle reduced $MaxF_{in}$ at lower interferences (0.4 mm interference, no taper 147 N vs combined tapered 66 N, p=0.0032), but this difference was lost in higher interferences (1.2 mm interference, no taper 357 N vs combined tapered 359 N, p=0.865). Increasing taper angle caused an apparent 'right shifting' of the $MaxF_{out}$-interference curve, resulting in significantly lower $MaxF_{out}$ in lower interferences (0.4 mm interference, no taper 83 N vs combined tapered 35 N, p=0.0105) and significantly higher $MaxF_{out}$ at higher interferences (1.2 mm interference, no taper 89 N vs combined tapered 146 N, p=0.0042) (**Figure 6.7**).

Patterns were similar with smooth pegs, and results have been included in **Appendix E**.

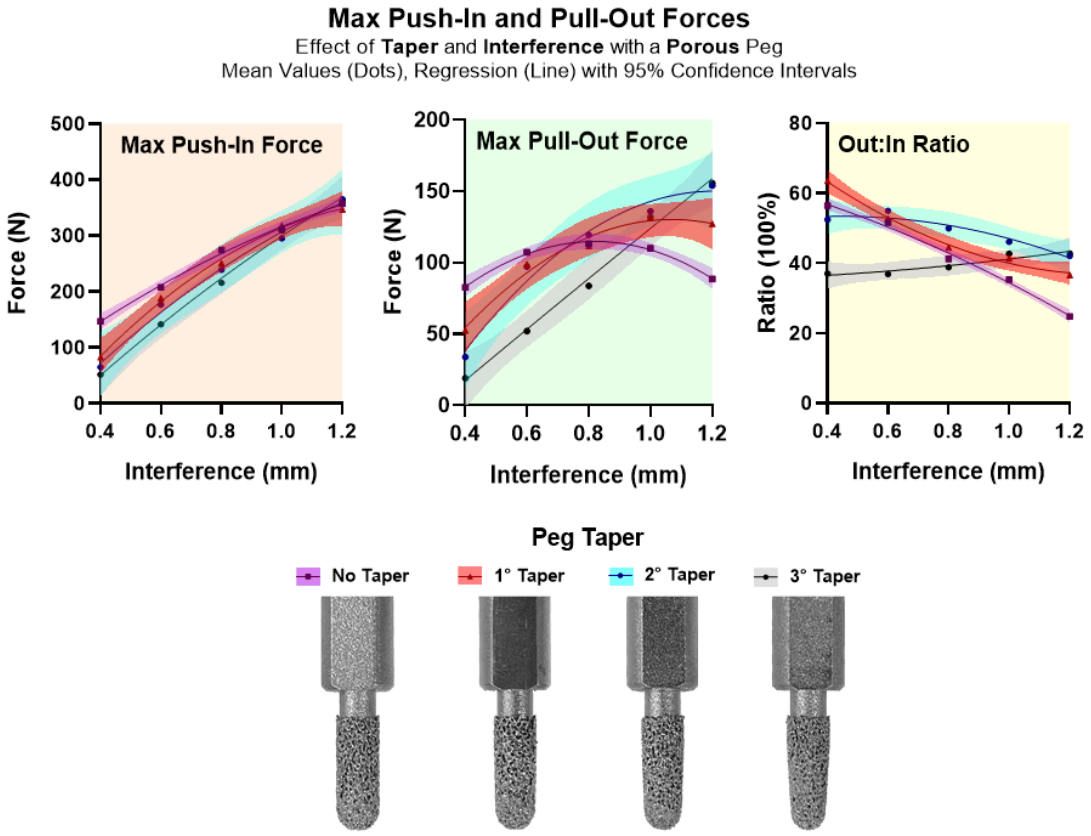


Figure 6.7: *Maximum Push-In, Pull-Out Forces, and ratio of values, with varying peg taper angle and interference in a porous peg. Quadratic regression was performed for each variant across interferences.*

6.5.3.3 Effect of Surface Roughness

$MaxF_{in}$ was similar across between smooth and porous pegs at lower interferences (0.4 mm interference, smooth 147.1 N vs porous 147.0 N, p=0.996), with a small divergence at higher interferences where porous pegs required greater $MaxF_{in}$ (1.2 mm interference, smooth 305 N vs porous 357 N, p=0.005). $MaxF_{out}$ values for smooth pegs was double that of porous pegs at lower interferences (0.4 mm interference, smooth 135 N vs porous 83 N, p=0.001), and further diverged at higher interferences across interferences (1.2 mm interference, smooth 180 N vs porous 81 N, p<0.0001). Consequently, the ratio of $MaxF_{out}$: $MaxF_{in}$ for smooth pegs remained approximately double that of porous pegs across all interferences (ratio of $MaxF_{out}$: $MaxF_{in}$, porous peg as a proportion of smooth peg at each interference, 0.4 mm: 61%, 0.6 mm: 65%, 0.8 mm: 59%, 1.0 mm: 55%, 1.2 mm: 42%, total: 56%) (**Figure 6.8**).

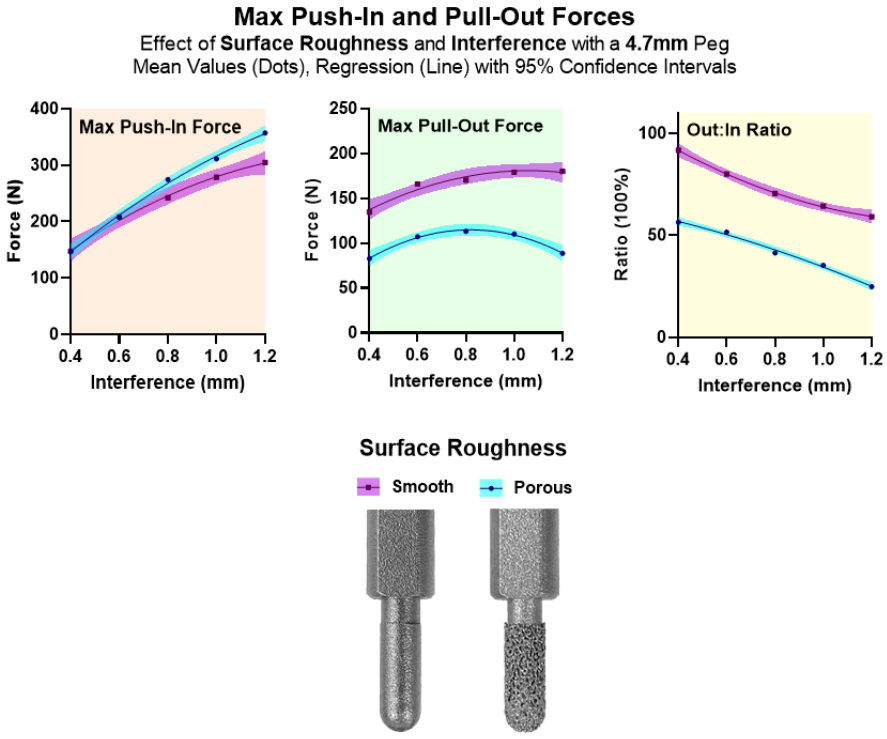


Figure 6.8: *Maximum Push-In, Pull-Out Forces, and ratio of values, with varying interference in a 4.7mm smooth and porous pegs. Quadratic regression was performed for each variant across interferences.*

6.5.3.4 Effect of Tip Profile

With greater interferences, $MaxF_{in}$ increased in both rounded tips, and flat-angle tips, on porous pegs. There was a large and significant difference in $MaxF_{out}$ between rounded and flat angled tips across all interferences tested. This was greatest at 0.8 mm interference, due to an increase in $MaxF_{out}$ in the rounded peg (0.8 mm interference, round-tipped peg 113 N vs flat-angle tipped peg 59N, p=0.0004), and the minimum difference was at 0.4 mm interference (round-bottomed peg 83 N vs flat angled peg 59 N, p=0.0039). Both tip profiles shared a similar downward gradient on $MaxF_{out}$: $MaxF_{in}$ ratio, with the rounded tip being approximately 10% higher in all interferences (**Figure 6.9**).

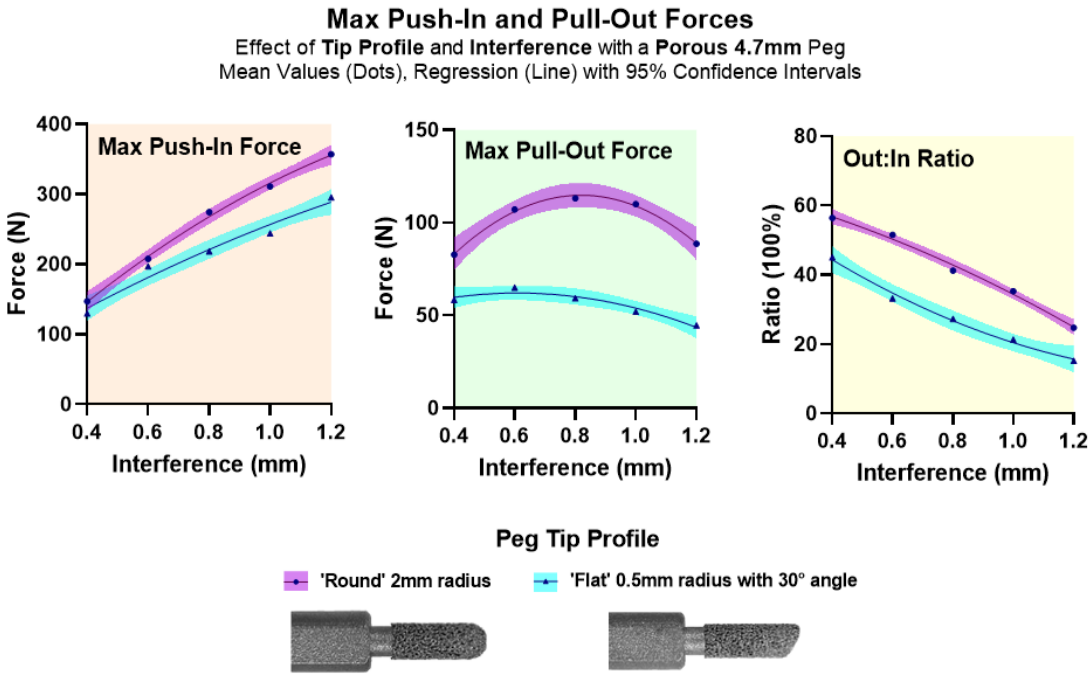


Figure 6.9: *Maximum Push-In, Pull-Out Forces, and ratio of values, with varying interference in a rounded tip vs a flat-angled tip. Quadratic regression was performed for each variant across interferences.*

6.5.3.5 Effect of Base Gap

The introduction of a 2 mm gap at the base of the peg reduces the overall height of the peg's porous surface from 9 mm to 7 mm. The effective change in interference, given the 2 mm radius at the bottom of the peg, is 5.4 mm at 0.4 mm of interference, increasing to 6.2 mm at 1.2 mm of interference (**Figure 6.10**). $MaxF_{in}$ diverged and $MaxF_{out}$ converged with increasing interference between variants, with the base gap variant experiencing lower $MaxF_{in}$ (0.4 mm interference, no gap 147 N vs gap 120 N, p=0.278. 1.2 mm interference, no gap 357 N vs gap 292 N, p=0.0353) and $MaxF_{out}$ (0.4 mm interference, no gap 83 N vs gap 62 N, p=0.120. 1.2 mm interference, no gap 89 N vs gap 81 N, p=0.358). Both variants had a similar $MaxF_{out}$: $MaxF_{in}$ ratio (**Figure 6.10**).

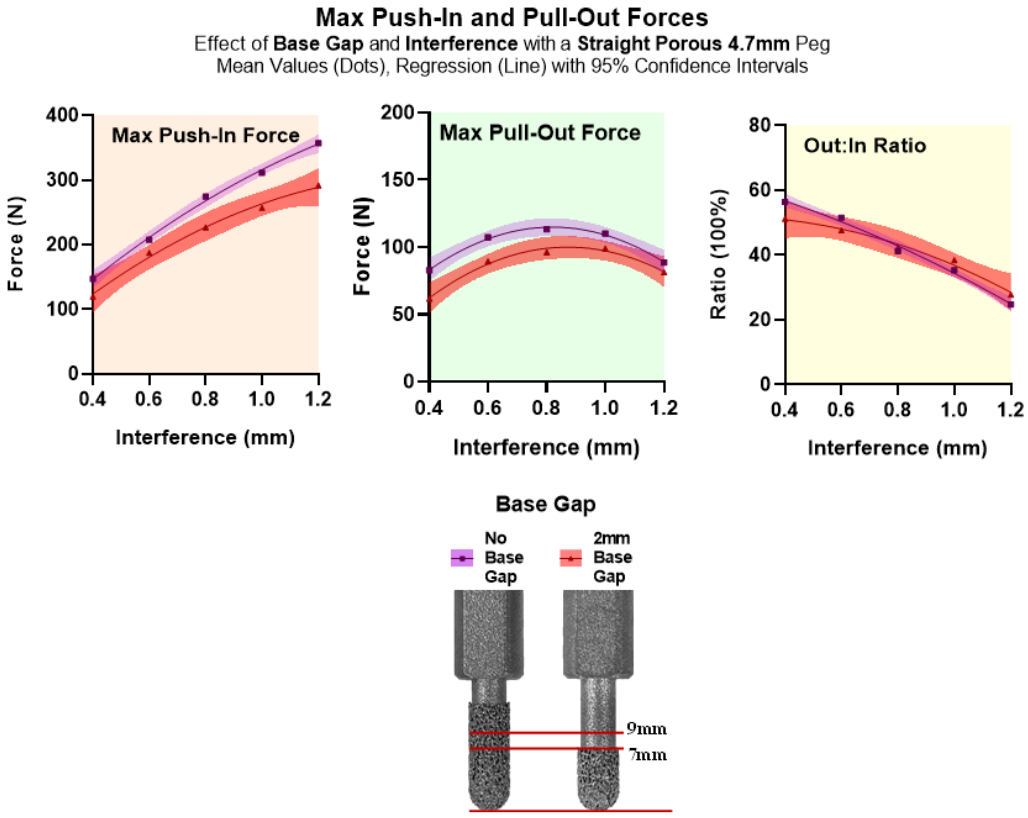


Figure 6.10: *Maximum Push-In, Pull-Out Forces, and ratio of values, with varying interference in without a gap at the base, and a 2mm base gap. Quadratic regression was performed for each variant across interferences.*

6.5.3.6 Effect of Insertion Depth

A deeper insertion of the peg increases $MaxF_{in}$ and $MaxF_{out}$ in both smooth and porous pegs. The rate of increase of both $MaxF_{in}$ and $MaxF_{out}$ is greater with the smooth peg compared to the porous peg. This difference is greatest with $MaxF_{out}$, which was near-identical in both smooth and porous pegs at 3 mm insertion depth (smooth 17 N vs porous 16 N, p=0.339) and 55% higher at 9 mm insertion depth (smooth 165 N vs porous 107 N, p=0.002). This resulted in a similar, substantial divergence in $MaxF_{out}$:$MaxF_{in}$ ratio with increasing peg insertion depth, where the ratio for the smooth peg increased at a higher rate relative to the porous peg (**Figure 6.11**).

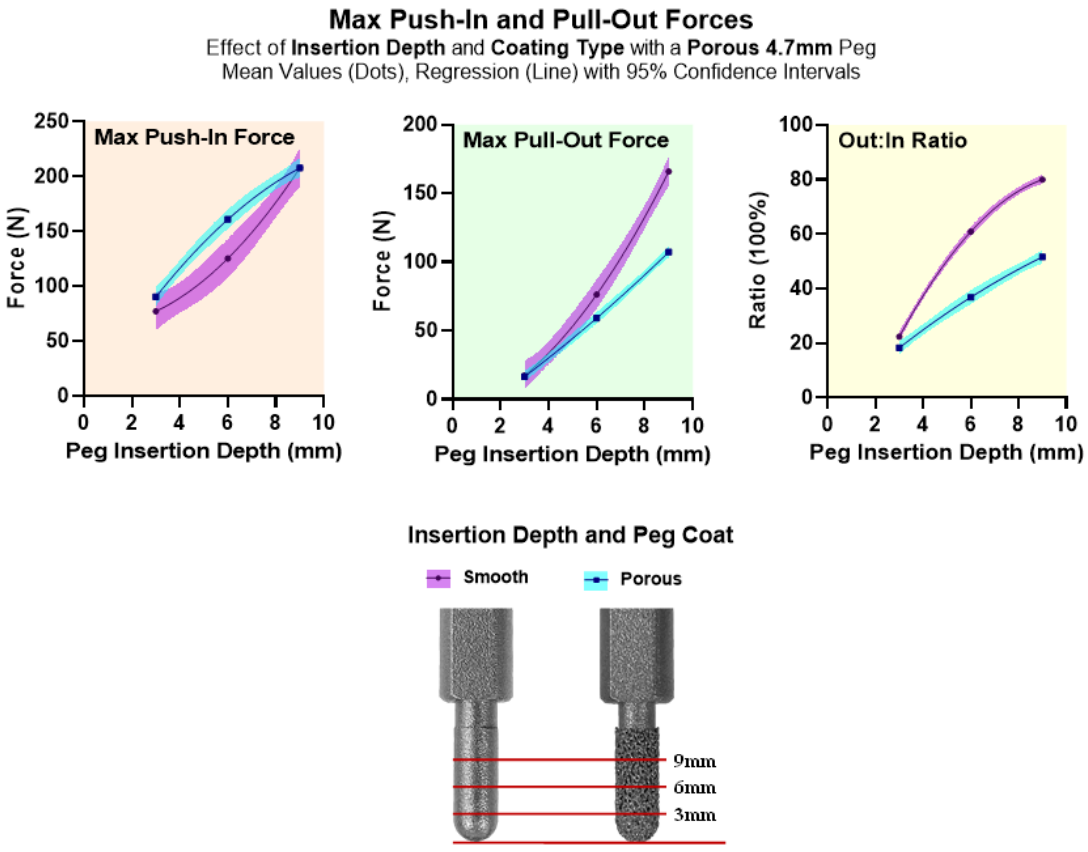


Figure 6.11: *Maximum Push-In, Pull-Out Forces, and ratio of values, with varying peg insertion depth in smooth and porous pegs. Quadratic regression was performed for each variant across insertion depths.*

6.5.3.7 Effect of Angle

Peg insertion angle had the greatest effect on $MaxF_{out}$ seen across different design elements tested. There is a 22% increase in $MaxF_{out}$ in straight vs angled pegs in smooth pegs (straight 166 N vs combined angled 214 N, p=0.004) and a greater 80% increase in porous pegs (straight 107 N vs combined angled 193 N, p<0.0001) (**Figure 6.12**).

$MaxF_{out}$ of smooth pegs increased 25% from 190 N in 20° pegs to 237 N in 40° pegs (p=0.0004). $MaxF_{out}$ of porous pegs similarly increased 19% from 178 N in 20° pegs to 211 N in 40° pegs (p=0.0162). Across angled pegs, $MaxF_{out}$ of smooth pegs was significantly and consistently 10% greater than porous pegs (comparison of curves, p<0.0001) (**Figure 6.12**).

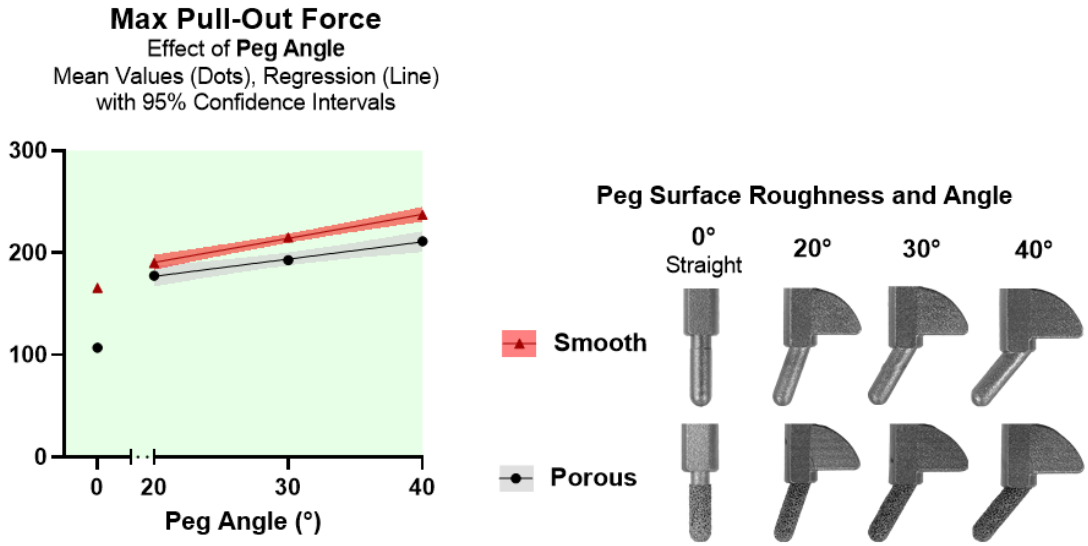


Figure 6.12: *Maximum Pull-Out Forces with a straight peg and with pegs angled 20°, 30°, and 40° against vertical, with smooth and porous pegs. Linear regression was performed between the angled pegs.*

6.5.3.8 Effect of Tip Surface Roughness

With a smooth tip, there was a 12% reduction in $MaxF_{in}$ compared to a porous tip (porous 208 N vs smooth 183 N, p=0.0138), and $MaxF_{out}$ was similar (porous 107 N vs smooth 113 N, p=0.112). This is notably different from the difference between porous and smooth-edged keels found in **Chapter 5**, where there was a 26% lower $MaxF_{in}$ and 31% higher $MaxF_{out}$ (**Figure 6.13**)

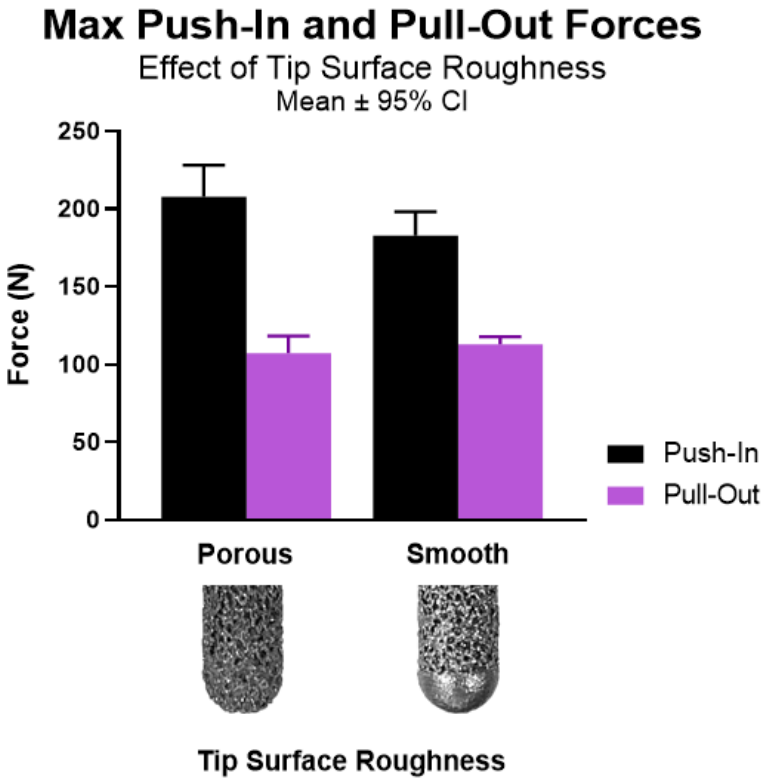


Figure 6.13: *Maximum Push-In and Pull-Out Forces with a porous vs smooth tip.*

6.5.4 Discussion of Findings

Changes in peg design elements resulted in multiple significant changes in maximum push-in and pull-out forces ($MaxF_{in}$ and $MaxF_{out}$) in pegs. The most striking improvement in $MaxF_{out}$ was following the use of a constrained angled peg – this will form the basis of eventual peg design discussed in **Section 6.6**. In this section, the effect of each of the tested design elements, and suggestions for patterns seen, are proposed.

A 4.7 mm peg with a porous coat inserted with 0.6-1.0 mm of interference had the highest ratio of $MaxF_{in}$:$MaxF_{out}$ forces across the diameters and interferences tested. This is consistent with findings by Campi et al who show ideal interference in a keel to be 0.7 mm, with minor changes between 0.6-1.0 mm [118].

Taper angle progressively reduced $MaxF_{in}$ at lower interferences, which is likely associated with less force and energy used for rasping the foam surface as it enters the hole (the phenomenon is discussed with the tapered keel and slot in **Section 5.5.5**). Taper angle progressively increased $MaxF_{out}$ at the higher interferences tested (0.8–1.2 mm) but substantially decreased $MaxF_{out}$ at lower interferences. The increase at higher interferences was likely due to the reduced damage at the wall hole due to less rasping, while the decrease at lower interferences may be attributed to the low surface area of contact and low surface pressures that result. A safe peg design would minimise changes in fixation due to varying interference which can occur clinically. Therefore, a straight peg would be preferred over a tapered one.

A porous coat reduces $MaxF_{out}$ by approximately half across all interferences compared to a smooth coat. A flat-bottomed porous peg had a further halving of $MaxF_{out}$ compared to a round-bottomed peg. Both phenomena are most likely due to successive increases in

rasping of the hole by the peg on entry (discussed in detail with the porous keel in **Section 5.5.5**).

The difference in $MaxF_{out}$ between smooth and porous pegs is diminished in constrained angled pegs. When pull-out was constrained to a vertical only motion, $MaxF_{out}$ of porous and smooth pegs remained within 90% of one another across the angles tested, and increased by 19-25% from 20° pegs to 40° pegs. The close similarity and pattern in $MaxF_{out}$ between smooth and porous pegs strongly suggest that a common mode of failure exists between them. When constrained, the foam above the angled peg applies a bony constraint and will need to fail to peg to be pulled up. Therefore, the $MaxF_{out}$ would be dependent on the failure of the foam itself, instead of friction-based interactions at the foam-peg interface, resulting in similar results between smooth and porous pegs. The small increase in $MaxF_{out}$ at steeper angles is likely due to a larger foam volume being recruited by the longer pegs at higher angles. The small but consistently lower $MaxF_{out}$ in the porous compared to the smooth pegs may be attributed to structural damage caused by the peg on push in – it is possible that the rasping effect of the porous surface leads to the introduction of micro-cracks extending from the surface of the hole which weaken the foam.

Increasing peg depth appears from 3 mm to 9 mm causes a linear increase in $MaxF_{out}$ in porous pegs and a greater-than-linear increase in $MaxF_{out}$ in smooth pegs. Despite this appearance, it is likely that there is a proportional increase in $MaxF_{out}$ with the surface area of foam-peg contact in smooth pegs. This is because the leading edge of the peg has a round bottom of 2 mm radius and therefore will not experience any interference in the first ~1.5 millimetres. On balance, there is likely a less-than-proportional increase in $MaxF_{out}$ with the porous peg, which may be due to a continuous rasping action as the peg

enters further into the hole. This difference is consistent with the findings of the base-gap test, where the introduction of a 2 mm gap at the base of the peg (2 mm removed from 7.5 mm in interference height - a 27% decrease) resulted in a less-than-proportional decrease in $MaxF_{out}$ by 15%.

The smooth-bottomed peg did not introduce the same decrease in $MaxF_{in}$ and increase in $MaxF_{out}$ seen with the smooth-edged keel in **Chapter 5**. It is not immediately clear why this might be. This difference is most attributable to the difference in the radii of the leading edges. Keels are designed to have a 1.0 mm radius at their edge whilst the pegs have a 2 mm radius. Similar to the difference seen with the round vs flat-tipped pegs and the effect of peg taper, the smaller radius may result in greater rasping of the hole on entry in keels, which is mitigated by the smooth edge. However, this rasping may already be minimised the peg which has a larger radius and therefore a more parallel surface contacting the slot, diminishing the added benefit of a smooth bottom.

The Push-In Pull-Out (PIPO) study design used in this study was based on its earlier use in studying keel design. Therefore, several of the methodological limitations apply to this chapter as well, namely limitations in comparability, applicability of foam mechanics to trabecular bone, need for further measurements to be analysed, and the need for validation with more physiological tests (discussed in more detail in **Section 5.5.6,** physiological tests of fracture and fixation are performed in **Chapters 7 and 8**).

Interferences are assumed in this study based on the size of drill bits measured and used. While this is adequate for the aims of this study, a more precise characterisation of these effects ought to require measurement of interferences and assessment of force-interference data as two continuous variables.

There are multiple statistically significant patterns noted in this study, and several hypotheses are made in the discussion (**Section 6.5.4**). Several of these explanations apply the concept of a porous or flatter/smaller-radii leading edge rasping a hole. While intuitive, this observation is likely the culmination of multiple complex mechanical phenomena, including static and dynamic friction, foam deformation, and foam failure models. There is limited understanding of these concepts in literature, and further limited understanding of how applicable they are to bone. Empirical characterisation of these properties would require a combination of mechanical and computational testing to validate this 'rasping' effect and other hypotheses proposed. This applies to hypotheses made about the keel-slot interactions in **Section 5.5.5** as well.

Finally, due to the wide scope of design elements explored in this study, not all permutations of design elements were compared. Where such comparison was not done, it is assumed that the effects of each design element would be independent. A more detailed characterisation would empirically assess all permutations to determine if design element effects are indeed independent or confound one another.

Finally, hole depth was kept constant across all tests and its effect was not tested. However, hole depth is unlikely to influence results of this study, excluding excessively short holes where pegs interact with the base of the hole. This will be further discussed in **Section 6.6.2**.

6.6 A New Tibial Component with Peg Fixation

6.6.1 Proposed Peg Profile

When an angled peg is constrained, the increase in pull-out force compared to an equivalent straight peg is greater than all other differences seen in the other design elements tested. Therefore, the final design aims to maximise this effect of constrained pull-out. This can be done through the use of an angled peg with an angled, flat, tip profile. The addition of a base gap will reduce the likelihood of stress concentrations in the bone and peg (**Section 6.5.2**), thereby improving the safety of the peg. While a flat-angled tip and a base gap reduced the pull-out forces in the straight pegs, the change in mode of failure when an angled peg is used (from friction-based constraint to failure of bone superior to the peg) would likely diminish any reductions in pull-out force.

Based on the height of the existing keel, a maximum vertical peg height of 9 mm can be considered safe. However, a longer peg of a fixed diameter has a smaller aspect ratio (i.e. is thinner) which increases susceptibility to shear failure [203]. Furthermore, a longer peg increases the pivot arm between base of the peg at the component floor and tip of the peg, which increases risk of bone damage due to surgical errors (such as inaccurate positioning or impaction). Similarly, a greater peg angle geometrically increases the length of peg. However, a smaller (i.e., more vertical) peg angle restricts access to posterior regions of the tibial floor to drill holes [204]. Therefore, a conservative vertical peg height of 6 mm with a 30° angle was chosen. The base gap will be scaled proportionally from 2 mm with 9 mm insertion, to 1.3 mm with 6 mm insertion.

A 4.7 mm non-tapered peg was found to be the safest from the various peg diameters and tapers tested, as it had the least variability in $MaxF_{out}$ across the 0.6-1.0 mm interference range.

While the importance of bone ingrowth in pegs has not been tested, the findings in **Chapter 3** suggest that porous surface should be used in all bone-implant interfaces. As the porous pegs performed within 90% of the pull-out force of the smooth pegs, they can be deemed safe.

In summary, based on the findings of this study, the peg profile which best benefits fixation of the tibial component would likely:

- Be 4.7 mm in diameter, inserted with 0.8 mm interference (0.6-1.0 mm is safe).
- Sit at a 30° angle to the vertical.
- Be inserted 6 mm in depth.
- Have a porous surface, no taper, an angled tip profile, and a 1.3 mm base gap.

This design is visualised in **Figure 6.14**.

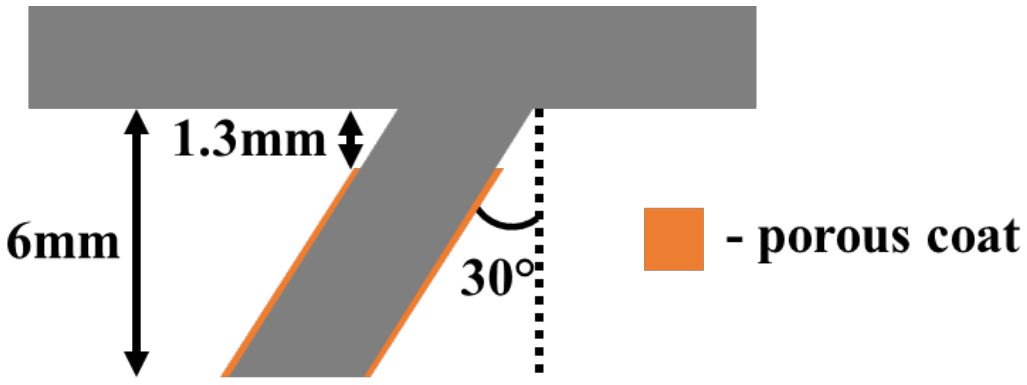


Figure 6.14: *Proposed peg profile incorporating all suggested design elements (not to scale).*

6.6.2 Proposed Peg Number and Distribution

In **Chapter 5**, the mean $FMax_{out}$ of the standard keel was 178 N and small PWSE keel is 234 N. In this chapter, the peg 30° angled peg tested had a $FMax_{out}$ of 193 N, and the changes to the design discussed in **Section 6.5.1** (shortening height from 9 mm to 6 mm and addition of a base gap) would likely reduce this value. Therefore, one peg is likely to be insufficient to replace a keel design.

Grigori et al [203] suggests that pegs placed further apart are more likely to act independently. If more than one peg is used, the pegs would need to be adequately far apart to ensure that the resulting combined $FMax_{out}$ is closer to the sum of the $FMax_{out}$ of single pegs. Furthermore, it can be mechanically expected that more than one peg would be necessary for rotational stability.

Therefore, the use of two pegs on a tibial component is proposed. To allow them to be positioned as far as possible away from one another, one will be positioned at the sagittal midpoint of the tibial component which is the posterior limit for making a hole intraoperatively [204]. The other will be positioned as anteriorly as possible within known safe range to constrain anterior lift-off (**Figure 6.2**); this would be at the anterior aspect of the tibial component.

It is not immediately clear where on the coronal axis (i.e., horizontally on an AP view) the pegs should be placed. If too close to the tibial wall, pegs/holes may act as an extension of the vertical cut used to prepare the tibia; which is known to increase the risk of fracture [192, 205]. Conversely, if the pegs are too close to the medial edge, there would be relatively less bone mass available for fixation. Therefore, the pegs can be positioned on the same horizontal position as the current keel.

Based on these findings, the use of two anteriorly placed, angled pegs is proposed, positioned as shown in **Figure 6.15a**. This design will henceforth be termed the Two-Peg. To implant the Two-Peg tibial component, appropriately positioned and congruently aligned angled holes are necessary. To achieve this, a new drill template is proposed (**Figure 6.15b**). Holes will be made to be 2mm deeper than depth of the pegs, which is the same clearance in existing and new keel designs, where peg is unlikely to interact with the base of the hole.

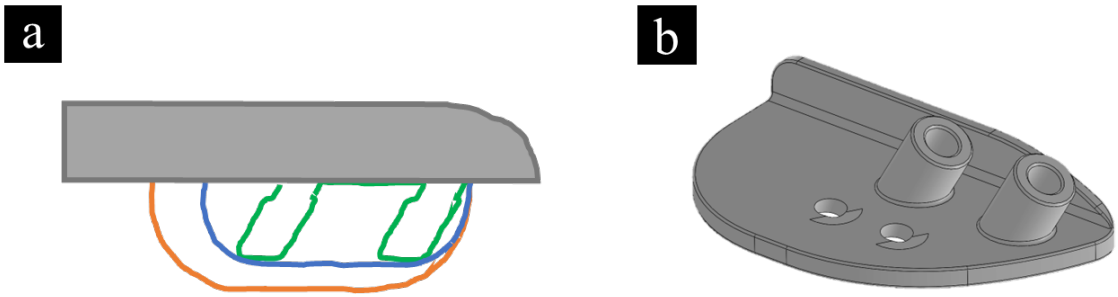


Figure 6.15: (a) *Position of the two pegs in new design in a lateral view of the tibial component (in green), overlayed on the positions of the small keel (in blue), and standard keel (in orange).* ***(b)*** *A custom designed template for the positioning and congruent alignment of holes to be drilled for a Two-Peg tibial component.*

This new design will need to be assessed compared to the existing and new keel designs. This will be performed in **Chapters 7 and 8**.

6.7 Chapter Summary

It is expected that the tibial component motion involves anterior lift-off which is constrained to vertical motion (outlined in **Section 6.5.2**). Based on this, a new approach to fixation with two anteriorly positioned angled pegs, in place of a keel, has been proposed.

Based on PIPO testing, this new tibial component is likely to provide superior primary fixation to the existing keel-based tibial component. Due to reduced bone resection and the lack of keel-induced splitting forces, it is also likely to reduce fracture risk compared to a keel design. However, these will need to be verified using more physiologically relevant tests of fracture and fixation. These will be explored in **Chapter 7** with load-to-fracture testing, and **Chapter 8** with assessment of anterior lift-off.

Compared to the change in keel size proposed in **Chapter 5**, this change in tibial component design shifts away from current keel-cut instrumentation and technique. This removes the need for a keel cut, eliminating the risk of posterior cortex compromise, but may itself introduce new complications which are not presently identifiable. New templates, and a drill in place of a keel cut saw, is also needed. The implications and next steps of these factors are discussed in **Chapter 9**.

7 Fracture Risk in a Very Small Tibia: The Effect of Different Fixation Elements on Load-to-Fracture

7.1 Chapter Motivation and Aims

In **Chapters 5 and 6**, an assumption was made that interference and keel depth increased fracture risk. While this may seem intuitive due to the introduction of splitting forces by the keel, and reduction of bone mass below the keel, it was not verified.

At the end of **Chapter 5 and Chapter 6**, new designs were proposed to replace the existing keel structure for tibial component fixation – a smaller porous, or porous-walled smooth-edged keel, and a Two-Peg design. Preliminary testing with Push-In Pull-Out tests have found that they demonstrate lower push-in forces and higher pull-out forces than the standard keel. They also travel less deeply into the tibia, and require less bone resection than the existing keel.

In this chapter, a more physiologically relevant test of fracture risk was designed and used to:

Aim 1. Determine the effect of keel interference and depth on fracture risk.

Aim 2. Determine if, and to what extent, the new replacement designs for the existing keel are able to decrease fracture risk.

Tests will be performed using a very small tibia, where incidence of fracture has been shown to be higher than in larger sizes (discussed in **Chapter 5**).

7.2 Why a keel may cause a fracture

The exact mechanical and physiological processes underlying peri-prosthetic stress fractures are not known. As described in **Chapter 5,** fractures tend to present a few weeks after surgery: they are generally believed to be initiated during surgery, and then progress thereafter.

In this chapter, two potential fracture-inducing processes are described and assessed. First, creating the keel slot requires resection of bone, which is hypothesised to increase the stress in the remaining bone and increase risk of fracture. Second, interference between the keel and the slot produces internal splitting forces in the proximal tibia. The greater forces needed to push-in a keel would induce splitting forces along the slot [118, 119, 196]. These could initiate a fracture, or induce structural damage that propagates upon weight bearing to result in a fracture. Bone can remodel to support these loads, but this process takes months [206]. It is hypothesised that in the early postoperative period prior to bone remodelling, such adaptations would have yet to occur, and increase fracture risk.

A combination of bone resection and internal stresses would weaken the structural integrity of the of the proximal tibia, and therefore be expected to reduce the loads needed to pass through the joint and induce a fracture. This will be assessed by performing a mechanical study of loads needed to induce fracture, and using force required to fracture as a metric for estimating fracture risk, as previously performed in literature [106, 207].

7.3 Testing Load-to-Fracture

7.3.1 Study Aims and Methods

This *in-vitro* comparative mechanical study of load-to-fracture aims to explore the effect of creating a slot and inserting a keel, on load-to-fracture in an anatomically very small tibia, at two physiologically relevant loading positions. This study also aims to explore potential changes to the existing keel design to determine if and how much they change the load-to-fracture.

This study was performed using titanium tibial components inserted into polyurethane foam which acts as a trabecular bone analogue. Components were designed by an engineer using CAD (SOLIDWORKS, Dassault Systèmes, France) to be structurally identical to the Size 'A' Cementless Oxford medial UKR tibial component. Components were additively manufactured from powdered titanium (Cp-Ti Grade 2, AP&C, Saint-Eustache, Canada) with a Direct Metal Laser Melting system (Concept Laser MLAB200, General Electric, Boston, Massachusetts, USA). These were inserted into solid rigid polyurethane foam with a density of 20 pounds per cubic feet (PCF) which has material properties similar to subchondral trabecular bone found in the proximal tibia (PCF 20 foam: density 0.32g/cm^3 and compressive modulus 210 MPa, vs trabecular bone: 0.3g/cm^3, range 14–345 MPa, Sawbones, Malmo, Sweden) [197-199].

The foam was machined to the shape of the proximal medial tibia which had experienced a peri-prosthetic fracture (**Figure 7.8**). The patient had a Size 'A' tibial component, which is classed as a 'very small tibia' [105]. Foam was machined to the anatomy of a medial tibial condyle (VMC 1000II, Hardinge, St. Gallen, Switzerland) based on a 3-

dimensional reconstruction of the patient created by an engineer from Computer Tomography (CT) scans of the patient knee prior to fracture (**Figure 7.8**).

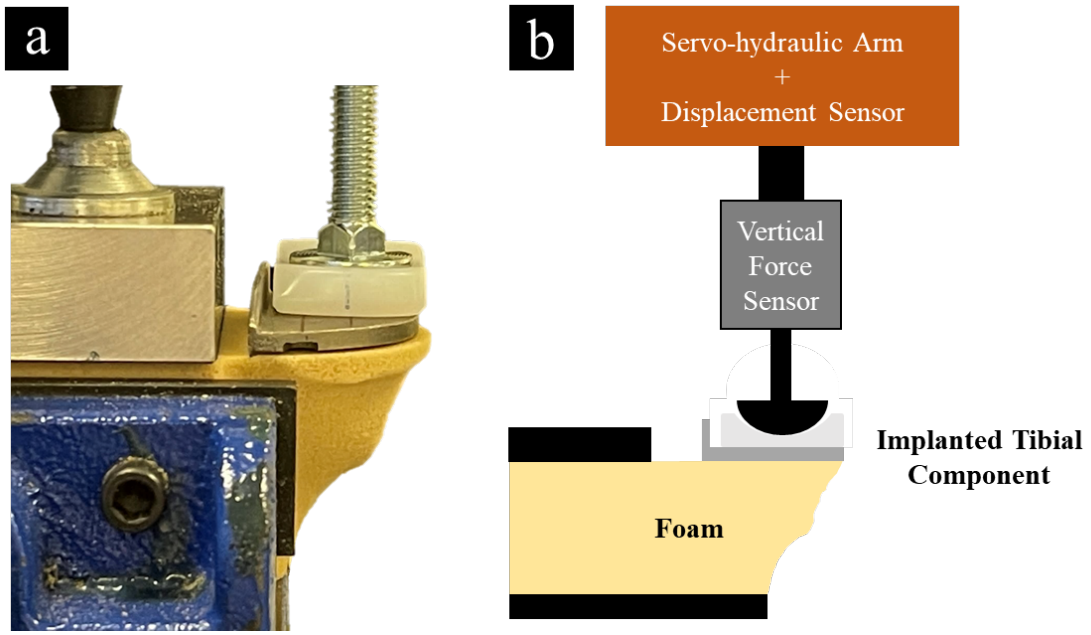


Figure 7.1: (a) *Image of setup for load-to-fracture testing.* ***(b)*** *Diagram of components in test setup.*

Testing was performed using printed Size 'A' tibial components, implanted using the standard surgical technique and instruments: the use of a keel cut saw, guided by a template, to create the vertical slot for insertion of keel. Keels were inserted using the clinically used keel impaction tool [86]. The custom clip-on template modifier designed for use with the small keel in **Chapter 5** was used for the small keels; when used with the keel cut saw, it produces a smaller slot with the same clearance in length, depth, and width as the standard template produces for the standard keel (**Figure 5.7**). The template and method for the Two-Peg component proposed in **Section 6.6.2** was used for preparing the tibial floor for Two-Peg fixation. Implantation was performed using the same impaction tool used for keel-based components.

Five keel variants were tested. Standard keel, small porous keel, and no keel variants were tested towards the first aim of this study to determine the effect of slot size and interference on load-to-fracture. Small porous and porous-walled smooth-edged (PWSE) keels, and Two-Peg, were tested to determine if, and how much, they change load-to-fracture compared to the standard keel. All variants were used with Size 'A' tibial components.

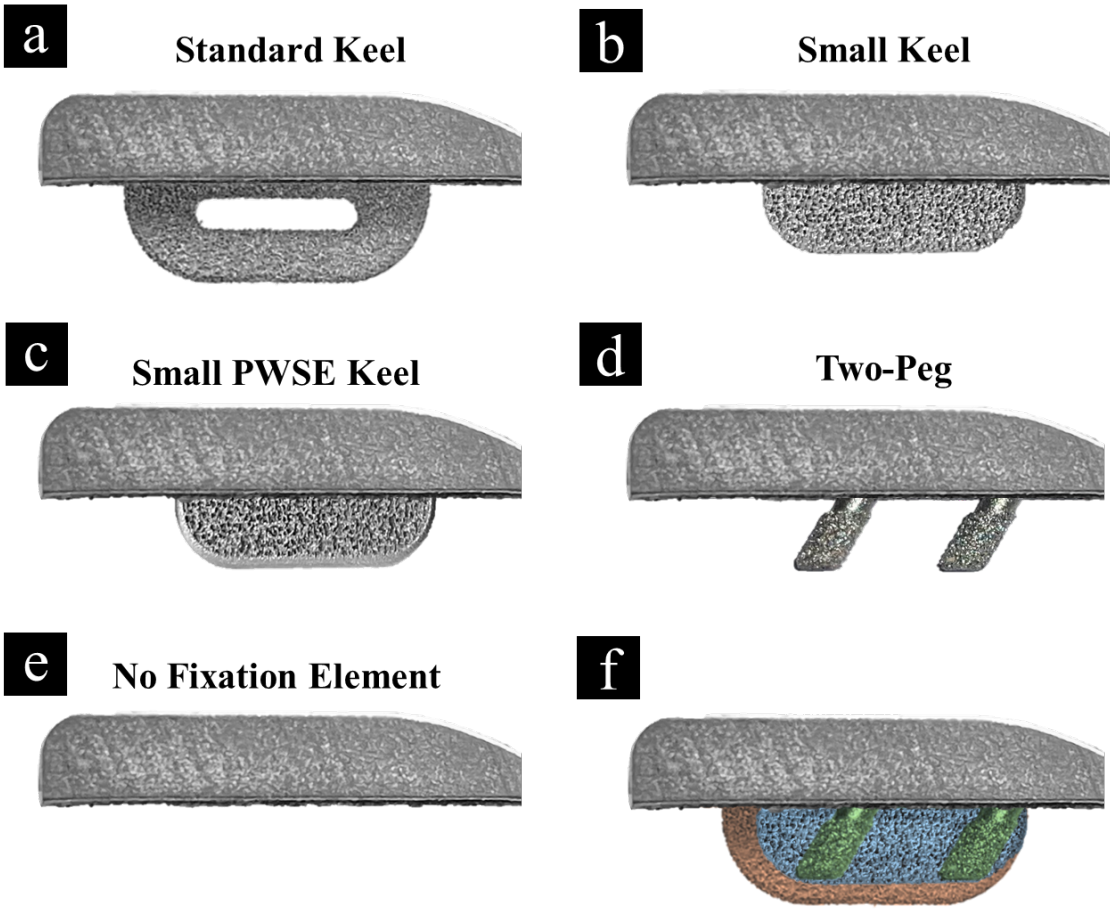


Figure 7.2: *Keel Designs explored in this study.* ***(a)*** *Standard keel found in currently used clinical components,* ***(b)*** *Small porous keel,* ***(c)*** *Small porous-walled smooth-edged keel,* ***(d)*** *Two-Peg, and* ***(e)*** *no keel.* ***(f)*** *Different fixation elements overlayed – standard in orange, small in blue, Two-Peg in green. Small keel designs are as described in* ***Chapter 5****. Two-Peg design is as described in* ***Chapter 6****.*

Load-to-fracture testing was performed using a servo-hydraulic testing machine (Dartec HC 10, Zwick Ltd, Herefordshire, UK) which measures displacement, and a S-beam load cell (FSB-01, Force Logic, Berkshire, UK) which measures vertical force. Loading was performed at a rate of 0.5 mm s^{-1} until fracture occurred. Loading was performed 13 mm away from the tibial wall based on estimated neutral bearing position on tibial condyle.

A no-keel tibial component was used to test load-to-fracture without a slot, as a negative control test to obtain a baseline load needed for fracture. This was compared with loads needed to fracture tibias with slots but without a keel inserted, to assess the effect of the keel cut alone in inducing fractures. Tests were then repeated with a standard and small keel tibial component inserted into a slot, to assess the added effect of inserting keels (thereby introducing interferences) of different depths on load-to-fracture. The small PWSE keel and Two-Peg were then similarly assessed.

To determine if there was any effect of loading position, tests with varying slot and keel depths were performed first at the midpoint of the component in the sagittal plane/AP axis, identified to be the anterior-most position encountered in motions expected in key activities of daily living patients can be expected to perform post-operatively: step-up motions (e.g., when walking up stairs) and knee-bend motions (e.g., when rising from a chair) [208, 209]. Tests comparing the standard, small, and no keel variants were repeated at 8 mm posterior to the midpoint of the implant, identified to be the posterior-most position encountered in step-up and knee-bend motions [208, 209]. These positions are henceforth referred to as ‘central’ and ‘posterior’.

Fracture load was defined as the force recorded at the point immediately preceding failure of the test specimen. Fractures were further characterised by an analysis of the path taken by the fracture. Path taken on the coronal plane was measured as the angle made by the

fracture relative to vertical, from the top of the fracture to its lateral-most position, as observed anteriorly and posteriorly. The average of anterior and posterior measurements was used to calculate a coronal fracture path angle (CFPA).

All tests were performed n=5. All datasets were tested for normality using Shapiro-Wilk. Statistical comparisons were performed using two-tailed Student's t-test if both groups compared were parametric; else Mann-Whitley U-test was performed.

7.3.2 Results

7.3.2.1 Effect of Slot and Keel Depth

When centrally loaded and the standard keel design/instrumentation were used, the introduction of a slot without insertion of a keel reduced fracture load by 50% (No Slot 1422 N vs Standard Slot 710 N, $p<0.0001$). Insertion of a keel into this slot further reduced fracture load by 40% (Standard Slot 710 N vs Current Keel 423 N, $p=0.0001$). Using a smaller slot, and inserting a smaller (porous) keel, both independently increased fracture load substantially: the slot without keel by 27% (710 N vs 904 N, $p=0.0003$), and the keel by 70% (423 N vs 721 N, $p=0.0003$). The added effect of the keel on fracture load is significantly greater with the standard keel than the small keel: fracture load was reduced by 40% when a standard keel is inserted into a standard slot vs 20% when a small keel was inserted into a small slot ($p=0.0002$, Chi-Square Test) (**Figure 7.3**).

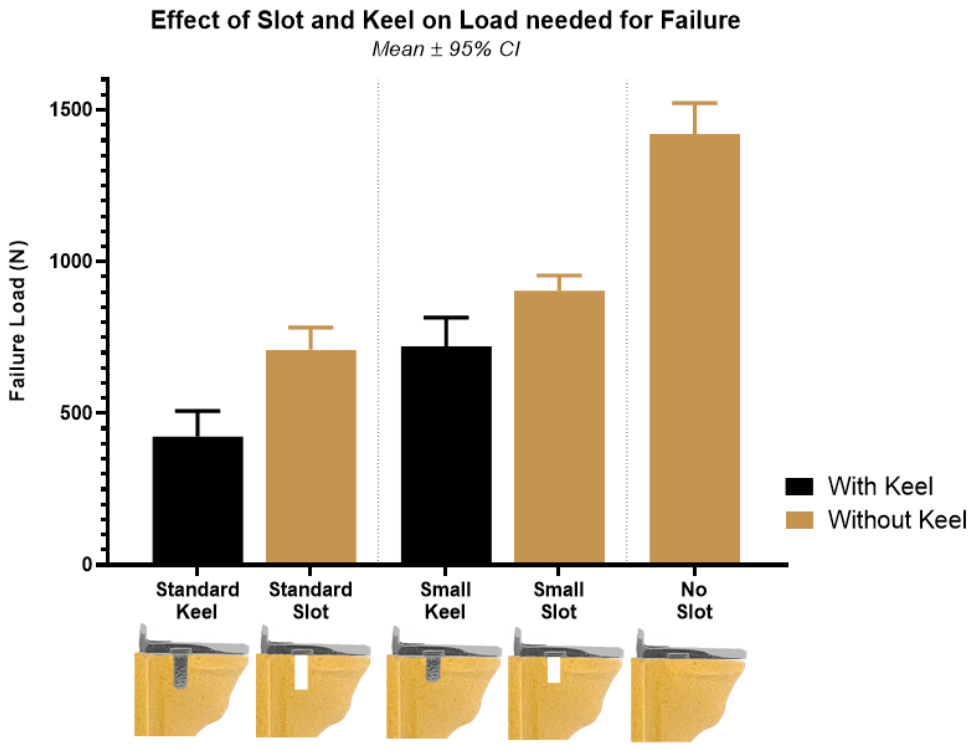


Figure 7.3: *Effect of Slot and Keel on load needed for fracture in standard, small, and no keel designs.*

7.3.2.2 Effect of Loading Position

Posterior loading consistently resulted in lower fracture loads than central loading by 10-13%, but this was only significant when there was no slot (13%, 1422 N vs 1231 N, p=0.0038). Differences between loading positions were not statistically significant when in the presence of a standard keel (11%, 423 N vs 376 N, p=0.330) or small keel (10%, 721 N vs 656 N, p=0.238) (**Figure 7.4**).

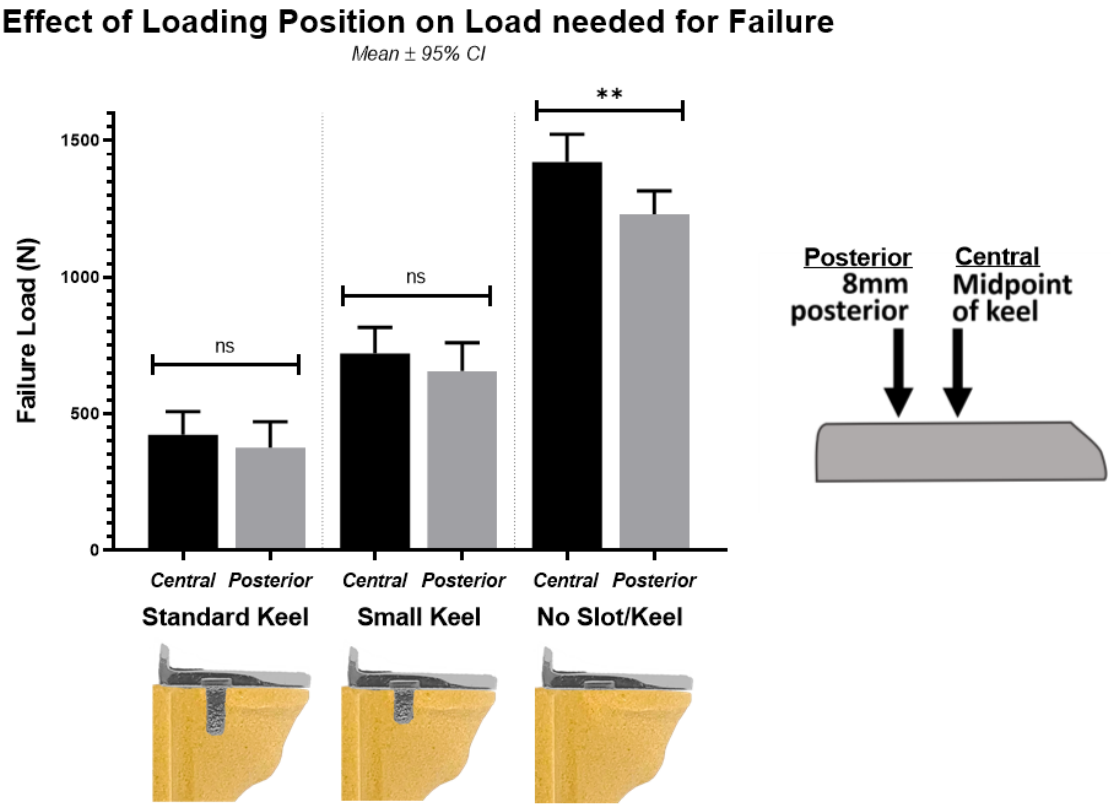


Figure 7.4: *Effect of loading position and keel design on load needed for failure, in standard keel design and a smaller keel design.*

7.3.2.3 Load-to-Fracture in New Fixation Elements

Fracture loads of new fixation designs were tested with central loading until fracture occurred. The small PWSE keel had a near identical fracture load to the small porous keel (741 N vs 720 N, p=0.722), which was 75% greater than the standard keel. The Two-Peg had a significantly higher fracture load than the small PWSE keel (1215 N vs 741 N, p<0.0001), which was 190% greater than the standard keel and 14% lower than having no slot made. Inserting the keels/pegs into their respective slots/holes had a decreasing effect on load-to-fracture from standard keel (40% reduction, p=0.0001) to small keel (18-20% reduction, ANOVA p=0.005) to Two-Peg (2% reduction, p=0.732) (**Figure 7.5**).

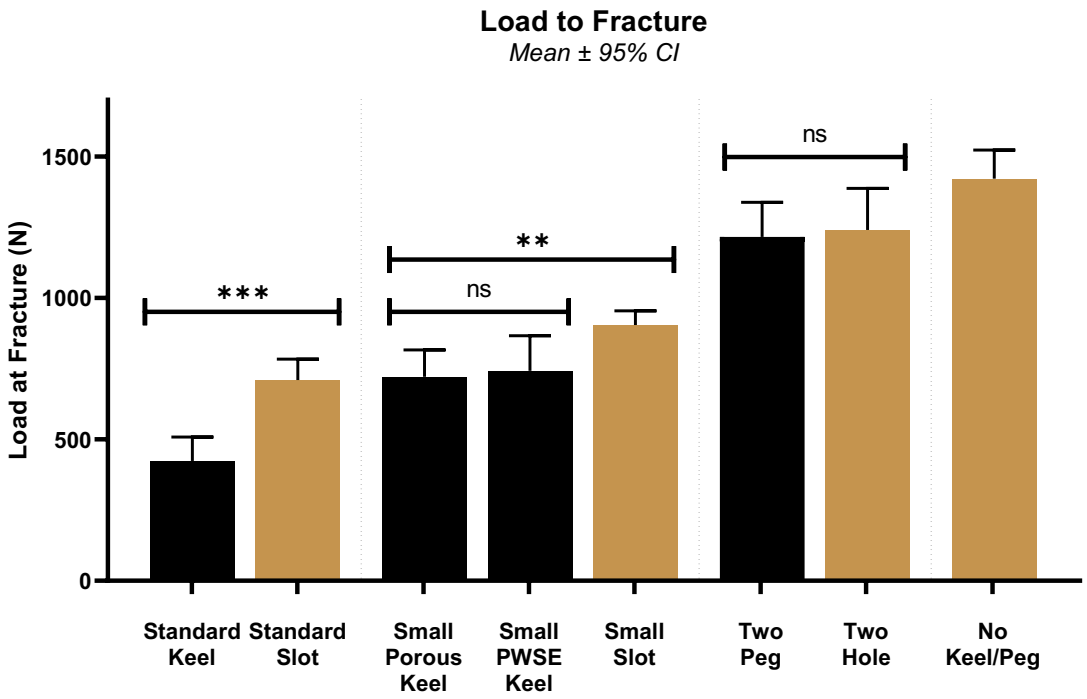


Figure 7.5: *Fracture loads in the standard, small, small porous-walled smooth-bottomed (PWSE), Two-Peg, an no fixation elements, at central loading.*

7.3.2.4 Fracture Path Angle

In central loading, further to fracture loads, fracture paths were characterised to determine if patterns existed. The Coronal Fracture Path Angle (CFPA) was calculated as the average of the anterior and posterior angles of the fracture in the coronal plane. When no keel was implanted, fractures travelled obliquely into the bone. Fractures travelled more vertically when a standard keel slot was introduced (No slot 21° vs Standard slot 12.1°, p=0.0009), and further vertically when a standard keel was inserted (Standard slot 12.1° vs Standard keel 8.2°, p=0.0316). Fractures travelled less vertically when a small keel slot was made (No slot 21° vs Small slot 14.8°, p=0.0154), but inserting a small keel did not induce a further change (Small slot only 14.8° vs Small keel 15.4°, p=0.635). CFPA did not change significantly when two holes (for Two-Peg) was made or when Two-Peg was implanted compared to having no slot (No slot 21° vs two holes 19.5° vs Two-Peg 18.9°, ANOVA p=0.358) (**Figure 7.6, Figure 7.7**).

The abovementioned analyses were for repeated for tests performed with posterior loading (standard keel, small porous keel, no keel). There was no difference in results between central and posterior loading (standard central 8.2° vs posterior 8.4°, small central 15.4° vs posterior 15.0°, no keel 21.0° vs 22.8°, p>0.05 in all comparisons).

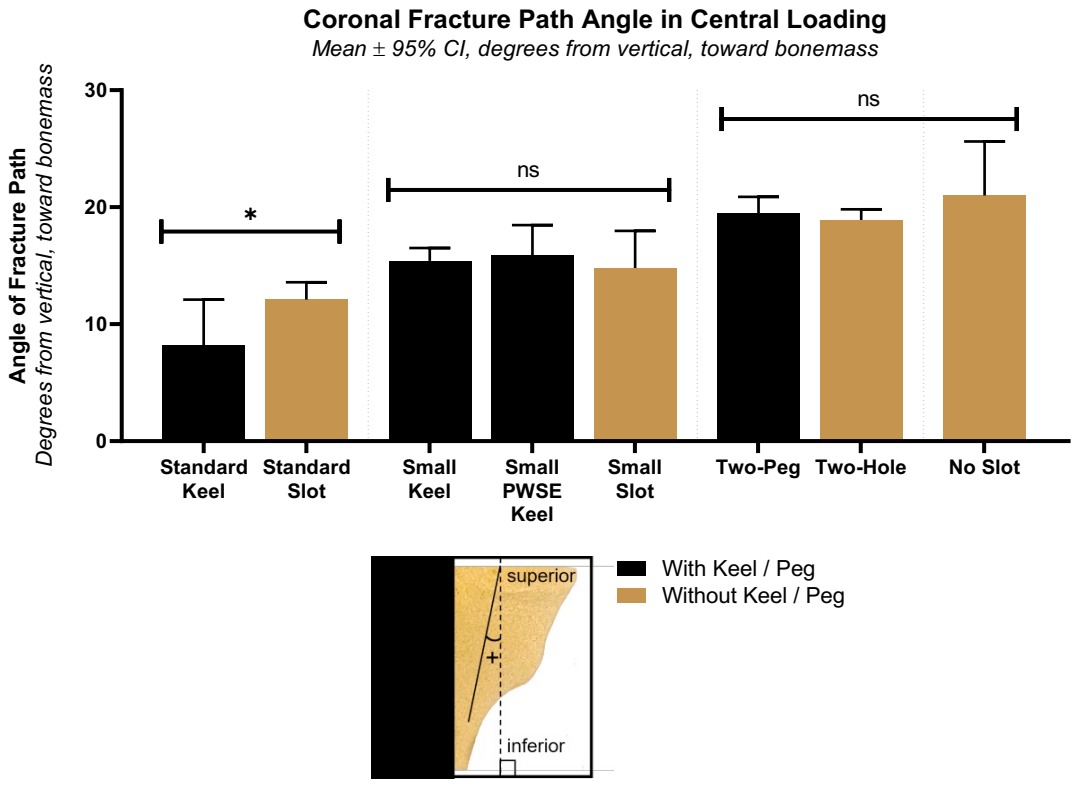


Figure 7.6: *Coronal Fracture Path Angle (CFPA) with and without slot, and with standard, small, Two-Peg, and no keels/pegs.*

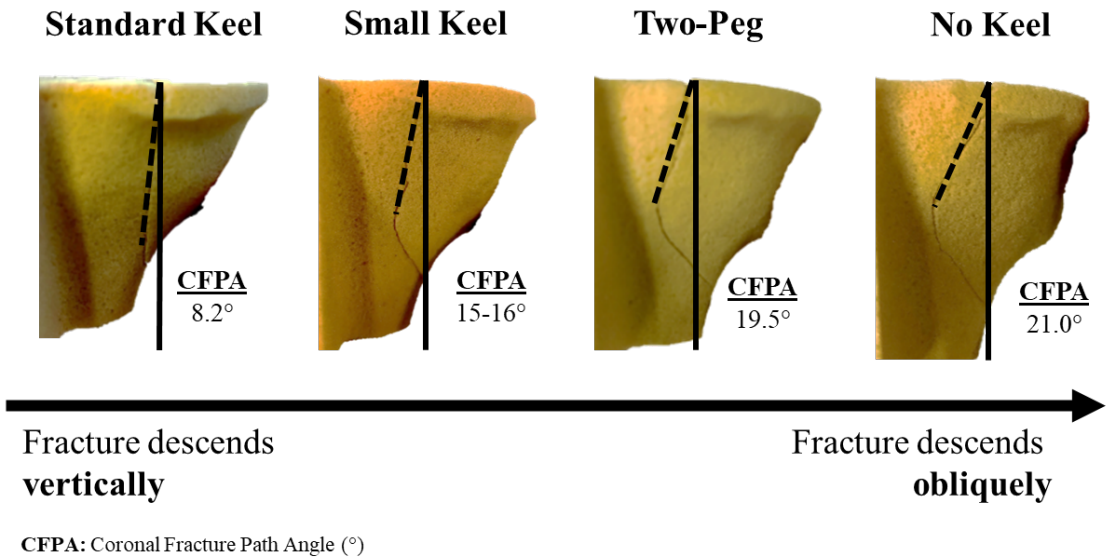


Figure 7.7: *Visualisation of fracture paths in standard, small, Two-Peg, and no keel variants.*

7.3.3 Discussion of Findings

This study shows that for very small tibial components, cutting a slot for a keel, and the insertion of a keel with interference, both reduced the load-to-fracture. Therefore, a large slot or excess interference would likely increase the risk of a peri-prosthetic fracture. Reducing the size of the keel and the keel slot increases load-to-fracture, and thereby likely reducing the risk of a peri-prosthetic fracture.

The risk of revision for fracture is about 2-3 times higher following cementless UKR (0.2-0.3%) compared to cemented (0.1%) [100, 176]. As the keel slots are similar for cemented and cementless components, it is likely that the interference fit is responsible for the increased risk of fracture for the cementless components. It is therefore important to ensure that interference in the keel with cementless tibial fixation is not too large. The recommended method to achieve this is to ensure the trial tibial component can be inserted into the slot with finger pressure alone [210]. If this is not possible, the slot should be enlarged. This also validates the hypothesis put forward in **Chapters 5 and 6** that interference induces splitting forces and increases fracture risk.

This study showed that larger slots are associated with a reduced load-to-fracture and therefore an increased risk of fracture. Therefore, care should be taken to avoid making the slot unnecessarily large. Slots that extend too far posteriorly can damage the posterior cortex have been shown to be an important cause of fracture in mechanical, cadaveric, and clinical studies [192-194]. With the current implant, to avoid this, the template which guides the saw has to be securely fixed with the pin and this should be held by the surgeon to prevent the template from moving posteriorly when using the keel cut saw [86].

In this study, foam was machined to have the shape of a tibia that required a Size 'A' component. Load-to-fracture of the tibia with a Size 'A' component was only 30% of the intact tibia, which explains, at least in part, the higher incidence of fracture in these very small tibias [105]. A small keel, which was approximately the same relative depth as the keel in the largest tibial components, had a >50% increase in load-to-fracture. Therefore, if smaller keels were introduced in these very small tibial component sizes, they would likely decrease the risk of fracture in very small tibias.

During step-up and knee-bend motions, the bearing, and thus the position of tibial component loading, moves. The site of loading load ranges from the centre of the component in the AP axis (anterior limit), to 8 mm posterior to this point (posterior limit) [208, 209]. Although there was a trend towards the load-to-fracture being higher with posterior rather than central loading, this was not statistically significant in implanted knees. Posterior loading tends to occur in flexed knees, which are often associated with activities where the loads across the knee are higher (such as a high step) [211]. Therefore, in very small patients who have an increased risk of fracture, it would be prudent to avoid high loads across a flexed knee for a few weeks after surgery, after which bone remodelling will occur and may reduce the splitting forces induced by interference, thereby reducing risk of fracture.

A comparison of loads causing fracture in this chapter, and maximum push-in forces ($MaxF_{in}$) from **Chapters 5 and 6**, provide useful insight into the mechanisms underlying these fractures (**Table 7.1**). Both load-to-fracture, and $MaxF_{in}$ were used as measures relating to fracture risk. In all keels, a reduction in $MaxF_{in}$ corresponded with an increase in load-to-fracture. However, their effects were not proportional – the small keel had a 11% reduction in $MaxF_{in}$ but a much greater 70% increase in load-to-fracture compared

to the standard keel. In contrast, the small PWSE keel had significant 25% increase[3] in $MaxF_{in}$ but an insignificant 5% increase in load to fracture compared to the small keel[4]. Conversely, the Two-Peg had a near-identical $MaxF_{in}$ but a significant 112% increase in load-to-fracture compared to the small PWSE keel. These differences suggest that the amount of bone resection performed plays a more important role in fracture risk than $MaxF_{in}$, as the small keel requires a less bone to be resected with a smaller slot, and the Two-Peg requires even less bone to be resected with two holes.

Table 7.1: *Load to Fracture and Maximum Push-In Force of keel designs tested.*

	Load to Fracture (N)		**Maximum Push-In Force (N)**	
	Mean	**Value as a % of Standard keel**	**Mean**	**Value as a % of Standard keel**
Standard Keel	423		738	
Small Porous Keel	720	70% higher	660	11% lower
Small PWSE Keel	741	75% higher	544	25% lower
Two-Peg	1215	187% higher	548 (274 × 2)	26% lower

The path of a peri-prosthetic fracture changes when a slot is made, and further changes when a keel is implanted. Without a keel, fractures travel obliquely in the coronal plane – this was quantified using the CFPA. Inserting a keel makes fractures travel more vertically, likely because they are following the path of the keel. A smaller keel results in a less vertical fracture path. The Two-Peg resulted in a near-identical CFPA to having no slot or holes made in the tibia (**Figure 7.7**). These findings implicate the keel in

[3] Maximum push-in force: Small (Porous) keel 738N vs Small PWSE keel 545N, p=0.0056.
[4] Load to Fracture: Small PWSE keel 741N vs Small (Porous) keel 720N, p=0.722.

inducing fractures, and demonstrate how it is partially mitigated with a smaller keel and almost fully mitigated with the Two-Peg.

This study is a comparative analysis between implant designs, based on the assumption that fractures initiation would likely to be the same as for a complete fracture. This is supported by the pattern of fracture seen in the study specimens, which is similar to that which occurred clinically in the knee which was used as the model for this study (**Figure 7.7, Figure 7.8, Figure 7.9**).

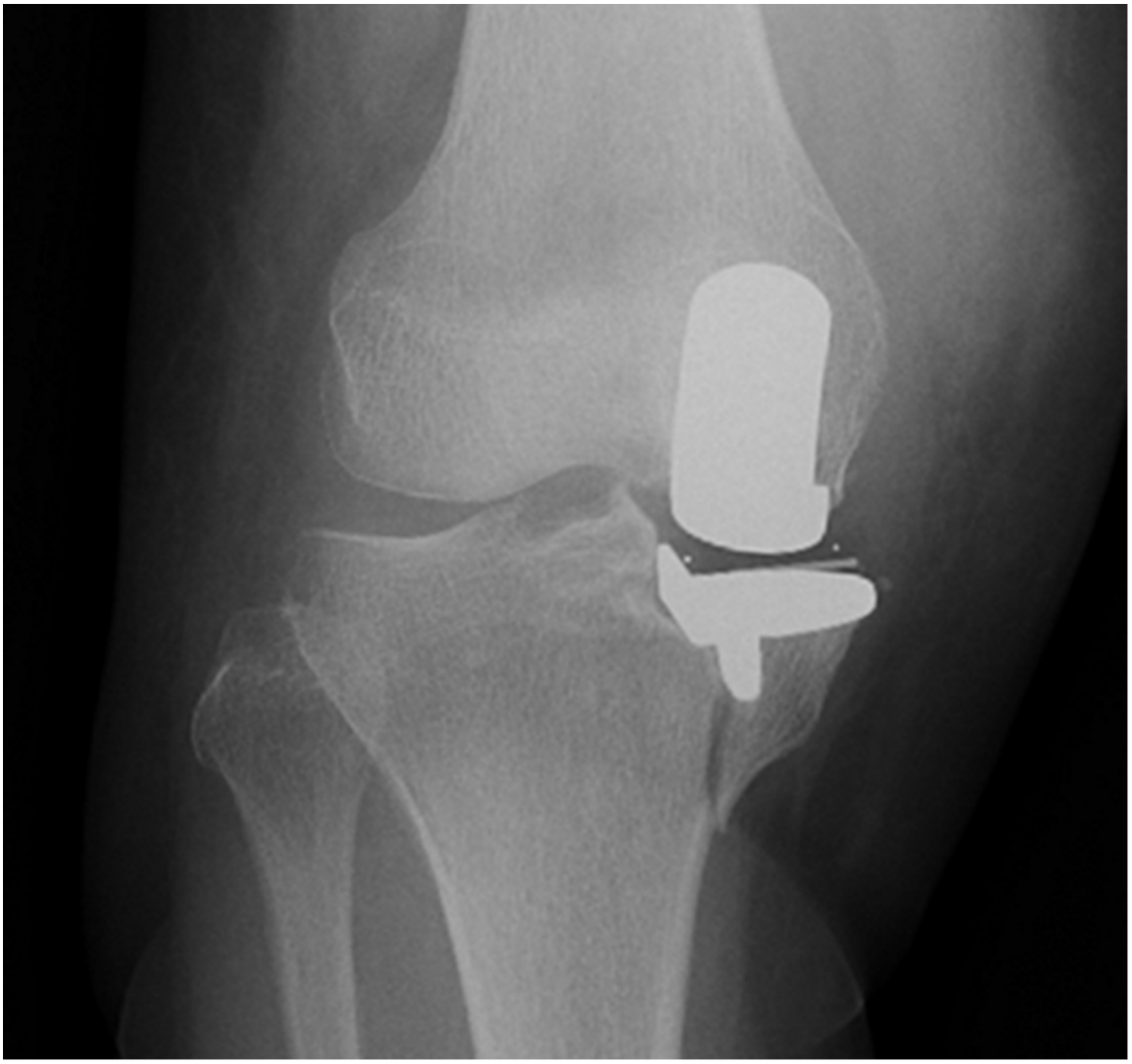


Figure 7.8: *Anterior-Posterior radiograph of peri-prosthetic tibial fracture occurring in knee used as model for this study. The implant used would have the standard keel.*

This study also used a single density foam, with the mechanical properties of trabecular bone. It therefore cannot reproduce the mechanical effects of the tibial cortex. However, the keel is surrounded by trabecular bone, and in this study, the fractures were seen to initiate in this trabecular bone region near the keel (**Figure 7.9**). Although composite bone analogues which represent both trabecular and cortical bone do exist, their metaphyses are unrealistic, with the cortex being excessively thick, and strong.

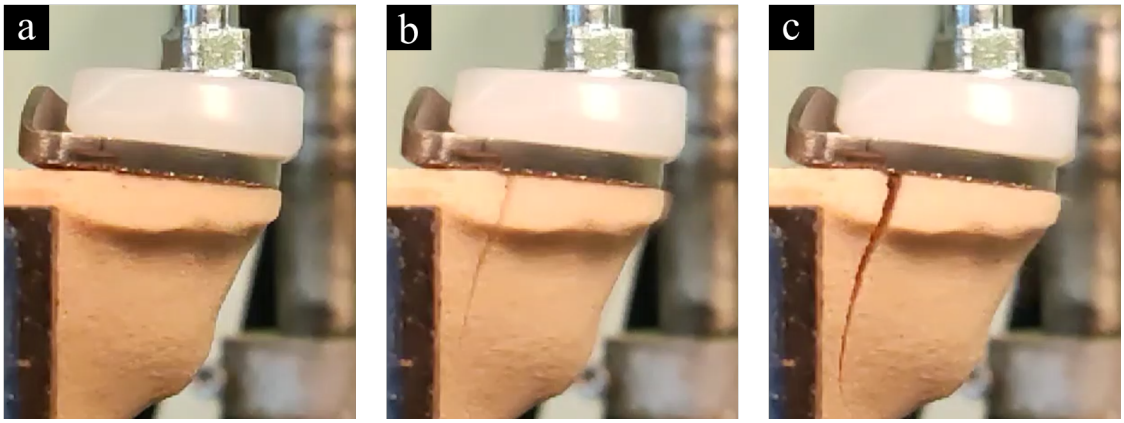


Figure 7.9: *Consecutive frames of a fracture test in this study with a standard keel, recorded at 240 frames per second. Changes from* ***7a-c*** *demonstrate fracture propagating inferiorly keel to bone below, with fracture path similar to clinical findings (see* ***Figure 7.8****).*

Radiographic evidence from clinical cases of peri-prosthetic fractures show an un-displaced fracture initiating from the keel before the fracture completes [105]. In this study of polyurethane foam (i.e., plastic bone), the fracture happens virtually instantaneously, in contrast to the usual clinical presentation of presenting in the weeks after surgery [105, 186]. This may be due to the presence of a cortex below the keel and soft tissue structures surrounding the medial condyle. It can be hypothesised that cracks are initiated around the keel perioperatively, which propagate through the cancellous bone and cortex until they complete. This process could be slowed as soft tissue needs to

stretch and cortex needs to deform progressively as fracture extends; these processes do not occur with the setup used in this study.

Another limitation is that the findings of this study are based on one tibial anatomy. However, this was from a high-risk tibia which actually sustained a fracture so was therefore an optimal candidate for this comparative study. Further cadaveric testing could be undertaken to estimate relevant fracture loads in human bone specimens. However, such analyses have limitations as well, as the mechanical properties of the metaphysis in non-arthritic cadaver specimens has been shown to be substantially different than in arthritic bone [212, 213], and such studies in literature present fracture which extend into the shaft of the tibia – a pattern not seen clinically [207].

7.4 Chapter Summary

Load-to-fracture testing of the Cementless Oxford UKR found that making a keel slot, and inserting a keel, both reduce the load needed to induce a fracture in a tibia. These fractures tend to follow the path of the keel. This validates the practice of using cemented tibial fixation with very small tibial components (size A or AA), as this removes interference and likely decreases fracture risk. In general, surgeons implanting cementless UKR tibias should avoid oversizing tibial components. They should also ensure the keel slot is neither too long, by preventing the template from moving, nor too narrow, by ensuring the trial component can be inserted with finger pressure.

The small porous keel and small porous-walled and smooth-edged (PWSE) keel designed in **Chapter 5** both require the same load to fracture the tibia. These smaller keels, and the Two-Peg designed in **Chapter 6**, require successively, significantly greater loads to fracture the tibia compared to the existing keel design, and are likely to reduce fracture risk. The increases in load-to-fracture with these designs are greater than those predicted by maximum push-in forces in Push-In Pull-Out testing, suggesting that the quantity of bone resection plays a more important role in fracture risk than maximum push-in forces.

8 Primary Fixation in a Very Small Tibia: The Effect of Different Fixation Elements on Sagittal Micromotion

8.1 Chapter Motivation and Aims

The interference between the keel and its bone slot is believed to play a key role in primary fixation of the Cementless Oxford UKR tibial component. While this is generally accepted, it has not been empirically demonstrated.

The work in **Chapter 5 and Chapter 6** helped identify three new designs to potentially replace the existing keel structure for tibial component fixation – a small porous keel, a small porous-walled smooth-edged (PWSE) keel, and a Two-Peg design. In **Chapter 7**, these designs were shown to successively, significantly, increase the load needed to fracture a tibia, suggesting reduced fracture risk.

However, the keel is important for primary fixation of the tibial component, and this function cannot be compromised in these efforts to reduce fracture risk. The existing keel has also been found to experience posterior tilting, suggesting that primary fixation with the existing design may be inadequate (further discussed in **Section 8.2.1**). Preliminary testing with Push-In Pull-Out (PIPO) tests demonstrated that the new designs require greater force for pull-out than the standard keel, suggesting improved primary fixation, which may address these concerns. However, these PIPO tests did not take account of tibial anatomy or physiological loading patterns.

In this chapter, a more physiologically relevant test of primary fixation was designed and used to:

Aim 1. Determine the effect of keel size and interference on primary fixation.

Aim 2. Determine how the new replacement designs compare to the existing keel in ensuring primary fixation.

8.2 Primary Fixation, Micromotion, and Subsidence of the Tibial Component

8.2.1 Implications of Inadequate Primary Fixation

Prior to bone remodelling, the keel of the tibial component serves as the main fixation element in the Cementless Oxford UKR tibial component. The interference between the keel and its slot results in friction, which resists translations and rotations on the sagittal plane of the implant (further discussed in **Section 6.2**). If this friction is overcome, then the implant moves independently of the bone surrounding it – this is defined in this thesis as micromotion. Therefore, micromotion along the plane of the keel, or sagittal micromotion, can be a measure of primary fixation.

The precise relationship between failure of primary fixation of the Cementless Oxford UKR and its clinical outcomes is not well understood.

Subsidence of the Cementless Oxford UKR tibial component has been reported in a small proportion of procedures, where the tibial component subsides posteriorly (termed increasing posterior slope) and laterally (termed increasing valgus), and affects clinical and patient reported outcomes (such as knee stiffness, flexion deformity, and pain) [102, 107]. This subsidence occurs in the early-postoperative period i.e., before the component becomes well-fixed due to secondary fixation [149]. Therefore, it can be hypothesised that subsidence occurs, at least in part, due to inadequate primary fixation.

A prospective time-course RSA study of Cementless Oxford UKR found that the tibial component, on average, experiences a significant increase in posterior slope of 0.4° [149]. This suggests that the increase in posterior slope due to inadequate primary

fixation is a common attribute of the Cementless Oxford UKR tibial component, regardless of symptom state.

It is not clear why this pattern of posterior sloping, which sometimes is extreme and relates to pain and stiffness, occurs. It is known that physiological loading of the tibial component occurs in the posterior aspect of the tibial floor [208], resulting in downward loads applied on the posterior aspect of the tibial component and bone below (**Figure 8.1a**). Clinical radiographs of cementless tibial components which undergo such posterior sloping also present an associated anterior lift-off (**Figure 8.1b-f**).

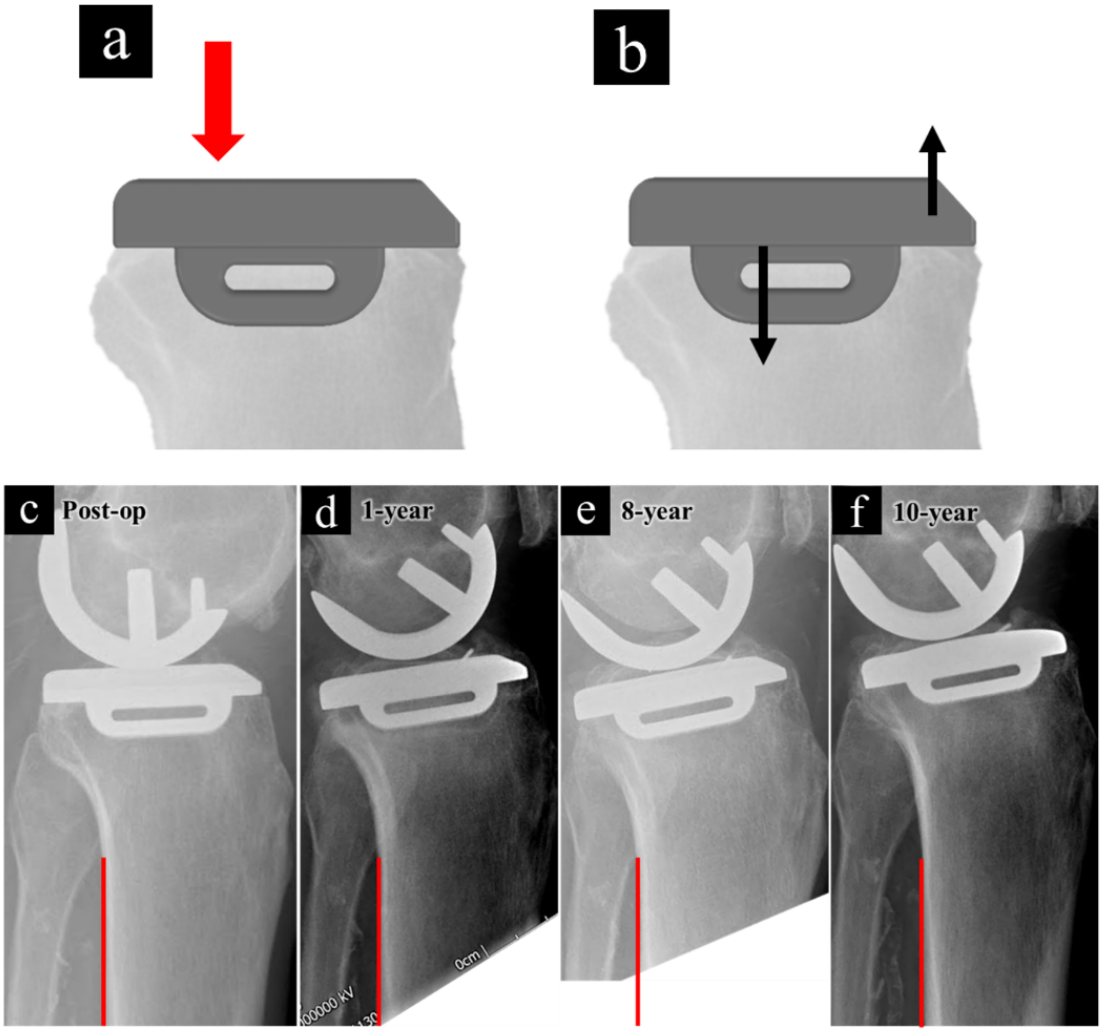


Figure 8.1: *First presented in Figure 6.2 and are re-presented here.* ***(a)*** *A load being applied at the location of the red arrow in the sagittal plane.* ***(b)*** *The predicted tilting implant motion that would result indicated with black arrows, demonstrating vertical lift-off of the anterior aspect of the tibial component.* ***(c,d,e,f)*** *Lateral views of a knee experiencing pain and stiffness, post-operatively, and 1,8, and 10 years after surgery.* ***(d)*** *presents increased posterior slope, and radiolucencies in the anterior keel slot and anterior tibial floor, demonstrating anterior lift-off at 1-year.* ***(e)*** *presents minimal further change in posterior slope and in-fill of apparent space in anterior keel slot, demonstrating arrest of subsidence by 8 years,* ***(f)*** *presents no further change at 10 years.*

When the increasing posterior slope, loading patterns which act on the posterior aspect of the tibial component, and the capacity for sagittal micromotion by the keel are considered together, there is compelling evidence to hypothesise that posterior loading

and inadequate fixation of the keel results in posterior tilting and anterior lift-off of the tibial component.

Therefore, the measurement of sagittal micromotion using anterior lift-off, in physiological loading patterns would be a viable and clinically relevant test for primary fixation.

8.2.2 Implant Factors Affecting Sagittal Micromotion

Keel-slot interference and keel size are both considered to be important factors in primary fixation of the tibial component, as discussed in **Chapter 5**. However, the relationship between these factors and implant micromotion has not been empirically assessed in literature.

In **Chapter 5**, a smaller keel design is proposed, with its size reduced through the removal of the keel 'window' (**Figure 5.5**). The window was initially designed to allow for cement in-fill to improve fixation [75]. With the Cementless Oxford UKR, this window has been retained, but its involvement in primary and secondary fixation are unclear. In the new small keel, removal of the window allows the total porous surface area on the wall of the keel to be retained while reducing the depth of the keel by approximately 30%. In **Chapter 7**, this smaller keel design has been shown to substantially reduce risk of fracture in a mechanical study of very small tibias, compared to the standard cementless keel. However, in **Chapter 5**, primary fixation of the tibial component was suggested to be compromised with a smaller porous keel, as less force was needed to pull the keel out of its slot. The addition of a smooth bottom to the keel, which likely reduced the damage to the slot as the implant is inserted, mitigated this: the

porous-walled smooth-edged (PWSE) keel required greater pull-out forces with a small keel than the standard keel.

In **Chapter 6**, the use of a Two-Peg structure as a replacement for the keel was proposed, which would have improved pull-out forces when constrained to vertical motion. Such vertically constrained pull-out is expected in the motion Oxford UKR tibial component (**Figure 8.1**). In **Chapter 7**, this Two-Peg design required significantly greater load to fracture a tibia compared to any of the keel-based designs.

While data on pull-out forces is available, it is not clear how they relate to micromotion, and therefore, cannot solely be used to ascertain strength of primary fixation with these new designs.

Therefore, the work outlined in this chapter seeks to determine the effect of interference and keel size on micromotion, and determine how primary fixation compares between the existing keel design and new keel/peg designs.

8.3 Measuring Micromotion

8.3.1 Available Methods for Implant Motion Tracking

There are limited methods available for the precise tracking of implant motion. Two commonly used methods reported in literature are radiostereometric analysis and image tracking.

Radiostereometric analysis (RSA) involves the imaging of an implant using paired radiographs taken from different planes, which are digitally aligned and processed to output the migration of the implant relative to reference structures, which are usually radio-opaque marker balls implanted into bone. RSA can be used to detect implant motion during dynamic load-unload testing, termed Dynamically Induced Micromotion (DIMM) [214], and has been used in literature [162]. It is reported to have an accuracy of 0.1 – 0.2 mm compared to reference measurements [215-217]. This method was developed for *in-vivo* use and requires radiography equipment.

Image tracking involves image capture, identification of key features in the image, and tracking the motion of the feature. These motions are then compared to reference lengths, thereby providing accurate motion data. This is generally performed in two ways – either through the use of highly reflective balls as optical features (commonly used in optical motion capture devices), or the use of high-contrast dots against a surface as features (commonly used in Digital Image Correlation (DIC) devices). A standard commercially-available optical motion capture setup was reported to have an uncertainty of 1.11 mm [218] in a laboratory setting. Similar uncertainty assessment of DIC setups was not found in orthopaedic literature. However, DIC is generally used in micro- and nano- scale

mechanical assessment [219], as it is limited only by speckle size, image accuracy, and image resolution.

RSA and optical motion capture do not have sufficient accuracy for micrometre scale measurements needed for micromotion assessment. Therefore, Digital Image Correlation (DIC) was pursued as a potential method for micromotion assessment. It has been used in the assessment of strain in UKR [146, 220, 221], based on displacement measurements.

Image acquisition devices for DIC designed for industrial and research use are expensive. Therefore, a novel method for DIC was developed for assessment of primary fixation using relatively low-cost materials.

8.3.2 A Low-Cost, High-Resolution, Micromotion Measurement Protocol

Two-dimensional DIC was performed in this study. Image acquisition was performed using a Digital Single Lens Reflex camera with a CMOS sensor (EOS 4000D, Canon, Uxbridge, UK) with a 75 mm focal length achieved with a stock lens (EF-S 18-55mm, Canon, Uxbridge, UK) and lens extender (Teleplus DG, Kenko, Tokyo, Japan). A shutter speed of 1/100s was used to avoid image blur and 1/100s was used to align with alternating current supply of 50Hz. A f/10 depth of focus was used to achieve adequate depth of field of imaging. A 1500 lumen diffused light source (Toolstation, Somerset, UK) was used with ISO 100 to obtain a sufficient signal to noise ratio. With these settings, the central 50% of images acquired were determined to be adequately undistorted, and thus used as the working field for the experiment (**Figure 8.2b**). Imaged surfaces were finely speckled using white and black matt paint (PlastiKote, Valspar Paint,

Wokingham, UK) (**Figure 8.2b,c**). Acquired images were processed using software (Correlate, GOM Metrology, Braunschweig, Germany) to compute the displacement of operator-labelled elements.

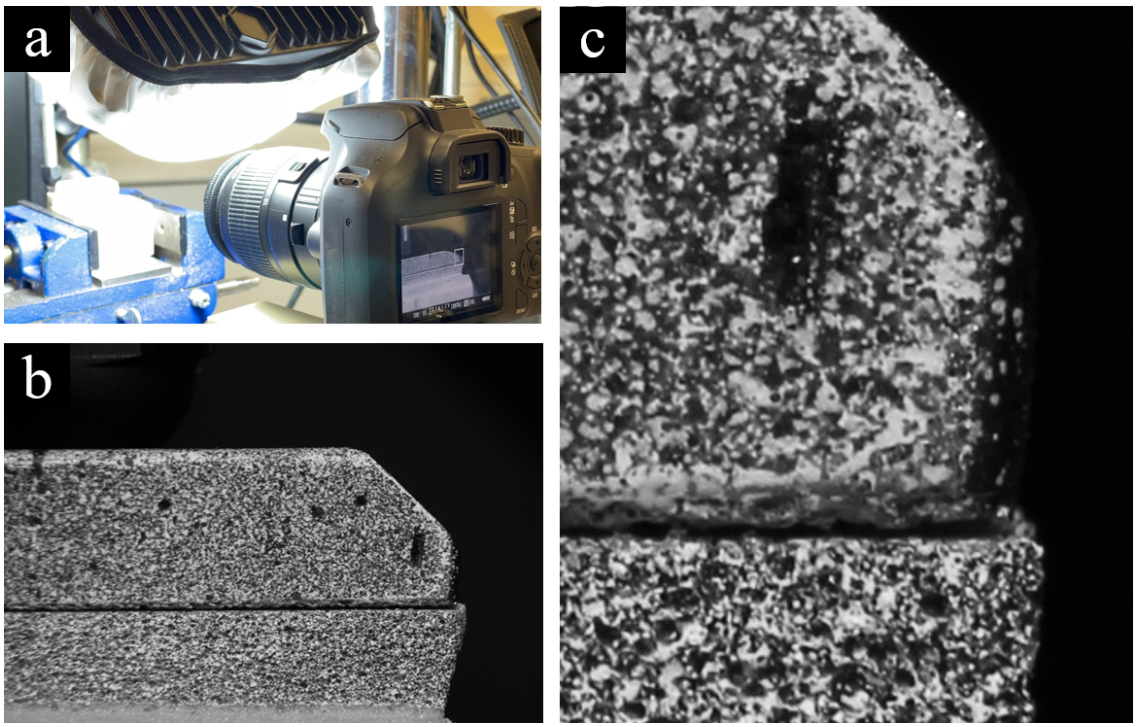


Figure 8.2: ***(a)*** *Image Acquisition Setup for DIC.* ***(b)*** *Example overall image acquired, demonstrating distortion at the lateral ends of image.* ***(c)*** *Zoomed-in image presenting high speckle fidelity and low image blur required for DIC. Note that two black dots in (b) are reference points for two identical lines 10.00mm apart, used were used as reference for image scaling in post-processing. Line at the front of component seen in (b) and (c) was used as measurement marker for anterior lift-off.*

Setup was scaled using consistent reference lengths, and measurements were validated using displacement comparison with a rigid, speckled reference frame held in the same imaging plane as the tibial component, moved using a servo-hydraulic testing machine (Dartec HC 10, Zwick Ltd, Herefordshire, UK) which measures displacement. The reference frame was displaced 20 times by 1 mm, 0.5 mm, 0.2 mm, 0.1 mm, 0.05 mm, 0.02 mm, and 0.01 mm, from which imaged and real displacements were compared.

Setup was reliably accurate to 50 µm (0.05 mm), where it had a SD of 6.2% of calculated displacement from reference displacement (**Figure 8.3**).

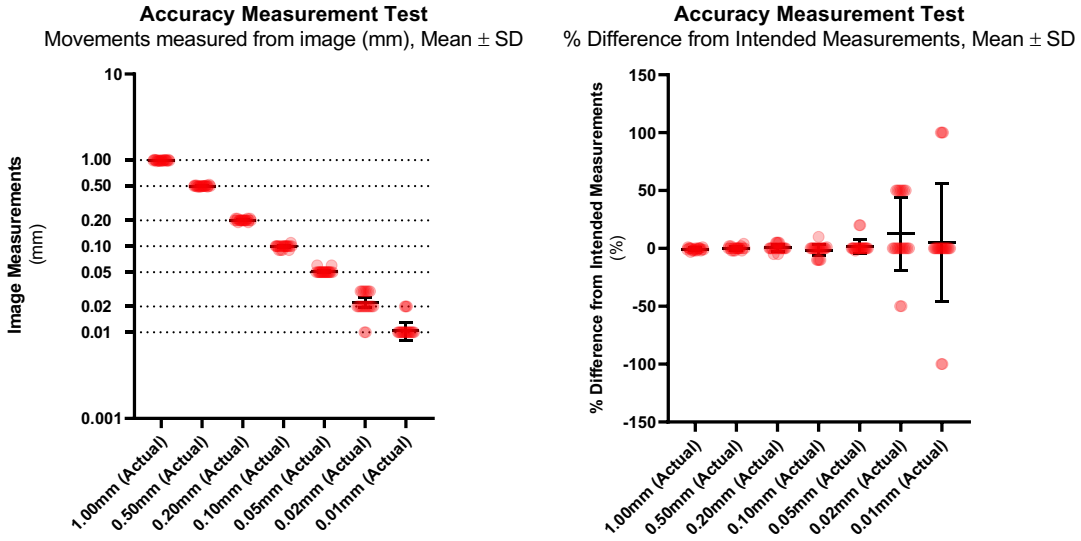


Figure 8.3: *Comparison of displacement calculated from Digital Image Correlation to real displacement, for setup validation. Standard deviations for 1.00mm was 1.1%, 0.50mm was 1.5%, 0.20mm was 2.8%, 0.10mm was 4.9%, 0.05mm was 6.2%, 0.02mm was 31.9% and 0.01mm was 51.0%.*

8.4 Measuring Sagittal Micromotion using Anterior Lift-Off

8.4.1 Study Aims and Methods

The primary aim of this study was to determine to effect of the keel in micromotion of the tibial component, by performing an *in-vitro* assessment of component fixation with and without keel in anatomically shaped tibias, when loaded at physiologically defined loading positions. The secondary aim of this study was to determine the change in fixation with new tibial component fixation designs. As micromotion was expected primarily to occur in the sagittal plane, sagittal micromotion was assessed.

Size 'A' additively manufactured titanium tibial components were made with identical design to clinically used cementless components (see **Section 7.3.1** for details). Six tibial component designs with varying tibial fixation structures were used – one with a 3.7 mm standard keel similar to clinically used cementless keel design, one with a standard-sized keel but with a narrower 3.0 mm width, one with no fixation element, one with a small porous keel and one with a small porous-walled smooth-edged (PWSE) keel based on the designs developed in **Chapter 5**, and one with a Two-Peg design developed in **Chapter 6**. The narrower standard keel tests the effect of the interference. Having no keel assesses the effect of a standard keel. The small porous keel assesses the effect of reducing the keel size. The small porous/PWSE keels and Two-Peg assesses the performance of these new designs (**Figure 8.4**).

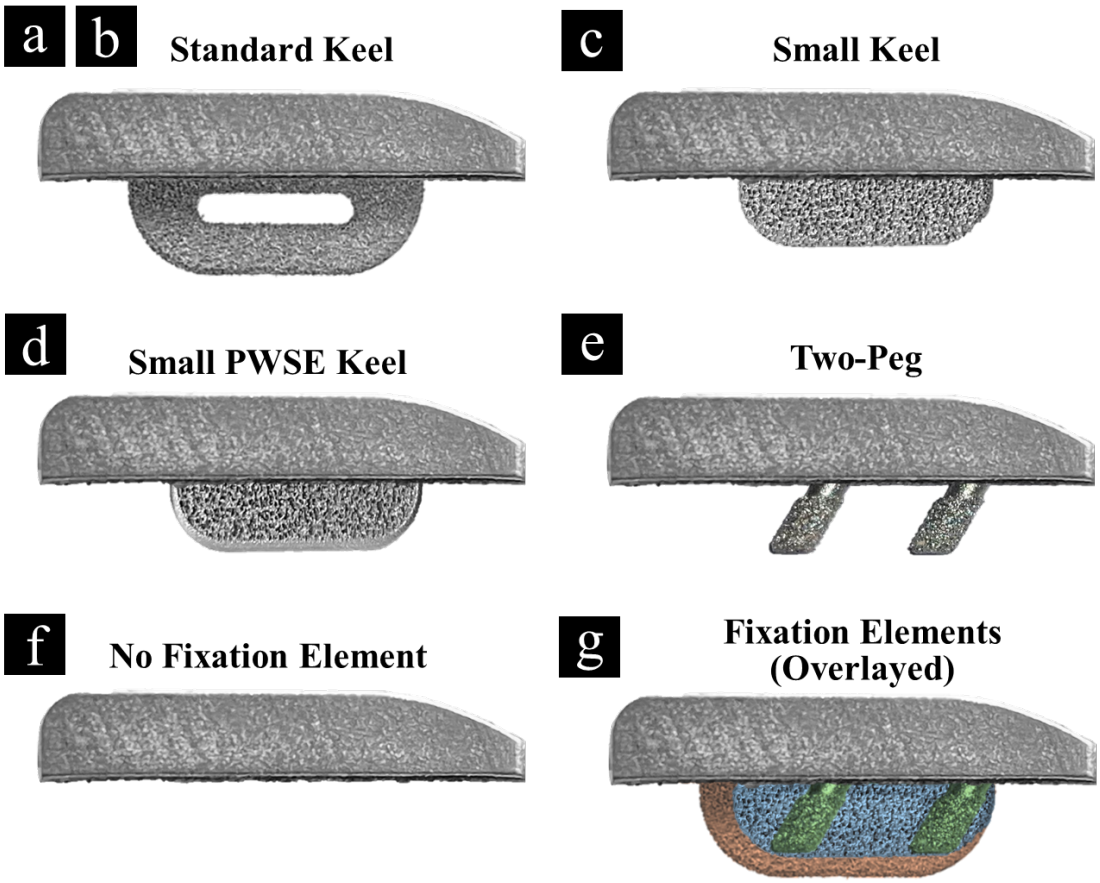


Figure 8.4: *Keel Designs explored in this study.* ***(a)*** *Standard keel found in currently used clinical components,* ***(b)*** *Standard keel with no interference,* ***(c)*** *no fixation element,* ***(d)*** *Small porous keel,* ***(e)*** *Small porous-walled smooth-edged keel, and* ***(f)*** *Two-Peg.* ***(g)*** *Fixation elements overlayed – standard in orange, small in blue, and Two-Peg in green. Small keel designs are as described in* ***Chapter 5****. Two-Peg design is as described in* ***Chapter 6****.*

These Size 'A' components were implanted into Size 'A' medial condyles which had an identical structure to a tibia which experienced a peri-prosthetic fracture (as performed in **Chapter 7**). Details of foam properties and machining specifications were as described in **Chapter 7**. An additional 5 mm vertical cut was made at the tibial wall to expose foam below the tibial wall for imaging (**Figure 8.5**).

Keels were implanted into the condyles using standard implanting techniques and instrumentation. The small keels cuts and Two-Peg holes were made using modified templates and instrumentation as outlined in **Chapters 5 and 6**.

Condyles with implanted tibial components were loaded following a defined protocol using a servo-hydraulic testing machine (Dartec HC 10, Zwick Ltd, Herefordshire, UK) which measured displacement, and a S-beam load cell (FSB-01, Force Logic, Berkshire, UK) which measured vertical force. One load cycle consisted of loading and unloading in 50 N increments to a maximum of 200 N. Loading was performed at a rate of 10 N s^{-1} with a 3 second dwell period between load changes to allow for image acquisition. The motion of the tibial keel relative to the condyle below was optically tracked. Digital Image Correlation (DIC) based on the protocol outlined in **Section 8.3.2** was used to image the tibial wall and adjacent foam.

Load testing involved repeated load cycles of midpoint and posterior loading consistent with the anterior and posterior limits of physiological loading expected in the post-operative period during primary fixation. Anterior loading was positioned at the midpoint implant in the sagittal plane, while posterior loading was positioned 8 mm posteriorly to represent shallow flexion (i.e., step-up loading), and 15 mm posterior to represent a more aggressive deep flexion (i.e., lunge loading). Sagittal loading positions were based on anterior and posterior limits reached by bearings in a study of lateral radiographs in implanted knees during these motions [208]. Loading was performed 13 mm away from the tibial wall based on estimated neutral bearing position on tibial condyle. Each implanted condyle was load-cycled at midpoint then 8 mm posteriorly until change in implant micromotion between posterior loads was less than 0.1 mm (defined as reaching

steady state). Following this, each implanted condyle was load-cycled at midpoint and 15 mm posteriorly in the same manner.

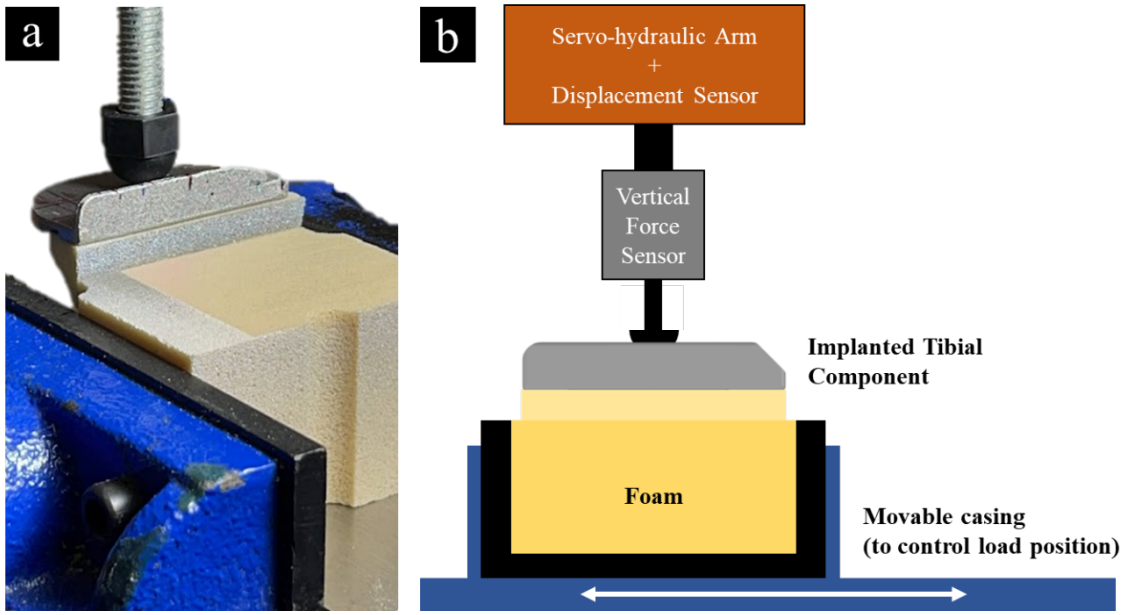


Figure 8.5: ***(a)*** *Image of setup for sagittal micromotion testing.* ***(b)*** *Diagram of components in test setup.*

Force, displacement, and time data were collected at 100 Hz for analysis. Image acquisition was performed for DIC during posterior loading sequences. In all such sequences, lift-off of the tibial component from the condyle was the largest micromotion observed within imaging setup. Therefore, this 'anterior lift-off' position was standardised (42 mm from the posterior edge of the tibial component in all components), and measured. Anterior lift-off was measured and using averaged between duplicate two-point displacement measurements – displacements were within 20 µm between all duplicates (**Figure 8.6**). This test was performed with all tibial component variants in three separate condyles (n=3).

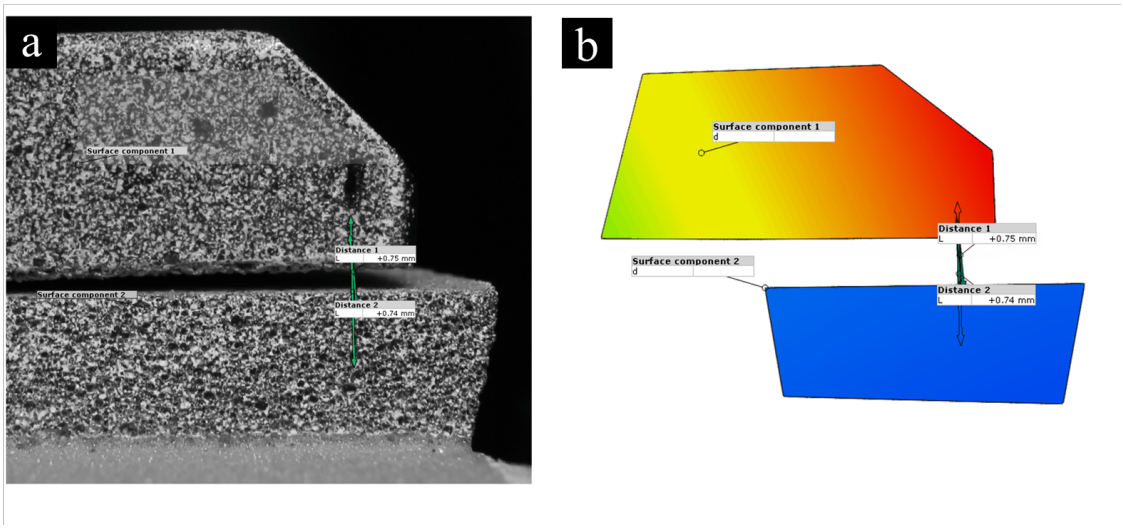


Figure 8.6: *A sample of how anterior lift-off was measured mid-sequence.* ***(a)*** *Mid-sequence image frame under study.* ***(b)*** *Surface components applied with a colour map of displacement (blue indicates less motion and red indicates more motion), and two-point distance was measured a at fixed distance from posterior edge of tibial component across all tests. Duplicate measurements were taken at different heights and were found to be within 20 μm in all cases.*

Maximum anterior lift-off comparisons were statistically performed using the unpaired Student t-test for parametric (Shapiro-Wilk $p>0.05$), and the Mann-Whitney U-test for non-parametric (Shapiro-Wilk $p<0.05$) distributions. Discrete categories were assessed with the chi-square test or Fisher's exact test, as appropriate. Anterior-lift off measurements from load-on and load-off sequences were used to calculate a 2-segment linear regression intersecting at the highest load (200N). Overall anterior lift-off between sequences was compared using extra sum-of-squares F test. GraphPad Prism (GraphPad Software, San Diego, California, USA) and Excel (Microsoft, Redmond, Washington, USA).

8.4.2 Results

When loaded posteriorly, there was an increase in anterior lift-off in all tests with loading, and decrease in anterior lift-off with unloading. For all tests, a greater load resulted in greater anterior lift-off, and maximum anterior lift-off was at maximum load in all tests. All anterior lift-off values reached steady state within four load cycles, with most reaching steady state within two cycles: n=24 (80%) in two cycles, n=5 (17%) in three cycles, and n=1 (3%) in four cycles. Four of six tests where steady state took greater than two cycles occurred where there was no interference (n=2 in no keel, and n=2 in standard keel with no interference, n=1 in small porous keel, n=1 in Two-Peg).

8.4.2.1 Effect of Interference and Keel Size on Anterior Lift-Off

When loaded to 200 N at 8 mm posteriorly (representing load position during shallow flexion), a standard keel with no interference experienced five times lesser maximum anterior lift-off than a standard keel with interference (63 μm vs 340 μm, p=0.0146). Removing the keel entirely further decreased this maximum anterior lift-off by half, but this was not statistically significant (30 μm vs 63 μm, p=0.176) (**Figure 8.7, Figure 8.9**). Comparing the whole load cycle, the anterior lift-off of the tibial component without a keel was lower than that of the standard keel with no interference (p=0.0043) (**Figure 8.7**).

The maximum anterior lift-off of the small porous keel was less than the standard keel but this was not significant (245 μm vs 340 μm, p=0.233), and more than the standard keel with no interference (63 μm vs 245 μm, p=0.0016). Over the whole load-unload sequence, the small porous keel experienced significantly less anterior lift-off than the

standard keel (p=0.0092). At the end of unloading, tibial components with no interference almost completely returned to their original positions while keels with interference remained slightly but significantly anterior (p=0.0054, comparing keels with no interference: no keel 1.6 µm and standard keel with no interference 3 µm, against keels with interference: standard keel 45 µm and small porous keel 47 µm) (**Figure 8.7**).

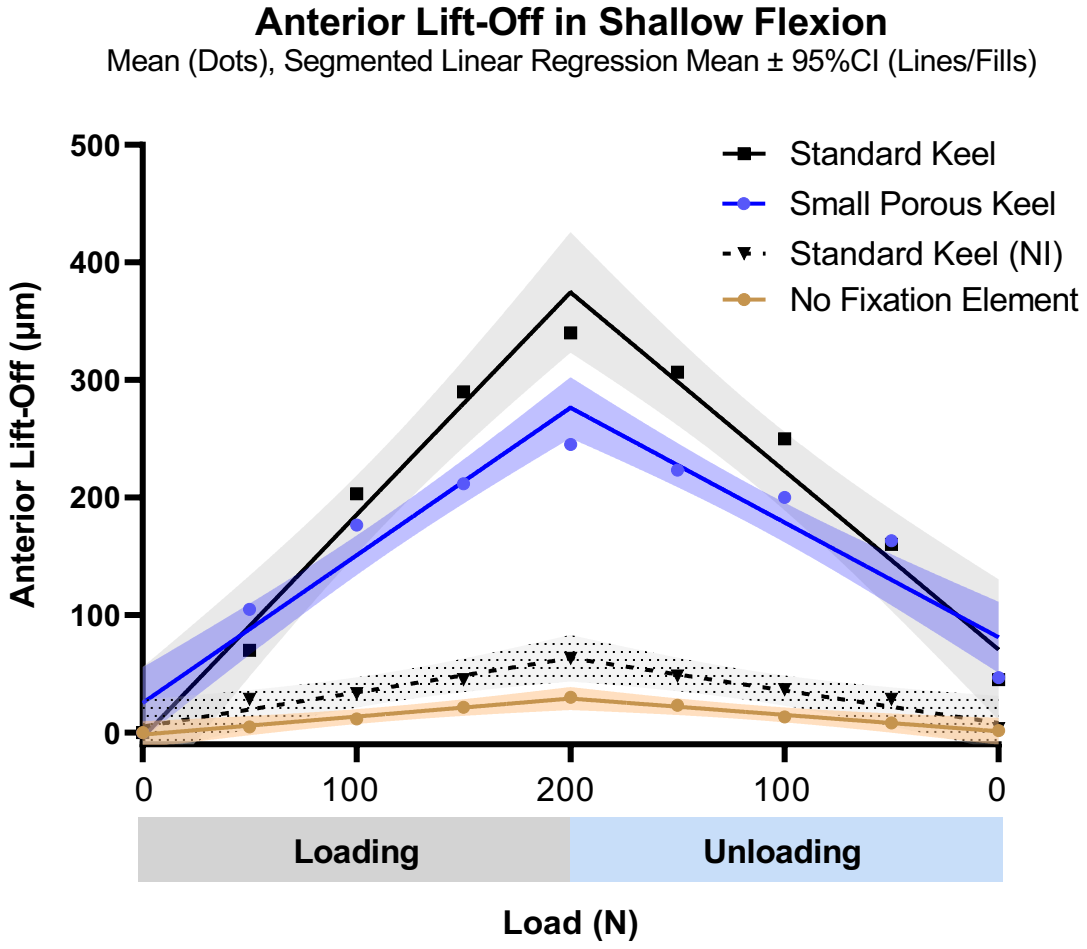


Figure 8.7: *Anterior Lift-Off during posterior loading of tibial components with a standard keel, standard keel with no interference (NI), and no fixation element, loaded at posterior-most position experienced in step-up loading position, located 8 mm posterior to midpoint of implant on the sagittal plane. Anterior lift-off measured using DIC at 50 N increments, with mean values in dots and linear regressions of data represented with solid lines.*

When loaded to 200 N 15 mm posteriorly (representing load position during deep flexion), the tibial components with no interference moved more than those which had interference. Having a standard keel with no interference reduced anterior lift-off compared to having no keel – this was not significant at maximum loading but was significant when comparing the whole load cycle (anterior lift-off at maximal loading: 1003 μm vs 817 μm, p=0.241, comparison of anterior lift-off across load cycle, p=0.0064) (**Figure 8.8, Figure 8.9**). A standard keel with interference had a lower anterior lift-off than a standard keel with no interference – this was close to significance at maximal loading, and significant across the load cycle (anterior lift-off at maximal loading: 817 μm vs 521 μm, p=0.077, comparison of anterior lift-off across load cycle p<0.0001) (**Figure 8.8, Figure 8.9**). The small porous keel had a lower anterior lift-off than the standard keel, which was not significant at maximal loading but significant across the load cycle (anterior lift-off at maximal loading: 378 μm vs 521 μm, p=0.265, anterior lift-off across load cycle, p=0.0062) (**Figure 8.8, Figure 8.9**).

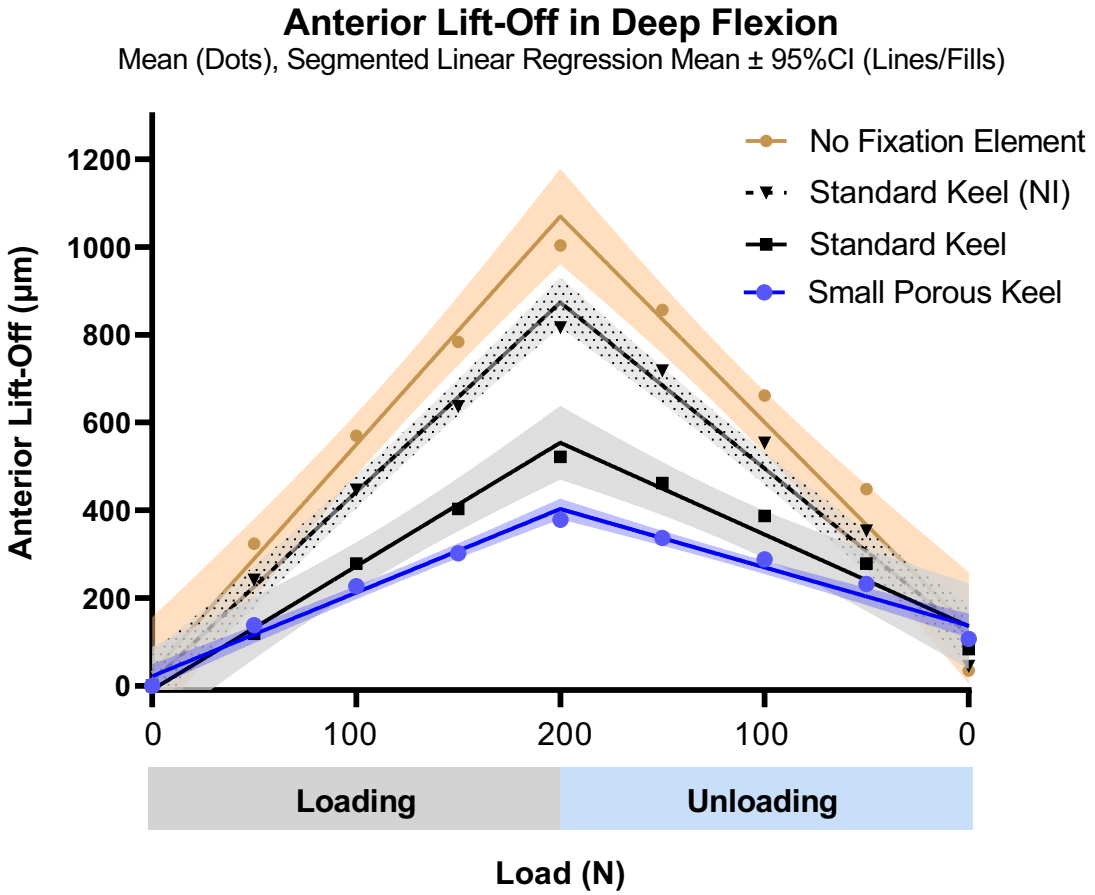


Figure 8.8: *Anterior Lift-Off during posterior loading of tibial components with a standard keel, standard keel with no interference (NI), and no fixation element, located 15 mm posterior to midpoint of implant on the sagittal plane. Anterior lift-off measured using DIC at 50 N increments, with mean values in dots and linear regressions of data represented with solid lines.*

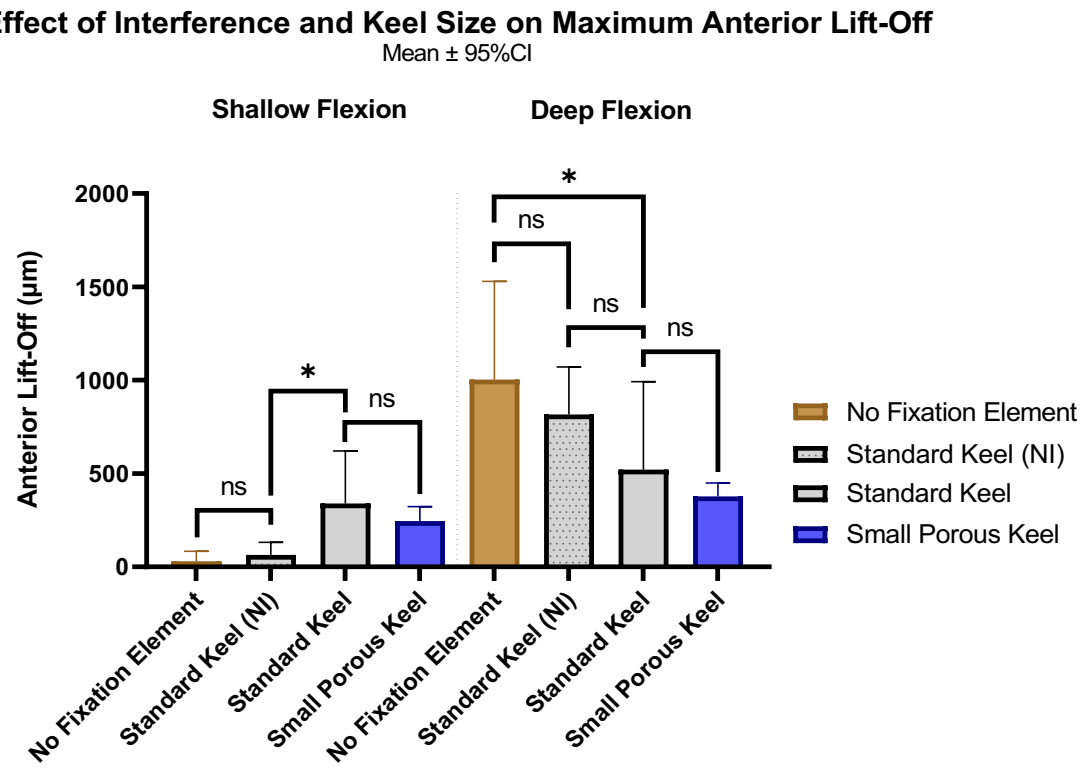


Figure 8.9: *Maximum anterior lift-off measurements, occurring during maximal loading of 200 N in a tibial component with a standard keel, standard keel with no interference (NI), and no fixation element. Tests statistically compared. ns: not significant, *:p<0.05.*

8.4.2.2 Anterior Lift-Off in New Fixation Designs

When loaded to 200 N 8 mm posteriorly (representing load position during shallow flexion), the tibial component with a small PWSE keel experienced a significant 60% reduction in maximum anterior lift-off comparted to the component with a standard keel, and the Two-Peg experienced a further significant 70% reduction in maximum anterior lift-off (Standard keel 340 μm vs Small PWSE keel 125 μm, p=0.0302, Small PWSE keel 125 μm vs Two-Peg 40 μm, one-way ANOVA p=0.0004) (**Figure 8.10, Figure 8.12)**. Once fully unloaded, both keel designs remained slightly anterior, while the Two-Peg returned to baseline (Standard keel 45 μm vs Small PWSE keel 23 μm vs Two-Peg 0 μm, t-test between average of keels and Two-Peg, p=0.0328) (**Figure 8.10)**.

A similar pattern was observed when loading 15 mm posteriorly (representing deep flexion). The tibial component with a small PWSE keel experienced a 50% reduction in maximum anterior lift-off compared to the component with a standard keel. This was not significant at maximal loading, but overall curves were significantly different (Standard keel 522 μm vs Small PWSE keel 273 μm, p=0.1159, comparison of anterior lift-off across load cycle p<0.0001) (**Figure 8.11, Figure 8.12**). The tibial component with the Two-Peg experienced a significant 74% reduction in maximum anterior lift-off compared to the component with a standard keel (522N vs 137N, p=0.0247). Both keel designs remained slightly anterior, while the Two-Peg returned to near baseline (Standard keel 83 μm vs Small PWSE keel 110 μm vs Two-Peg 7 μm, t-test between keels and Two-Peg, p=0.0531) (**Figure 8.11**).

Differences between standard and small porous keel have been discussed in the previous section (**Section 8.4.2.1**). The small PSWE keel experienced significant 50% less anterior lift-off the small porous keel when loaded 8mm posteriorly (PWSE 245 N vs porous 125

N, p=0.0030) and non-significant 30% less when loaded 15mm posteriorly (PWSE 378 N vs porous 273 N, p=0.160).

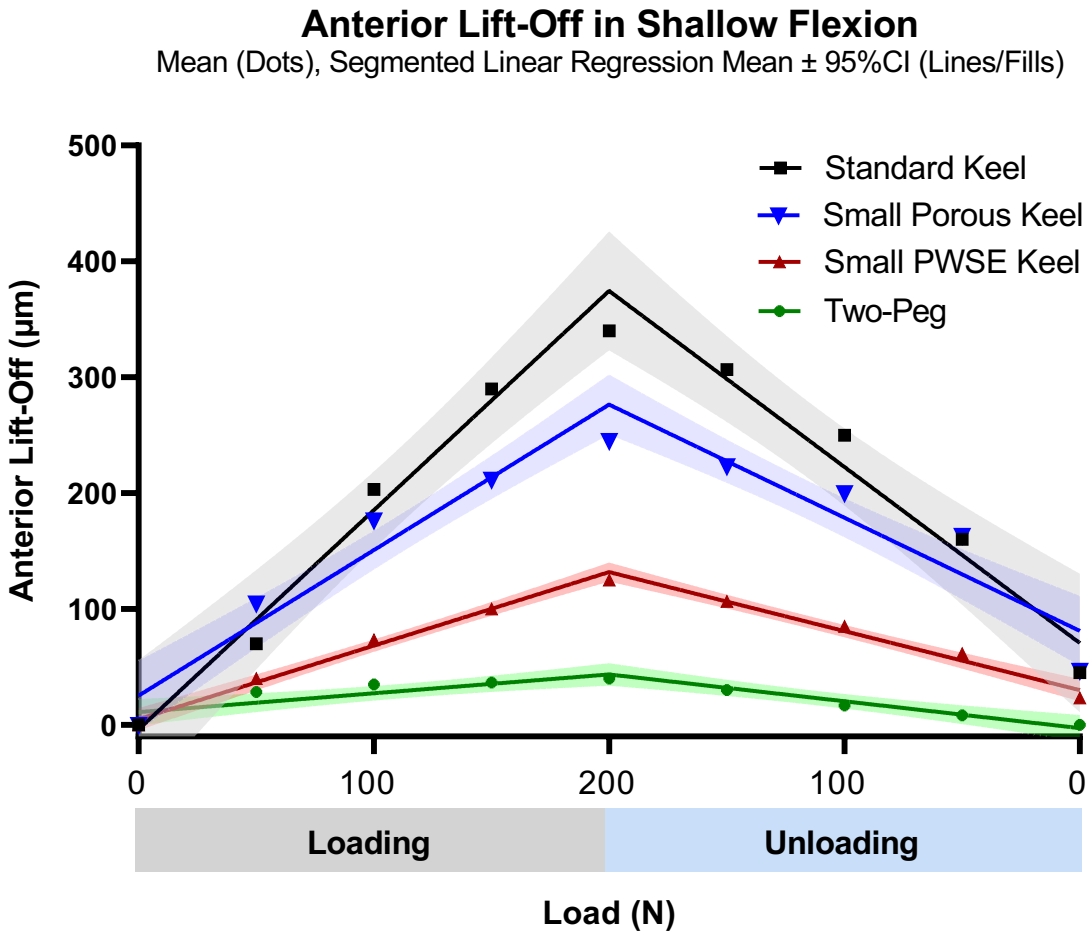


Figure 8.10: *Anterior Lift-Off during posterior loading of tibial components with a standard keel, small (porous) keel, small porous keel, small PWSE keel, and Two-Peg, located 15 mm posterior to midpoint of implant on the sagittal plane. Anterior lift-off measured using DIC at 50 N increments, with mean values in dots and linear regressions of data represented with solid lines.*

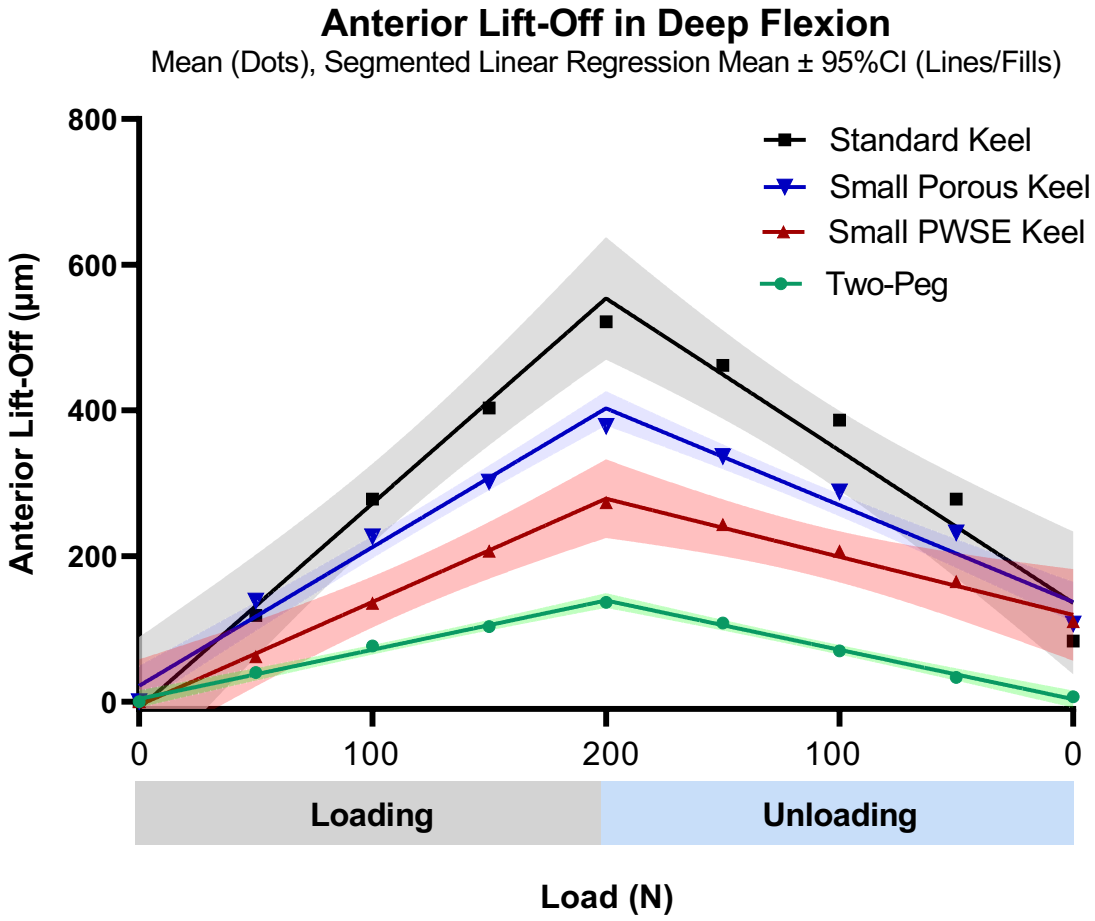


Figure 8.11: *Anterior Lift-Off during posterior loading of tibial components with a standard keel, small (porous) keel, small porous keel, small PWSE keel, and Two-Peg, located 15 mm posterior to midpoint of implant on the sagittal plane. Anterior lift-off measured using DIC at 50 N increments, with mean values in dots and linear regressions of data represented with solid lines.*

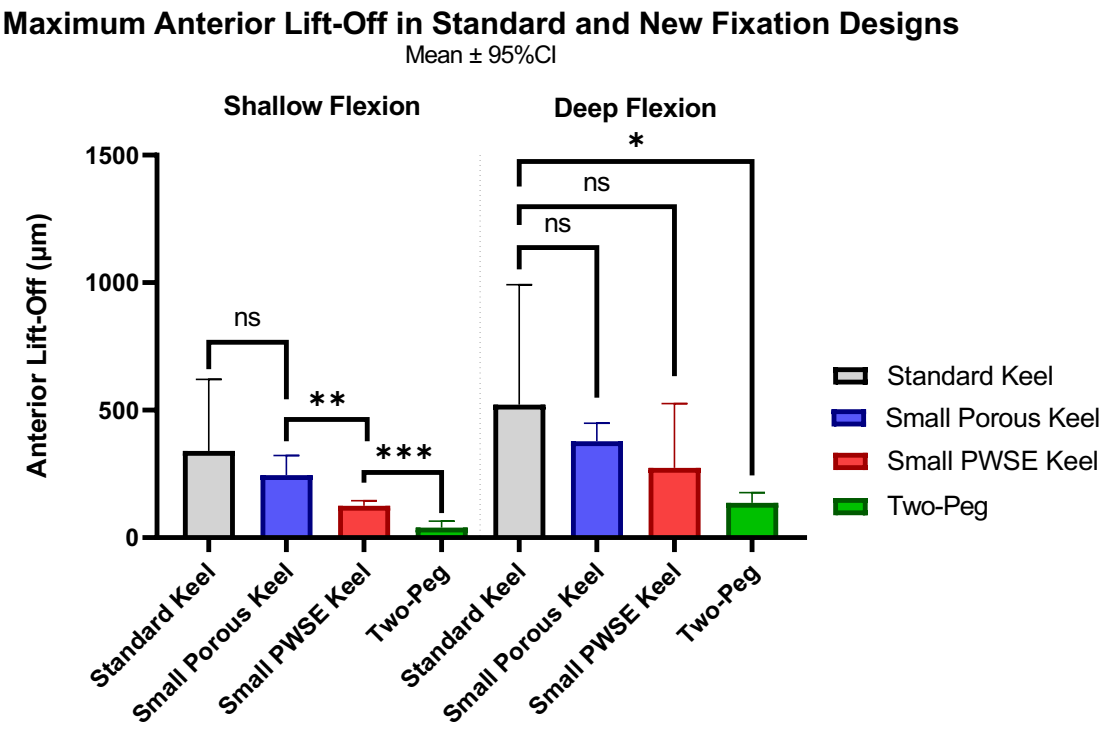


Figure 8.12: *Maximum anterior lift-off measurements, occurring during maximal loading of 200 N in a tibial component with a standard keel, small porous keel, small PWSE keel, and Two-Peg. Tests statistically compared. ns: not significant, *: p<0.05, ***: p<0.001.*

8.4.3 Discussion of Findings

This study found that interference increases anterior lift-off in shallow flexion, but is reduces anterior lift-off at higher flexion angles, suggesting two different mechanisms inducing sagittal micromotion. This is the first time this apparent duality has been described. The new fixation designs tested both demonstrate significant reductions in anterior lift-off, suggesting improved primary fixation.

Using interference for primary fixation of a tibial component keel has the counterintuitive effect of increasing anterior lift-off in shallow fixation (as in a step-up motion, when the loading position is not excessively posterior). Data showed that, compared to a standard keel, having no keel reduces the anterior lift-off by more than tenfold, from 340 μm to 30 μm. A variant of the standard keel, which is thinner to avoid having an interference fit, also had a drastically lower 63 μm of anterior lift-off, which has a five-fold reduction in anterior lift-off compared to the standard keel. It is not immediately clear why. When the loading position is moved to represent deep flexion (with a more extreme position 15 mm posterior to midpoint), the pattern observed is reversed. Interference fit is beneficial, reducing anterior lift-off by 50%, from 1003 μm with no keel to 521 μm with the standard keel. Having a standard keel with no interference sits between having no keel and a standard keel with interference at 816 μm. In both loading positions, a smaller keel demonstrates a significant reduction in anterior lift-off across the load cycle. This is inconsistent with the standard keel, which experienced greater anterior lift-off at lower interferences.

A hypothesis is proposed which is consistent with these findings. Firstly, Push-In Pull-Out studies of the keel in **Chapter 5** demonstrate that there is a small but consistent upward displacement (i.e., a ‘bounce back’) of the keel after Push-In (**Figure 5.4**). This

may result in the keel and component sitting slightly proud of the slot. This would mechanically allow for greater pivoting along the plane of the keel, resulting in the greater anterior lift-off in shallow flexion. A smaller keel can be expected to proportionally bounce back less, thereby permitting less pivoting and less anterior lift-off. Over the early post-operative period, successive load cycles are likely to result in the keel being pushed down into the slot, making it fully seated and stopping this pivoting motion, arresting the progression of subsidence. This is consistent with what is described in routine clinical follow-up [75], RSA findings of a small inferior translation and posterior sloping of the cementless tibial component in the first year before getting fixed [149], as well as clinical findings of progression of posterior-slope-inducing subsidence which is arrested after the first year [107]. In the absence of interference at the keel, the interaction between the tibial component and the condyle occurs at the floor of the tibial component; this may explain the low anterior lift-off seen at shallow flexion (where the pivoting motion does not occur), but much greater anterior lift-off seen with deep flexion (where implant motion is not constrained by interference).

With the new keel designs, the maximum anterior lift-off of was successively and significantly reduced from standard > small porous > small PWSE > Two-Peg (**Figure 8.12**) in shallow fixation. While the same pattern was seen in deep flexion, differences in maximum anterior lift-off were smaller and not significant between the keels, but remained significant between the standard keel and Two-Peg (**Figure 8.12**), and differences were successively significant across variants when whole load cycles were compared (**Figure 8.11**).

It should be noted that the whole range of motion of the Two-Peg in shallow flexion and motion when loaded below 100 N in deep flexion are less than 50 μm, which is the tested

accuracy limit of the setup (**Figure 8.3**). Therefore, it is possible that trends below this value are inaccurate.

The large anterior lift-off in deep flexion 'lunge' tests reinforce clinically given advice that patients should be advised against such deep motion in the early postoperative period [75]. Avoiding excessive micromotion during this early remodelling stage is known to be important as it can lead to formation of fibrous tissue and inhibition of bone ingrowth, which likely compromise secondary fixation [201].

It is notable that a tibial component with a standard keel with no interference has small but statistically significant interference-like action, increasing micromotion with 8 mm posterior loading and decreasing micromotion with 15 mm posterior loading. This is suggestive of a 'yaw' rotation (rotation on the axial plane) of the tibial component, as although this keel is narrower than the slot it is in, such rotation of the implant can result in the keel interfacing with the slot and inducing frictional forces which would mimic those seen in a fixed keel.

In **Chapter 7**, it was found that maximum push-in forces from Push-In Pull-Out testing were not a reliable predictor of load-to-fracture (**Section 7.3.3**). Similar inconsistencies were found between maximum pull-out forces ($MaxF_{out}$) from **Chapters 5 and 6**, and anterior lift-off values from this chapter.

Table 8.1: *Maximum Anterior Lift-Off and Maximum Push-In Force of keel designs tested.*

Maximum Anterior Lift-Off				
	Shallow Flexion (-8mm, step up)		**Deep Flexion (-15mm, forward lunge)**	
	Mean (μm)	**Value as a % of Standard keel**	**Mean (μm)**	**Value as a % of Standard keel**
Standard Keel	340		522	
Small Porous Keel	245	28% lower	378	28% lower
Small PWSE Keel	125	63% lower	273	48% lower
Two-Peg	40	89% lower	137	74% lower

Maximum Pull-Out Force		
	Mean (N)	**Value as a % of Standard keel**
Standard Keel	178	
Small Porous Keel	113	37% lower
Small PWSE Keel	234	31% higher
Two-Peg	385 (193 × 2)	116% higher

The small PWSE keel experienced 31% greater $MaxF_{out}$ and 56% less maximum anterior lift-off, and the Two-Peg experienced 116% greater $MaxF_{out}$ and 82% less maximum anterior lift-off. Most interestingly, the small porous keel which had a 37% lower $MaxF_{out}$ than the standard keel still experienced an average of 28% less maximum anterior lift-off than the standard keel (**Table 8.1**). The relatively better performance of the small keels in micromotion compared to pull-out forces is consistent with the 'reduced bounce back' hypothesis discussed earlier. The relatively poorer performance with the Two-Peg may be due to methodological limitations (as its maximum anterior lift-off of 40 μm is below the setup's precision limit of 50 μm) and mechanical interaction between pegs (resulting

in two proximally placed pegs having a combined less pull-out force compared to two separate pegs) [203].

In all, these new keel and peg designs, in addition to potentially reducing fracture risk (**Chapter 7**), also appear to reduce anterior lift-off and thereby potentially improve primary fixation, likely reducing the risk of micromotion and subsidence (**Chapter 8.2.1**). This is especially as the posterior sloping [149] and posterior subsidence [107] seen clinically occur in patients who are advised to perform only activities of daily living where shallow flexion occurs [208]; the new fixation designs are most protective within the limits of posterior loading seen in such shallow flexion (**Figure 8.12**).

A limitation of this study is that the displacement of the foam condyle and component were only measured on the lateral (i.e., sagittal) view, and micromotion on the AP view is not assessed. This is due to the two-dimensional DIC algorithm used in this study. Further exploration of implant motion, by means of three-dimensional DIC or otherwise, would be needed to validate the rotational movement suggested to occur with the standard narrow keel.

The condyles used in this mechanical study have notable differences to clinical anatomy. Tests were performed on machined medial condyles which did not have a cortical surface as a result of manufacturing technique. It is unlikely that the absence of the cortex influenced results, as micromotion would be the result of interaction between the keel and the surrounding trabecular bone it is implanted in. In addition, the condyles tested had a 5 mm vertical cut on the plane of the tibial wall to enable DIC analysis. It can be expected that this vertical cut may have an effect on micromotion. Nonetheless, as a comparative study, it is unlikely that the cut would influence the different keel designs differently, and is therefore unlikely to be of concern.

8.5 Chapter Summary

Primary fixation of the tibial component is conferred by the keel. Interference at the keel results in reduced sagittal micromotion in deep flexion, but counterintuitively, greater sagittal micromotion in shallow flexion. A smaller keel protects against this micromotion in both shallow and deep flexion, likely due to reduced bounce back and pivoting at the keel. Mechanisms for these patterns are proposed and consistent with clinical evidence.

The small porous keel demonstrates similar if not slightly reduced sagittal micromotion compared to the standard keel. Adding a smooth edge further reduces this. The new Two-Peg provides even better primary fixation of the tibial component – the largest anterior lift-off measurement made in this study was within the limits of tolerable micromotion found in literature, and upon unloading, the Two-Peg component returned to its initial position with no residual displacement. Improvements to primary fixation, specifically through limiting anterior lift-off, would likely reduce the early posterior sloping of the cementless tibial component observed clinically, thereby potentially reducing the risk of subsidence.

These new designs are promising candidates for reduced fracture risk (as found in **Chapter 7**), and now have been found in this chapter to provide equal or better primary fixation compared to the existing keel design. If found safe, and used clinically, they are likely to reduce fracture risk in very small tibias, and potentially also the risk of subsidence.

9 Conclusion

9.1 Summary of Findings

The work done in this thesis had two aims: firstly, to compare the symptoms following Cementless and Cemented Oxford UKR and explore factors that may influence them, and secondly to assess design changes which may reduce the risk of fracture.

In **Chapter 2**, a study comparing Cementless and Cemented Oxford UKR demonstrated that most pain reported by patients is nociceptive, that stronger pain is more likely to occur where there are co-morbidities, and that 42% more patients with the cementless implant report having no pain compared to cemented.

In **Chapter 3**, the cementless tibial component was shown to have significantly less radiolucencies than the cemented, and that these radiolucencies were associated with an increased likelihood of patients reporting pain. Radiolucencies in the cementless tibial component were found only where there was no porous coat. This finding lends compelling evidence to apply porous surfaces to all bone-implant interfaces of the tibial component.

In **Chapter 4**, bone density around the keel was found to change in the years following surgery, but these changes were unrelated to pain and therefore unlikely to be of clinical concern. Changes suggest that tibial component loading occurs disproportionately through the keel, and that this was greater in smaller tibial components. This potentially implicates the keel in fractures occurring with the cementless tibial component.

The Cementless Oxford UKR experiences a greater incidence of fracture, particularly in very small tibias. Around 7% of patients who get the Oxford UKR implant in the UK are given the cemented tibial component in part due to concerns about fracture. This proportion is estimated to be 17% in Asia-Pacific populations. Therefore, design changes which may reduce the risk of fracture were explored.

The high fracture risk is attributed to a relatively deeper keel in very small tibias, and surgical errors leading to extended cuts that compromise the posterior cortex. In **Chapter 5**, Push-In Pull-Out tests were used to assess the effect of design changes to fracture risk and primary fixation. From these tests, two new keel designs were proposed: a small porous keel and a small porous-walled smooth-edged keel. In **Chapter 6**, similar testing was performed with pegs and a more radical fixation design, replacing keels with two anterior angled pegs, was proposed to address fundamental limitations of a keel.

Chapter 7 and **Chapter 8** evaluate designs in plastic bone blocks machined to the shape of a very small tibia, using load-to-fracture and anterior lift-off with posterior loading as more physiological metrics for fracture risk and primary fixation. Greater keel size and interference were shown to likely increase fracture risk. Smaller keel size appeared to have similar or better primary fixation to larger keel size. Interference was related to greater anterior lift-off with shallow flexion but less anterior lift-off with deep flexion. Reasons for these patterns are proposed.

The small porous keel, compared to the standard keel, increased load-to-fracture and had similar primary fixation. The small smooth-edged keel similarly increased the fracture load but had better primary fixation. The Two-Peg greatly increased fracture load and primary fixation.

Based on these findings, two changes to the existing Cementless Oxford UKR tibial component are recommended. First is the expansion of the porous surface to all implant surfaces that interface with bone. Second is the modification of the existing keel to one or more of three new designs. The most immediately implementable design is the small porous keel, which can be manufactured with current clinical techniques. The second design is the small porous-walled smooth-edged keel, which requires modification to manufacturing techniques. The final design is the Two-Peg, which requires modifications to manufacturing, surgical technique, and instrumentation.

This **concluding chapter** will outline the next steps to bridge the findings of this thesis to clinical use of these new tibial components. If found safe for clinical use, these design changes can be implemented as a new 'Phase 2' Cementless Oxford UKR. This will allow future comparison of outcomes to the existing Cementless Oxford UKR. These new tibial components will likely improve fixation and reduce fracture and subsidence risk in patients.

9.2 Further Work on Outcome Assessment

Patterns in radiolucency and bone density around the keel have been assessed in the AP view in this thesis. However, it is not known how radiolucencies and bone density vary along the AP axis of the tibial component (i.e., as seen in a lateral radiographic view). Given existing knowledge about posterior loading, posterior subsidence, and anterior tilt (discussed in **Chapter 8**), it is possible that radiolucencies and bone density may vary along the AP axis of the tibial keel. In addition, only sagittal micromotion was assessed in this thesis. While tibial component micromotion is likely to vary the most in the sagittal plane (discussed in **Chapter 8**), it is possible that micromotion also occurs in the coronal and axial planes.

The underlying mechanisms of keel-slot and peg-hole interactions (discussed in **Chapters 5 and 6**), such as rasping, are only discussed speculatively in this thesis. They are likely to involve multiple complex mechanical phenomena which are not well characterised in orthopaedic literature, such as static and dynamic friction, foam deformation, and foam failure models.

There are methodological limitations limiting the testing of these hypotheses and mechanical interactions. For radiolucencies in a lateral view, more rigorous methods to address alignment will need to be developed, as there are fewer implant elements available to quantify alignment than in the AP view. For bone density measurements, there are difficulties in accurately sizing and segmenting bone regions without a reference area such as the keel, and accounting for changes in bone mass in bone outside of the peri-keel region. For micromotion in coronal and axial views, changes to imaging setup, the use of more expensive three-dimensional DIC, and a two-axis loading machine, would likely be required as well. Interactions at the bone-implant interface will require

precise characterisation of mechanical properties likely involving a combination of mechanical testing and computational modelling.

Nonetheless, if such hypotheses are explored, better understanding of these presently unknown patterns and properties will provide greater insight into the clinical and mechanical interactions of the bone and the tibial component, and may help to potentially identify further areas for improvement.

9.3 Further Work on Design Changes

9.3.1 Expanding the Porous Surface of the Tibial Component

The bone-facing surfaces of the current Cementless Oxford UKR are shown in **Figure 9.1**. Data from **Chapter 3** suggests that the bone-implant interfaces without porous coating have the highest risk of experiencing a radiolucency, which is associated with incidence of pain. Based on this, it is suggested that all bone-facing surfaces, including those which are currently smooth or have a microporous surface, are replaced with porous-coated surface. All bone-facing surfaces should have a further application of a hydroxyapatite coat, which is already present on current Cementless Oxford UKR.

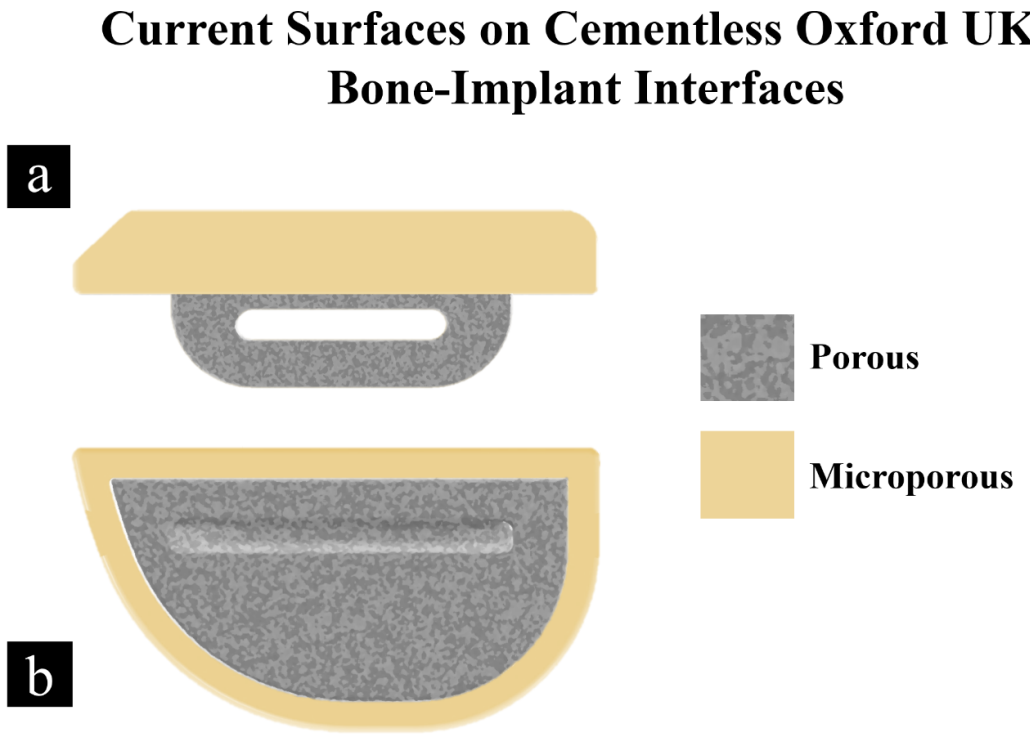


Figure 9.1: *Current Surfaces on* ***(a)*** *lateral and* ***(b)*** *inferior views of the current Cementless Oxford UKR presenting implant surfaces that interface with bone.*

9.3.2 Testing Fracture and Fixation in Larger Tibial Sizes and with Cortex

In this thesis, new keel/peg designs have been tested with the structure of one Size 'A' tibia. Prior to routine clinical use, these new tibial component designs will need to be tested and found to be safe for all sizes of tibias. Therefore, tests of fracture risk and primary fixation, similar to those performed in this thesis, will need to be performed across a representative sample of implant sizes (e.g., smallest, middle, and largest sizes). It would also be prudent to reproduce findings in new designs when tested with a cortex. However, the modality of testing to be used is unclear. Cadaveric testing is unlikely as osteoarthritic and non-osteoarthritic knees are believed to have notably different material properties [212, 213]. In addition, existing cadaveric testing does not accurately represent fracture patterns seen clinically [207] – see **Section 5.2.1** for clinical fracture patterns. Alternatively, validation may be performed using computational modelling to determine the added effect of an osteoarthritic cortex.

9.3.3 Replicating Findings with True Porous Surfaces

All tests presented in the thesis have been performed with additively manufactured (i.e., 3D-printed) implants. Preliminary comparisons of surface similarities between 3D-printed and true porous surfaces showed that the surface microstructures were similar (**Figure 5.6**).

However, implant manufacturing uses considerably different approach to prepare surfaces to additive manufacturing. This is most relevant for the porous surfaces. 3D-printed porous surfaces produce a fine titanium 'mesh' which is limited to the resolution of the printer. In contrast, true porous surfaces are produced using high-energy plasma

sprayed titanium, which deposits on the surface of the implant and cools [223]. A layer of hydroxyapatite is also sprayed onto these surfaces.

The mechanical differences between 3D-printed and true porous surfaces have not been characterised in the Oxford UKR, and therefore tests which rely on implant-bone surface interactions, such as Push-In Pull-Out and anterior lift-off, need to be validated with a true porous surface.

9.3.4 Producing New Component Designs with Clinical Manufacturing Techniques

Existing Cementless Oxford UKR tibial components are produced by casting Cobalt-Chrome-Molybdenum alloys into the specific shapes of the implants. These casts are then finished as follows: polishing where smooth surfaces are desired such as the implant-bearing interfaces, shot-blasting where rough surfaces are desires such as the external tibial wall with plasma-sprayed titanium where a porous coat is desired, and with a final coat of hydroxyapatite on all surfaces interfacing with bone.

Based on this, the production of small porous keel would require minimal changes to existing manufacturing techniques, as a new casting mould would be able to produce the new keel size.

The small PWSE keel requires modification the application of the spray coat. A preliminary technique was trialled where a mask was applied to the keel edge (which was to be smooth). This process was successful in producing a porous-walled, smooth-edged keel, but also produced a ‘lip’ between the smooth and porous surfaces (**Figure 9.2b**).

This component was trialled using Push-In Pull-Out testing, where the lip was found to limit bone-slot interaction during the push-in phase, and cause substantial rasping during the pull-out phase (**Figure 9.2c**), resulting in low maximum push-in and pull-out forces (**Figure 9.3**), compared to a standard keel. Removing this lip by planing and filing (**Figure 9.2d**) improves push-in and pull-out forces, though not to the levels seen with the 3D-printed PWSE keel (**Figure 5.8, Chapter 5**). Further work is necessary to further optimise manufacture of the PWSE keel. The process of manufacturing a Two-Peg tibial component will likely involve a new casting mould as well – this will need to be explored.

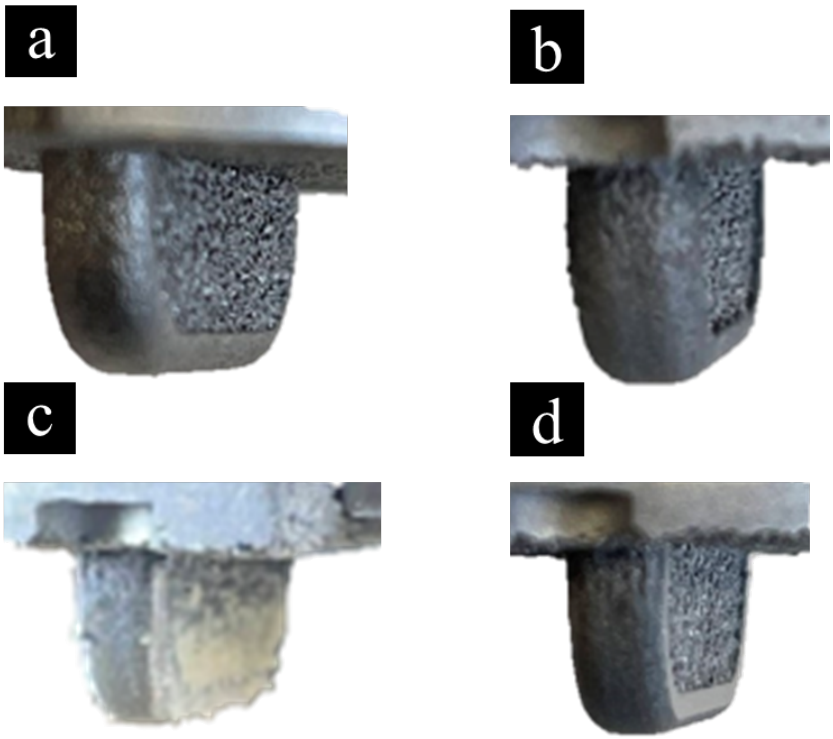


Figure 9.2: *Differences in small PWSE keels when* ***(a)*** *3D printed, and* ***(b)*** *manufactured using clinical techniques.* ***(c)*** *Rasping effect of upper lip of clinically manufactured keel.* ***(d)*** *Removal of lip from clinically manufactured keel by planing and filing.*

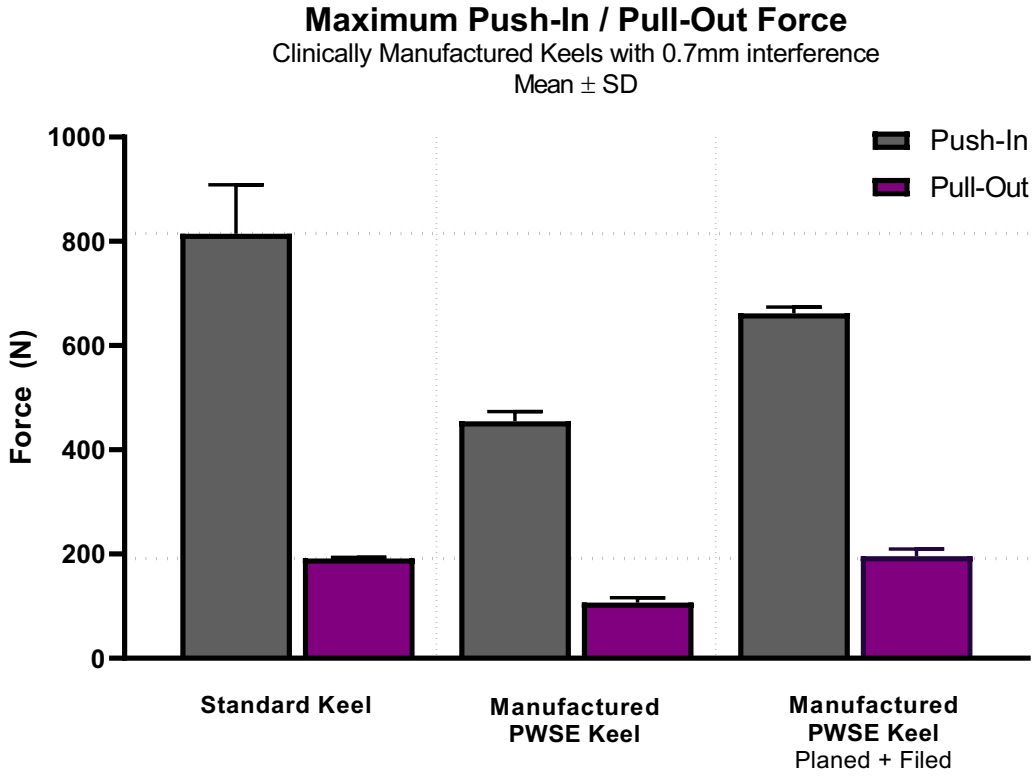


Figure 9.3: *Maximum Push-In and Pull-Out Forces in clinically manufactured standard and small PWSE keels, and a small PWSE keel where the lip is planed and filed. Tests performed at n=3.*

9.3.5 Safety and Regulatory Approval

Once new tibial components with expanded porous surfaces and new keel/peg fixation elements are manufactured, they will need to be deemed to be safe for clinical assessment, followed by further approval for wider clinical testing and routine use. Such regulatory approval in the UK is provided by the Medicines and Healthcare products Regulatory Agency (MHRA), and detailed review of MHRA guidelines will be necessary to determine what steps need to be taken to obtain regulatory approval.

It is likely that the new keel designs, due to their similarity to the existing keel design, are structurally safe. However, the newer peg design is radically different, thus likely

requiring fatigue studies to ensure that it is safe from structural failure (such as fracture of a peg from the rest of the component).

9.3.6 Clinical Assessment

9.3.6.1 Assessing Safety and Primary Fixation

The new tibial component designs proposed have a smaller keel/peg profile than the existing standard keel. This keel plays a key role in providing primary implant fixation. While primary fixation has been shown in this thesis to be similar or better in new designs, this remains the greatest safety concern and will need to be a primary outcome assessed in early clinical trials. Poor fixation is believed to be related to implant subsidence, and in particular posterior subsidence (**Figure 8.1**). Therefore, if the new designs perform as expected based on findings in this thesis, they will experience similar or lesser posterior subsidence compared to the standard keel. This can be assessed using radiostereometric analysis (RSA), which allows measurement of implant migration, and thus, subsidence (discussed further in **Section 8.3.1**).

Therefore, the first clinical trial of this 'Phase 2 Cementless Oxford UKR tibial component' should be a randomised control trial (RCT) incorporating RSA, where the new tibial component design is compared against the existing design monitoring implant fixation, and in particular, posterior subsidence. The RSA study could incorporate Dynamically Induced Micromotion (DIMM) testing, to assess *in-vivo* implant motion during knee loading and unloading [214].

It is unlikely that the new designs, which are highly similar to existing designs except for the less resection of bone for the new keel/pegs, would increase risk of peri or post-operative complications (such as fracture). Nonetheless, such complications should be monitored in early trials to ensure new designs are not less safe than the existing design, with constant monitoring of data to ensure use of new designs can be rapidly stopped if the implant is found to be unsafe.

9.3.6.2 Assessing Secondary Fixation

Following early trials, the mid-to-long term fixation of the new designs is another important unknown that was not tested within the scope of this thesis, and requires assessment of bone remodelling. While the porous surface area interfacing with the bone slot in the new small porous and PWSE keels is the same as the current standard keel, there may be 'unknown unknowns' which may adversely affect fixation. This is even more applicable to the Two-Peg design, particularly as it has a reduced porous surface area compared to the keels.

Secondary fixation therefore should be carefully monitored before routine use of new implant designs. This can be assessed by continued mid-to-long term follow-up of the RSA-based RCT cohort discussed in **Section 9.3.6.1**. In addition, studies assessing radiolucency (as performed in **Chapter 3**) can be used to further assess secondary fixation.

9.3.6.3 Assessing Patient-Reported Outcomes

Once early safety-related trials are successful, further assessment can be performed monitoring patient-related outcomes. While the early RCT can incorporate elements of such outcome measures, they would likely be underpowered to identify differences. Therefore, once the new tibial components are deemed safe and the implant is used routinely, larger studies on patient-reported outcomes (as performed in **Chapter 2**) should be performed to determine if the new implant designs improve pain, function, and ultimately, patient satisfaction.

BIBLIOGRAPHY

1. Standring S. *Gray's Anatomy*. 42 ed. The Anatomical Basis of Clinical Practice. 2020: Elsevier.

2. Baratta R, Solomonow M, Zhou BH, Letson D, Chuinard R, and D'Ambrosia R. Muscular coactivation:The role of the antagonist musculature in maintaining knee stability. *The American Journal of Sports Medicine*. 1988; **16**(2): p. 113-122.

3. Wilson A. *Knee Anatomy*. Available from: https://profadrianwilson.co.uk/knee-treatments/knee-anatomy/.

4. Anonymous. *Articular surfaces and joints in the knee*. Available from: https://www.earthslab.com/anatomy/knee-joint/.

5. Papas PV, Cushner FD, and Scuderi GR. The History of Total Knee Arthroplasty. *Techniques in Orthopaedics*. 2018; **33**(1): p. 2-6.

6. Shetty AA, Tindall A, Ting P, and Heatley FW. The evolution of total knee arthroplasty. Part II: the hinged knee replacement and the semi-constrained knee replacement. *Current Orthopaedics*. 2003; **17**(5): p. 403-407.

7. Turcotte RE, Sim FH, Pritchard DJ, Chao EYS, and Donati D. *Long-Term Follow-Up of Walldius-Hinged Total Knee Arthroplasties*. 1991. Berlin, Heidelberg: Springer Berlin Heidelberg.

8. Moll JM, Chesterman PJ, Meanock RI, and Andrews FM. Walldius arthroplasty of the knee. Follow-up study of 51 operations. *Annals of the Rheumatic Diseases*. 1973; **32**(5): p. 397-405.

9. Font-Rodriguez DE, Scuderi GR, and Insall JN. Survivorship of cemented total knee arthroplasty. *Clinical Orthopaedics and Related Research*. 1997;(345): p. 79-86.

10. Hsu H and Siwiec RM. *Knee Arthroplasty*, in *StatPearls*. 2022, StatPearls Publishing: Treasure Island (FL).

11. Rodríguez-Merchán EC. Total knee arthroplasty using hinge joints: Indications and results. *EFORT Open Reviews*. 2019; **4**(4): p. 121-132.

12. *National Joint Registry 16th Annual Report 2019*. 2019, National Joint Registry: London.

13. Glyn-Jones S, Palmer AJR, Agricola R, Price AJ, Vincent TL, Weinans H, and Carr AJ. Osteoarthritis. *Lancet*. 2015; **386**(9991): p. 376-387.

14. van den Bosch MHJ. Osteoarthritis year in review 2020: biology. *Osteoarthr Cartil*. 2021; **29**(2): p. 143-150.

15. Madry H, Luyten FP, and Facchini A. Biological aspects of early osteoarthritis. *Knee Surg Sports Traumatol Arthrosc*. 2012; **20**(3): p. 407-422.

16. Khokhar K and Conaghan PG. Bone in osteoarthritis: imaging and interventions. *Curr Opin Rheumatol*. 2022; **34**(1): p. 73-78.

17. Poulsen E, Goncalves GH, Bricca A, Roos EM, Thorlund JB, and Juhl CB. Knee osteoarthritis risk is increased 4-6 fold after knee injury – a systematic review and meta-analysis. *Br J Sports Med*. 2019; **53**(23): p. 1454-1463.

18. Katz JN, Arant KR, and Loeser RF. Diagnosis and Treatment of Hip and Knee Osteoarthritis A Review. *JAMA*. 2021; **325**(6): p. 568-578.

19. Kellgren JH and Lawrence JS. Radiological Assessment of Osteo-Arthrosis. *Annals of the Rheumatic Diseases*. 1957; **16**(4): p. 494-502.

20. Jonsson K and Boegård T. *Radiography*, in *Imaging of the Knee: Techniques and Applications*, A.M. Davies and V. Cassar-Pullicino, Editors. 2003, Springer Berlin Heidelberg: Berlin, Heidelberg. p. 3-17.

21. Murphy L, Schwartz TA, Helmick CG, Renner JB, Tudor G, Koch G, Dragomir A, Kalsbeek WD, Luta G, and Jordan JM. Lifetime risk of symptomatic knee osteoarthritis. *Arthritis Care Res (Hoboken)*. 2008; **59**(9): p. 1207-1213.

22. Christensen R, Bartels EM, Astrup A, and Bliddal H. Effect of weight reduction in obese patients diagnosed with knee osteoarthritis: a systematic review and meta-analysis. *Ann Rheum Dis*. 2007; **66**(4): p. 433-439.

23. Kan HS, Chan PK, Chiu KY, Yan CH, Yeung SS, Ng YL, Shiu KW, and Ho T. Non-surgical treatment of knee osteoarthritis. *Hong Kong Med J*. 2019; **25**(2): p. 127-133.

24. McAlindon TE, Bannuru RR, Sullivan MC, Arden NK, Berenbaum F, Bierma-Zeinstra SM, Hawker GA, Henrotin Y, Hunter DJ, Kawaguchi H, Kwoh K, Lohmander S, Rannou F, Roos EM, and Underwood M. OARSI guidelines for the non-surgical management of knee osteoarthritis. *Osteoarthr Cartil*. 2014; **22**(3): p. 363-388.

25. Raja K and Dewan N. Efficacy of knee braces and foot orthoses in conservative management of knee osteoarthritis: a systematic review. *Am J Phys Med Rehabil*. 2011; **90**(3): p. 247-262.

26. Jones A, Silva PG, Silva AC, Colucci M, Tuffanin A, Jardim JR, and Natour J. Impact of cane use on pain, function, general health and energy expenditure during gait in patients with knee osteoarthritis: a randomised controlled trial. *Ann Rheum Dis*. 2012; **71**(2): p. 172-179.

27. Simic M, Hinman RS, Wrigley TV, Bennell KL, and Hunt MA. Gait modification strategies for altering medial knee joint load: A systematic review. *Arthritis Care Res (Hoboken)*. 2011; **63**(3): p. 405-426.

28. Bannuru RR, Natov NS, Obadan IE, Price LL, Schmid CH, and McAlindon TE. Therapeutic trajectory of hyaluronic acid versus corticosteroids in the treatment of knee osteoarthritis: a systematic review and meta-analysis. *Arthritis Rheum*. 2009; **61**(12): p. 1704-1711.

29. Bellamy N, Campbell J, Robinson V, Gee T, Bourne R, and Wells G. Intraarticular corticosteroid for treatment of osteoarthritis of the knee. *Cochrane Database Syst. Rev*. 2006;(2): p. Cd005328.

30. Katz JN, Earp BE, and Gomoll AH. Surgical management of osteoarthritis. *Arthritis Care Res (Hoboken)*. 2010; **62**(9): p. 1220-1228.

31. He M, Zhong X, Li Z, Shen K, and Zeng W. Progress in the treatment of knee osteoarthritis with high tibial osteotomy: a systematic review. *Syst Rev*. 2021; **10**(1): p. 56.

32. Ollivier B, Berger P, Depuydt C, and Vandenneucker H. Good long-term survival and patient-reported outcomes after high tibial osteotomy for medial compartment osteoarthritis. *Knee Surg Sports Traumatol Arthrosc*. 2021; **29**(11): p. 3569-3584.

33. Diaz CC, Lavoie-Gagne OZ, Knapik DM, Korrapati A, Chahla J, and Forsythe B. Outcomes of Distal Femoral Osteotomy for Valgus Malalignment: A Systematic Review and Meta-analysis of Closing Wedge Versus Opening Wedge Techniques. *Am J Sports Med*. 2022: p. 3635465211051740.

34. Moseley JB, O'Malley K, Petersen NJ, Menke TJ, Brody BA, Kuykendall DH, Hollingsworth JC, Ashton CM, and Wray NP. A controlled trial of arthroscopic surgery for osteoarthritis of the knee. *N Engl J Med*. 2002; **347**(2): p. 81-88.

35. Kirkley A, Birmingham TB, Litchfield RB, Giffin JR, Willits KR, Wong CJ, Feagan BG, Donner A, Griffin SH, D'Ascanio LM, Pope JE, and Fowler PJ. A randomized trial of arthroscopic surgery for osteoarthritis of the knee. *N Engl J Med*. 2008; **359**(11): p. 1097-1107.

36. Baeten D, Demetter P, Cuvelier C, Van den Bosch F, Kruithof E, Van Damme N, Verbruggen G, Mielants H, Veys EM, and De Keyser F. Comparative study of the synovial histology in rheumatoid arthritis, spondyloarthropathy, and osteoarthritis: influence of disease duration and activity. *Annals of the Rheumatic Diseases*. 2000; **59**(12): p. 945-953.

37. Dougados M, Linden SVD, Juhlin R, Huitfeldt B, Amor B, Calin A, Cats A, Dijkmans B, Olivieri I, Pasero G, Veys E, and Zeidler H. The European Spondylarthropathy Study Group Preliminary Criteria for the Classification of Spondylarthropathy. *Arthritis & Rheumatism*. 1991; **34**(10): p. 1218-1227.

38. Jones GB. Arthroplasty of the knee by the Walldius prosthesis. *J Bone Joint Surg Br*. 1968; **50**(3): p. 505-510.

39. Phillips H and Taylor JG. The Walldius hinge arthroplasty. *J Bone Joint Surg Br*. 1975; **57**(1): p. 59-62.

40. Lee JK and Choi CH. Total knee arthroplasty in rheumatoid arthritis. *Knee Surg Relat Res*. 2012; **24**(1): p. 1-6.

41. Ahlbäck S, Bauer GCH, and Bohne WH. Spontaneous Osteonecrosis of the Knee. *Arthritis & Rheumatism*. 1968; **11**(6): p. 705-733.

42. Yamamoto T and Bullough PG. Spontaneous osteonecrosis of the knee: the result of subchondral insufficiency fracture. *J Bone Joint Surg Am*. 2000; **82**(6): p. 858-866.

43. Duany NG, Zywiel MG, McGrath MS, Siddiqui JA, Jones LC, Bonutti PM, and Mont MA. Joint-preserving surgical treatment of spontaneous osteonecrosis of the knee. *Arch Orthop Trauma Surg*. 2010; **130**(1): p. 11-16.

44. Myers TG, Cui Q, Kuskowski M, Mihalko WM, and Saleh KJ. Outcomes of total and unicompartmental knee arthroplasty for secondary and spontaneous osteonecrosis of the knee. 2006; **88**(Suppl. 3): p. 76-82.

45. Lotz MK and Kraus VB. New developments in osteoarthritis. Posttraumatic osteoarthritis: pathogenesis and pharmacological treatment options. *Arthritis Res Ther*. 2010; **12**(3): p. 211.

46. Benazzo F, Rossi SMP, and Ghiara M. Partial knee arthroplasty: Patellofemoral arthroplasty and combined unicompartmental and patellofemoral arthroplasty implants - general considerations and indications, technique and clinical experience. *Knee*. 2014; **21**(S1): p. S43-S46.

47. Abdel MP, von Roth P, Cross WW, Berry DJ, Trousdale RT, and Lewallen DG. Total Knee Arthroplasty in Patients With a Prior Tibial Plateau Fracture: A Long-Term Report at 15 Years. *J Arthroplasty*. 2015; **30**(12): p. 2170-2172.

48. Guccione AA, Felson DT, Anderson JJ, Anthony JM, Zhang Y, Wilson PW, Kelly-Hayes M, Wolf PA, Kreger BE, and Kannel WB. The effects of specific medical conditions on the functional limitations of elders in the Framingham Study. *Am J Public Health*. 1994; **84**(3): p. 351-358.

49. Cieza A, Causey K, Kamenov K, Hanson SW, Chatterji S, and Vos T. Global estimates of the need for rehabilitation based on the Global Burden of Disease study 2019: a systematic analysis for the Global Burden of Disease Study 2019. *The Lancet*. 2020; **396**(10267): p. 2006-2017.

50. Christensen K, Doblhammer G, Rau R, and Vaupel JW. Ageing populations: the challenges ahead. *Lancet*. 2009; **374**(9696): p. 1196-1208.

51. Kelly T, Yang W, Chen CS, Reynolds K, and He J. Global burden of obesity in 2005 and projections to 2030. *Int J Obes (Lond)*. 2008; **32**(9): p. 1431-1437.

52. *The National Joint Registry 18th Annual Report*. 2021, National Joint Registry: London.

53. Price AJ, Alvand A, Troelsen A, Katz JN, Hooper G, Gray A, Carr A, and Beard D. Knee replacement. *The Lancet*. 2018; **392**(10158): p. 1672-1682.

54. Culliford D, Maskell J, Judge A, Cooper C, Prieto-Alhambra D, and Arden NK. Future projections of total hip and knee arthroplasty in the UK: results from the UK Clinical Practice Research Datalink. *Osteoarthritis Cartilage*. 2015; **23**(4): p. 594-600.

55. Willis-Owen CA, Brust K, Alsop H, Miraldo M, and Cobb JP. Unicondylar knee arthroplasty in the UK National Health Service: an analysis of candidacy, outcome and cost efficacy. 2009; **16**: p. 473-478.

56. Liddle AD, Pandit H, Judge A, and Murray DW. Optimal usage of unicompartmental knee arthroplasty: a study of 41,986 cases from the National Joint Registry for England and Wales. *Bone Joint J*. 2015; **97-b**(11): p. 1506-1511.

57. Carlos Rodríguez-Merchán E and Gómez-Cardero P. Unicompartmental knee arthroplasty: Current indications, technical issues and results. *EFORT Open Reviews*. 2018; **3**(6): p. 363-373.

58. Jones G, Kotti M, Wiik A, Collins R, Brevadt M, Strachan R, and Cobb J. Gait comparison of unicompartmental and total knee arthroplasties with healthy controls. *The Bone & Joint Journal*. 2016; **98-B**(10_Supple_B): p. 16-21.

59. Liddle A, Pandit H, Judge A, and Murray D. Patient-reported outcomes after total and unicompartmental knee arthroplasty: a study of 14,076 matched patients from the National Joint Registry for England and Wales. *The Bone & Joint Journal*. 2015; **97-B**(6): p. 793-801.

60. Burn E, Sanchez-Santos MT, Pandit HG, Hamilton TW, Liddle AD, Murray DW, and Pinedo-Villanueva R. Ten-year patient-reported outcomes following total and minimally invasive unicompartmental knee arthroplasty: a propensity score-matched cohort analysis. *Knee Surgery, Sports Traumatology, Arthroscopy*. 2018; **26**(5): p. 1455-1464.

61. Chawla H, Ghomrawi HM, van der List JP, Eggman AA, Zuiderbaan HA, and Pearle AD. Establishing Age-Specific Cost-Effective Annual Revision Rates for Unicompartmental Knee Arthroplasty: A Meta-Analysis. *Journal of Arthroplasty*. 2017; **32**(1): p. 326-335.

62. Wilson HA, Middleton R, Abram SGF, Smith S, Alvand A, and Jackson WF. Patient relevant outcomes of unicompartmental versus total knee replacement: systematic review and meta-analysis. 2019; **364**: p. l352.

63. Mohammad HR, Liddle AD, Judge A, and Murray DW. A Matched Comparison of Long-Term Outcomes of Total and Unicompartmental Knee Replacements in Different Ages Based on National Databases: Analysis of Data From the National Joint Registry for England, Wales, Northern Ireland, and the Isle of Man. *J Arthroplasty*. 2022; **37**(2): p. 243-251.

64. Pandit H, Hamilton TW, Jenkins C, Mellon SJ, Dodd CA, and Murray DW. The clinical outcome of minimally invasive Phase 3 Oxford unicompartmental knee arthroplasty: a 15-year follow-up of 1000 UKAs. *The bone & joint journal*. 2015; **97-B**(11): p. 1493-1500.

65. Lisowski LA, Meijer LI, van den Bekerom MP, Pilot P, and Lisowski AE. Ten- to 15-year results of the Oxford Phase III mobile unicompartmental knee arthroplasty: a prospective study from a non-designer group. *Bone & Joint Journal*. 2016; **98 B**(10 Supple B): p. 41-47.

66. Kim KT, Lee S, Kim JH, Hong SW, Jung WS, and Shin WS. The Survivorship and Clinical Results of Minimally Invasive Unicompartmental Knee Arthroplasty at 10-Year Follow-up. *Clin Orthop Surg*. 2015; **7**(2): p. 199-206.

67. Epinette JA, Brunschweiler B, Mertl P, Mole D, and Cazenave A. Unicompartmental knee arthroplasty modes of failure: wear is not the main reason for failure: a multicentre study of 418 failed knees. *Orthop Traumatol Surg Res*. 2012; **98**(6 Suppl): p. S124-130.

68. Vasso M, Antoniadis A, and Helmy N. Update on unicompartmental knee arthroplasty: Current indications and failure modes. *EFORT Open Rev*. 2018; **3**(8): p. 442-448.

69. Goodfellow JW, O'Connor JJ, and Murray DW. A critique of revision rate as an outcome measure: re-interpretation of knee joint registry data. *J Bone Joint Surg Br*. 2010; **92**(12): p. 1628-1631.

70. Robertsson O, Knutson K, Lewold S, and Lidgren L. The routine of surgical management reduces failure after unicompartmental knee arthroplasty. *Journal of Bone & Joint Surgery - British Volume*. 2001; **83**(1): p. 45-49.

71. Badawy M, Espehaug B, Indrekvam K, Havelin LI, and Furnes O. Higher revision risk for unicompartmental knee arthroplasty in low-volume hospitals. *Acta Orthopaedica*. 2014; **85**(4): p. 342-347.

72. van der List JP, Sheng DL, Kleeblad LJ, Chawla H, and Pearle AD. Outcomes of cementless unicompartmental and total knee arthroplasty: A systematic review. *Knee*. 2017; **24**(3): p. 497-507.

73. Mohammad HR, Judge A, and Murray DW. A matched comparison of cementless unicompartmental and total knee replacement outcomes based on the National Joint Registry for England, Wales, Northern Ireland and the Isle of Man. *Acta Orthop*. 2022; **93**: p. 478-487.

74. Goodfellow JW and O'Connor J. Clinical results of the Oxford knee. Surface arthroplasty of the tibiofemoral joint with a meniscal bearing prosthesis. *Clin Orthop Relat Res*. 1986;(205): p. 21-42.

75. Goodfellow J, O'Connor, J., Pandit, H., Dodd, C. & Murray, D. *Unicompartmental Arthroplasty with the Oxford Knee 2nd edition*. 2015, Oxford: Goodfellow Publishers.

76. *Zimmer Biomet*. 2022; Available from: https://www.zimmerbiomet.eu/en.

77. Goodfellow J and O'Connor J. The anterior cruciate ligament in knee arthroplasty. A risk-factor with unconstrained meniscal prostheses. *Clin Orthop Relat Res*. 1992;(276): p. 245-252.

78. White SH, Ludkowski PF, and Goodfellow JW. Anteromedial osteoarthritis of the knee. *J Bone Joint Surg Br*. 1991; **73**(4): p. 582-586.

79. Murray DW, Goodfellow JW, and O'Connor JJ. The Oxford medial unicompartmental arthroplasty: a ten-year survival study. *J Bone Joint Surg Br*. 1998; **80**(6): p. 983-989.

80. Svärd UC and Price AJ. Oxford medial unicompartmental knee arthroplasty. A survival analysis of an independent series. *J Bone Joint Surg Br*. 2001; **83**(2): p. 191-194.

81. Pandit H, Jenkins C, Barker K, Dodd CAF, and Murray DW. The Oxford medial unicompartmental knee replacement using a minimally-invasive approach. *Journal of Bone and Joint Surgery - Series B*. 2006; **88**(1): p. 54-60.

82. Price AJ, Webb J, Topf H, Dodd CA, Goodfellow JW, and Murray DW. Rapid recovery after oxford unicompartmental arthroplasty through a short incision. *J Arthroplasty*. 2001; **16**(8): p. 970-976.

83. Forsythe ME, Englund RE, and Leighton RK. Unicondylar knee arthroplasty: A cementless perspective. *Canadian Journal of Surgery*. 2000; **43**(6): p. 417-424.

84. White SH, Roberts S, and Kuiper JH. The cemented twin-peg Oxford partial knee replacement survivorship: a cohort study. *Knee*. 2015; **22**(4): p. 333-337.

85. Mohammad HR, Matharu GS, Judge A, and Murray DW. A matched comparison of revision rates of cemented Oxford Unicompartmental Knee Replacements with Single and Twin Peg femoral components, based on data from the National Joint Registry for England, Wales, Northern Ireland and the Isle of Man. *Acta Orthopaedica*. 2020; **91**(4): p. 420-425.

86. *Oxford®Partial Knee Microplasty® Instrumentation Surgical Technique*. 2019, Zimmer Biomet: Bridgend, UK.

87. Botterill J and Khatkar H. The role of hydroxyapatite coating in joint replacement surgery - Key considerations. *J Clin Orthop Trauma*. 2022; **29**: p. 101874.

88. Kendrick BJL, Simpson DJ, Kaptein BL, Valstar ER, Gill HS, Murray DW, and Price AJ. Polyethylene wear of mobile-bearing unicompartmental knee replacement at 20 years. *Journal of Bone and Joint Surgery - Series B*. 2011; **93 B**(4): p. 470-475.

89. Kendrick BJ, Longino D, Pandit H, Svard U, Gill HS, Dodd CA, Murray DW, and Price AJ. Polyethylene wear in Oxford unicompartmental knee replacement: a retrieval study of 47 bearings. *Journal of Bone & Joint Surgery - British Volume*. 2010; **92**(3): p. 367-373.

90. Kozinn SC and Scott R. Unicondylar knee arthroplasty. *J Bone Joint Surg Am*. 1989; **71**(1): p. 145-150.

91. Goodfellow JW, Kershaw CJ, Benson MK, and O'Connor JJ. The Oxford Knee for unicompartmental osteoarthritis. The first 103 cases. *J Bone Joint Surg Br*. 1988; **70**(5): p. 692-701.

92. Pandit H, Jenkins C, Gill HS, Smith G, Price AJ, Dodd CAF, and Murray DW. Unnecessary contraindications for mobile-bearing unicompartmental knee replacement. *Journal of Bone and Joint Surgery - Series B*. 2011; **93 B**(5): p. 622-628.

93. Molloy J, Kennedy J, Jenkins C, Mellon S, Dodd C, and Murray D. Obesity should not be considered a contraindication to medial Oxford UKA: long-term patient-reported outcomes and implant survival in 1000 knees. *Knee surgery, sports traumatology, arthroscopy : official journal of the ESSKA*. 2019; **27**(7): p. 2259-2265.

94. Kennedy JA, Matharu GS, Hamilton TW, Mellon SJ, and Murray DW. Age and Outcomes of Medial Meniscal-Bearing Unicompartmental Knee Arthroplasty. *Journal of Arthroplasty*. 2018; **33**(10): p. 3153-3159.

95. Mohammad HR, Mellon S, Judge A, Dodd C, and Murray D. The effect of age on the outcomes of cementless mobile bearing unicompartmental knee replacements. *Knee Surg Sports Traumatol Arthrosc*. 2022; **30**(3): p. 928-938.

96. Mohammad HR, Kennedy JA, Mellon SJ, Judge A, Dodd CA, and Murray DW. Ten-year clinical and radiographic results of 1000 cementless Oxford unicompartmental knee replacements. *Knee Surgery, Sports Traumatology, Arthroscopy*. 2019.

97. John McKie, Peter Devane, Simon Young, Brendon Coleman, Dawson Muir, Perry Turner, Hugh Griffin, Peter Larmer, Andrea Pettett, Toni Hobbs, and Frampton. C. *Nineteen Year Report: January 1999 to December 2017*. 2018.

98. Kendrick BJL, Kaptein BL, Valstar ER, Gill HS, Jackson WFM, Dodd CAF, Price AJ, and Murray DW. Cemented versus cementless Oxford unicompartmental knee arthroplasty using radiostereometric analysis. *The Bone & Joint Journal*. 2015; **97-B**(2): p. 185-191.

99. Pandit H, Liddle AD, Kendrick BJ, Jenkins C, Price AJ, Gill HS, Dodd CA, and Murray DW. Improved fixation in cementless unicompartmental knee replacement: five-year results of a randomized controlled trial. *J Bone Joint Surg Am*. 2013; **95**(15): p. 1365-1372.

100. Mohammad HR, Matharu GS, Judge A, and Murray DW. Comparison of the 10-year outcomes of cemented and cementless unicompartmental knee replacements: data from the National Joint Registry for England, Wales, Northern Ireland and the Isle of Man. *Acta Orthop*. 2020; **91**(1): p. 76-81.

101. Li ZX and Tan AHC. An Early Periprosthetic Fracture of a Cementless Oxford Unicompartmental Knee Arthroplasty: Risk Factors and Mitigation Strategies. *J Orthop Case Rep*. 2021; **11**(4): p. 65-69.

102. Hefny MH, Smith NA, and Waite J. Cementless medial Oxford unicompartmental knee replacement. Five-year results from an independent series. *Knee*. 2020; **27**(4): p. 1219-1227.

103. Panzram B, Mandery M, Reiner T, Gotterbarm T, Schiltenwolf M, and Merle C. Cementless Oxford Medial Unicompartmental Knee Replacement—Clinical and Radiological Results of 228 Knees with a Minimum 2-Year Follow-Up. *Journal of Clinical Medicine*. 2020; **9**(5): p. 1476.

104. Nandra R, Rajgor HD, Winkworth C, and Aslam N. Regional five-year clinical outcomes of 289 consecutive cementless oxford uni-compartmental knee replacements at a non-inventor centre. *J Clin Orthop Trauma*. 2021; **17**: p. 176-181.

105. Hiranaka T, Yoshikawa R, Yoshida K, Michishita K, Nishimura T, Nitta S, Takashiba K, and Murray D. Tibial shape and size predicts the risk of tibial plateau fracture after cementless unicompartmental knee arthroplasty in Japanese patients. *The Bone & Joint Journal*. 2020; **102-B**(7): p. 861-867.

106. Seeger JB, Haas D, Jager S, Rohner E, Tohtz S, and Clarius M. Extended sagittal saw cut significantly reduces fracture load in cementless unicompartmental knee arthroplasty compared to cemented tibia plateaus: An experimental cadaver study. *Knee Surgery, Sports Traumatology, Arthroscopy*. 2012; **20**(6): p. 1087-1091.

107. Liddle A, Pandit H, Jenkins C, Lobenhoffer P, Jackson W, Dodd C, and Murray D. Valgus subsidence of the tibial component in cementless Oxford unicompartmental knee replacement. *The Bone & Joint Journal*. 2014; **96-B**(3): p. 345-349.

108. Mohammad HR, Matharu GS, Judge A, and Murray DW. The Effect of Surgeon Caseload on the Relative Revision Rate of Cemented and Cementless Unicompartmental Knee Replacements: An Analysis from the National Joint Registry for England, Wales, Northern Ireland and the Isle of Man. *J Bone Joint Surg Am*. 2020; **102**(8): p. 644-653.

109. Heckmann N, Ihn H, Stefl M, Etkin CD, Springer BD, Berry DJ, and Lieberman JR. Early Results From the American Joint Replacement Registry: A Comparison With Other National Registries. *Journal of Arthroplasty*. 2019; **34**(7 Supplement): p. S125-S134.e121.

110. *Hip, Knee & Shoulder Arthroplasty Report*. 2020, Australian Orthopaedic Association National Joint Replacement Registry (AOANJRR).

111. Gioe TJ, Killeen KK, Hoeffel DP, Bert JM, Comfort TK, Scheltema K, Mehle S, and Grimm K. Analysis of Unicompartmental Knee Arthroplasty in a Community-Based Implant Registry. *Clinical Orthopaedics and Related Research®*. 2003; **416**: p. 111-119.

112. Hunt LP, Ben-Shlomo Y, Clark EM, Dieppe P, Judge A, Macgregor AJ, Tobias JH, Vernon K, and Blom AW. 45-day mortality after 467779 knee replacements for osteoarthritis from the National Joint Registry for England and Wales: An observational study. *The Lancet*. 2014; **384**(9952): p. 1429-1436.

113. NJR. *16th Annual Report 2019 - National Joint Registry for England, Wales, Northern Ireland and the Isle of Man*. 2019.

114. Bin Abd Razak HR, Acharyya S, Tan SM, Pang HN, Tay KJD, Chia SL, Lo NN, and Yeo SJ. Predictors of midterm outcomes after medial unicompartmental knee arthroplasty in Asians. *CiOS Clinics in Orthopedic Surgery*. 2017; **9**(4): p. 432-438.

115. Bordini B, Stea S, Falcioni S, Ancarani C, and Toni A. Unicompartmental knee arthroplasty 11-year experience from 3929 implants in RIPO register. *Knee*. 2014; **21**(6): p. 1275-1279.

116. Brinkman JM, Bubra PS, Walker P, Walsh WR, and Bruce WJM. Midterm results using a medial pivot total knee replacement compared with the Australian National Joint Replacement Registry data. *ANZ Journal of Surgery*. 2014; **84**(3): p. 172-176.

117. Burn E, Liddle AD, Hamilton TW, Judge A, Pandit HG, Murray DW, and Pinedo-Villanueva R. Cost-effectiveness of unicompartmental compared with total knee replacement: a population-based study using data from the National Joint Registry for England and Wales. *BMJ Open*. 2018; **8**(4): p. e020977.

118. Campi S, Mellon SJ, Ridley D, Foulke B, Dodd CAF, Pandit HG, and Murray DW. Optimal interference of the tibial component of the cementless Oxford Unicompartmental Knee Replacement. *Bone & Joint Research*. 2018; **7**(3): p. 226-231.

119. Mohammad HR, Campi S, Murray D, and Mellon S. Instruments to reduce the risk of tibial fracture following cementless unicompartmental knee replacement. *The Knee*. 2018; **25**(6): p. 988-996.

120. Akan B, Karaguven D, Guclu B, Yildirim T, Kaya A, Armangil M, and Cetin I. Cemented versus Uncemented Oxford Unicompartmental Knee Arthroplasty: Is There a Difference? *Advances in orthopedics*. 2013; **2013**: p. 245915-245915.

121. Hamilton TW, Pandit HG, Jenkins C, Mellon SJ, Dodd CA, and Murray DW. Evidence-Based Indications for Mobile-Bearing Unicompartmental Knee Arthroplasty in a Consecutive Cohort of Thousand Knees. *The Journal of Arthroplasty*. 2017; **32**(6): p. 1779-1785.

122. Hamilton T, Pandit H, Lombardi A, Adams J, Oosthuizen C, Clavé A, Dodd C, Berend K, and Murray D. Radiological Decision Aid to determine suitability for medial unicompartmental knee arthroplasty. *The Bone & Joint Journal*. 2016; **98-B**(10_Supple_B): p. 3-10.

123. Murray DW, Fitzpatrick R, Rogers K, Pandit H, Beard DJ, Carr AJ, and Dawson J. The use of the Oxford hip and knee scores. *The Journal of Bone and Joint Surgery. British volume*. 2007; **89-B**(8): p. 1010-1014.

124. Harris K, Dawson J, Doll H, Field RE, Murray DW, Fitzpatrick R, Jenkinson C, Price AJ, and Beard DJ. Can pain and function be distinguished in the Oxford Knee Score in a meaningful way? An exploratory and confirmatory factor analysis. *Quality of Life Research*. 2013; **22**(9): p. 2561-2568.

125. Murray DW and Parkinson RW. Usage of unicompartmental knee arthroplasty. *Bone Joint J*. 2018; **100-B**(4): p. 432-435.

126. Kalairajah Y, Azurza K, Hulme C, Molloy S, and Drabu KJ. Health Outcome Measures in the Evaluation of Total Hip Arthroplasties—A Comparison Between the Harris Hip Score and the Oxford Hip Score. *The Journal of Arthroplasty*. 2005; **20**(8): p. 1037-1041.

127. *Twenty Year Report: January 1999 to December 2018*. 2019, New Zealand Joint Registry.

128. Insall JN, Dorr LD, Scott RD, and Norman WS. Rationale of The Knee Society Clinical Rating System. *Clinical Orthopaedics and Related Research*. 1989; **248**: p. 13-14.

129. Gulati A, Pandit H, Jenkins C, Chau R, Dodd CA, and Murray DW. The effect of leg alignment on the outcome of unicompartmental knee replacement. *J Bone Joint Surg Br*. 2009; **91**(4): p. 469-474.

130. Herdman M, Gudex C, Lloyd A, Janssen M, Kind P, Parkin D, Bonsel G, and Badia X. Development and preliminary testing of the new five-level version of EQ-5D (EQ-5D-5L). *Quality of Life Research*. 2011; **20**(10): p. 1727-1736.

131. Devlin NJ, Shah KK, Feng Y, Mulhern B, and van Hout B. Valuing health-related quality of life: An EQ-5D-5L value set for England. *Health Economics*. 2018; **27**(1): p. 7-22.

132. Tegner Y and Lysholm J. Rating systems in the evaluation of knee ligament injuries. *Clin Orthop Relat Res*. 1985;(198): p. 43-49.

133. Pandit H, Jenkins C, Beard DJ, Gallagher J, Price AJ, Dodd CAF, Goodfellow JW, and Murray DW. Cementless Oxford unicompartmental knee replacement shows reduced radiolucency at one year. *The Journal of bone and joint surgery. British volume*. 2009; **91**(2): p. 185-189.

134. Altman DG. *Practical Statistics for Medical Research*. 1st Edition ed. 2018: Chapman and Hall/CRC.

135. Baker PN, Petheram T, Jameson SS, Avery PJ, Reed MR, Gregg PJ, and Deehan DJ. Comparison of patient-reported outcome measures following total and unicondylar knee replacement. *Journal of Bone and Joint Surgery - Series B*. 2012; **94 B**(7): p. 919-927.

136. Matthews DJ, Hossain FS, Patel S, and Haddad FS. A Cohort Study Predicts Better Functional Outcomes and Equivalent Patient Satisfaction Following UKR Compared with TKR. *HSS Journal*. 2013; **9**(1): p. 21-24.

137. Liddle AD, Judge A, Pandit H, and Murray DW. Adverse outcomes after total and unicompartmental knee replacement in 101,330 matched patients: a study of data from the National Joint Registry for England and Wales. *Lancet*. 2014; **384**(9952): p. 1437-1445.

138. Clement ND, MacDonald D, and Simpson AHRW. The minimal clinically important difference in the Oxford knee score and Short Form 12 score after total knee arthroplasty. *Knee Surgery, Sports Traumatology, Arthroscopy*. 2014; **22**(8): p. 1933-1939.

139. Hamilton TW, Rizkalla JM, Kontochristos L, Marks BE, Mellon SJ, Dodd CAF, Pandit HG, and Murray DW. The Interaction of Caseload and Usage in Determining Outcomes of Unicompartmental Knee Arthroplasty: A Meta-Analysis. *The Journal of Arthroplasty*. 2017; **32**(10): p. 3228-3237.e3222.

140. Lee WC, Kwan YH, Chong HC, and Yeo SJ. The minimal clinically important difference for Knee Society Clinical Rating System after total knee arthroplasty for primary osteoarthritis. *Knee Surg Sports Traumatol Arthrosc*. 2017; **25**(11): p. 3354-3359.

141. Devji T, Guyatt GH, Lytvyn L, Brignardello-Petersen R, Foroutan F, Sadeghirad B, Buchbinder R, Poolman RW, Harris IA, Carrasco-Labra A, Siemieniuk RAC, and Vandvik PO. Application of minimal important differences in degenerative knee disease outcomes: a systematic review and case study to inform BMJ Rapid Recommendations. *BMJ Open*. 2017; **7**(5): p. e015587.

142. Campi S, Pandit H, Hooper G, Snell D, Jenkins C, Dodd CAF, Maxwell R, and Murray DW. Ten-year survival and seven-year functional results of cementless Oxford unicompartmental knee replacement: A prospective consecutive series of our first 1000 cases. *Knee*. 2018; **25**(6): p. 1231-1237.

143. Price AJ and Svard U. A second decade lifetable survival analysis of the Oxford unicompartmental knee arthroplasty. *Clinical Orthopaedics & Related Research*. 2011; **469**(1): p. 174-179.

144. Panzram B, Bertlich I, Reiner T, Walker T, Hagmann S, Weber M-A, and Gotterbarm T. Results after Cementless Medial Oxford Unicompartmental Knee Replacement - Incidence of Radiolucent Lines. *PLOS ONE*. 2017; **12**(1): p. e0170324.

145. Grössner-Schreiber B and Tuan RS. [The influence of the titanium implant surface on the process of osseointegration]. *Dtsch Zahnarztl Z*. 1991; **46**(10): p. 691-693.

146. Small SR, Berend ME, Rogge RD, Archer DB, Kingman AL, and Ritter MA. Tibial loading after UKA: evaluation of tibial slope, resection depth, medial shift and component rotation. *J Arthroplasty*. 2013; **28**(9 Suppl): p. 179-183.

147. Simpson DJ, Price AJ, Gulati A, Murray DW, and Gill HS. Elevated proximal tibial strains following unicompartmental knee replacement—A possible cause of pain. *Medical Engineering & Physics*. 2009; **31**(7): p. 752-757.

148. Iolascon G, Resmini G, and Tarantino U. Mechanobiology of bone. *Aging Clin Exp Res*. 2013; **25 Suppl 1**: p. S3-7.

149. Kendrick BJ, Kaptein BL, Valstar ER, Gill HS, Jackson WF, Dodd CA, Price AJ, and Murray DW. Cemented versus cementless Oxford unicompartmental knee arthroplasty using radiostereometric analysis: a randomised controlled trial. *The bone & joint journal*. 2015; **97-B**(2): p. 185-191.

150. Nakagaki S, Iijima M, Handa K, Koike T, Yasuda Y, Saito T, and Mizoguchi I. Micro-CT and histologic analyses of bone surrounding immediately loaded miniscrew implants: comparing compression and tension loading. *Dent Mater J*. 2014; **33**(2): p. 196-202.

151. Dumbleton J and Manley MT. Hydroxyapatite-Coated Prostheses in Total Hip and Knee Arthroplasty. *JBJS*. 2004; **86**(11).

152. Ohgushi H, Goldberg VM, and Caplan AI. Heterotopic osteogenesis in porous ceramics induced by marrow cells. *Journal of Orthopaedic Research*. 1989; **7**(4): p. 568-578.

153. Okumura M, Ohgushi H, and Tamai S. Bonding osteogenesis in coralline hydroxyapatite combined with bone marrow cells. *Biomaterials*. 1991; **12**(4): p. 411-416.

154. Okumura M, Ohgushi H, Tamai S, and Shors EC. Primary Bone-Formation in Porous Hydroxyapatite Ceramic - A Light and Scanning Electron-Microscopic Study. *Cells and Materials*. 1991; **1**(1): p. 29-34.

155. Zhao G, Zinger O, Schwartz Z, Wieland M, Landolt D, and Boyan BD. Osteoblast-like cells are sensitive to submicron-scale surface structure. *Clinical Oral Implants Research*. 2006; **17**(3): p. 258-264.

156. Jiang P, Zhang Y, Hu R, Wang X, Lai Y, Rui G, and Lin C. Hydroxyapatite-modified micro/nanostructured titania surfaces with different crystalline phases for osteoblast regulation. *Bioact Mater*. 2021; **6**(4): p. 1118-1129.

157. Gulati A, Chau R, Pandit HG, Gray H, Price AJ, Dodd CA, and Murray DW. The incidence of physiological radiolucency following Oxford unicompartmental knee replacement and its relationship to outcome. *J Bone Joint Surg Br*. 2009; **91**(7): p. 896-902.

158. Panzram B, Bertlich I, Reiner T, Walker T, Hagmann S, Weber MA, and Gotterbarm T. Results after cementless medial oxford unicompartmental knee replacement-incidence of radiolucent lines. *PLoS ONE*. 2017; **12**(1).

159. Davison MJ, Ioannidis G, Maly MR, Adachi JD, and Beattie KA. Intermittent and constant pain and physical function or performance in men and women with knee osteoarthritis: data from the osteoarthritis initiative. *Clin Rheumatol*. 2016; **35**(2): p. 371-379.

160. Wautier D, Ftaïta S, and Thienpont E. Radiolucent lines around knee arthroplasty components : a narrative review. *Acta Orthop Belg*. 2020; **86**(1): p. 82-94.

161. Rahimizadeh A, Nourmohammadi Z, Arabnejad S, Tanzer M, and Pasini D. Porous architected biomaterial for a tibial-knee implant with minimum bone resorption and bone-implant interface micromotion. *J Mech Behav Biomed Mater*. 2018; **78**: p. 465-479.

162. Horsager K, Kaptein BL, Romer L, Jorgensen PB, and Stilling M. Dynamic RSA for the evaluation of inducible micromotion of Oxford UKA during step-up and step-down motion. *Acta Orthopaedica*. 2017; **88**(3): p. 275-281.

163. Frost HM. Wolff's Law and bone's structural adaptations to mechanical usage: an overview for clinicians. *Angle Orthod*. 1994; **64**(3): p. 175-188.

164. Hart NH, Newton RU, Tan J, Rantalainen T, Chivers P, Siafarikas A, and Nimphius S. Biological basis of bone strength: anatomy, physiology and measurement. *J Musculoskelet Neuronal Interact*. 2020; **20**(3): p. 347-371.

165. Andersen MR, Winther NS, Lind T, Schrøder HM, Flivik G, and Petersen MM. Low Preoperative BMD Is Related to High Migration of Tibia Components in Uncemented TKA—92 Patients in a Combined DEXA and RSA Study With 2-Year Follow-Up. *The Journal of Arthroplasty*. 2017; **32**(7): p. 2141-2146.

166. Krause M, Hubert J, Deymann S, Hapfelmeier A, Wulff B, Petersik A, Püschel K, Amling M, Hawellek T, and Frosch K-H. Bone microarchitecture of the tibial plateau in skeletal health and osteoporosis. *The Knee*. 2018; **25**(4): p. 559-567.

167. Mazess RB and Barden HS. Measurement of bone by dual-photon absorptiometry (DPA) and dua-energy X-ray absorptiometry (DEXA). *Annales Chirurgiae et Gynaecologiae*. 1988; **77**(5-6): p. 197-203.

168. Bakkum AJT, Janssen TWJ, Rolf MP, Roos JC, Burcksen J, Knol DL, and de Groot S. A reliable method for measuring proximal tibia and distal femur bone mineral density using dual-energy X-ray absorptiometry. *Medical Engineering & Physics*. 2014; **36**(3): p. 387-390.

169. Hirvasniemi J, Thevenot J, Kokkonen HT, Finnilä MA, Venäläinen MS, Jämsä T, Korhonen RK, Töyräs J, and Saarakkala S. Correlation of Subchondral Bone Density and Structure from Plain Radiographs with Micro Computed Tomography Ex Vivo. *Ann Biomed Eng*. 2016; **44**(5): p. 1698-1709.

170. Magnusson HI, Westlin NE, Nyqvist F, Gärdsell P, Seeman E, and Karlsson MK. Abnormally Decreased Regional Bone Density in Athletes with Medial Tibial Stress Syndrome. *The American Journal of Sports Medicine*. 2001; **29**(6): p. 712-715.

171. Magnusson HI, Ahlborg HG, Karlsson C, Nyquist F, and Karlsson MK. Low Regional Tibial Bone Density in Athletes with Medial Tibial Stress Syndrome Normalizes after Recovery from Symptoms. *The American Journal of Sports Medicine*. 2003; **31**(4): p. 596-600.

172. Simpson DJ, Kendrick BJL, Dodd CAF, Price AJ, Gill HS, and Murray DW. Load transfer in the proximal tibia following implantation with a unicompartmental knee replacement:a static snapshot. *Proceedings of the Institution of Mechanical Engineers, Part H: Journal of Engineering in Medicine*. 2011; **225**(5): p. 521-529.

173. Recker R, Lappe J, Davies KM, and Heaney R. Bone remodeling increases substantially in the years after menopause and remains increased in older osteoporosis patients. *J Bone Miner Res*. 2004; **19**(10): p. 1628-1633.

174. Jeyapalina S, Beck JP, Bloebaum RD, and Bachus KN. Progression of bone ingrowth and attachment strength for stability of percutaneous osseointegrated prostheses. *Clinical orthopaedics and related research*. 2014; **472**(10): p. 2957-2965.

175. Liddle AD, O'Brien S, Doran E, Penny ID, Hooper GJ, Burn PJ, Dodd CAF, Beverl DE, Maxwell AR, Pit H, and et al. Cementless fixation in Oxford Unicompartmental Knee Replacement: a multicentre study of 1000 knees. *Bone and joint journal*. 2013; **95B**(2): p. 181-187.

176. Mohammad HR, Bullock GS, Kennedy JA, Mellon SJ, Murray D, and Judge A. Cementless unicompartmental knee replacement achieves better ten-year clinical outcomes than cemented: a systematic review. *Knee Surgery, Sports Traumatology, Arthroscopy*. 2020; **01**: p. 01.

177. Crawford DA, Berend KR, and Lombardi AV. Management of the Failed Medial Unicompartmental Knee Arthroplasty. *J Am Acad Orthop Surg*. 2018; **26**(20): p. e426-e433.

178. Thoreau L, Morcillo Marfil D, and Thienpont E. Periprosthetic fractures after medial unicompartmental knee arthroplasty: a narrative review. *Arch Orthop Trauma Surg*. 2021.

179. Burger JA, Jager T, Dooley MS, Zuiderbaan HA, Kerkhoffs GMMJ, and Pearle AD. Comparable incidence of periprosthetic tibial fractures in cementless and cemented unicompartmental knee arthroplasty: a systematic review and meta-analysis. *Knee Surgery, Sports Traumatology, Arthroscopy*. 2022; **30**(3): p. 852-874.

180. Yoshikawa R, Hiranaka T, Okamoto K, Fujishiro T, Hida Y, Kamenaga T, and Sakai Y. The medial eminence line for predicting tibial fracture risk after unicompartmental knee arthroplasty. *CiOS Clinics in Orthopedic Surgery*. 2020; **12**(2): p. 166-170.

181. Leenders AM, Schotanus MGM, Wind RJP, Borghans RAP, and Kort NP. A high rate of tibial plateau fractures after early experience with patient-specific instrumentation for unicompartmental knee arthroplasties. *Knee surgery, sports traumatology, arthroscopy : official journal of the ESSKA*. 2018; **26**(11): p. 3491-3498.

182. Yue B, Varadarajan KM, Ai S, Tang T, Rubash HE, and Li G. Differences of Knee Anthropometry Between Chinese and White Men and Women. *The Journal of Arthroplasty*. 2011; **26**(1): p. 124-130.

183. Brown NM, Engh G, and Fricka K. Periprosthetic Fracture following Partial Knee Arthroplasty. *Journal of Knee Surgery*. 2019; **32**(10): p. 947-952.

184. Gleeson RE, Evans R, Ackroyd CE, Webb J, and Newman JH. Fixed or mobile bearing unicompartmental knee replacement? A comparative cohort study. *The Knee*. 2004; **11**(5): p. 379-384.

185. Kim YJ, Kim BH, Yoo SH, Kang SW, Kwack CH, and Song MH. Mid-Term Results of Oxford Medial Unicompartmental Knee Arthroplasty in Young Asian Patients Less than 60 Years of Age: A Minimum 5-Year Follow-up. *Knee Surg Relat Res*. 2017; **29**(2): p. 122-128.

186. Pandit H, Murray DW, Dodd CA, Deo S, Waite J, Goodfellow J, and Gibbons CL. Medial tibial plateau fracture and the Oxford unicompartmental knee. *Orthopedics*. 2007; **30**(5 Suppl): p. 28-31.

187. Song MH, Kim BH, Ahn SJ, Yoo SH, and Lee MS. Early Complications After Minimally Invasive Mobile-Bearing Medial Unicompartmental Knee Arthroplasty. *Journal of Arthroplasty*. 2009; **24**(8): p. 1281-1284.

188. Rudol G, Jackson MP, and James SE. Medial tibial plateau fracture complicating unicompartmental knee arthroplasty. *J Arthroplasty*. 2007; **22**(1): p. 148-150.

189. Vardi G and Strover AE. Early complications of unicompartmental knee replacement: The Droitwich experience. *Knee*. 2004; **11**(5): p. 389-394.

190. Yang KY, Yeo SJ, and Lo NN. Stress fracture of the medial tibial plateau after minimally invasive unicompartmental knee arthroplasty: a report of 2 cases. *J Arthroplasty*. 2003; **18**(6): p. 801-803.

191. Abram SGF, Marsh AG, Brydone AS, Nicol F, Mohammed A, and Spencer SJ. The effect of tibial component sizing on patient reported outcome measures following uncemented total knee replacement. *The Knee*. 2014; **21**(5): p. 955-959.

192. Clarius M, Aldinger PR, Bruckner T, and Seeger JB. Saw cuts in unicompartmental knee arthroplasty: An analysis of sawbone preparations. *The Knee*. 2009; **16**(5): p. 314-316.

193. Seeger JB, Haas D, Jäger S, Röhner E, Tohtz S, and Clarius M. Extended sagittal saw cut significantly reduces fracture load in cementless unicompartmental knee arthroplasty compared to cemented tibia plateaus: an experimental cadaver study. *Knee Surgery, Sports Traumatology, Arthroscopy*. 2012; **20**(6): p. 1087-1091.

194. Kamenaga T, Hiranaka T, Nakano N, Hayashi S, Fujishiro T, Okamoto K, Kuroda R, and Matsumoto T. Short distance from the keel to the posterior tibial cortex is associated with fracture after cementless Oxford UKA in Asian patients. *Knee Surg Sports Traumatol Arthrosc*. 2022; **30**(4): p. 1220-1230.

195. Lee YS, Yun JY, and Lee BK. Tibial component coverage based on bone mineral density of the cut tibial surface during unicompartmental knee arthroplasty: Clinical relevance of the prevention of tibial component subsidence. *Archives of Orthopaedic and Trauma Surgery*. 2014; **134**(1): p. 85-89.

196. Damm NB, Morlock MM, and Bishop NE. Friction coefficient and effective interference at the implant-bone interface. *J Biomech*. 2015; **48**(12): p. 3517-3521.

197. Szivek JA, Thompson JD, and Benjamin JB. Characterization of three formulations of a synthetic foam as models for a range of human cancellous bone types. *Journal of Applied Biomaterials*. 1995; **6**(2): p. 125-128.

198. Hvid I, Christensen P, Søndergaard J, Christensen PB, and Larsen CG. Compressive Strength of Tibial Cancellous Bone: Instron® and Osteopenetrometer Measurements in an Autopsy Material. *Acta Orthopaedica Scandinavica*. 1983; **54**(6): p. 819-825.

199. Linde F, Hvid I, and Pongsoipetch B. Energy absorptive properties of human trabecular bone specimens during axial compression. *Journal of Orthopaedic Research*. 1989; **7**(3): p. 432-439.

200. Berahmani S, Janssen D, van Kessel S, Wolfson D, de Waal Malefijt M, Buma P, and Verdonschot N. An experimental study to investigate biomechanical aspects of the initial stability of press-fit implants. *Journal of the Mechanical Behavior of Biomedical Materials*. 2015; **42**: p. 177-185.

201. Geraldes DM, Hansen U, Jeffers J, and Amis AA. Stability of small pegs for cementless implant fixation. *Journal of Orthopaedic Research*. 2017; **35**(12): p. 2765-2772.

202. *Peg n.1*, in *Oxford English Dictionary*. 2022, Oxford University Press.

203. Giori NJ, Beaupré GS, and Carter DR. The influence of fixation peg design on the shear stability of prosthetic implants. *J Orthop Res*. 1990; **8**(6): p. 892-898.

204. Murray DW. *Unpublished intraoperative assessment of access to tibial floor to drill holes*, A. Rahman, Editor. 2022.

205. Pegg EC, Walter J, Mellon SJ, Pandit HG, Murray DW, D'Lima DD, Fregly BJ, and Gill HS. Evaluation of factors affecting tibial bone strain after unicompartmental knee replacement. *J Orthop Res*. 2013; **31**(5): p. 821-828.

206. Li MG and Nilsson KG. Changes in bone mineral density at the proximal tibia after total knee arthroplasty: A 2-year follow-up of 28 knees using dual energy x-ray absorptiometry. *Journal of Orthopaedic Research*. 2000; **18**(1): p. 40-47.

207. Clarius M, Haas D, Aldinger PR, Jaeger S, Jakubowitz E, and Seeger JB. Periprosthetic tibial fractures in unicompartmental knee arthroplasty as a function of extended sagittal saw cuts: An experimental study. *Knee*. 2010; **17**(1): p. 57-60.

208. Pegg EC, Mancuso F, Alinejad M, Van Duren BH, O'Connor JJ, Murray DW, and Pandit HG. Sagittal kinematics of mobile unicompartmental knee replacement in anterior cruciate ligament deficient knees. *Clinical Biomechanics*. 2016; **31**: p. 33-39.

209. Wahal N, Gaba S, Malhotra R, Kumar V, Pegg EC, and Pandit H. Reduced Bearing Excursion After Mobile-Bearing Unicompartmental Knee Arthroplasty is Associated With Poor Functional Outcomes. *The Journal of Arthroplasty*. 2018; **33**(2): p. 366-371.

210. *HHE2016-005: Urgent Field Safety Notice for Cementless Oxford Partial Knee Unicompartmental Knee Replacement system*. 2017, Zimmer Biomet.

211. Bergmann G. *OrthoLoad*. 2008, Charité Universitaetsmedizin Berlin: http://www.OrthoLoad.com.

212. Patel V, Issever AS, Burghardt A, Laib A, Ries M, and Majumdar S. MicroCT evaluation of normal and osteoarthritic bone structure in human knee specimens. *J Orthop Res*. 2003; **21**(1): p. 6-13.

213. Holzer LA, Kraiger M, Talakic E, Fritz GA, Avian A, Hofmeister A, Leithner A, and Holzer G. Microstructural analysis of subchondral bone in knee osteoarthritis. *Osteoporos Int*. 2020; **31**(10): p. 2037-2045.

214. Downing MR, Ashcroft PB, Johnstone AJ, Bach O, Mackenzie S, and Ashcroft GP. Assessment of inducible fracture micromotion in distal radial fractures using radiostereometry. *J Orthop Trauma*. 2008; **22**(8 Suppl): p. S96-105.

215. Short A, Gill HS, Marks B, Waite JC, Kellett CF, Price AJ, O'Connor JJ, and Murray DW. A novel method for in vivo knee prosthesis wear measurement. *J Biomech*. 2005; **38**(2): p. 315-322.

216. Simpson DJ, Kendrick BJ, Kaptein BL, Price AJ, Murray DW, and Gill HS. Development of a model-based Roentgen stereophotogrammetric analysis system to measure polyethylene wear in unicompartmental arthroplasty. *Proceedings of the Institution of Mechanical Engineers*. 2010; **Part H, Journal of engineering in medicine. 224**(11): p. 1235-1243.

217. van Ijsseldijk EA, Valstar ER, Stoel BC, Nelissen RG, Reiber JH, and Kaptein BL. The robustness and accuracy of in vivo linear wear measurements for knee prostheses based on model-based RSA. *J Biomech*. 2011; **44**(15): p. 2724-2727.

218. Eichelberger P, Ferraro M, Minder U, Denton T, Blasimann A, Krause F, and Baur H. Analysis of accuracy in optical motion capture – A protocol for laboratory setup evaluation. *Journal of Biomechanics*. 2016; **49**(10): p. 2085-2088.

219. McCormick N and Lord J. Digital Image Correlation. *Materials Today*. 2010; **13**(12): p. 52-54.

220. Scott CEH, Eaton MJ, Nutton RW, Wade FA, Evans SL, and Pankaj P. Validated finite element analysis of metal backed versus all-polyethylene unicompartmental knee arthroplasty: the effect of implant thickness on proximal tibial strain. *Journal of Orthopaedic Research. Conference*. 2016; **34**(Supplement 1).

221. Ali AM, Newman SDS, Hooper PA, Davies CM, and Cobb JP. The effect of implant position on bone strain following lateral unicompartmental knee arthroplasty: A Biomechanical Model Using Digital Image Correlation. *Bone Joint Res*. 2017; **6**(8): p. 522-529.

222. Kohli N, Stoddart JC, and van Arkel RJ. The limit of tolerable micromotion for implant osseointegration: a systematic review. *Sci Rep*. 2021; **11**(1): p. 10797.

223. McCabe A, Pickford M, and Shawcross J. The History, Technical Specifications and Efficacy of Plasma Spray Coatings Applied to Joint Replacement Prostheses. *Reconstructive Review*. 2016; **6**(4).

APPENDICES

Appendix A PROMs used in 5-year Clinical Study

In **Chapter 2**, the following questionnaires were used. These forms used to collect the raw data for these questionnaires are presented below:

- Oxford Knee Score (OKS)
- Intermittent and Constant OsteoArthritis Pain (ICOAP) Score
- EQ-5D-5L
- painDETECT
- Tegner Activity Score (TAS)
- American Knee Society Score (AKSS)
- Charnley Classification

Oxford Knee Score (OKS) - Page 1 of 2

Oxford Knee Assessment - PART A: FOR PATIENT

PROBLEMS WITH YOUR KNEE

During the past 4 weeks.....

☯ tick one box for every question

1

During the past 4 weeks.....

How would you describe the pain you usually have from your knee?

None	Very mild	Mild	Moderate	Severe
☐4	☐3	☐2	☐1	☐0

2

***During the past 4 weeks*.....**

Have you had any trouble with washing and drying yourself (all over) because of your knee?

No trouble at all	Very little trouble	Moderate trouble	Extreme difficulty	Impossible to do
☐4	☐3	☐2	☐1	☐0

3

***During the past 4 weeks*.....**

Have you had any trouble getting in and out of a car or using public transport because of your knee? (whichever you would tend to use)

No trouble at all	Very little trouble	Moderate trouble	Extreme difficulty	Impossible to do
☐4	☐3	☐2	☐1	☐0

4

***During the past 4 weeks*.....**

For how long have you been able to walk before pain from your knee becomes **severe**? (*with or without a stick)*

No pain/more than 30 mins	16 to 30 mins	5 to 15 mins	Around the house only	Not at all - pain severe when walking
☐4	☐3	☐2	☐1	☐0

5

***During the past 4 weeks*.....**

After a meal (sat at a table), how painful has it been for you to stand up from a chair because of your knee?

Not at all painful	Slightly painful	Moderately painful	Very painful	Unbearable
☐4	☐3	☐2	☐1	☐0

Oxford Knee Score (OKS) - Page 2 of 2

6

***During the past 4 weeks*.....**

Have you been limping when walking, because of your knee?

Rarely/never	Sometimes, or just at first	Often, not just at first	Most of the time	All of the time
☐4	☐3	☐2	☐1	☐0

7

***During the past 4 weeks*.....**

Could you kneel down and get up again afterwards?

Yes, easily	With little difficulty	With moderate difficulty	With extreme difficulty	No, impossible
☐4	☐3	☐2	☐1	☐0

8

***During the past 4 weeks*.....**

Have you been troubled by pain from your knee in bed at night?

No nights	Only 1 or 2 nights	Some nights	Most nights	Every night
☐4	☐3	☐2	☐1	☐0

9

***During the past 4 weeks*.....**

How much has pain from your knee interfered with your usual work *(including housework)*?

Not at all	A little bit	Moderately	Greatly	Totally
☐4	☐3	☐2	☐1	☐0

10

***During the past 4 weeks*.....**

Have you felt that your knee might suddenly 'give way' or let you down?

Rarely/never	Sometimes, or just at first	Often, not just at first	Most of the time	All of the time
☐4	☐3	☐2	☐1	☐0

11

***During the past 4 weeks*.....**

Could you do the household shopping on your own?

Yes, easily	With little difficulty	With moderate difficulty	With extreme difficulty	No, impossible
☐4	☐3	☐2	☐1	☐0

12

***During the past 4 weeks*.....**

Could you walk down one flight of stairs?

Yes, easily	With little difficulty	With moderate difficulty	With extreme difficulty	No, impossible
☐4	☐3	☐2	☐1	☐0

A measure of Intermittent and Constant Osteoarthritis Pain,

ICOAP: Knee Version

People have told us that they experience different kinds of pain (including aching or discomfort) in their knee. To get a better sense of the different types of knee pain you may experience, we would like to ask you about any "constant pain" (pain you have all the time) separately from any pain that you may experience less often, that is, "pain that comes and goes". The following questions will ask you about the pain that you have experienced in your knee in the PAST WEEK. Please answer ALL questions.

A. CONSTANT PAIN (for each of the following questions, please select the response that best describes, on average, your constant knee pain in the PAST WEEK.

1. In the past week, how intense has your constant knee pain been?

Not at all / No constant knee pain ☐ Mildly ☐ Moderately ☐ Severely ☐ Extremely ☐

2. In the past week, how much has your constant knee pain affected your sleep?

Not at all / No constant knee pain ☐ Mildly ☐ Moderately ☐ Severely ☐ Extremely ☐

3. In the past week, how much has your constant knee pain affected your overall quality of life?

Not at all / No constant knee pain ☐ Mildly ☐ Moderately ☐ Severely ☐ Extremely ☐

4. In the past week, how frustrated or annoyed have you been by your constant knee pain?

Not at all / No constant knee pain ☐ Mildly ☐ Moderately ☐ Severely ☐ Extremely ☐

5. In the past week, how upset or worried have you been by your constant knee pain?

Not at all / No constant knee pain ☐ Mildly ☐ Moderately ☐ Severely ☐ Extremely ☐

B. PAIN THAT COMES AND GOES (for each of the following questions, please select the response that best describes your knee pain that comes and goes, on average, in the PAST WEEK.

6. In the past week, how intense has your most severe knee pain that comes and goes been?

Not at all/No knee pain that comes and goes ☐ Mildly ☐ Moderately ☐ Severely ☐ Extremely ☐

7. In the past week, how frequently has this knee pain that comes and goes occurred?

Never/No knee pain that comes and goes ☐ Rarely ☐ Sometimes ☐ Often ☐ Very Often ☐

8. In the past week, how much has your knee pain that comes and goes affected your sleep?

Not at all/No knee pain that comes and goes ☐ Mildly ☐ Moderately ☐ Severely ☐ Extremely ☐

9. In the past week, how much has your knee pain that comes and goes affected your overall quality of life?

Not at all/No knee pain that comes and goes ☐ Mildly ☐ Moderately ☐ Severely ☐ Extremely ☐

10. In the past week, how frustrated or annoyed have you been by your knee pain that comes and goes?

Not at all/No knee pain that comes and goes ☐ Mildly ☐ Moderately ☐ Severely ☐ Extremely ☐

11. In the past week, how upset or worried have you been by your knee pain that comes and goes?

Not at all/No knee pain that comes and goes ☐ Mildly ☐ Moderately ☐ Severely ☐ Extremely ☐

EQ-5D-5L - Page 1 of 2

Under each heading, please tick the ONE box that best describes your health TODAY

MOBILITY

- I have no problems in walking about ❑
- I have slight problems in walking about ❑
- I have moderate problems in walking about ❑
- I have severe problems in walking about ❑
- I am unable to walk about ❑

SELF-CARE

- I have no problems washing or dressing myself ❑
- I have slight problems washing or dressing myself ❑
- I have moderate problems washing or dressing myself ❑
- I have severe problems washing or dressing myself ❑
- I am unable to wash or dress myself ❑

USUAL ACTIVITIES *(e.g. work, study, housework, family or leisure activities*)

- I have no problems doing my usual activities ❑
- I have slight problems doing my usual activities ❑
- I have moderate problems doing my usual activities ❑
- I have severe problems doing my usual activities ❑
- I am unable to do my usual activities ❑

PAIN / DISCOMFORT

- I have no pain or discomfort ❑
- I have slight pain or discomfort ❑
- I have moderate pain or discomfort ❑
- I have severe pain or discomfort ❑
- I have extreme pain or discomfort ❑

ANXIETY / DEPRESSION

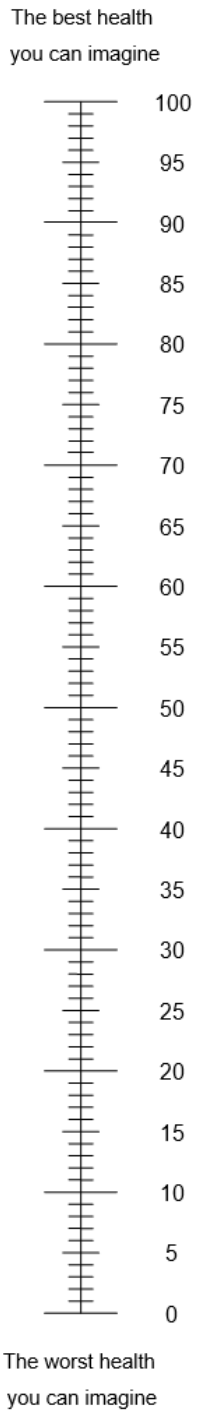
- I am not anxious or depressed ❑
- I am slightly anxious or depressed ❑
- I am moderately anxious or depressed ❑
- I am severely anxious or depressed ❑
- I am extremely anxious or depressed ❑

UK (English) v.2 © 2009 EuroQol Group. EQ-5D™ is a trade mark of the EuroQol Group

EQ-5D-5L Score - Page 2 of 2

- We would like to know how good or bad your health is TODAY.
- This scale is numbered from 0 to 100.
- 100 means the best health you can imagine.
  0 means the worst health you can imagine.
- Mark an X on the scale to indicate how your health is TODAY.
- Now, please write the number you marked on the scale in the box below.

YOUR HEALTH TODAY =



UK (English) v.2 © 2009 EuroQol Group. EQ-5D™ is a trade mark of the EuroQol Group

painDETECT™

PAIN QUESTIONNAIRE

Date: ..... Patient: Last name: ..... First name: .....

How would you assess your pain **now**, at this moment?

0 1 2 3 4 5 6 7 8 9 10

none max.

How strong was the **strongest** pain during the past 4 weeks?

0 1 2 3 4 5 6 7 8 9 10

none max.

How strong was the pain during the past 4 weeks **on average**?

0 1 2 3 4 5 6 7 8 9 10

none max.

Mark the picture that best describes the course of your pain:



Persistent pain with slight fluctuations ☐



Persistent pain with pain attacks ☐



Pain attacks without pain between them ☐



Pain attacks with pain between them ☐

Please mark your **main area of pain**



Does your pain radiate to other regions of your body? yes ☐ no ☐

If yes, please draw the direction in which the pain radiates.

Do you suffer from a burning sensation (e.g., stinging nettles) in the marked areas?

never ☐ hardly noticed ☐ slightly ☐ moderately ☐ strongly ☐ very strongly ☐

Do you have a tingling or prickling sensation in the area of your pain (like crawling ants or electrical tingling)?

never ☐ hardly noticed ☐ slightly ☐ moderately ☐ strongly ☐ very strongly ☐

Is light touching (clothing, a blanket) in this area painful?

never ☐ hardly noticed ☐ slightly ☐ moderately ☐ strongly ☐ very strongly ☐

Do you have sudden pain attacks in the area of your pain, like electric shocks?

never ☐ hardly noticed ☐ slightly ☐ moderately ☐ strongly ☐ very strongly ☐

Is cold or heat (bath water) in this area occasionally painful?

never ☐ hardly noticed ☐ slightly ☐ moderately ☐ strongly ☐ very strongly ☐

Do you suffer from a sensation of numbness in the areas that you marked?

never ☐ hardly noticed ☐ slightly ☐ moderately ☐ strongly ☐ very strongly ☐

Does slight pressure in this area, e.g., with a finger, trigger pain?

never ☐ hardly noticed ☐ slightly ☐ moderately ☐ strongly ☐ very strongly ☐

(To be filled out by the physician)

never	hardly noticed	slightly	moderately	strongly	very strongly
☐ x 0 = 0	☐ x 1 = ☐	☐ x 2 = ☐☐	☐ x 3 = ☐☐	☐ x 4 = ☐☐	☐ x 5 = ☐☐

Total score ☐☐ **out of 35**

R. Freynhagen, R. Baron, U. Gockel, T.R. Tölle, Current Medical Research and Opinion vol 22 (10) 2006; 1911-1920 ©Pfizer Pharma GmbH 2006

Tegner Activity Score (TAS) - Page 1 of 1

Please circle the number, which best describes the activity you are able to do.

TEGNER ACTIVITY SCORE	
10	**Competitive Sports**: soccer – National & International Elite
9	**Competitive Sports**: soccer – lower divisions, ice hockey, wresting, and gymnastics
8	**Competitive Sports**: bandy, squash/badminton, athletics (jumping etc.), downhill skiing
7	**Competitive Sports**: tennis, athletics (running), motocross, speedway, handball, basketball **Recreational Sports**: soccer, badminton, ice hockey, squash, athletics (jogging), cross-country.
6	**Recreational Sports**: tennis, badminton, handball, basketball, downhill skiing, jogging at least 5 times a week
5	**Work**: heavy labour (building, forestry) **Competitive Sports**: (cycling/cross-country skiing) **Recreational Sports**: (jogging on uneven grounds at least 2 times a week)
4	**Work**: moderate heavy labour eg. truck driving, heavy domestic work **Recreational Sports**: cycling, cross-country skiing, jogging on even ground at least 2 times a week
3	**Work**: light labour eg. nursing **Competitive and recreational sports**: swimming, walking in forest possible
2	**Work**: light labour Walking on uneven ground possible but walking in forest impossible
1	**Work**: sedentary work, walking on even ground possible
0	**Sick Leave / Disability** pension due to knee problems

American Knee Society Score (AKSS)

Pain	Points	✓
None	50	
Mild or Occasional	45	
Mild – Stairs only	40	
Mild Walking and Stairs	30	
Moderate – Occasional	20	
Moderate – Continual	10	
Severe	0	

Stability (maximum movement in any position)

AP	Points	✓
<5mm	10	
5-10mm	5	
>10mm	0	

Med-Lat	Points	✓
<5°	15	
6-9°	10	
10-14°	5	
>15°	0	

Flexion ROM		
Degrees	**Points**	✓
≥125	25	
120	24	
115	23	
110	22	
105	21	
100	20	
95	19	
90	18	
85	17	
80	16	
75	15	
70	14	
65	13	

Flexion ROM (continued)		
Degrees	**Points**	✓
60	12	
55	11	
50	10	
45	9	
40	8	
35	7	
30	6	
25	5	
20	4	
15	3	
10	2	
5	1	
0	0	

Maximum Flexion: _____

Extension: _____

Subtotal: ☐☐☐/100

DEDUCTIONS

Flexion contracture			Extension Lag			Alignment		
	Points	✓		Points	✓	ASIS – Knee- Ankle	Points	✓
0-4°	**0**		0	**0**		Normal Knee (in 5-10° valgus)	**0**	
5-9°	**-2**		1-9°	**-5**		Minor Valgus Knee (in 0-4° valgus)	**-10**	
10-15°	**-5**		10-20°	**-10**		Moderate Valgus Knee (in 11-15° valgus)	**-10**	
16-20°	**-10**		>20°	**-15**		Severe Valgus or Varus (>15° or < 0°)	**-20**	
>20°	**-15**					**Goniometer Measurement** in degrees: Please circle **valgus or varus**		°

Total Deductions ☐☐/50

Objective Knee Score ☐☐☐/100

FUNCTION SCORE

Walking			Stairs			Support (deductions)		
	Points	✓		Points	✓		Points	✓
Unlimited	50		Normal	50		No Support	0	
500m-1km	40		Down with rail	40		Stick	-5	
100-500m	30		Up & down with rail	30		2 sticks	-10	
<100m	20		Unable down	15		Crutches/walker	-20	
Housebound	10		Unable	0				
Unable	0							

Functional Knee Score ☐☐☐/100

Comments:

Charnley ABC
A: Single knee affected ☐
B: Both knees affected ☐
C: Multiple arthritis or medical infirmity ☐

Appendix B Additional Results for Tibial Component Fixation

In **Chapter 3**, radiolucencies around the tibial component were shown to be related to incidence of pain. This was determined based on analysis of ICOAP 'Total' scores (see **Section 3.7**). This difference was found to stem from ICOAP 'B' scores. No relationship to OKS and TAS were found. This was based on a F test performed on simple linear regressions of outcome scores against radiolucency scores. This data shown in the following pages. Note that TWF/TFF/TKF refer to Tibial Wall/Floor/Keel Fixation. Significance test results and equations for of ICOAP 'Total' and ICOAP 'B' have been highlighted in yellow for quick reference.

TWF Cemented	5 Year OKS Pain Subtotal	5 Year OKS Fn Subtotal	5 Year OKS Total	5 Year ICOAP A Total Actual	5 Year ICOAP B Total Actual	ICOAP Total	TAS
Goodness of Fit							
R squared	0.006893	0.001498	0.003696	0.03136	0.001249	0.007324	0.0009914
Is slope significantly non-zero?							
F	0.3887	0.08402	0.2077	1.813	0.07002	0.4132	0.05557
P value	0.5355	0.7730	0.6503	0.1836	0.7923	0.5230	0.8145
Deviation from zero?	Not Significant	Not Significant	Not Significant	Not Significant	Not Significant	Not Significant	Not Significant
Equation	Y = -0.01595*X + 17.53	Y = -0.009357*X + 24.62	Y = -0.02531*X + 42.15	Y = 0.1459*X + 2.630	Y = -0.03097*X + 13.52	Y = 0.05746*X + 8.077	Y = 0.002745*X + 3.143

TWF Cementless	5 Year OKS Pain Subtotal	5 Year OKS Fn Subtotal	5 Year OKS Total	5 Year ICOAP A Total Actual	5 Year ICOAP B Total Actual	ICOAP Total	TAS
Goodness of Fit							
R squared	0.01020	0.005254	3.643e-005	0.03165	0.003893	0.02008	0.0004481
Is slope significantly non-zero?							
F	0.4429	0.2271	0.001567	1.406	0.1681	0.8810	0.01928
P value	0.5093	0.6361	0.9686	0.2423	0.6839	0.3532	0.8902
Deviation from zero?	Not Significant	Not Significant	Not Significant	Not Significant	Not Significant	Not Significant	Not Significant
Equation	Y = 0.007476*X + 17.79	Y = -0.008509*X + 25.44	Y = -0.001033*X + 43.23	Y = -0.04047*X + 4.539	Y = -0.02214*X + 9.077	Y = -0.03130*X + 6.808	Y = 0.0008181*X + 3.222

TFF Cemented	5 Year OKS Pain Subtotal	5 Year OKS Fn Subtotal	5 Year OKS Total	5 Year ICOAP A Total Actual	5 Year ICOAP B Total Actual	ICOAP Total	TAS
Goodness of Fit							
R squared	0.01244	0.01515	0.01512	0.0006374	0.07076	0.03575	0.002648
Is slope significantly non-zero?							
F	0.7052	0.8615	0.8595	0.03572	4.264	2.076	0.1487
P value	0.4046	0.3573	0.3579	0.8508	0.0436	0.1552	0.7012
Deviation from zero?	Not Significant	Not Significant	Not Significant	Not Significant	Significant	Not Significant	Not Significant
Equation	Y = 0.02885*X + 14.79	Y = 0.04007*X + 21.03	Y = 0.06892*X + 35.82	Y = -0.02800*X + 7.484	Y = -0.3138*X + 39.88	Y = -0.1709*X + 23.68	Y = 0.006041*X + 2.672

TFF Cementless	5 Year OKS Pain Subtotal	5 Year OKS Fn Subtotal	5 Year OKS Total	5 Year ICOAP A Total Actual	5 Year ICOAP B Total Actual	ICOAP Total	TAS
Goodness of Fit							
R squared	0.001225	0.05217	0.02953	0.002553	0.01091	0.003344	0.008323
Is slope significantly non-zero?							
F	0.05272	2.367	1.308	0.1101	0.4741	0.1443	0.3609
P value	0.8195	0.1313	0.2590	0.7417	0.4948	0.7059	0.5512
Deviation from zero?	Not Significant	Not Significant	Not Significant	Not Significant	Not Significant	Not Significant	Not Significant
Equation	Y = -0.01536*X + 19.65	Y = -0.1589*X + 39.96	Y = -0.1743*X + 59.61	Y = 0.06813*X - 4.090	Y = -0.2196*X + 28.57	Y = -0.07573*X + 12.24	Y = -0.02090*X + 5.237

TKF Cemented	5 Year OKS Pain Subtotal	5 Year OKS Fn Subtotal	5 Year OKS Total	5 Year ICOAP A Total Actual	5 Year ICOAP B Total Actual	ICOAP Total	TAS
Goodness of Fit							
R squared	0.05369	0.04546	0.05325	0.009407	0.1597	0.1026	0.0004614
Is slope significantly non-zero?							
F	3.177	2.667	3.150	0.5318	10.64	6.401	0.02585
P value	0.0801	0.1080	0.0814	0.4689	0.0019	0.0142	0.8728
Deviation from zero?	Not Significant	Not Significant	Not Significant	Not Significant	Significant	Significant	Not Significant
Equation	Y = 0.05462*X + 12.24	Y = 0.06323*X + 18.65	Y = 0.1178*X + 30.89	Y = -0.09801*X + 14.10	Y = -0.4295*X + 52.50	Y = -0.2638*X + 33.30	Y = 0.002297*X + 2.978

TKF Cementless	5 Year OKS Pain Subtotal	5 Year OKS Fn Subtotal	5 Year OKS Total	5 Year ICOAP A Total Actual	5 Year ICOAP B Total Actual	ICOAP Total	TAS
Goodness of Fit							
R squared	0.0004446	0.001836	0.001484	0.006410	0.005084	0.0002569	0.0001813
Is slope significantly non-zero?							
F	0.01913	0.07910	0.06390	0.2774	0.2197	0.01105	0.007797
P value	0.8907	0.7799	0.8016	0.6011	0.6416	0.9168	0.9300
Deviation from zero?	Not Significant	Not Significant	Not Significant	Not Significant	Not Significant	Not Significant	Not Significant
Equation	Y = 0.02582*X + 15.63	Y = 0.08319*X + 16.70	Y = 0.1090*X + 32.34	Y = 0.3012*X - 27.62	Y = -0.4183*X + 49.47	Y = -0.05857*X + 10.93	Y = -0.008606*X + 4.122

Appendix C Additional Results for Peri-Keel Remodelling

In **Chapter 4**, assessment of ΔSOV between post-operative and 5-year radiographs was performed. An intermediate assessment of ΔSOV between post-operative and 1-year radiographs has been included below (**Figure C1**).

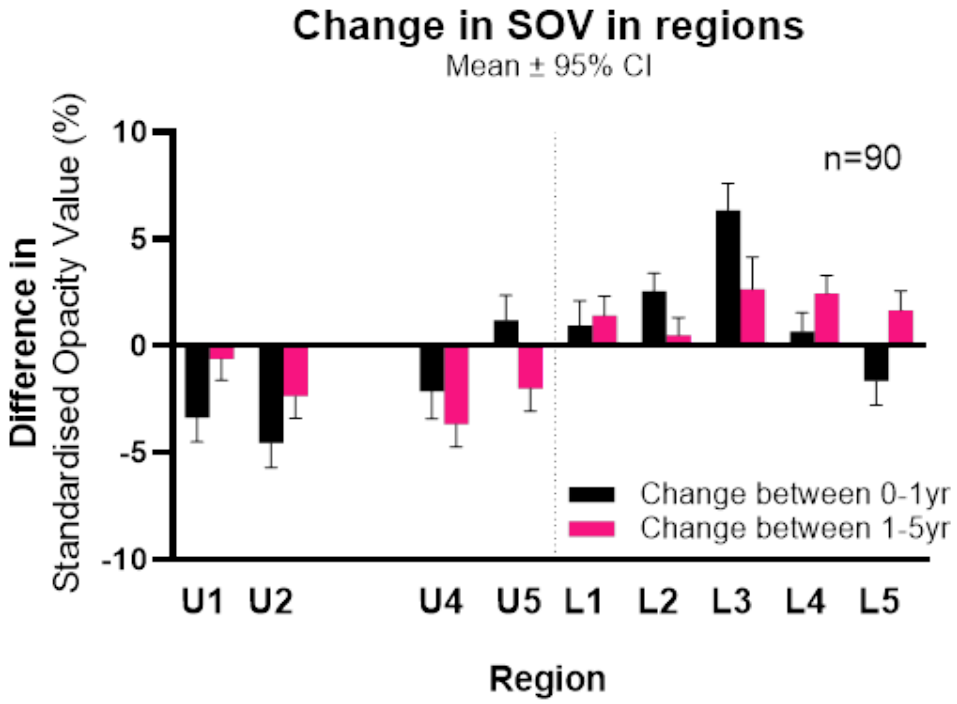


Figure C1: *Change in SOV in regions between 0-1 year and 1-5 years after surgery.*

1-year postoperative radiographs were collected from patients in the final study cohort. 90 of the 115 patients had further 1-year radiographs (i.e., had post-op, 1-year, and 5-year radiographs). Change in SOV between 0-1 and 1-5 year was calculated. It was found that 70% of the densification seen under the keel occurred within 1-year. Furthermore, there appears to be a generalised densification of the region below the keel L3-L5 only after 1-year, resulting in a 1.6-2.6% increase in standardised opacity. Finally, U5 and L5 are the only regions that demonstrate differing changes in density between 0-1 year and 1-5 years, though these changes are small: <2%.

Appendix D Code for data extraction in PIPO testing

In **Chapters 5 and 6**, displacement and force data from PIPO tests were extracted using code written in MATLAB (Natick, Massachusetts, USA). Key elements of code have been included below – these were used and adapted as needed to collect displacement and force data for analysis, and process data to obtain maximum force values, and total energy (N.mm) values for push-in and pull-out phases.

```
%% Open and extract data from a .txt file to a matrix

%Column1: Time [s]
%Column2: HC10 Displacement [mm]
%Column3: HC10 Load 25kN [N]
%Column4: HC10 Load 2.5kN [N]
filename = '<FILENAME> ';
fileID = filename(1:end-4);  %name without extension

fid = fopen(filename,'rt');

%Makes CellArray
CellArray = textscan(fid, '%f%f%f', 'HeaderLines',3);
fclose(fid);
DataMatrix = cell2mat(CellArray);

%Define variables used in code
timeaxis = DataMatrix(:,1);
displacementaxis = DataMatrix(:,2);
rawloadaxis = DataMatrix(:,3);

%% Turning Points and Graphs

%Use 2nd der to find key turning/inflexion points in load graph.
%Savitzky-Golay smoothening used to remove noise. Parameters determined iteratively
to optimise Signal:Noise Ratio.
%pks and locs identify key points separating test phases.

sgolayflit_dim = <as appropriate>;
sgolayflit_range = <as appropriate>;

2ndDerForceAxis =
sgolayfilt(gradient(gradient((rawloadaxis))),sgolayflit_dim,sgolayflit_range)*10^3;
[pks,locs] = findpeaks(Smoothed2ndDerForceAxis,'MinPeakHeight', <as
appropriate>,'MinPeakDistance', <as appropriate>);
```

```
%% Point Measurements

MaxPushInForceRaw               =   min(DataMatrix(:,3)) ;
MaxPushInForceRawIndex          =   find(DataMatrix(:,3)==min(DataMatrix(:,3)));
%%gives index value of maxpushin

MaxPushInForceRawTime           =   DataMatrix(MaxPushInForceRawIndex,1);
MaxPushInForceRawDisp           =   DataMatrix(MaxPushInForceRawIndex,2);

Locs1_MaxPushIn_Time            =   timeaxis(locs(1));
Locs1_MaxPushIn_Disp            =   displacementaxis(locs(1));
Locs1_MaxPushIn_ForceRaw        =   rawloadaxis(locs(1));

Locs2_10saftMaxPushIn_Time      =   timeaxis(locs(2));
Locs2_10saftMaxPushIn_Disp      =   displacementaxis(locs(2));
Locs2_10saftMaxPushIn_ForceRaw  =   rawloadaxis(locs(2));

MaxPullOutForceRaw              =   max(DataMatrix(:,3)) ;
MaxPullOutForceRawIndex         =   find(DataMatrix(:,3)==max(DataMatrix(:,3)));
%%gives index value of maxpullout
MaxPullOutForceRawTime          =   DataMatrix(MaxPullOutForceRawIndex,1);
MaxPullOutForceRawDisp          =   DataMatrix(MaxPullOutForceRawIndex,2);

Locs3_MaxPullOut_Time           =   timeaxis(locs(3));
Locs3_MaxPullOut_Disp           =   displacementaxis(locs(3));
Locs3_MaxPullOut_ForceRaw       =   rawloadaxis(locs(3));

%% Getting Area Under Curves (AUC) Values

P1a_time                = timeaxis(1:locs(1));
P1a_disp                = displacementaxis(1:locs(1));
P1a_load_raw            = rawloadaxis(1:locs(1));
P1a_AUC_wrtT_raw        = trapz(P1a_time, P1a_load_raw); %Phase1a AUC wrt time
P1a_AUC_wrtD_raw        = trapz(P1a_disp, P1a_load_raw); %Phase1a AUC wrt
displacement

P1b_time                = timeaxis(locs(1):locs(2));
P1b_disp                = displacementaxis(locs(1):locs(2));
P1b_load_raw            = rawloadaxis(locs(1):locs(2));
P1b_AUC_wrtT_raw        = trapz(P1b_time, P1b_load_raw); %Phase1b AUC wrt time
P1b_AUC_wrtD_raw        = trapz(P1b_disp, P1b_load_raw); %Phase1b AUC wrt
displacement

P1_AUC_wrtT_raw         = P1a_AUC_wrtT_raw + P1b_AUC_wrtT_raw; %Phase1 AUC total wrt
time
P1_AUC_wrtD_raw         = P1a_AUC_wrtD_raw + P1b_AUC_wrtD_raw; %Phase1 AUC total wrt
displacement

P2_time                 = timeaxis(locs(2):locs(3));
P2_disp                 = displacementaxis(locs(2):locs(3));
P2_load_raw             = rawloadaxis(locs(2):locs(3));
P2_AUC_wrtT_raw         = trapz(P2_time, P2_load_raw); %Phase2 AUC wrt time
P2_AUC_wrtD_raw         = trapz(P2_disp, P2_load_raw); %Phase2 AUC wrt displacement

P3_time                 = timeaxis(locs(3):length(timeaxis));
P3_disp                 = displacementaxis(locs(3):length(displacementaxis));
P3_load_raw             = rawloadaxis(locs(3):length(rawloadaxis));

P3_AUC_wrtT_raw         = trapz(P3_time, P3_load_raw); %Phase3 AUC wrt time
P3_AUC_wrtD_raw         = trapz(P3_disp, P3_load_raw); %Phase3 AUC wrt time
```

Appendix E Additional Results from Peg PIPO Testing

In **Chapter 6**, data from smooth pegs was collected across peg diameters in non-tapered pegs, and separately across taper angles. Patterns were similar to results from porous pegs and therefore not included in main text for brevity (**Figure E1, 2**).

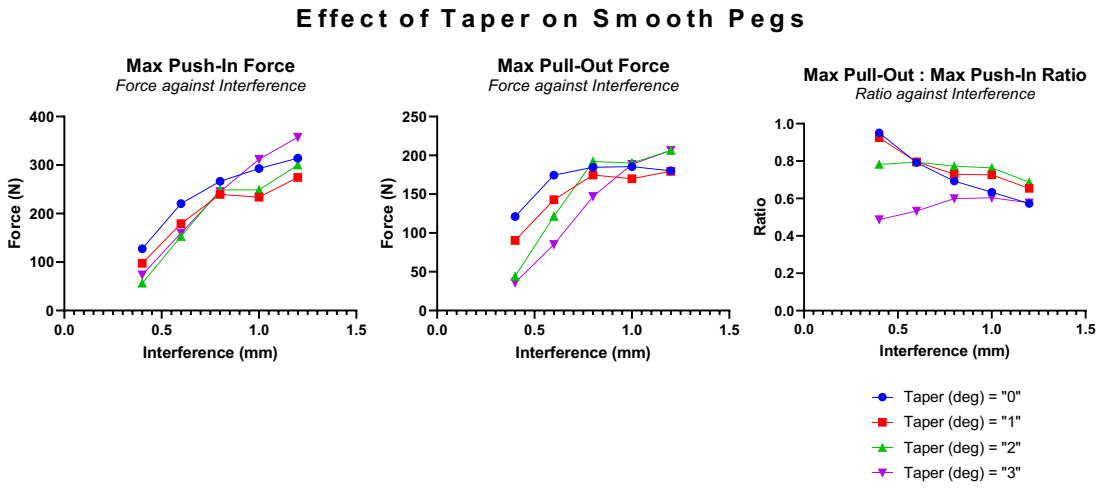


Figure E1: *Maximum Push-In, Pull-Out Forces, and ratio of values, with varying peg taper and interference with a smooth coat.*

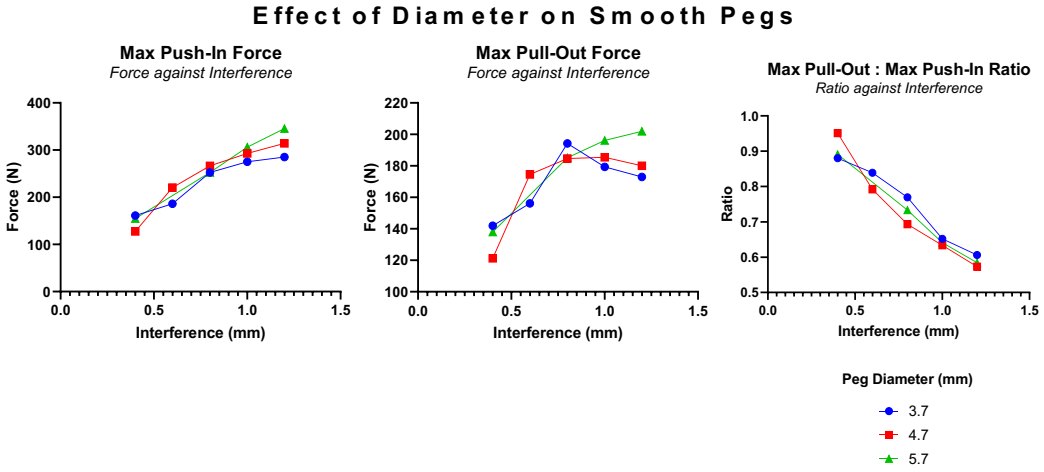


Figure E2: *Maximum Push-In, Pull-Out Forces, and ratio of values, with varying peg diameter and interference in a smooth coat.*

Further in **Chapter 6**, both smooth and porous angled pegs were tested without constraint. These tests had limited applicability to the aims of the study and had methodological limitations, and therefore excluded from final analysis (**Figure E2, Figure E3**).

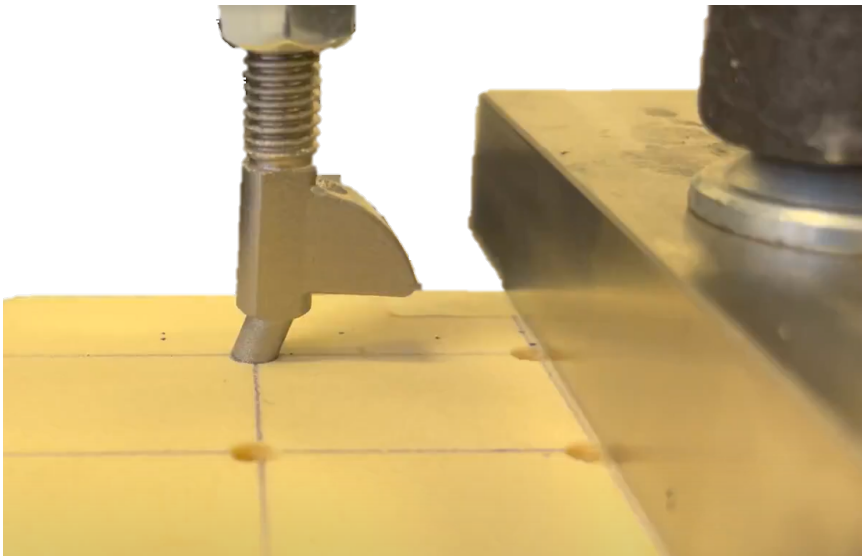


Figure E2: *Setup used for an angled peg pull-out test without constraint.*

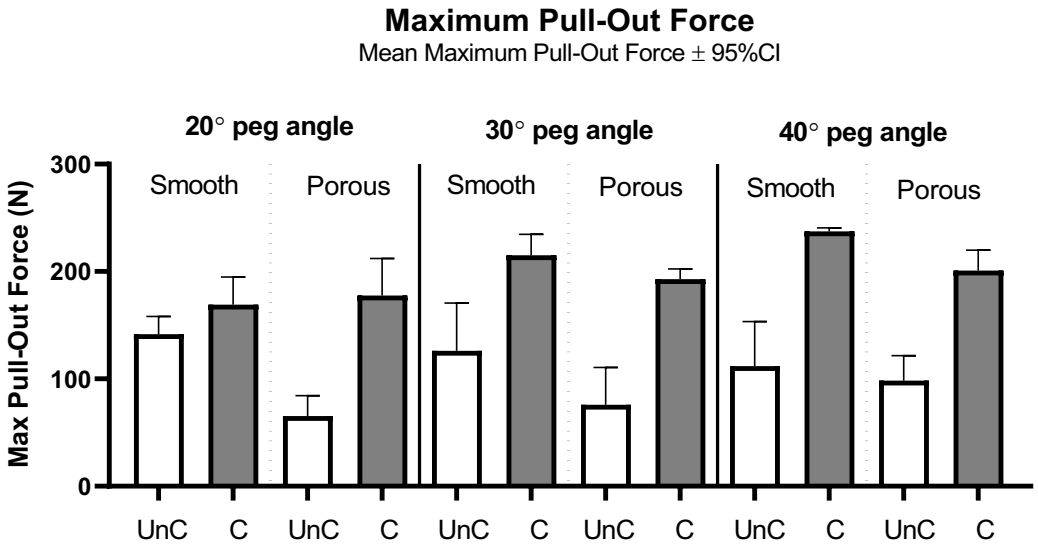


Figure E3: *Maximum Pull-Out Forces in constrained and unconstrained tests, performed on smooth and porous coats, with peg angles of 20°, 30°, and 40° from vertical.*

Appendix F Additional Results from Fracture Testing

In **Chapter 7**, fracture angles in tibias with the standard keel were described to be more vertical, based on coronal fracture path angle (CFPA) measurements. In addition, the axial fracture path angle (AFPA) was also measured. Data is shown below.

Axial fracture path angle (AFPA) was assessed where variants were tested with both central and posterior loading. AFPA indicates the path taken by fractures in the axial plane at the base on the tibial component. Anterior loading resulted in fractures angled medially towards the tibial tubercle, and posterior loading resulted in fractures angling away from the tubercle. AFPA was most oblique with no keel, and had the largest difference central and posterior loading (central -7.4° vs posterior 8.2°, p=0.0018) (**Figure F2**).

Inserting a keel makes the AFPA more vertical in both central and posterior loading. In central loading, AFPA changes from -7.4° with no keel to -2.0° in standard and -2.6° with a small porous keel (ANOVA p=0.0637), though this is not significant. In posterior loading, AFPA changes from 8.2° with no keel to 6.8° in small keel and 2.2° in standard keel (ANOVA p=0.0328); differences are significant (**Figure F2**).

The difference in AFPA between central and posterior loading was significant in all keel designs (standard p=0.0067, small p<0.0001, no keel p=0.0018). There was no difference in AFPA between slot-only and keel-in-slot tests (p>0.05 in all tests).

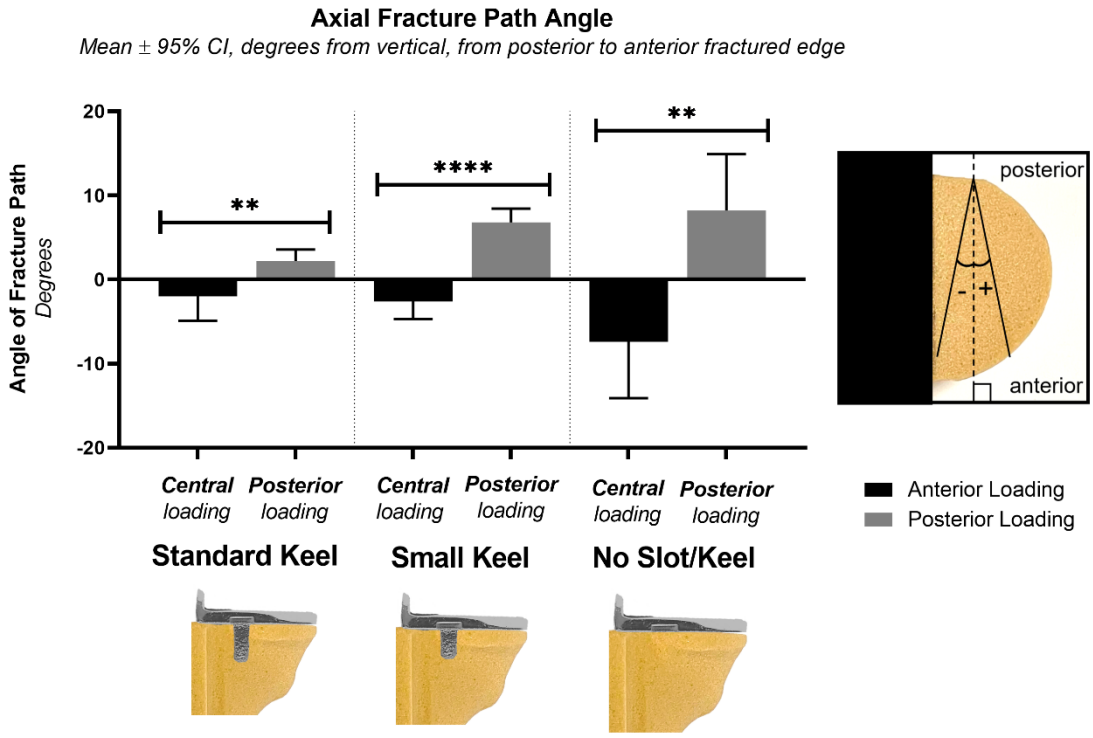


Figure F1: *Axial Fracture Path Angle (AFPA) in with standard, small porous, and no keels, with anterior and posterior loading.*

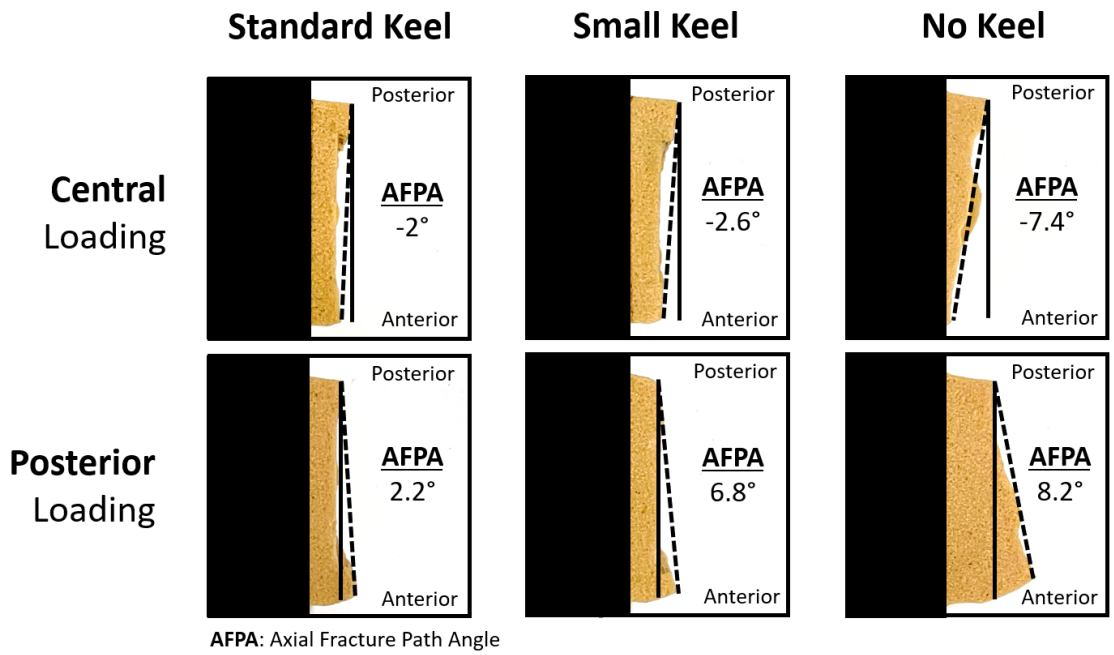


Figure F2: *Visualisation of axial fracture path angles analysed in* ***Figure F1****.*